SIMONE ZANARINI

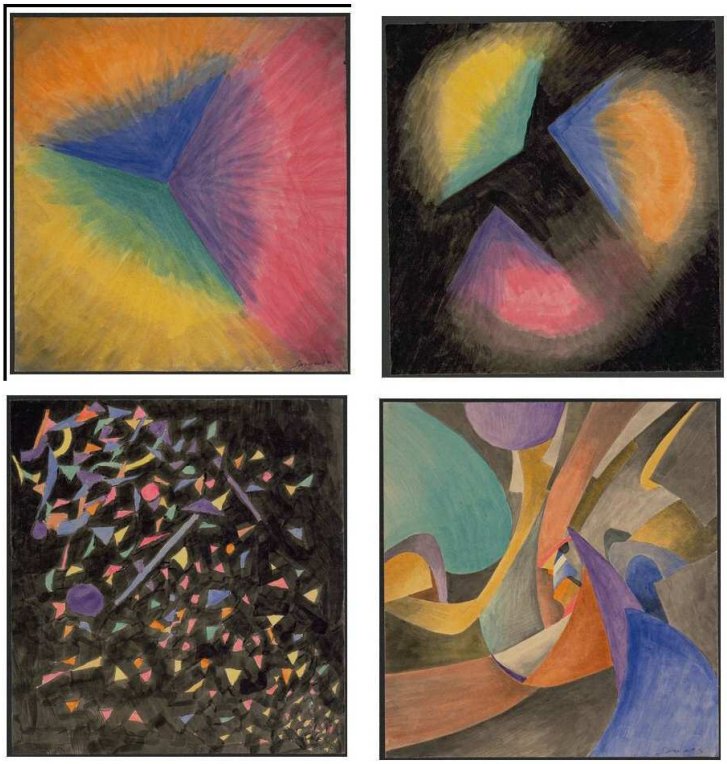

NEW MATERIALS FOR ELECTROCHEMILUMINESCENCE

BOLOGNA 2007

Alma Mater Studiorum-Università di Bologna

DOTTORATO DI RICERCA IN SCIENZE CHIMICHE

XIX ciclo

Dipartimento di Chimica "G. Ciamician"

Coordinatore: Prof. Vincenzo Balzani

NEW MATERIALS FOR ELECTROCHEMILUMINESCENCE

Tesi di dottorato di:

Dr. **Simone Zanarini**

Relatore:

Chiar.mo Prof.

Francesco Paolucci

Coordinatore:

Chiar.mo prof.

Vincenzo Balzani

Settore scientifico disciplinare:
Area 03 - Scienze chimiche; CHIM/02 CHIMICA FISICA

Marzo 2007

A mio padre e mia nonna da poco mancati

COVER AND BACK COVER PICTURES*: Leopold Survage: Colored Rhythm, study for the film;* 1913; MoMa New York.

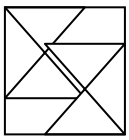

Preface

L'elettrochemiluminescenza (ECL) è un fenomeno il cui studio coinvolge sia aspetti fotofisici che elettrochimici. Lo stato eccitato viene raggiunto attraverso uno stimolo elettrochimico. Le sue applicazioni più importanti sono di tipo diagnostico; infatti la maggior parte delle molecole biologicamente rilevanti come ad esempio le proteine e gli oligonucleotidi possono essere riconosciute e quantificate con una sensibilità e specificità senza precedenti. L'elettrochimica infatti a differenza delle più classiche tecniche della fluorescenza e chemiluminescenza consente di controllare temporalmente e spazialmente la generazione dello stato eccitato.

Sono stati veramente preziosi i due periodi passati presso i laboratori del Prof. A. J. Bard, uno dei pionieri dell'ECL che tra gli altri meriti fu il primo a mettere a punto la tecnica ed a riportare nel 1972 la sorprendente emissione del $Ru(bpy)_3^{2+}$. *In questa introduzione non posso non ringraziare di cuore i miei supervisori Massimo e Francesco prima di tutto per il loro aiuto ed in seconda battuta per la irripetibile opportunità di entrare in contatto con questa grande personalità che ha finito per entusiasmarmi profondamente. Non potrò mai essere grato abbastanza…*

Considerando che le tecniche ECL sono da diversi anni fondamentalmente le stesse la ricerca è finita per indirizzarsi fondamentalmente verso lo sviluppo di nuovi materiali con proprietà migliori dei precedenti.

Nel capitolo I vengono introdotti i concetti ed i meccanismi di base necessari per comprendere gli esperimenti ECL senza comunque scendere troppo nel dettaglio; infine vengono descritte le direzioni fondamentali delle indagini.

Nel capitolo II partendo dagli apparati sperimentali dei laboratori di A. J. Bard viene descritto accuratamente il design, la realizzazione e la messa a punto del nuovo strumento ECL di Bologna. Questa fase di assemblaggio ha richiesto non pochi sforzi ma ha consentito introducendovi la nuova tecnica di proseguire gli studi ECL in Italia.

Nel capitolo III vengono introdotti i risultati degli studi elettrochimici ed ECL su alcuni complessi del Ru(II) di nuova sintesi contenti leganti basati sulle tetrazoline. L'emissione ECL è stata studiata sia in soluzione che allo stato solido. L'effetto sull' ECL della protonazione dell' anello tetrazolinico per via chimica è stata altresì oggetto di indagine evidenziando il presunto effetto catalitico di uno dei complessi nella generazione di idrogeno molecolare in un solvente organico. Da ultimo, dopo alcuni studi preliminari sull'emissione ECL in buffer acquosi, è stata testata l'interazione diretta di alcuni complessi con DNA timoidale mediante titolazione ECL e PL.

Nel capitolo IV diversi complessi dell Ir(III) sono stati caratterizzati sia da un punto di vista elettrochimico che ECL. Alcuni complessi erano già noti in letteratura per la loro alta efficienza mentre i rimanenti sono nuove molecole contenenti leganti tetrazolinici analoghi a quelli studiati nel capitolo precedente. Interessante è stata la possibilità evidenziata da un complesso alogenato di poter studiare la cinetica di una reazione chimica elettro-indotta tramite ECL.

Nel capitolo V infine viene investigata la possibilità di utilizzare chip di silicio monouso, sui quali sono sputterati gli elettrodi, come devices analitici

ECL. Iniziando dalla fabbricazione dei chip, gli studi di riproducibilità del segnale ECL e l'ottimizzazione della geometria viene poi descritta in dettaglio la sintesi di un marcatore ECL basato sul $Ru(bpy)_3^{2+}$ e la funzionalizzazione dei chip utilizzando un SAM di acido lipoico come strato di ancoraggio. Dopo alcune caratterizzazioni di verifica con spettroscopia di massa (TOF) è mostrato come tramite una rapida e semplice misura ECL sia possibile confermare la presenza del prodotto di coupling sui chip funzionalizzati con un elevatissima sensibilità. Nessun segnale è stato invece evidenziato utilizzando sullo stesso sistema metodi fluorimetrici.

Spero che questa tesi sia uno stimolo verso il miglioramento della conoscenze in quel universo ancora poco esplorato che è l'ECL…

The study of electrochemiluminescence (ECL) involves photophysical and electrochemical aspects. Excited states are populated by an electrical stimulus. The most important applications are in the diagnostic field where a number of different biologically-relevant molecules (e.g. proteins and nucleic acids) can be recognized and quantified with a sensitivity and specificity previously not reachable. As a matter of fact the electrochemistry, differently to the classic techniques as fluorescence and chemiluminescence, allows to control the excited state generation spatially and temporally. The two research visits into A. J. Bard electrochemistry laboratories were priceless. Dr. Bard has been one of ECL pioneers, the first to introduce the technique and the one who discovered in 1972 the surprising emission of $Ru(bpy)_3^{2+}$. I consider necessary to thank by now my supervisors Massimo and Francesco for their help and for giving me the great opportunity to know this unique science man that made me feel enthusiastic. I will never be grateful enough…
Considering that the experimental techniques of ECL did not changed significantly in these last years the most convenient research direction has been the developing of materials with new or improved properties.

In Chapter I the basics concepts and mechanisms of ECL are introduced so that the successive experiments can be easily understood. In the final paragraph the scopes of the thesis are briefly described.

In Chapter II by starting from ECL experimental apparatus of Dr. Bard's laboratories the design, assembly and preliminary tests of the new Bologna instrument are carefully described. The instrument assembly required to work hard but resulted in the introduction of the new technique in our labs by allowing the continuation of the ECL studies began in Texas.

In Chapter III are described the results of electrochemical and ECL studies performed on new synthesized Ru(II) complexes containing tetrazolate based ligands. ECL emission has been investigated in solution and in solid thin films. The effect of the chemical protonation of the tetrazolate ring on ECL emission has been also investigated evidencing the possibility of a catalytic effect (generation of molecular hydrogen) of one of the complexes in organic media. Finally, after a series of preliminary studies on ECL emission in acqueous buffers, the direct interaction with calf thymus DNA of some complexes has been tested by ECL and photoluminescence (PL) titration.

In Chapter IV different Ir(III) complexes have been characterized electrochemically and photophysically (ECL and PL). Some complexes were already well-known in literature for their high quantum efficiency whereas the remaining were new synthesized compounds containing tetrazolate based ligands analogous to those investigated in Chapt. III. During the tests on a halogenated complex was unexpectedly evidenced the possibility to follow the kinetics of an electro-induced chemical reaction by using ECL signal.

In the last chapter (V) the possibility to use mono-use silicon chips electrodes as ECL analitycal devices is under investigation. The chapter begins

by describing the chip structure and materials then a signal reproducibility study and geometry optimization is carried on by using two different complexes. In the following paragraphs is reported in detail the synthesis of an ECL label based on $Ru(bpy)_3^{2+}$ and the chip functionalization by using a lipoic acid SAM and the same label. After some preliminary characterizations (mass spectroscopy TOF) has been demonstrated that by mean of a simple and fast ECL measurement it's possible to confirm the presence of the coupling product SAM-label into the chip with a very high sensitivity. No signal was detected from the same system by using photoluminescence.

I hope this thesis will be a boost to expand knowledge of the partially explored ECL universe…

Contents

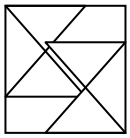

Chapter One: electrochemiluminescence

Non sibi sed aliis

The electrochemiluminescence[1] (ECL) is an emission of light at electrodes in electrochemical cells caused by electron transfer reactions of electrogenerated species in solution. A typical system includes a solution containing reactants A and B with supporting electrolyte. The reaction sequence to generate an excited state and light emission is:

$A + e^- \rightarrow A^-\bullet$ (reduction at electrode)

$B - e^- \rightarrow B^+\bullet$ (oxidation at electrode)

$A^-\bullet + B^+\bullet \rightarrow {}^1A^* + B$ (excited state formation)

$^1A^* \rightarrow A + h\nu$ (light emission)

A and B could be the same species, e.g. $Ru(bpy)_3^{2+}$ in oxydized and reduced form. The term *electrogenerated chemiluminescence* (ECL) is used to distinguish from generic systems where light is emitted in electrochemical cells. Let's consider some well known phenomena showing light emission at electrodes in electrochemical cell that are not ECL.

Chemiluminescence reactions. There are numerous chemical reactions in solution on a species that causes light emission. Often the production of excited states is mediated by the reaction with peroxide and oxygen[2-3]. Some well known examples are luminol, oxalate esters and luciginen with many pratical applications. Considering the luminol (5-amino-2,3-dihydro-1,4-phthalazinedione) the chemiluminescent reaction is generally carried by the addition of hydrogen peroxide in the presence of an ion which generates hydroxyl radical.

Glow discharge electrolysis. If electrolysis is carried out with a small electrode, high voltages and very high current densities the evolution of gas (e.g., oxygen at the anode) forms a gas layer that separates solution[4] contact from the electrode. At higher applied voltages, breakdown occurs in the gas film leading to a glow discharge and emission of light.[5]

Electroluminescence (EL). There are several different mechanisms by which light is emitted in solids, usually semiconductors or insulators.[6] Dielectric breakdown, similar to the glow discharge phenomenon that occurs in gases, can produce light emission. This involves rather high electric fields. Another high field form of luminescence in solids is related to cathodoluminesence that occurs when cathode rays (beams of electrons) strike a phosphor, as in cathode ray tubes in oscilloscopes. An EL process that is closer to ECL is one that involves electron-hole recombination in the solid following injection of carriers (sometimes called *injection electroluminescence*). This is the process

responsible for light emission at suitable p-n junctions in light-emitting diodes (LEDs), for example of GaAs.

1.1
A brief history of ECL

The beginning of ECL experiments was in the middle 1960s years. The main problem in most experiments was the use of aqueous or partially aqueous solvents. This way the developing of organic electrochemistry was not possible. Water has the disadvantage of having a limited range of available potentials before it is oxidized to oxygen or reduced to hydrogen (i.e. it has a small *potential window*). The situation began to improve with the introduction of the use of aprotic solvents like acetonitrile (MeCN).[7] MeCN has a large potential window allowing difficult oxidations and reductions to be examined. Many organic compounds show reasonable solubility in MeCN and the solvent itself has negligible acid and base properties. A problem with the early studies with MeCN however, was that the solvent was often contaminated with small amounts of water (and sometimes oxygen), so that even with this solvent, electrogeneration of radical ions was not noticed.[8] However with the advent of electrochemical cells that could be used on vacuum lines or in glove boxes, with highly purified and degassed solvents and electrolytes, electrochemical experiments showed that reduction of many aromatic hydrocarbons led to rather stable radical anions and oxidations produced radical cations.[9] The application of electron spin resonance to study electrogenerated radical ions showed that they were the same as those prepared chemically and was also important in proving the ready production of these species at electrodes.[10]

A chronology of essential ECL experiments from the sixty to the ninety years is shown in the time line reported in fig.1 . In 1964 Hercules[11] used Pt electrodes in MeCN or DMF solutions and showed emission of light with a number of hydrocarbons, including anthracene, diphenyl-anthracene (DPA) and rubrene when the electrode potential was cycled at frequencies up to 10

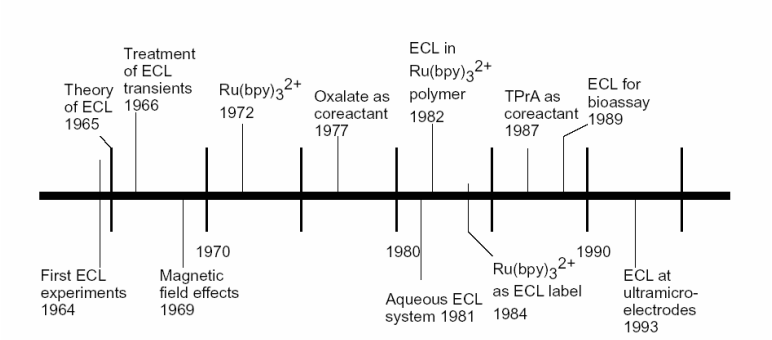

Figure 1: Time line showing the evolution of ECL experiments from 1960 to present days.

Hz. No detailed electrochemical or spectroscopic results were reported, with detection of the emitted light by eye. Approaches to a theoretical understanding of the ECL response, both in terms of the reason for excited state formation and for the shape of the electrochemical ECL transients, followed soon after the first experiments. The photoluminescence of $Ru(bpy)_3^{2+}$ was reported in 1959[12] and its spectroscopy was studied rather extensively in the late 60s.[13] The ECL of this species in MeCN solution was reported in 1972[14] and ascribed to the reaction sequence

$$\mathbf{Ru(bpy)_3^{2+} - e \rightarrow Ru(bpy)_3^{3+}} \qquad \textbf{(oxidation during anodic step)}$$

$$\mathbf{Ru(bpy)_3^{2+} + e \rightarrow Ru(bpy)_3^{+}} \qquad \textbf{(reduction during cathodic step)}$$

$$\mathbf{Ru(bpy)_3^{+} + Ru(bpy)_3^{3+} \rightarrow Ru(bpy)_3^{2+*} + Ru(bpy)_3^{2+}}$$

$$\mathbf{Ru(bpy)_3^{2+*} \rightarrow Ru(bpy)_3^{2+} + h\nu}$$

The discovery of ECL with the water soluble $Ru(bpy)_3^{2+}$ suggested that aqueous ECL was a possibility, especially since it was also known that $Ru(bpy)_3^{3+}$ was reasonably stable in aqueous solution. The problem however was that the potential window of water is rather small compared to that in aprotic solvents like MeCN. What was needed was a water soluble species

that could generate the reductant for reaction with $Ru(bpy)_3^{3+}$ by *oxidation* rather than by reduction. Such a species has become known as a *coreactant*.. The discovery that oxalate anion would behave as a coreactant via the reaction sequence:

$$\mathbf{C_2O_4^{2-} - e \rightarrow CO_2^- + CO_2}$$
$$\mathbf{Ru(bpy)_3^{2+} + CO_2^- \rightarrow Ru(bpy)_3^{2+*} + CO_2}$$

meant that ECL could be generated simply by oxidizing $Ru(bpy)_3^{2+}$ and oxalate in a mixture.[15] A more efficient coreactant for $Ru(bpy)_3^{2+}$, tri-n-propylamine (TPrA), at pHs near 7 was found a few years later.[16-17]

1.2
Pratical applications

Analytical Applications. The advent of aqueous ECL , and especially the discovery of coreactants made the ECL suitable for analysis . Since different coreactants, like oxalate and pyruvate would react with $Ru(bpy)_3^{3+}$ to produce emission. A different type of analytical application involves the use of $Ru(bpy)_3^{2+}$ or other ECL active emitter as a label , usually on a biologically interesting molecule like an antibody replacing the previously used radioactive or fluorescent labels. The sensitivity of $Ru(bpy)_3^{2+}$ ECL determinations is high, down to pM levels, and the linearity of response with concentration is good.[18] ECL has an advantage over fluorescent labels, since it does not require a light source and is free from effects of scattered light and fluorescent impurities in the sample. ECL has thus been used commercially for immunoassay and DNA analysis.[19-20] A more detailed overview of diagnostic applications of ECL will be presented in section 1.4.

Display and OLEDs. From the earliest days of ECL there was interest in using this phenomenon for lighting, displays and LED. Early research efforts did not lead to commercial devices, perhaps because the operating life was not adequate as well as the difficulty at the time with encapsulation of the emitting material. However ECL was also observed in polymer films, such as a film of polymerized $Ru(bpy)_3^{2+}$ and poly(vinyl-9,10-diphenylanthracene.[21-22] Polymeric and solid state light emitting electrochemical cells (LECs) have been investigated in recent years.[23]

Thin layers. When a chemical reaction is performed using a self assembled monolayer or a Langmuir-Blodgett film as substrate to confirm the occurrency of occurrence by NMR or Fluorescence is often not straightforward. If the segment added in the chemical reaction contains an ECL tag is possible to detect the presence of a single layer of molecules deposited in conductive substrates. Using ECL tags the study of structure change on surfactant molecules is also possible following the modification of emission spectra. This particular aspect will be illustrated in chapter V.

1.3
Preliminary concepts of electrochemistry and photochemistry

In the following paragraph some basic concept of electrochemistry and photo chemistry will be introduced .[24]

1.3.1
Electrochemistry

Electrode potential and cyclic voltammetry(CV).

The standard potentials E°(A, A^-) and E° (D, D^-) for the electrodic reactions

$\mathbf{A + e \leftrightarrow A^-}$

$\mathbf{D^+ + e \leftrightarrow D}$

measured respect to reference electrode, based on the pair O/R

O + e ↔ R

represents the ΔG^0 of the combined reactions

A + R ↔ A$^-$ + O

D$^+$ + R ↔ D + O

When electrochemical experiments are performed in water the formal reference electrode is the H/H_2 couple when all other reactants have activity equal to unit. For practical purposes Ag/AgCl or saturated calomel electrode (SCE) are normally used.[24] In organic solvents as DMF and MeCN the couple that is more often used is the Ferrocene/Ferrocenium (Fc/Fc^+). Under the assumption that its potential remains constant a quasi reference silver wire electrode can be used when measuring the difference between two redox processes. The potential of a couple (A/A- or D/D-) is the energy necessary at equilibrium to remove an electron from A^- (D^-) or to add an electron to A (D). In the fig. 2 a molecular orbital (MO) scheme is presented. This energy is that needed to place an electron in the lowest unoccupied MO (LUMO) of A or to remove an electron to the highest occupied MO (HOMO) of D.

The Fermi level is the higher energetic level occupied in the conductive band of a metal at 0 K. The energy of this level depends on the material of working electrode and is proportional to the density of the metal free electrons.

The overall ECL electrochemical reaction is

D$^+$ + A$^-$ ↔ D + A

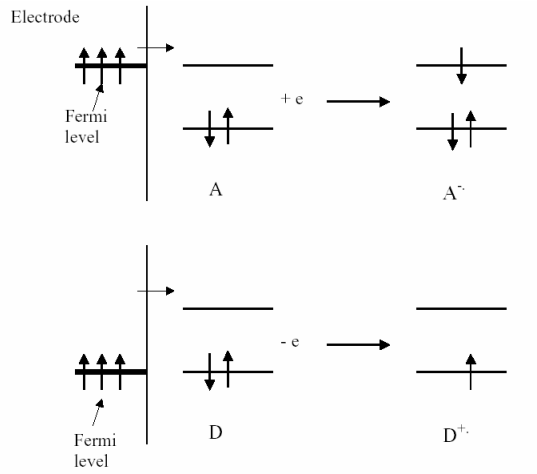

Figure 2: Molecular orbital scheme showing electronic states involved in electrochemical processes.

the relative free energy is

$$\Delta G_r^\circ = -FE_r^\circ$$

where

$E_r^\circ = E^\circ(D^+,D) - E^\circ(A,A^-)$ and **F** is the Faraday's constant

The entropy of reaction is function of the derivative respect to temperature (T) of the reaction potential (E_r°) according to the following expression

$$\Delta S^0_r = FT(\partial E^\circ_r/\partial T)_P$$

In the case of ECL reactions ΔG_r° is in the range of 2-3 eV whereas $T\Delta S^0_r$ is lower of 0.1 eV.

Prior to ECL experiments, electrochemical characterization of the system and CV is typically performed. A current-potential curve (*i vs. E*) of the compound object of study is obtained in appropriate solvent and electrolyte with an inert electrode (Pt) swepting the potential with time (scan rate *v).* The voltammetric curve shows the typical peaks of reduction and oxydation of the system. In nerstian systems where the electron transfer reactions at electrode interface are fast and the positive and negative charged radical produced are stable, the analysis of oxydation and reduction waves can be used to calculate E° values. Considering a typical case in which the processes are mono electronic ($n = 1$) and the reactant and products have the same diffusion coefficient (D) one can write

$$E^0 = E_p \pm 1.109(RF/T) = E_p \pm 28.5\ mV \text{ at } 25\ ^{\circ}C$$

Where E_p is the potential of the peak and positive sign is for reduction and the negative for oxidation. The diffusion coefficient D [cm^2/s] can be practically calculated from peak current i_p when the concentration of the species, C^* [mol/L] is known using the following expression:

$$i_p = (2.69 \times 10^5) A D C^* v^{1/2}$$

where A is the area of electrode [cm^2] and v is the scan rate [V/s]. The stability of the electrogenerated species can be estimated analizing voltammetric waves. The existence of waves on reversal scan is an evidence that the produced species e.g. D^+, formed by oxidation of D, is reduced back on reverse scan. If instead D^+ is instable for the time necessary to cross the wave at the present scan rate the reverse peak will

be absent (or i_p lower) and the anodic wave will be shifted to less positive potentials.

Chronoamperometry and potential impulses

In ECL studies of new molecules the potential is often stepped (rather than swept) between oxidation and reduction processes. A first potential step from a potential where no reactivity is present to one well beyond the E_p where reduction or oxydation occurs is accompanied with a current i that decays with time (t) according to the Cottrell model:

$$I = FAC^*D^{1/2}/(\pi t)^{1/2}$$

The decay of current intensity i in function of $t^{-1/2}$ represents a growing of diffusion layer of formed product. The use of fast potential impulses normally produces higher time integrated light intensity with respect to that obtained using fast cyclic voltammetry as switching potential. On the other hand the use of fast potential impulses require a good reversibility of the included electrochemical processes or ECL emission could fast disappear.

1.3.2
Photochemistry and spectroscopy

Here is a brief introduction of some basics principles needed to understand luminescent phenomena of importance in ECL.[25-26]

Energy Levels

Energy states available to a molecule can be usually represented by an energy level diagram like the one shown in fig.3. The scheme includes electronic and vibrational levels. The molecular orbital HOMO and LUMO of the molecule can be assigned to specific electronic energy levels. Shown in this diagram is

the lowest, singlet, electronic state of the molecule, S_0 where electrons are paired in the same HOMO. The multiplicity of a state can be calculated using the simple expression 2s + 1, where s is the spin quantum number. In the case of paired electrons the multiplicity is 1. The first excited state, S_1 and T_1 (with 2 unpaired electrons) are also shown into the diagram. Higher energy levels as S_2 and T_2 are usually not of importance in ECL emissions. The vibrational levels for each of the states are numbered v= 0, 1, 2… It is of interest to consider the lifetime of a molecule in different states. The lifetime of an excited vibrational state in solution is in the ps regime, since energy can be easily transferred to the solvent. This way, in normal conditions excited vibrational states rapidly decay to the fundamental v = 0 vibration level (see for example in fig. 2 the S_1 levels). The radiative lifetime of the excited singlet state, S_1 for organic compounds is tipically in the scale of ns and triplet states are much longer (from ms to s regime) since radiational transitions to the ground state are "forbidden". In the case of metal chelates the lifetime of triplet state is much shorter because the presence of an heavy nucleus promote spin-orbit coupling. For example triplet charge transfer excited state of $Ru(bpy)_3^{2+}$ emits with lifetime lower than 1 μs.

Photoluminescence

Light emission results from transitions between excited and ground states. Absorption causes transitions from S_0 to various vibrational levels in S_1 giving the observed absorption band. Emission occurs from the v=0 state of S_1 to different vibration states of S_0 resulting in the emission band. An example of absorbance spectra and its corresponding emission is reported in fig.4. The wavelengths of emission band are higher (or red shifted) compared to absorption. (fig.4)

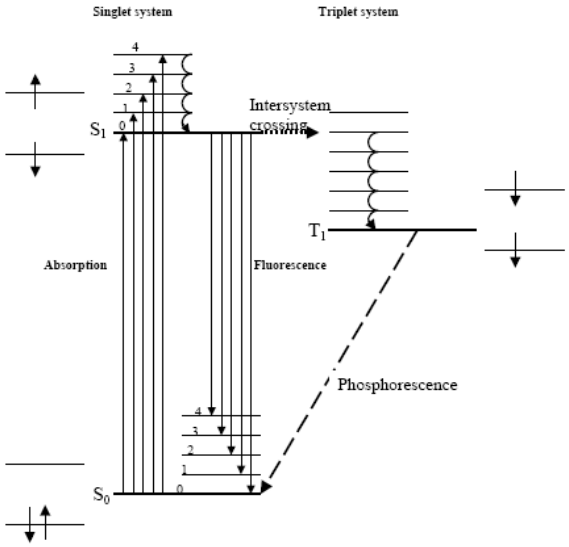

Figure 3: Energy levels and molecular orbitals involved in the absorption and emission of radiation.

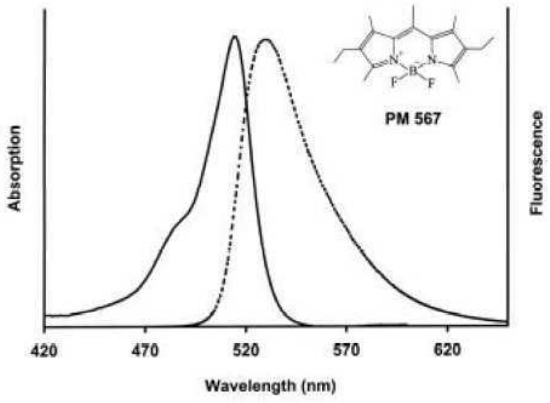

Figure 4: A typical example[1] of specular absorption (solid line) and emission (dashed line) spectra.

There is a difference in energy between the absorption and emission bands for the transition between the v=0 states, the so-called 0,0-band. This difference,

known as the Stoke's shift, is the result of the optical transitions being essentially instantaneous (~10-15 s), so that there are no structural or solvation changes occurring during the transition. Thus during excitation,
the transition is from a ground state structure to an excited state structure of the same configuration. However the excited state, because of the different electronic configuration, can undergo some structural changes, for example, reorientation of solvent, to relax to a lower energy state. Emission from this state then occurs to a ground state that has the configuration of the excited state (which then relaxes to the original ground state). The energy of the singlet transition can be estimated from the spectra, for example as the average of the energies of the 0,0-bands for excitation and emission, if they are discernable, or sometimes from the wavelength, λ , where the excitation and emission bands cross, by the formula:

$$E_S \text{ (in eV)} = 1239.81/\lambda \text{ (in nm)}$$

Emission from the triplet state results in phosphorescence. This is rarely seen for organic molecules in solution, because these molecules are readily quenched by solution species before emission. Oxygen, because it is a triplet molecule, is an effective triplet quencher.
Emission from triplet states is found however with metal chelates, which have much shorter emission lifetimes than organic molecules. The triplet states can produce excited singlets, a type of energy up-conversion, by triplet-triplet annihilation (TTA). This is observed spectroscopically as delayed fluorescence. Note that in spectroscopy, some singlet states, for example 9,10-diphenylanthracene, have close to a 100% efficiency for radiation to the ground state, with very few triplets,[27] formed by intersystem crossing. In this case delayed fluorescence is not observed. However with such systems, triplets can be formed in ECL by adjustment of the energetics of the annihilation reaction, where TTA is then observed. Thus states are sometimes accessible in ECL that are not available spectroscopically.

Quenching

An excited states can be quenched by another molecule (a quencher, Q) to produce the ground state, i.e.

$$D^* + Q \rightarrow D + Q^*$$

where Q* can often decay to the ground state without emission. Quenching can occur by either energy transfer or electron transfer. Energy transfer, sometimes called Förster transfer, is favored by the electronic energy of D* being larger than that of Q*, and a large overlap of the emission band of D* with the absorption band of Q. The energy transfer occurs by a direct electrodynamic interaction between D* and Q and occurs at short distances between the reactants.[28]

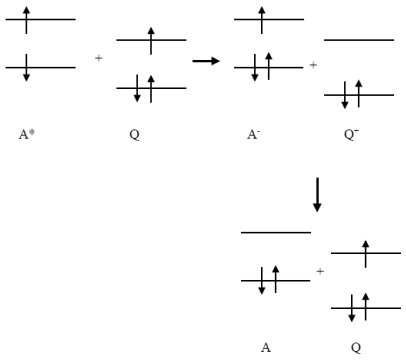

Figure 5. Scheme of the mechanism of electron transfer quenching

Electron transfer quenching (fig.5) occurs because the excited state is easier to oxidize and easier to reduce than the corresponding ground state of the same molecule, by an amount essentially equal to the excitation energy of the molecule. The kinetics of a quenching reaction, is governed by the Stern-Volmer equation:

$$\varphi^0/\varphi - 1 = R^0/R - 1 = k_Q\tau_0[Q]$$

where φ^0 and φ are the fluorescence efficiencies and R^0 and R are the fluorescence responses, in the absence and presence of a quencher at concentration [Q], respectively, k_Q is the rate constant for quenching, and τ_0 is the lifetime of the excited state in the absence of a quencher. Metal electrodes can similarly act as quenchers by either energy transfer or electron transfer processes. The energy transfer mode is analogous to Förster transfer, and results from coupling of the oscillating field of the excited dipole to the surface plasmon modes of the metal.[29,30] Quenching by electron transfer follows the same arguments as given above.[31]

Excimers and exciplexes

An *excimer* (originally short for excited dimer) is a short-lived dimeric or heterodimeric molecule formed from two species, at least one of which is in an electronic excited state. Excimers are often diatomic and are formed between two atoms or molecules that would not bond if both were in the ground state. The lifetime of an excimer is very short, on the order of nanoseconds. The wavelength of an excimer's emission is longer than that of the excited monomer's emission, because the excimer is stabilized compared to the excited monomer. Because excimer formation is dependent on a bimolecular interaction, it is promoted by high monomer density. Low-concentration conditions produce excited monomers that decay to the ground state before they interact with an unexcited monomer to form an excimer.

The term excimer is, strictly speaking, limited to cases in which a true dimer is formed; that is, both components of the dimer are the same molecule or atom. The term *exciplex* refers to the heterodimeric case; however, common usage expands excimer to cover this situation.

1.4
Fundamental requirements and conditions for ECL

The essential requirements for efficient annihilation ECL where radical cation and radical anion of the same specie disappear producing excited state are:

(1) stable radical cation and anion of the precursor molecule in the electrolyte of interest ;
(2) good photoluminescence efficiency of excited state;
(3) sufficient energy in the electron transfer reaction to produce the excited state. When these criteria are met, ECL will usually be observed, although the efficiency often depends upon kinetics of the electron transfer reaction.

1.4.1
Energetic Requirements.

The produced excited states depends on the energy of electron transfer reaction. Since the excitation energy is fundamentally closest to a thermodynamic internal energy, the usual energy criterion for production of an excited singlet state of energy E_S (in eV) is:

$$-\Delta H_0 = E^0(D^{+\cdot},D) - E^0(A,A^{-\cdot}) - T\Delta S\ 0 > E_S$$

The value of TΔS 0 is usually estimated as 0.1 (±0.1) eV.[32-38] Frequently the criterion is given based on CV peak potentials (in V) at T = 298 K in the following form:

$$E_p(D^{+\cdot},D) - E_p(A,A^{-\cdot}) - 0.16 > E_S$$

Reactions that satisfy this criterion are usually called “energy sufficient”, and is said to follow the S-route.[11]

When $-\Delta H^0 > E_T$, the reaction energy can produce the triplet and reactions are said to follow the T-route. Sometimes, both excited singlets and triplets are formed in significant amounts in the annihilation and reaction is said to follow the ST-route. If excimers or exciplexes are produced the reaction it is said to proceed by the E-route.

1.4.2
Coreactants

Energetics of ECL reactions that occur in presence of coreactants is more difficult, because the energies of the reactive intermediates may not be known. Fundamental principles are the same as with annihilation reactions as concerns the energy of the final electron transfer step. A number of coreactants for ECL have been tested. For example, tri-n-propylamine (TPA) has been used in the oxidative ECL of $Ru(bpy)_3^{2+}$.[16,17] The mechanism involves ultimate generation of a radical that acts as the reductant with the electrogenerated $Ru(bpy)_3^{2+}$. Mechanism can be summarized as follows:

$$\mathbf{Ru(bpy)_3^{2+} - e^- \rightarrow Ru(bpy)_3^{3+}}$$

$$\mathbf{Pr_2NCH_2CH_2CH_3 - e^- \rightarrow Pr_2NCH_2CH_2CH_3^{+\cdot}}$$

$$\mathbf{Pr_2NCH_2CH_2CH_3^{+\cdot} \rightarrow Pr_2NC^{\bullet}HCH_2CH_3 + H^+}$$

$$\mathbf{Ru(bpy)_3^{3+} + Pr_2NC^{\bullet}HCH_2CH_3 \rightarrow Ru(bpy)_3^{2+*} + Pr_2NC^{+}H_2CH_2CH_3}$$

The oxidation of TPA can occur by reaction directly at the electrode or by reaction with $Ru(bpy)_3^{3+}$. Another class of coreactants has been tested and successfully used: molecules that form strong oxidants upon reduction .
The most active reductive coreactant has been found to be the $S_2O_8^{2-}$ which reduction proceeds as follows:

$$S_2O_8^{2-} + e^- \rightarrow SO_4^{2-} + SO_4^{\cdot-}$$

Where $SO_4^{\cdot-}$ is a strong oxidant that reacting with $Ru(bpy)_3^+$ or anion radicals produces the excited state.[39]

1.4.3
Monolayers, films and nanoparticles

In addition to studies of solution phase species, ECL has also been observed in monolayers on electrode surfaces and in various types of films.

For example a monolayer of a surfactant derivative of $Ru(bpy)_3^{2+}$ (i.e. containing a C18 chain linked through an amide link to a bipyridine) on Pt, Au, or ITO electrodes showed ECL when oxidized in the presence of oxalate as a coreactant.[40] Similarly, a film of a $Ru(bpy)_3^{2+}$-surfactant can be formed at the air/water interface and contacted by the horizontal touch method with an ITO electrode and the ECL was observed .[41,42] ECL active layers on the surface of beads or electrodes forms the basis of the ECL based immunoassays. Films of polymers or solids can also show ECL and are the basis of light-emitting devices. Recently $Ru(bpy)_3^{2+}$ and $Os(bpy)_3^{2+}$ doped silica nanoparticles have been successfully synthesised using a microemulsion.[43] ECL Emission was detected in suspension and from the same nanoparticles deposited at electrode surface.[44] The use of this particles as ECL label for DNA and other biologically relevant molecules is actually an interesting direction of investigation.

1.5
ECL as a diagnostic tool

1.5.1
ECL as an analytical tool

Electrochemiluminescence has been successfully applied in clinical laboratories of analysis and industry. At the beginnings interest arise because

of possibility to detect very low analyte concentrations. During his development the technique revealed other advantages as the absence of matrix effects and flexibility; this way diagnostic analytical applications grew of importance. ECL allows the combination of the specificity and sensitivity of a spectroscopic analysis with electrochemistry (EC) . Combining the two techniques It's possible the generation of excited states without the need of a light source that is substituted by an electric stimulus. The absence of scattered light and emission from impurities makes the sensitivity improved. Another advantage of electrochemical excitation is the possibility to accurately control spatially the emission trough working electrode position. Analytical methods based on ECL allow today the detection of biomolecules in a wide range of molecular weights. Trough ECL the concentration or simply the presence of specific proteins and DNA sequences can be carefully monitored. Another line of application has been the tracking of enzymes activity inside living cells. Last but not least feature of ECL is the low cost of instrumentation especially if compared with other techniques that can reach similar performances. The simplicity and high specificity of every ECL measurement is the key feature which lead the technique to the success in the field of clinical diagnosis, food analysis and new materials research.

1.5.2
Immunometric methods

The assay format more commonly used for bio-molecules tests at very low concentrations is the introduction of a traceable label in the analyte and the successive use of the specific signal of the marker for detection. With this approach the intensity of detected signal is proportional to analyte concentration. Classical labelling methodologies used in immunoassay are chemiluminescence (e.g. Fluorescein), fluorescence, the use of enzymes and radioactive isotopes. This approach has been successfully extended to electrochemiluminescent dyes. The majority of commercially available ECL based detection systems are based on the contemporary oxidation of

$Ru(bpy)_3^{2+}$ and trypropilammine in phosphate buffer solutions (PBS). This method has been found to be very effective in pH 7 buffered acqueous solution even in presence of air.

In general immunometric methods can be classified in two fundamental classes: homogeneous and heterogeneous. In heterogeneous methods detection can not discriminate if the label is attacked or not to the analyte. In this case is necessary to separate free label before measurement can be performed. Normally separation is made by immobilizing one of the component in a solid substrate. Homogeneous methods, on the other hand, can distinguish between the free and bond tag. With those methods no separation is necessary and test can be performed directly in solution. Methodologies that use solid substrate for separation evidenced however a great increase of sensitivity and selectivity with respect to homogeneous ones. In this case the driving force is the high affinity between two biomolecules that causes very specific interactions. As depicted in fig. 6 a probe molecule is immobilized in working electrode surface.[45] When the target marked molecules in solution are captured by the probe ECL signal will be proportional to the number of coupling sites.

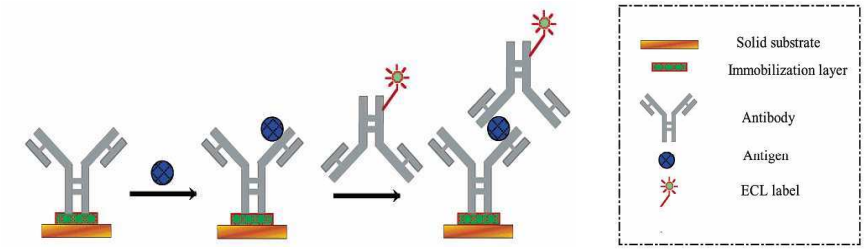

Figure 6. Typical assay format of immunological heterogeneous methods based on ECL.[45]

Immunometric methods can be also divided in competitive and not competitive. In non competitive methods all analyte is captured from antibody and the signal is directly proportional to his concentration (fig. 7 B). in competitive methods the signal is modulated by the presence of analyte which normally has an higher affinity with respect to labelled target. In this case the signal decreases when concentration of analyte increases (fig. 7 A).

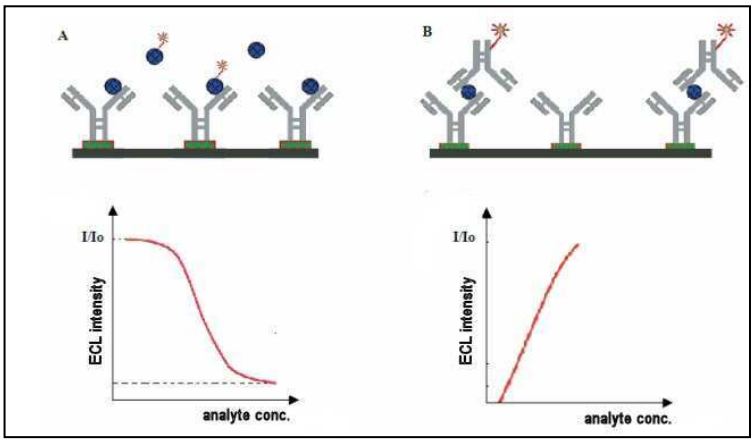

Figure7. Dependence of signal on analyte concentration for competitive heterogeneous method (A) and not competitive heterogeneous method (B).

The use of different types of specific interactions lead to different assay formats. (fig. 8) An example is the sandwich interaction antigen/antibody/antigen (fig. 8 B).

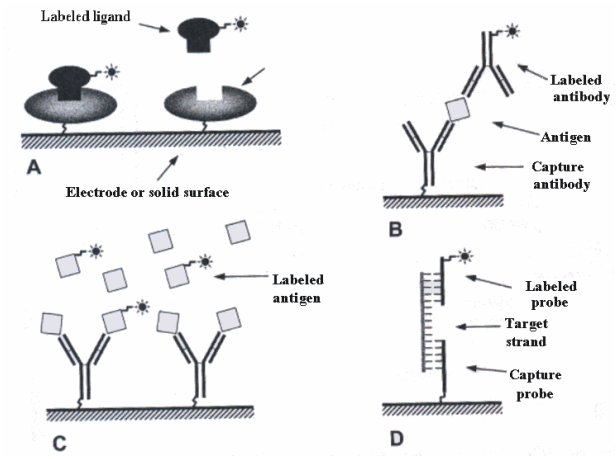

Figure 8. Commonly used assay formats for ECL based genomics and proteomics. a) Receptor – ligand assay; b) "Sandwich" immunoassay; c) Competition assay; d) Capture of a target oligonucleotyde using two partially complementary capture and labelled strands.

This case is an heterogeneous non competitive method in which the labelled specie in solution is an antibody specific for antigenic analyte. A similar technique is also used in genomics. Nucleic acids can be detected using a “sandwich” hybridization method by a labelled probe strand and another partially complementary immobilized probe. Each probe is complementary to analyte in a different sequence. (fig 8 D) . The immolization of the probe on solid substrate can be obtained by different techniques, (i. e. by the use of thyolate olygonucleotides) . First commercial instrument which used ECL as detection system was in 1992 “ORIGEN Analyzer” (fig. 9) by IGEN inc. In this instrument the solid phase was constituted of labelled magnetic beads.

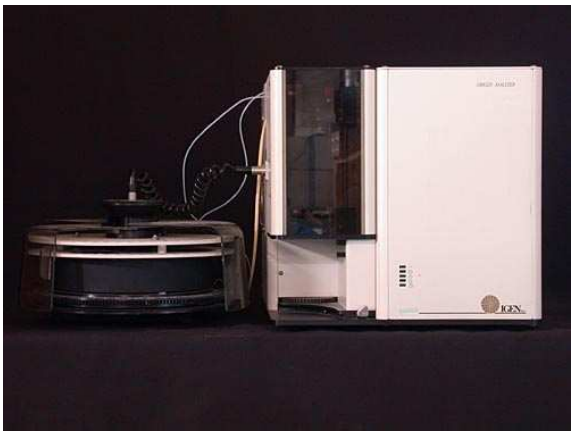

Figure 9. “ORIGEN” Analyzer (1992)

General setup is summarized in fig. 10. The hearth of the instrument is the flow cell which is filled by a peristaltic pump that charges in appropriate sequence magnetic beads, analyte and reagents. Prior to measurement magnetic beads are attracted in front of working electrode surface by a magnet (fig. 11) . At this point the coreactant tripropylammine is introduced and electrical stimulus is applied. The emitted light is detected by a photomultiplier (PMT) positioned in front of working electrode. After each

experiment cell is washed by a NaOH 3 M acqueous solution introduced by the same peristaltic pump.

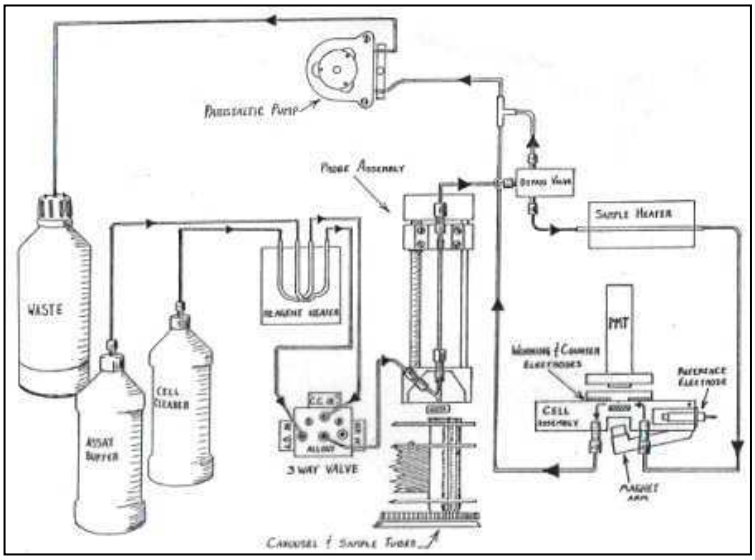

Figure 10. Scheme of ORIGEN ECL analyzer

The use of ECL based homogeneous methods has been found to be of scarce practical interest. The main problem encountered in this approach is the ECL intensity drift that follows aggregation of antigen with antibody most probably

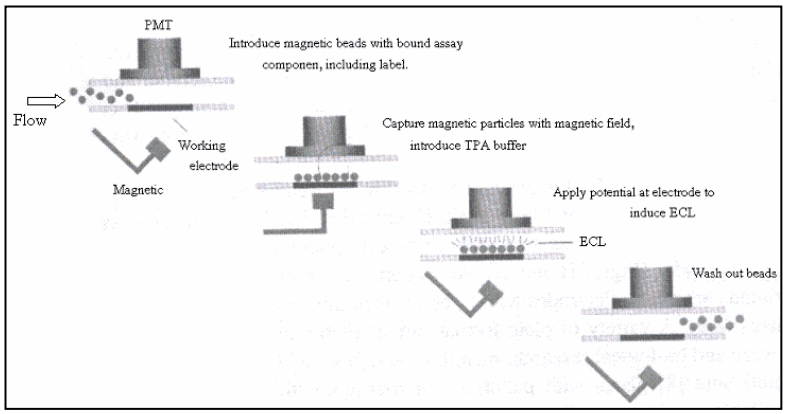

Figure 11. Work cycle of ECL analytical cell with the use of magnetic beads.

caused by big decrease of diffusion coefficient caused by the formation of the high molecular weight aggregate in solution.

1.5.3
Clinical applications

Most successful application of ECL techniques was in clinical area there is for monitoring biomolecules which presence is associated with genetic or viral diseases and dysfunctions of human metabolism. The main classes of investigated compounds are: hormones, enzymes, proteins, nucleic acids and antibodies. The assay can be qualitative or quantitative depending on the necessity to ensure the presence of the searched compound or to quantify his concentration. The tests are normally performed in biologic fluids such as: blood, serum, plasma, urines… As already stated above ECL is an high sensitivity and matrix independent technique; this features allow successful employment in clinical tests where well established techniques (e. g. fluorescence) encounter difficulties. The number of ECL based clinical tests is increasing each day. A number of ECL based clinical tests have been recently summarized in a review;[46] the majority of the methods employs the N-tripropylammine as coreactant in acqueous buffer. For example ECL detection can be used in cancer diagnosis, in some cases the disease can be recognized at the early stages increasing the percentage of success of the therapy. Another interesting example is the quantification of thyroidal hormones in blood useful tool to track important dysfunctions. Although ECL has found many interesting diagnostic applications the most important remains genomics. DNA (deoxyribonucleic acid) is essentially an organic polymer which monomers are the single nucleotides. Each nucleotide is formed by a molecule of sugar (deoxyribose), a phosphate group and a base (cytosine, guanine, adenine or thymine) and is connected with many others to form strands. The order of bases in a single strand is called primary structure. The secondary structure is known as double helix where two separate strands are coupled

through base pairs by hydrogen bonds (fig. 12) DNA can be found in the nucleus of eukaryotic and prokaryotic cells inside mitochondria and viruses. DNA is the place where genetic information is stored. Inside the cell each protein is synthesized according to the sequence of the base pairs in a specific portion of DNA. When a base pairs sequence or a nucleotide is modified the consequence is most probably a disease. The cancer is unfortunately one of the possible consequences of DNA mutations. This consideration reveals the importance of a sensitive method to detect flaws in DNA structure. To recognize specific DNA sequences synthetic oligonucleotides are used as probes. Only if the target nucleic acid strand is complementary to the probe they will combine together to form double helix structure (hybridization). If at this point the target oligonucleotide is labelled with an ECL active molecule as $Ru(bpy)_3^{2+}$ the detection of light is a confirmation of the presence of the searched sequence in the sample. The necessity of DNA mapping and analysis requires normally that many different sequences need to be searched for. This aspect justifies the great interest for LAB ON CHIP devices; in this miniaturized laboratories many analytes can be quickly detected with great reproducibility.

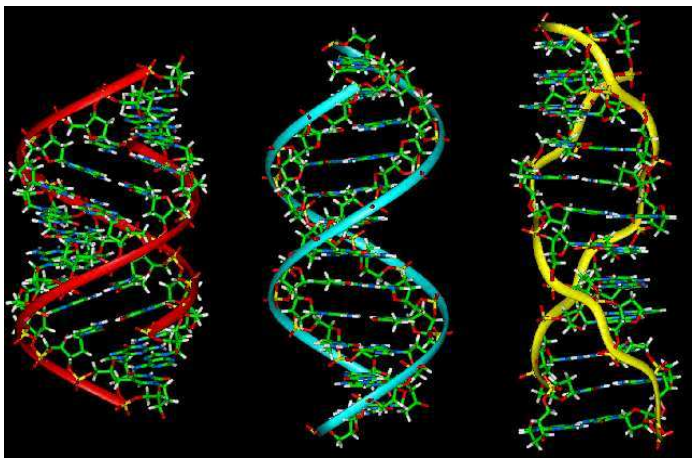

Figure 12. From left to right, three possible double helix structures of DNA: A, B and Z.

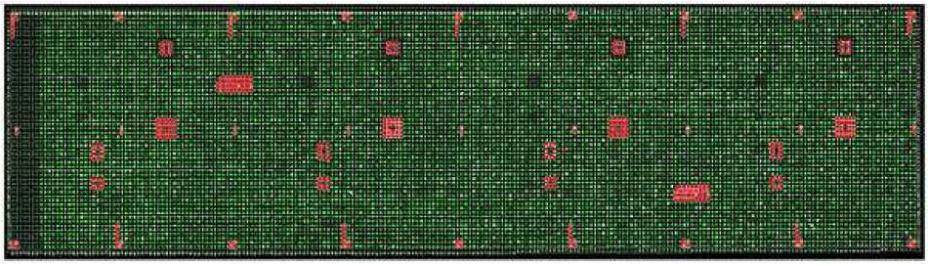

Figure 13. A lab on chip example: 12,000 different nucleotides sequences are detected in a single experiment.

This multi sample microchips are intended to replace actual DNA analysis techniques that require slow and sophisticated procedures in combination to very expensive instruments. An example of an actual LAB ON CHIP commercial system is shown in fig. 13. This microchips arrays can detect up to 12,000 different nucleotides in a single experiment. There is not still an ECL based LAB on CHIP similar to this but considering that the detection signal is an electrochemical current the extension will probably follow briefly with the possibility of greatly improve sensitivity. The advantages of LAB ON CHIP use are also automation, standardization and lower probability of error. Some examples of existing ECL methods based on DNA sequence analysis are those for HIV and A and B hepatitis recognition.[1,46] With this scope ultra sensitive methodologies have been realized [47]

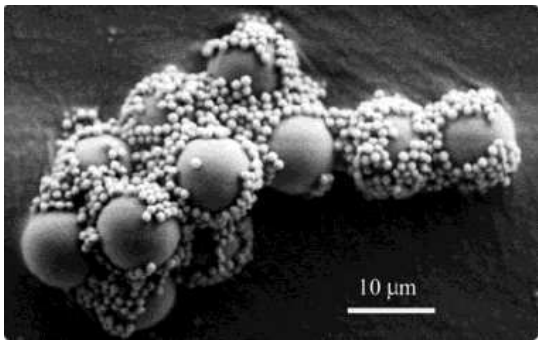

Figure 14. SEM image obtained after hybridization between DNA-MB and DNA-PSB/ $Ru(bpy)_3^{2+}$. Ref. 47

using Polystyrene Microspheres (PSB) as ECL label carrier (fig. 14). DNA probe (p-DNA) single strand is bound to Magnetic beads (MB) whereas target DNA (t-DNA) , labelled with $Ru(bpy)_3^{2+}$ is bound to PSB. Using PSB for each strand of t-DNA bound to the bead are present $7.9x10^9$ molecules of label. This causes a great increase of sensitivity that is close to 1fM in t-DNA. Figure 15 depicts previously described approach. The complementary strands will be magnetically separated after hybridization and formation of p-DNA-MB - t-DNA-PSB/ $Ru(bpy)_3^{2+}$ complex. The final step will be dissolution in acetonitrile of PSB. The $Ru(bpy)_3^{2+}$ is released in solution from the complex and ECL emission generated by oxidation in presence of N-trypropylammine. The intensity of the signal is proportional to t-DNA concentration with ultra high sensitivity.

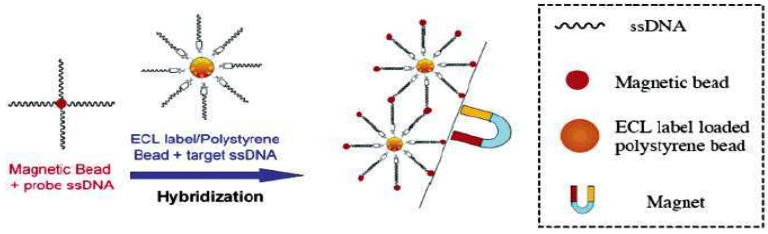

Figure 15. Hybridization scheme of DNA using polystyrene beads as ECL carrier and magnetic beads for p-DNA-MB ↔ t-DNA-PSB/ $Ru(bpy)_3^{2+}$ complex separation in flow cell. Ref. 47

1.6

ECL new materials: the philosophy of this thesis.

A fundamental topic in ECL research is the developing of new molecules and materials that show high quantum efficiency and red or blue shift with respect to $Ru(bpy)_3^{2+}$. Reliability to modification for using as label in biologically relevant molecules or to prepare light emitting solid devices are other suitable features . Fundamental electrochemical, photophysical and ECL properties of many new materials have been carefully studied. The word material has been translated in different ways: molecule of the emitter, aggregation state of the emitter, immobilization state, material of the electrodes… This way ECL characterization has been performed in different conditions depending on the

nature of the material and the scope of the measurement. Accordingly ECL has been obtained from thin solid films and functionalized chips. Together with basic qualitative studies quantitative studies have been performed to check the effect on ECL of interaction with DNA or protonation of the dye.

The two research visits in A. J. Bard group at university of Texas made me to understand the many possibilities of ECL technique. When I was back in Bologna I wanted to make possible the continuation of this very promising and interesting investigations. For this reason one of the priorities was also the developing of an instrument for ECL measurements. The machine was intended for characterization of whatever class of new materials. What We obtained is a flexible and modular instrument that I hope will be useful to find the bright side of each new material.

References

[1] A. J. Bard, *Electrogenerated chemiluminescence*, Marcel Dekker, New York (2004)

[2] V. Vojir, *Coll. Czech. Chem. Commun.*, 19, 862 (1954).

[3] T. Kuwana, B. Epstein, E. T. Seo, *J. Phys. Chem.*, 67, 2243 (1963)

[4] A. J. Bard, K. S. V. Santhanam, S. A. Cruser, L. R. Faulkner, *Fluorescence*, Marcel Dekker, New York, (1967)

[5] A. Hickling, M. D. Ingram, *Trans. Faraday Soc*., 60, 783 (1964).

[6] Henry F. Ivey, *Electroluminescence and Related Effects*, Academic Press, New York, 1963.

[7] (a) I. M. Kolthoff, J. F. Coetzee, *J. Am. Chem. Soc*., 79, 870 (1957); (b) A. I. Popov, D. H. Geske, *J. Am. Chem. Soc*., 80, 1340 (1958).

[8] H. Lund, *Acta Chem. Scand.* 11, 1323 (1957).

[9] For reviews of this early work, see, e.g. (a) A. J. Bard, K. S. V. Santhanam, J. T.Maloy, J. Phelps, L. O. Wheeler, *Disc. Faraday Soc.* 45, 167 (1968); (b) M. E. Peover, *Electroanalytical Chemistry*, Marcel Dekker, New York, 1967, Vol. 2, p. 1; (c) R. N. Adams, *Electrochemistry at Solid Electrodes*, Marcel Dekker, New York, 1969, p. 309.

[10] (a) D. H. Geske, A. H. Maki, *J. Am. Chem. Soc*., 82, 2671 (1960); (b) L. O. Wheeler, K. S. V. Santhanam and A. J. Bard, "Electron Spin Resonance Spectra of 9-Phenylanthracene and 9,10-Diphenylanthracene Anion Radicals," *J. Phys. Chem.*, 71, 2223 (1967).

[11] D. M. Hercules, *Science*, 145, 808 (1964).

[12] J. P. Paris, W. W. Brandt, *J. Am. Chem. Soc*. 81, 5001 (1959).

[13] G. A. Crosby, *Acct. Chem. Res.* 8, 231 (1975).

[14] N. E. Tokel, A. J. Bard, *J. Am. Chem. Soc*. 94, 2862 (1972).

[15] M. Chang, T. Saji, A. J. Bard, *J. Am. Chem. Soc*. 99, 5399 (1977).

[16] J. B. Noffsinger, N. D. Danielson, *Anal. Chem.* 59, 865 (1987).

[17] J. K. Leland, M. J. Powell, *J. Electrochem. Soc.* 137, 3127 (1990).

[18] D. Ege, W. G. Becker, A. J. Bard, *Anal. Chem.* 56, 2413 (1984).

[19] A. J. Bard and G M. Whitesides. *U.S. Patent* No. 5,221,605.

[20] G F. Blackburn, H. P. Shah, J. H. Kenten, J. Leland, R. A. Kamin, J. Link, J. Peteran,M. J. Powell, A. Shah, D. B. Talley, S. K.. Tyuagi, E. Wilkins, T. G. Wu, R. J. Massey, *Clin. Chem.* 37, 1534 (1991).

[21] H. D. Abruña, A. J. Bard, *J. Am. Chem. Soc.* 104, 2641 (1982).

[22] F. R. Fan, A. Mau, A. J. Bard, *Chem. Phys. Lett.* 116, 400 (1985).

[23] B. J. Piersma,E. Gileadi, *Mod. Asp. Electrochem.*, 4, 47 (1966).

[24] A. J. Bard, L. R. Faulkner, *Electochemical Methods*, Wiley, New York, 2001

[25] C. A. Parker, *Photoluminescence of Solutions*, Elsevier, Amsterdam, 1968.

[26] J. B. Birks, *Photophysics of Aromatic Molecules*, Wiley-Interscience, New York, 1970.

[27] A. Zweig, *Advan. Photochem.*, 6, 425 (1968).

[28] C. A. Parker, *Photoluminescence of Solutions*, Elsevier, Amsterdam, 1968.

[29] H. Kuhn, *J. Chem. Phys*. 53, 101 (1970).

[30] R. R. Chance, A. Prock, R. Silbey, *J. Chem. Phys.* 62, 2245 (1975).

[31] E. A. Chandross, R. E. Visco, *J. Phys Chem*.. 72, 378 (1968).

[32] L. R. Faulkner, A. J. Bard in *Electroanalytical Chemistry*, A. J. Bard, Ed., Marcel Dekker, N. Y., Vol. 10, p. 1.

[33] A. Weller, K. Zachariasse, *J. Chem. Phys.* 46, 4984 (1967).

[34] L. R. Faulkner, H. Tachikawa, A. J. Bard, *J. Am. Chem. Soc.* 94, 691 (1972).

[35] G. J. Hoytink, *Disc. Faraday Soc*. 45, 14 (1968).

[36] R. P. Van Duyne, C. N. Reilley, *Anal. Chem.* 44, 142 (1972).

[37] R. E. Visco, E. A. Chandross, *Electrochim. Acta*, 13, 1187 (1968).

[38] A. Pighin, *Can. J. Chem.* 51, 3467 (1973).

[39] H. S. White and A. J. Bard, *J. Am. Chem. Soc.* 104, 6891 (1982).

[40] X. Zhang and A. J. Bard, *J. Phys. Chem.* 92, 5566 (1988).

[41] C. J. Miller, P. McCord, and A. J. Bard, *Langmuir*, 7, 2781 (1991).

[42] C. J. Miller and A. J. Bard, *Anal. Chem.* 63, 1707 (1991).

[43] L. Wang, C.Yang, and W.Tan, *NanoLett.* 5, 37 (2005)

[44] L. Zhang and S. Dong, *Anal. Chem.*78,5119 (2006)

[45] W.Miao, A.J. Bard, *Anal Chem*. 75, 5825 (2003)

[46] M. M. Richter, *Chem. Rev.* 104, 3003 (2004)

[47] W.Miao, A.J. Bard, *Anal. Chem.* 76, 5379 (2004)

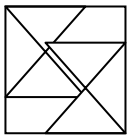

Chapter Two: ECL instrument design

"I Believe that innovative research is a mix of many failures and few successes"
R. Zare

In this chapter an overview of the techniques used to generate ECL will be presented. The design and setup of the new instrument assembled in Bologna is carefully described and compared with that of Bard's lab in university of Texas that has been taken as a model.

2.1
Switching potential and instruments for ECL

As stated in previous chapter light can be generated during appropriate electrochemical experiments.[1] Excited singlet or triplet states can be populated

in two different ways. The first is the classical annihilation method in which ECL active compound is alternatively oxidized and reduced. Second method involves addiction of an appropriate coreactant and generation of excited states is obtained by a single oxidation or reduction step. For light generation the fundamental parameters of the switching potential are substantially two: the maximum potential reached and function of variation respect to time. The more commonly used potential programs are linear swept and repeated continuous impulses which correspond to the classical techniques of respectively cyclic voltammetry (CV) and chronoamperometry (CHRONO). Assuming that radicalic species generated electrochemically will not decompose prior to generation of excited states the use of a fast scan rate (CV) or fast impulse (CHRONO) increasing electric current (see previous chapter for scan rate functions) will cause generation of an higher amount of excited species and thus higher light intensity. For the ease of detection a pretty high scan rate is normally sufficient to obtain the limit current and maximize the emission (i. e. 10 V/s scan rate in CV and 100 ms impulses in CHRONO). The use of scan rates higher than this values will not improve significantly the intensity of generated light and will increase the probability of decomposition reactions on ECL active compound. In some case however a small increase of scan rate steadily leads to decomposition reactions causing complete disappearance of ECL signal. In this cases ECL signal must be carefully optimized taking in account the kinetics of excited state formation and decomposition reactions.

An instrument intended for ECL measurements is substantially made of an *electrochemical* and *spectrometric* unit. *Electrochemical* unit must include electrochemical cell, electrodes, potentiostat, current amplifiers and wave function generator. *Spectrometric* section deals with measurement of emitted light and is basically made of a dark box, monochromator, optics, signal amplificators and photon detectors. According to this general scheme many different setups can be designed depending on information required about emission. The main parameters necessary prior to whatever instrument design

are fundamentally spectral range, sensitivity to light, response time and maximum accumulation time of the detector.
According to this general approach two distinct ECL instruments will be presented and analyzed in detail. Starting from ECL experimental setup of Bard's group in Austin (Texas, USA) taken as model, the new assembled instrument will be then introduced motivating addictions and modifications to reference scheme. Signal optimization, optics calibrations and preliminary tests will be also described to clarify system performances and possibilities.

2.2
ECL instrumental setup in A. J. Bard's group

In Austin lab (TX, USA) two different approaches to ECL measurements were possible. The use of three different detectors and setups allows the study of emission phenomena from different point of views. Experimental techniques employed can be called as:

- *ECL-PMT system*
- *ECL-CCD system*
- *ECL-PD system*

ECL-PMT system. (fig.1*)* An autolab (ECOCHEMIE, Holland) electrochemical station is used to supply appropriate switching voltage to an ECL cell placed inside dark box which also contains a photomultiplier tube (PMT, Hamamatsu R4220p) placed in front of emitting surface of working

electrode. A voltage of 750 V is supplied to the PMT by an external high voltage generator.

Figure 1. ECL-PMT setup in Austin (TX,USA).

With this setup is possible to measure integrated ECL intensity in the approximate range of 200-1000 nm (PMT detection interval). There is not discrimination between wavelengths; the fact that photo detector is placed a few centimetres from emitting surface makes this setup very sensitive so that very weak emissions can be detected. Because emission intensity can vary in many order of magnitude an accurate control of signal to noise ratio is necessary. In Austin lab the signal from PMT is filtered and amplified by a low noise multimeter and sent to autolab as second signal (the first is electrical current i). As ECL emission becomes weaker by selecting a high amplification range (i. e. amplification factor 1 nA/V) dark box insulation from light sources (even very weak) become vital to ensure experimental signal detection that can be easily masked by the noise.

The collection at the same time of electrical current intensity and ECL photocurrent signal makes possible to evidence the dependence of ECL intensity on applied potential (Cyclic voltammetry) and time (chronoamperometry). A plot that shows current i and photocurrent intensity registered simultaneously is called light/current curve. Typical examples of ECL light/current curves registered with this ECL-PMT system are reported in fig.2.

ECL-CCD system (fig.3)

A charge-coupled device (CCD) camera (Photometrics CH260) cooled below -100 °C with liquid nitrogen to shut down dark currents, interfaced to a personal computer is used to obtain ECL spectra. The camera is focused on the output of a grating spectrometer (Holographics, Inc.) that acting as a prism separates linearly emitted light in different wavelength .[2] As described above for *ECL-PMT* setup the necessary switching potential can be provided using AUTOLAB electrochemical station or an equivalent instrument.

This second setup allows collection of ECL emission spectra accumulating simultaneously all wavelengths. This method can successfully register relatively short lived emissions if intense enough. Due to the high sensitivity of the camera system must be operated in a darkroom with very low background light intensity to ensure the absence of extraneous photons appearing as “spikes” in collected spectra. The time of exposure necessary is inversely proportional to emission intensity and normally of about 4 minutes. In CCD camera raw data light intensity is expressed in arbitrary units (A. U.; the number of photons detected) versus pixel number (column number in CCD array) . Pixel number is converted in wavelength (nm) using a standard spectra. After sample measurement an Hg lamp is inserted in the same slit of electrochemical cell and spectra is accumulated for 50 ms. Four bright peaks of Hg lamp spectra are then used for calibration. (94, 115, 189 and 211 nm). A typical ECL spectra recorded with this system is shown in fig.4.

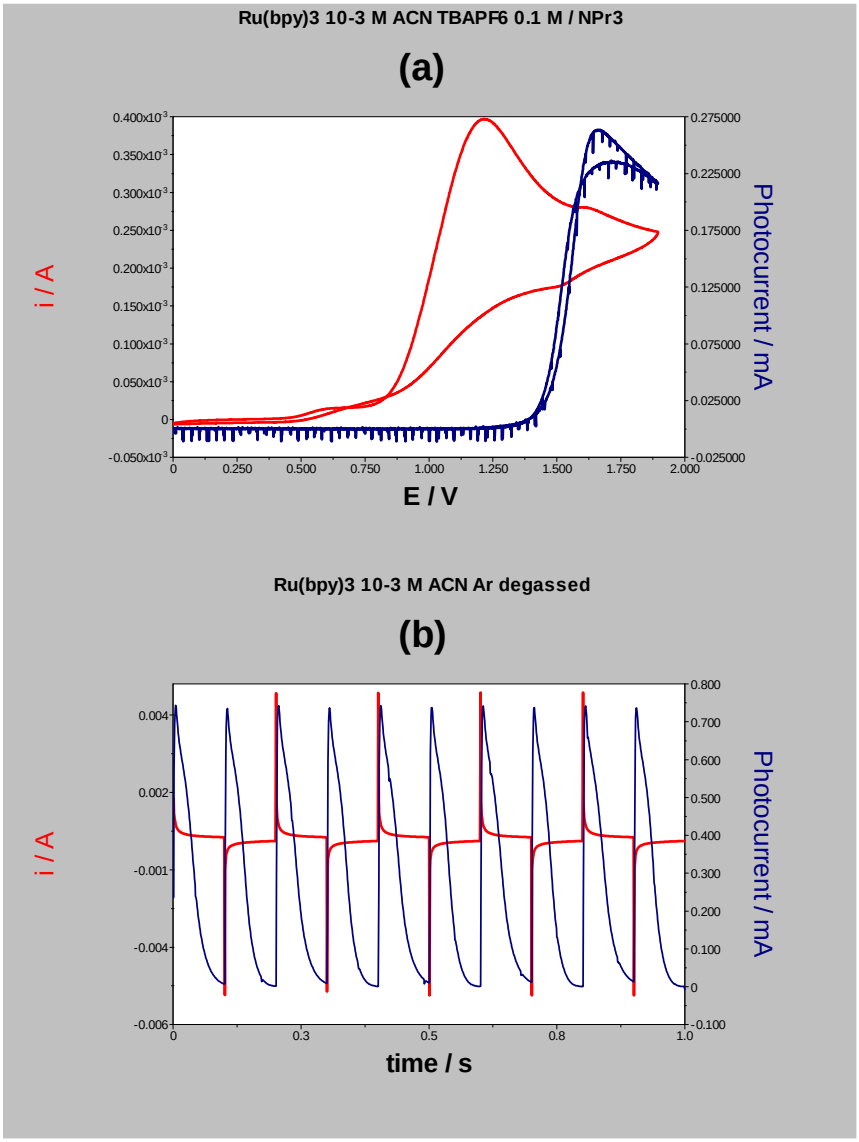

Figure 2. (a) Typical light\current ECL curve registered during cyclic voltammetry. Scan rate: 1 V/sec. Solvent: acetonitrile (MeCN or ACN). Active compound: $Ru(bpy)_3^{2+}$; Mechanism: oxidation in presence of NPr_3; (b) Light\current ECL curve obtained by chronoamperometry; Pulse width: 0.1 s; Solvent: Ar degassed MeCN; Compound: $Ru(bpy)_3^{2+}$ Mechanism: annihilation.

Figure 3. ECL-CCD setup in Austin (TX,USA).

Data collected with *ECL-CCD* and *ECL-PMT* provide complementary information for understanding the behaviour of active species. Normally the test with *ECL-PMT* is performed first because of higher sensitivity in order to optimize emission intensity (e. g. max. potential applied, scan rate, switching method). Cycling potential one can also realize if the emission is stable respect to time. If the maximum ECL intensity is in the order of μA of photocurrent is possible to register spectra by CCD camera. In the opposite case necessary CCD accumulation time becomes relatively high: about 30 minutes to get a low quality spectra. On the other hand the much more sensitive PMT can not detect emission wavelength changes and thus to identify produced excited states.

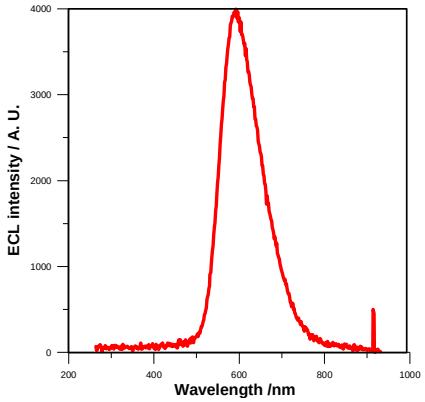

Figure 4. Typical ECL emission spectra registered by CCD camera. Pulse width: 0.1 s; Solvent: Ar degassed MeCN; Compound: $Ru(bpy)_3^{2+}$ Mechanism: annihilation. A "spike" is visible at about 920 nm.

ECL-PD system (fig.5)

This setup is fundamentally very close to *ECL-PMT* one.[3] Differences are due to necessity to perform ECL measurement in solid thin films (TL). As consequence because of the much higher light intensity (about 3 orders of magnitude in photocurrent scale) of organic light emitting solid devices (OLED) the use of photodiode (PD) instead of the much more sensitive PMT detector is necessary to prevent signal saturation. Another aspect, the necessary combination of correct electrical contacting and insulation from external light sources makes darkbox and sample holder change significantly. On the other hand light/current curves are obtained using AUTOLAB electrochemical station as described above *for ECL-PMT system*.

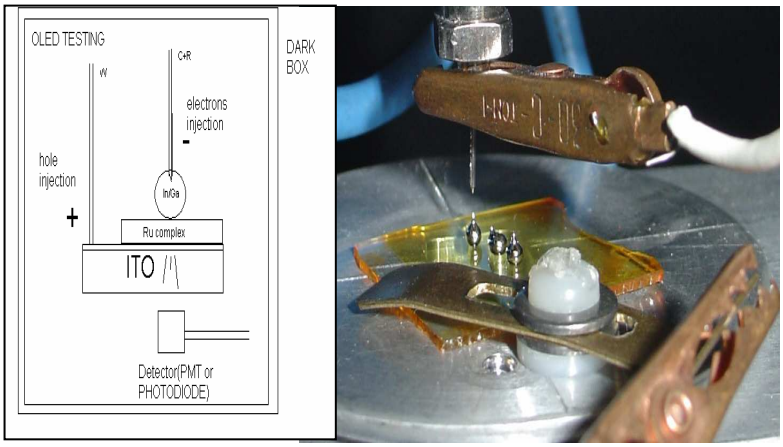

Figure 5. Scheme of *ECL-PD* experimental setup for ECL measurements from solid films.

The thin layer of ECL active compound is prepared on ITO glass (Delta Technologies, Ltd.) by spin coating from a MeCN solution (1-4% w/v of compound). A small drop of In/Ga eutectic (from Aldrich) over the active layer was used as counter electrode and was connected to the reference electrode lead. Positive charge is injected through the underlying ITO glass used as working electrode.

Electrodes, cell and sample preparation

The three electrodes, working (W), counter (C), and reference (ref) (fig.6) are polished with 0.05 μm alumina and then sonicated and thoroughly rinsed with Milli-Q water and acetone before each run. The quasi-reference electrode is a coiled silver wire. A platinum disk (approximate diameter 2 mm) is used as working electrode and a coiled Pt wire is used as an auxiliary electrode. The $E_{1/2}$ values for electrochemical processes are referred to SCE (saturated calomel electrode), and are calculated adding ferrocene as an internal standard according to a well established method. In ECL and electrochemical experiments, acetonitrile (MeCN or ACN) or other organic solvent such as tetrahydrofurane (THF), dicloromethane (DCM) or dimethylformamyde (DMF) (Fisher scientific HPLC grade) is used as received and 1 mM solution of the active compound is prepared with 0.1 M Tetrabutylammonium-PF_6 ($TBAPF_6$) (Aldrich) as supporting electrolyte. Similar results can be alternatively obtained with Tetrabutylammonium-BF_4 (Aldrich). Before each ECL experiment, the sample is deaerated with Ar for about 10 minutes in a specially made cell to minimize quenching effect and interaction

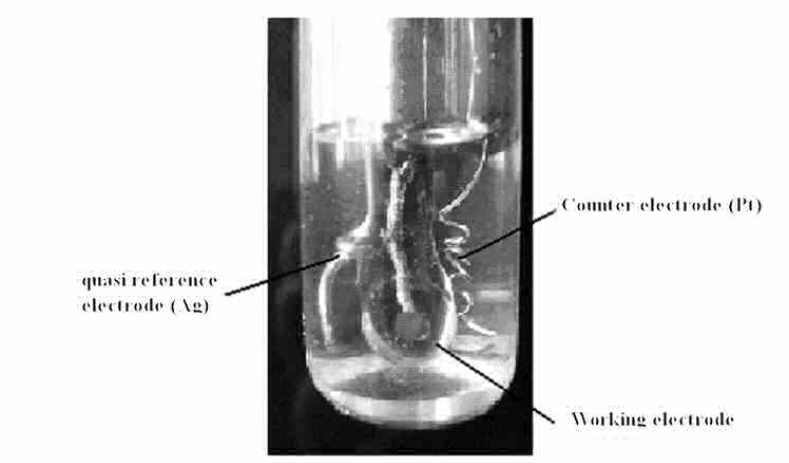

Figure 6. Classical three electrodes electrochemical cell for electrochemiluminescence. Working electrode surface is facing the side of the cell (L shape) toward light detector. (CCD or PMT)

with molecular oxygen. (fig.7) The exact concentration of oxygen in solution following degassing is not measured. Preliminary potential cycling is then performed systematically until a reproducible voltammogram is obtained. More drastical conditions can be obtained keeping supporting electrolytes, samples and solvent into dry box. When cell is prepared and o-ring sealed inside dry box oxygen and water impurities in the sample are lowered preventing quenching and decomposition processes that often seriously affect electrochemical behaviour and ECL performances.

2.3
The design of Bologna ECL instrument

2.3.1
General aspects

The basic idea was building from scratch (see fig. 9) an instrument as simple as possible to perform all measurements that in Austin

Figure 7. The ECL cell geometry allows an accurate degassing of solution by a 5 minutes Ar bubbling and exposure of the sample to air when required. Ar is saturated with solvent vapours to avoid his evaporation from sample.

were possible with three separate setups. Necessary requirements were essentially:

- Recording of ECL spectra (spectral range 200-1000 nm)
- Registering of light/current ECL integrated curves during cyclic voltammetry and chronoamperometry.
- Supporting of solution and solid film samples
- Detection of photocurrents in a wide range of intensities (nA-mA) .

Starting from Austin experimental setups some aspects needed to be carefully improved. No great importance was in general attribuited to reproducibility of measured ECL signal. This because for the study of mechanicistic and basic aspects of ECL emission a semiqualitative approach is often sufficient. Normally measured ECL intensity can be assumed as an estimation of the order of magnitude but is not sufficiently accurate for analytical purposes. Considering that now an accurate comparison of ECL efficiency of the new materials with that considered as standard has become necessary many efforts have been made to significantly improve reproducibility. As will be explained in detail cell holder, cell geometry, introduction of fixed electrodes and flow cell, the use of silicon chip electrodes has been made to keep emitting electrode surface as constant and reproducible as possible. Quantitative analysis is an hard aspect of electrochemical experiments due to frequent formation of filming products and modification of electrode surfaces; for this reasons an accurate optimization of experimental conditions in necessary. As example reproducibility is fundamental to be statistically confident in an ECL intensity change that follows protonation or interaction with DNA of active species.

The scope of the new instrument is thus not only to reproduce the model one but also to make possible:

- quantitative measurements (± 5 %)
- biological testing based on ECL (flow cell)
- measurements in high vacuum and ultra dry conditions

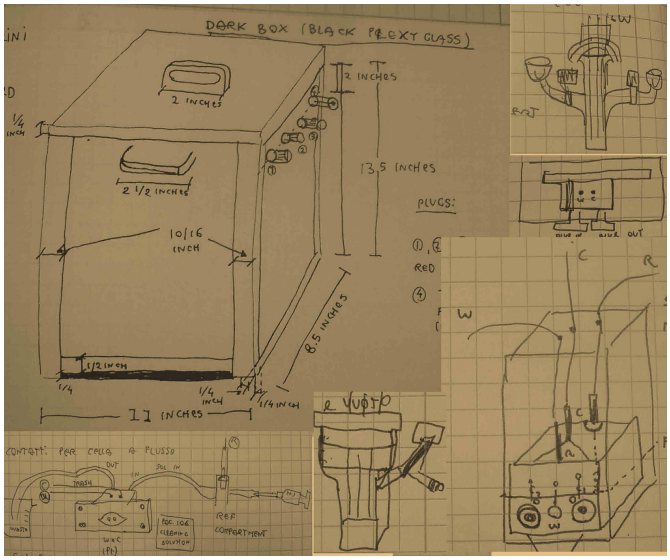

Figure 8.Fragments of dark box and cells scratches from Austin laboratory notebook

2.3.2

The new ECL instrumentation

In this thesis, the job has not only been the study ECL properties of new materials but as stated above also the setup of new ECL instrumentation. The optimization of the many experimental parameters has been obtained to find out more convenient work conditions. The reference compound, with suitable and stable well established ECL properties is the complex $Ru(bpy)_3^{2+}$.[4]

The instrument assembled in Bologna is not commercial and made of single commercially available or home built components to obtain the specifics described in previous paragraph. Main spectroscopic components are:

- a dual exit monochromator (Mod. Spectra-Pro 2300i Acton Research) (fig.9)
- a photo diode silicon detector (Mod. SI 440 Acton research; detecting range: 400-1100 nm)
- a photomultiplier detector (Mod. PD 471 Acton research; with built in high voltage power supply; max Voltage 1250 V; detecting range: 300-1100 nm)
- a control module (Mod. Spectra Hub Acton)
- a dark box with mobile cell holder (home built)
- a current sensitive preamplifier (Mod. 181 Princeton applied research)

Figure 9. Dual exit monochromator in ECL instrument. One of the two exit slits can also supportCCD camera detector.

The presence of two detectors allows to measure photoemission of very weak sources (PMT) and very intense.(silicon photodiode) For example direct light bulb or laser pointer emission spectra can be collected when photodiode is in

use. Detector change can be easily made by software controlling position of a motorized mirror. General setup of spectroscopic and electrochemical components is shown in fig. 10. Electrochemical cell is positioned inside dark box which is inserted on the side of monochromator entrance slit. A circular hole in dark box directed to monochromator allows to send signal to the detector. Spectra hub interface allows to control via software monochromator parameters and PMT high voltage. This hub is also used to acquire data and send it to Spectra Sense 4 software. Monochromator is provided of one entrance slit and two exit slits. Width of all slits can be adjusted using micrometric screws positioned in the top of the slot; maximum allowed width is 5 mm.

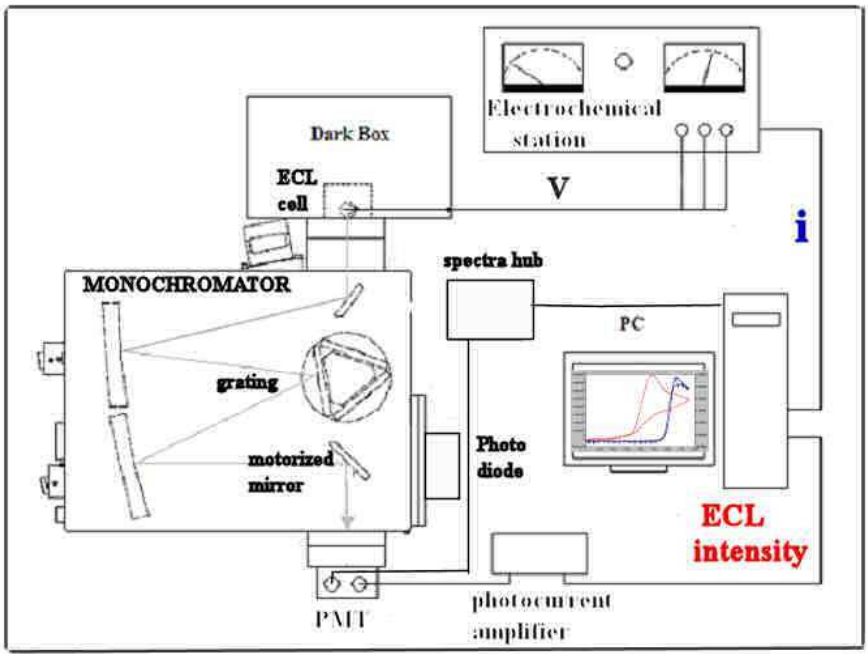

Figure 10. General scheme of ECL instrument.

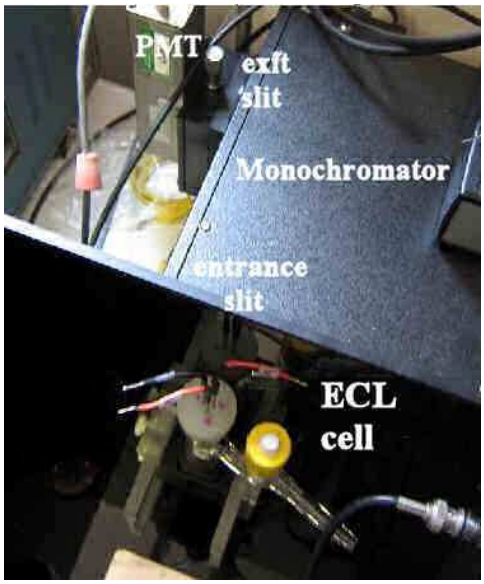

Figure 11. Top view of ECL cell and monochromator from entrance slit.

The output signal of PMT (an electrical current) can be treated in two different ways depending in the type of measurement performed:

1) *PMT output is connected to SPECTRA HUB to collect spectra or to obtain ECL intensity vs time graph using the Acton software SPECTRASENSE.*

Although SPECTRA HUB and SPECTRA SENSE allow a satisfactory signal to noise ratio (20 bit processing) in a wide range of emission intensities (good dynamicity) due to the electronic onboard processing prior to software elaboration, the response time is too slow (declared: 5 ms) to register emission during fast CV and chronoamperometry. On the other hand is not possible to directly send PMT signal from SPECTRA HUB to AUTOLAB because the data is sent from HUB to PC by an USB cable data. For this reasons an alternative setup is necessary for fast signal acquisition and time transients analysis which is the one presented in point 2.

2) *PMT output signal is sent to a current sensitive preamplifier module (CSP) which after processing sends the signal directly to the second input channel of AUTOLAB.*

In this case SPECTRA HUB is just used to control monochromator and PMT high voltage. With this connection scheme, which is the one depicted in fig.10 is possible to synchronize electrical current i and ECL photocurrent signals during cyclic voltammetry (CV) and chronoamperometry (CA). Using then AUTOLAB software GPES light/current curves are obtained in function of applied potential (V) or time (t). The sample time can be lowered to μs regime so that emission transients can be followed accurately even in fast chronoamperometric experiments. What Model 181 CSP does is to convert electric current from PMT to an appropriate voltage for AUTOLAB input. The module is a sophisticated ultra low noise electronic board that keeps a good signal to noise ratio in a huge range of input photocurrents. The sensitivity range can be selected in the range of 10^{-9}-10^{-4} A/V with minimal noise in the order of fA. Another selectable feature is the input signal attenuation of a 0.1 x factor which enlarge usability scale to mA/V.

When measuring integrated ECL intensities vs t or V (e.g. light current curves) the use of monochromator in position 0 nm (acts as a mirror) causes signal loss due to the many reflection steps between in and out slit. In those cases monochromator is bypassed and PMT is positioned inside darkbox a few millimetres from emitting electrode surface (fig.12). With this alternative setup signal loss is avoided and sensitivity greatly increased.

Electrochemical cell and electrodes

Electrochemical cell, the same typology used and built in Austin, is in glass and supports the already described three electrodes. Working electrode is slightly different from conventional upright geometry being "L shaped".

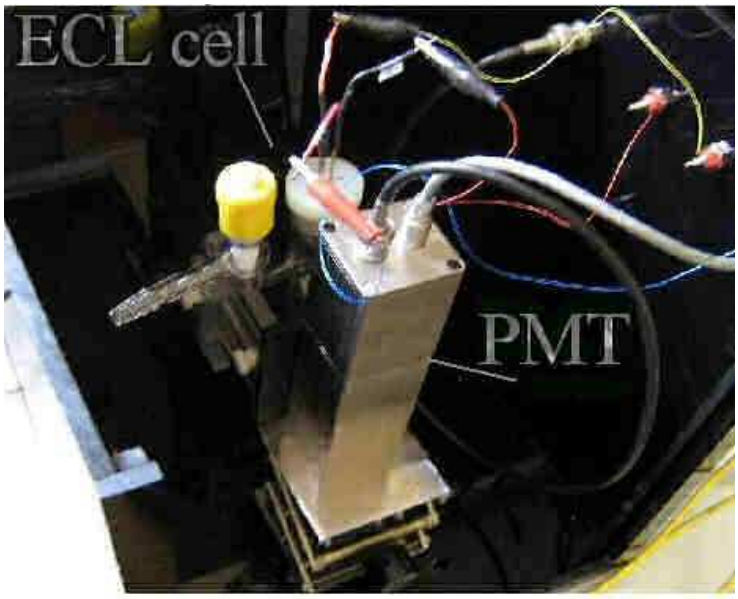

Figure 12. Alternative setup during light/current curves acquisition

This platinum disk electrode has been obtained by bending of about 90 degrees a Pt wire soldered carefully into glass tube. This geometry, exposing electrode surface to the side of the cell is necessary to direct emitted light toward monochromator entrance slit or detector. Cell design and components are summarized for clarity in fig. 13.

It's necessary during ECL experiments that working electrode surface is completely immersed in solution otherwise only a limited region of electrode will emit. Optimal distance between the glass side and emitting disk should be around 3-5 mm. This value, empirically obtained, ensures an appropriate diffusion layer and at the same time limits re-absorption of emitted light by sample solution. The electrodes cleaning procedures together with degassing method with Ar has been already described in a previous paragraph (sect. 2.2 and fig.7).

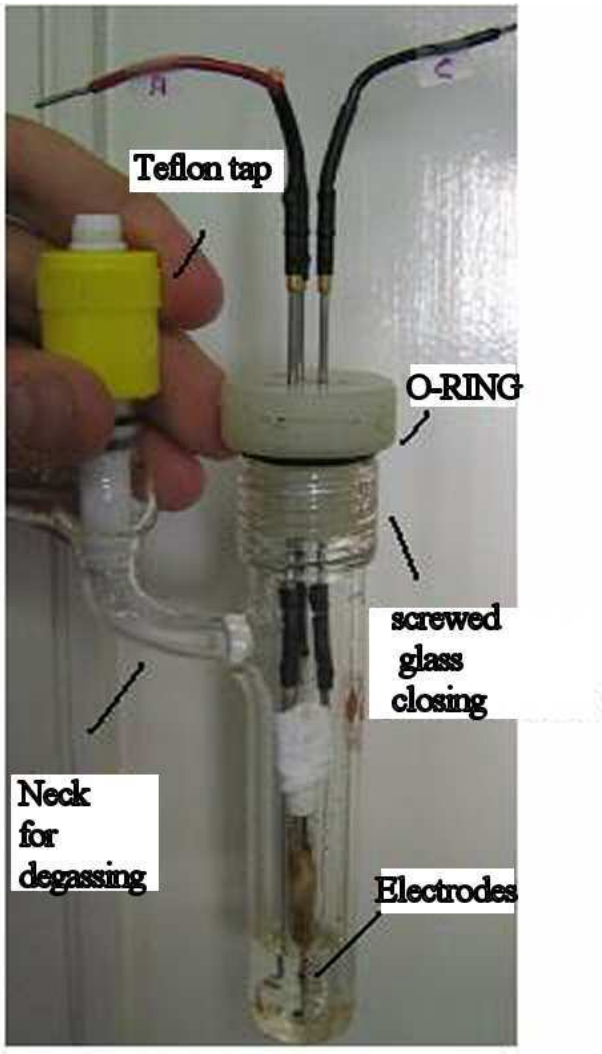

Figure 13. ECL electrochemical cell and electrodes. The cell was built is Austin glass shop and designed to allow an accurate Ar blowing degassing (depicted in fig. 7). Cell also supports connection to a vacuum rotative pump.

Dark box

Dark box was designed and built during second Austin research visit in black Plexiglas especially for the new instrument. His presence is fundamental to

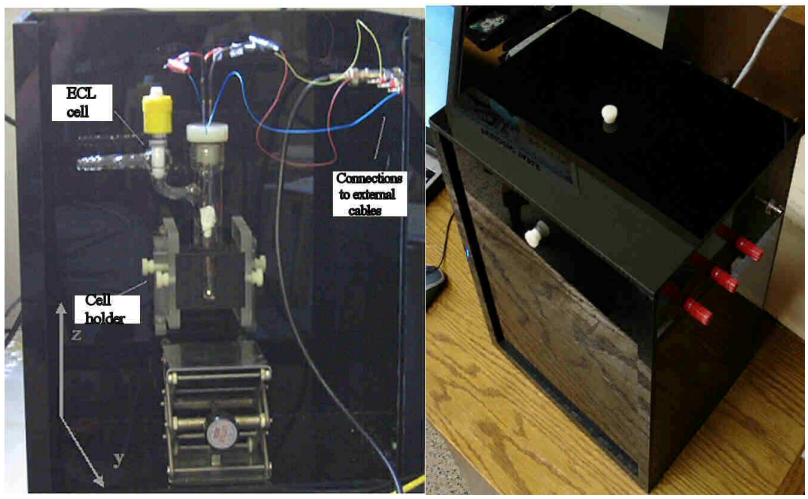

Figure 14. Darkbox inside and outside view.

insulate the sample emission from external light sources especially when PMT is in use. The box, which is depicted in fig. 14, has be thought to be large enough to conveniently work inside Besides the top and

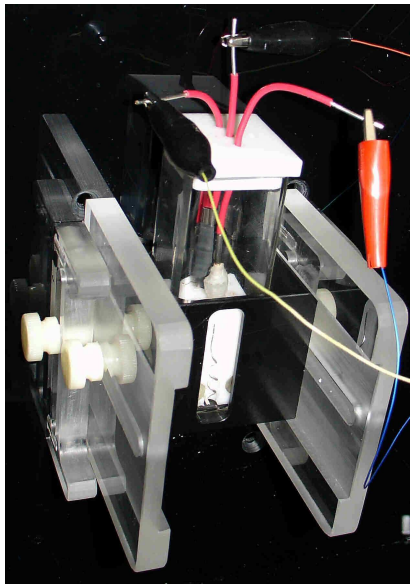

Figure 15. Detailed image of mobile cell holder. A square cell is mounted.

front side can be easily removed when necessary. Dark box can easily content PMT or PD if necessary allowing to bypass monochromator. Actually 5 holes are present in the top of his right side to allows connections with the 3 electrodes, output and eventual control cable of the detector. All 5 cables can be connected in o-ring sealed plugs preventing external light to get inside.

Mobile cell holder and cell formats

A mobile cell holder in Plexiglas has been built together with dark box and positioned in the side of entrance slit where a 1 inch diameter hole, completely including the slit is present. (fig.15). The holder can be accurately positioned respect to two directions as evidenced in fig. 14 :

1) Toward and outward of entrance slit (y direction)
2) Up and down (z direction)

The position of the cell can be changed and fixed independently in y and z direction with two plastic screws. In normal conditions to maximize signal at detector the entrance end exit slits are fixed at the maximum possible width (5 mm). Movement in y direction allows focusing light source. Attempts were made in Austin of to put a lens between source and slit without further signal improvements. Movement in z direction is necessary to align exactly working electrode with “input rectangle”. This alignment is important when acquiring spectra especially for low emitting species.

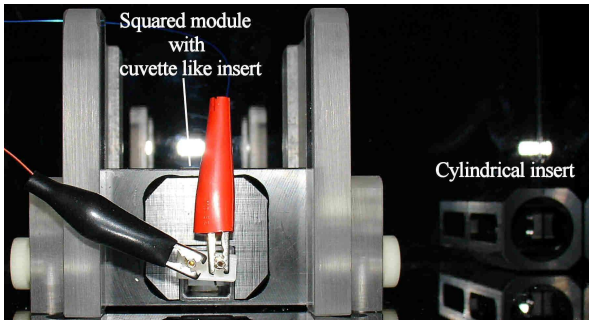

Figure 16. Mobile cell holder with cuvette like cell inside. A specific insert is put into square module. Another cylindrical insert is shown in the right.

The parallelepiped shaped module (PSM) in which glass cell is inserted, built in black Plexiglas supports three different types of cell:

- Cylindrical
- Square
- Fluorescence cuvette like.

As shown in fig. 16 the basic supported shape is square cell; using two especially made black Plexyglas inserts cylindrical and cuvette like cells can be fixed. An additional module has then been made to support flow cell. To make alignment easier each module has a passing rectangular hole that allows seeing the position of electrodes when cell is inserted.

2.4
Unconventional electrochemical cells for ECL

Cylindrical cell reported in fig.13 has been successfully used in many ECL experiments but reproducibility of intensity is estimated to be only of ± 50 % . This relatively poor feature is a consequence of possible cell partial rotation respect to holder and of working electrode respect to the rest of cell. The key point is that emitting surface position and orientation slightly changes in different experiments causing variations in detected intensities. For this reason and for other specific practical requirements several unconventional electrochemical cell for ECL have been built. A brief description of each geometry introduced is reported in following sections.

square cell

This type of cell has been built in two different versions o-ring sealed (fig.17) to allow operation in Ar degassed atmosphere and air opened (fig.15). One working and two symmetric counter electrodes are fixed and contacted by

screw pressing with a three holes mask in a Teflon rigid block that fits tightly in glass square bottom of the cell. Reference electrode (e.g. Ag/AgCl or Ag wire) can be directly inserted in a apposite hole in the back of Teflon cube.

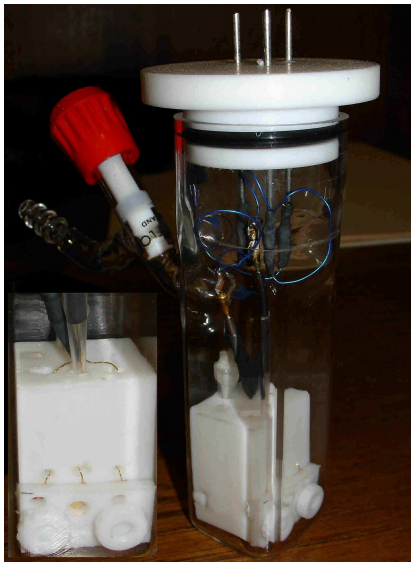

Figure 17. Left: rigid Teflon block containing electrodes; Right: Overall view of O-Ring sealed square cell

Benefits of that geometry are:

- fixed electrodes position respect to glass cell
- no rotation of cell in holder
- possibility of employing different material as working or counter electrodes: Au, Ag, Pt foils, carbon, B doped diamond or ITO glass
- both aqueous and organic solvents can be employed

Chip cell

In this cell (fig.18) as previous rigid components are completely made of Teflon to allow organic solvents usage when necessary. This cell has been made to support and correctly contact electrically ECL chip electrodes made of silicon containing gold W and C electrodes sputtered on. (see Chapter 5 for further details). Silicon chip is inserted and pressed down by a screw toward

two separated Pt wires similarly to square cell. Solid support can be then inserted into a glass or plastic monouse fluorescence standard cuvette. No true reference electrode can be used so a quasi reference Ag wire is normally employed. A cell image has been published in a Italian engineering journal ("Ingegneri e Architetti del politecnico di Torino" n° 1/2006 p. 15) for his catchy design.

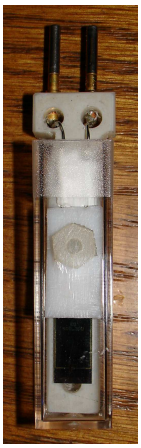

Figure 18. This cell allows connection of chip miniaturized contacts with electrochemical instrument without soldering.

High vacuum cell

This cell has been prepared to operate in ultra dry (total absence of water) and ultra vacuum conditions (10^{-5} mbar of internal pressure). Sample can be prepared in the same ultra clean conditions used in Bologna's Lab to perform cyclic voltammetries in ultra aprotic conditions ensuring conditions even more drastic that what obtained with dry box. This setup is particularly useful when treating species very sensitive to oxygen and water presence (e.g. Antracene and derivatives) or simply to maximize ECL performance of a system moderately sensitive to oxygen. As a matter of fact the degassing with Ar is hard to standardize and a small difference in oxygen concentration in solution can often seriously affect ECL intensity and stability so that the use of extreme

conditions can definitely solve the problem and can be assumed as limit performance condition very useful for comparisons. The cell depicted in fig. 19 has two distinct spherical joints used for connection to turbomolecular pump vacuum line and to perform trap to trap ultra dry solvent distillation from o-ring sealed schlenks . For further details on Cyclic voltammetry performed in high vacuum conditions see the relative appendix at the end of this chapter.

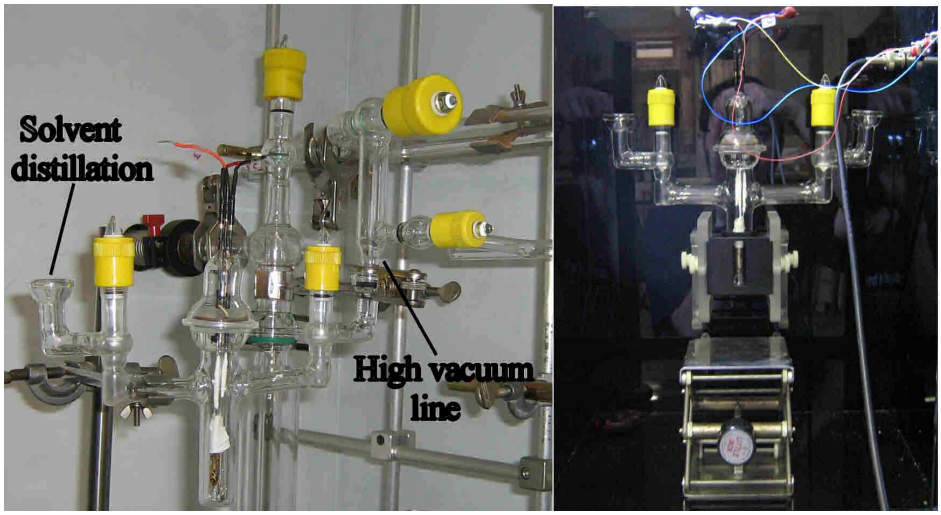

Figure 19. Cell preparation (left) and ECL measurement (right) in high vacuum conditions.

Flow cell

Flow cell system (fig.20) is the type of electrochemical cell commonly used in ECL based immunological tests. The benefits from an analytical point of view are substantially two:

1) Good reproducibility of ECL intensity.

Electrodes and cell are fixed in front of detector. Sample and washing solution are inserted and removed by a peristaltic pump.

2) Small amount of solution required (50-100 μL).

Electrochemical Plexiglas cell is about 500 μL thick and "eye shaped". Solution is inserted and removed from small holes located in the left and right side of the cell by capillary Teflon tubes.
Electrochemical cell contains two equivalent Pt disks of 2 mm diameter tightly soldered into a polymeric matrix that acts as working and counter electrode.
There is also the possibility to use a true reference electrode in an external Plexiglas compartment (not shown) that can be inserted between peristaltic pump and electrochemical cell. Electrodes can be also manually cleaned by removing the four screws that put together the two sides of the cell. Depending on required setup flow cell can be fixed into mobile holder to collect spectra or placed in horizontal position directly under photo detector. (fig.21)

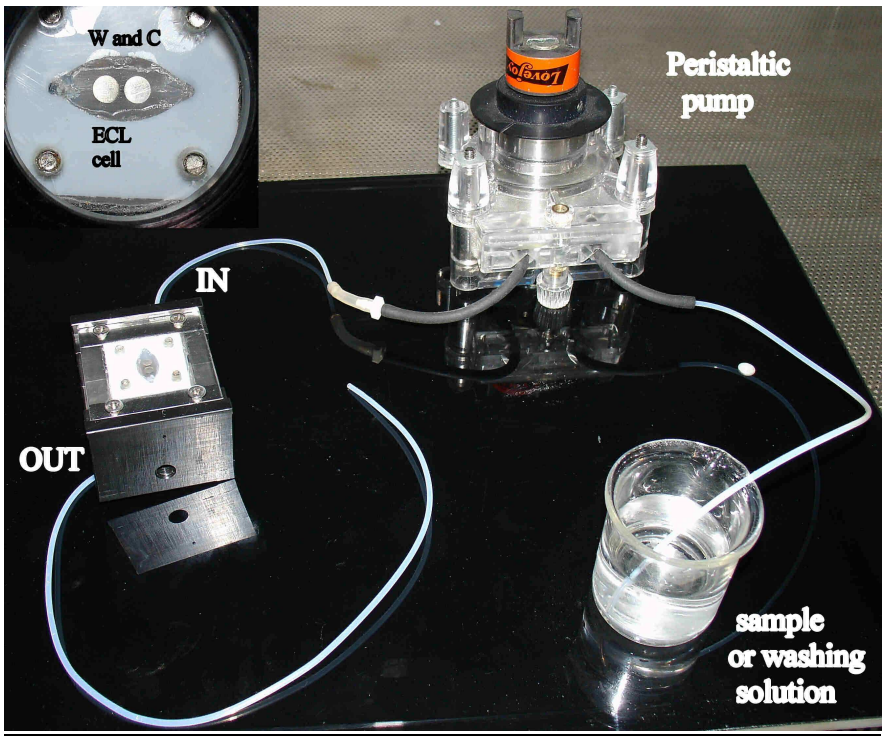

Figure 20. Scheme of ECL flow cell and solution charging system.

Vertical OLED holder

This solid sample holder (fig.22) has been made to collect spectra of ECL emission from solid films and can be easily placed on top of cell holder inside dark box. The connection scheme is analogous to that of horizontal setup reported in fig.5 and previously described.

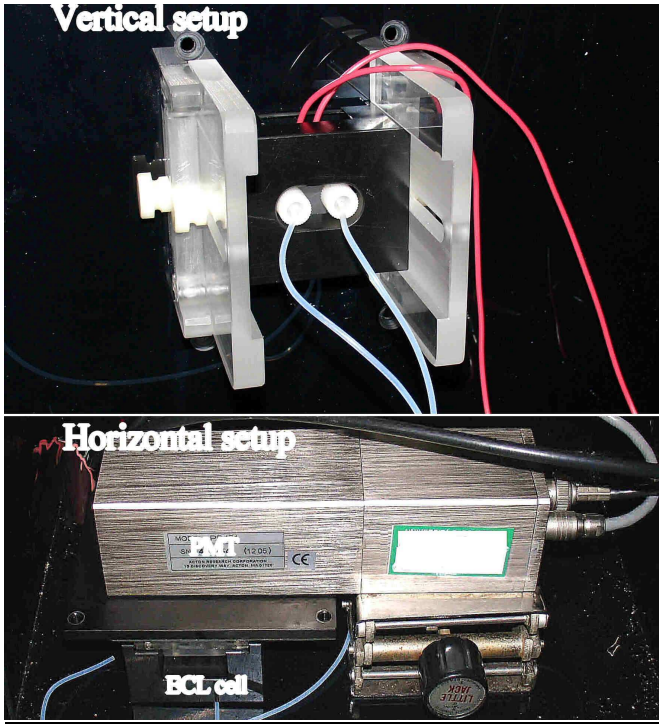

Figure 21. (top) ECL flow cell in vertical position towards monochromator; (bottom) cell is positioned directly under photomultiplier tube.

The In/Ga eutectic drop used to inject electrons in active layer is however in electrical contact with a Copper wire placed in opposite side respect to hole in Teflon support from which light emission is collected.

2.5
Monochromator basics and setup

A monochromator is an optical device that transmits a mechanically selectable narrow band of wavelengths of light chosen from a wider range of wavelengths available at the input.

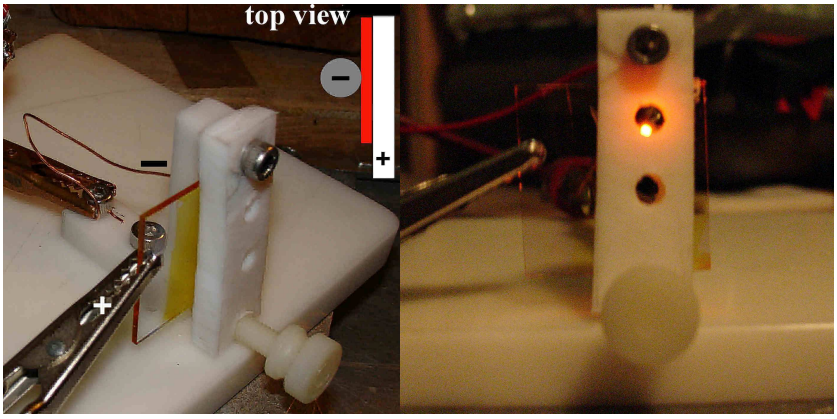

Figure 22. (Left) vertical holder electrical connections scheme; (right) ECL emission from a $Ru(bpy)_3^{2+}$ solid film spin coated on ITO glass.

A monochromator can use either the phenomenon of optical dispersion in a prism, or that of diffraction using a diffraction grating, to spatially separate the colors of light. It usually has a mechanism for directing the selected color to an exit slit. Usually the grating or the prism are used in a reflective mode. A reflective prism is made by making a right triangle prism (typically, half of an equilateral prism) with one side mirrored. The light enters through the hypotenuse face and is reflected back through it, being refracted twice at the same surface. The total refraction, and the total dispersion, is the same as would occur if an equilateral prism were used.

The dispersion or diffraction is only controllable if the light is collimated, that is if all the rays of light are parallel, or practically so. A source, like the sun,

which is very far away, provides collimated light. Newton used sunlight in his famous experiments. In a practical monochromator however, the light source is close by, and an optical system in the monochromator converts the diverging light of the source to collimated light. Although some monochromator designs do use focusing gratings that do not need separate collimators, most use collimating mirrors. Reflective optics are preferred because they do not introduce dispersive effects of their own.

In the common *Czerny-Turner design* (fig.23), the broad band illumination source (A) is aimed at an entrance slit (B). The amount of light energy available for use depends on the intensity of the source in the space defined by the slit and the acceptance angle of the optical system. The slit is placed at the effective focus of a curved mirror (the collimator C, usually a spherical mirror) so that the light from the slit reflected from the mirror is collimated (focused at infinity). The collimated light is refracted by the prism or diffracted from the grating (D) and then is collected by another mirror (E) which refocuses the light, now dispersed, on the exit slit (F). At the exit slit, the colors of the light are spread out (in the visible this shows the colors of the rainbow). Because each color arrives at a separate point in the exit slit plane, there are a series of images of the entrance slit focused on the plane. Because the entrance slit is finite in width, parts of nearby images overlap. The light leaving the exit slit (G) contains the entire image of the entrance slit of the selected color plus parts of the entrance slit images of nearby colors. A rotation of the dispersing element causes the band of colors to move relative to the exit slit, so that the desired entrance slit image is centered on the exit slit. The range of colors leaving the exit slit is a function of the width of the slits. The entrance and exit slit widths are adjusted together.

When a *diffraction grating* is used, care must be taken in the design of broad band monochromators because the diffraction pattern has overlapping orders. Sometimes extra, broadband filters are inserted in the optical path to limit the width of the diffraction orders so they do not overlap. The original high resolution diffraction gratings were ruled. The construction of high quality

ruling engines was a large undertaking, and good gratings were very expensive. The slope of the triangular groove in a ruled grating is typically adjusted to enhance the brightness of a particular diffraction order. This is called *blazing* a grating. Ruled gratings have imperfections that produce "ghost" diffraction orders that raise the stray light level of a monochromator. A later photolithographic technique allows gratings to be created from a holographic interference pattern. Holographic gratings have sinusoidal grooves and so are not as bright, but have a much lower stray light level than blazed gratings, and are generally preferred. The wavelength where light intensity is brighter is called λ of Blaze and is specific for each grating. At this λ the energetic yield is maximum and approximately 80-90 % of source intensity.

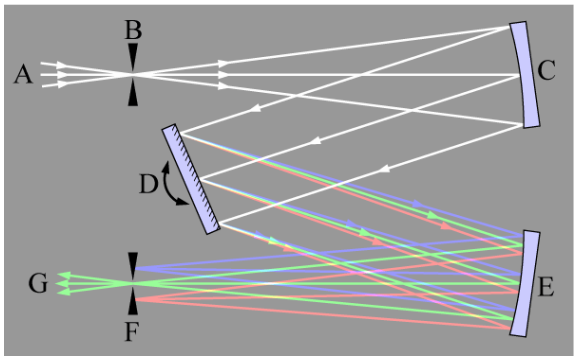

Figure 23. Diagram of a Czerny-Turner monochromator

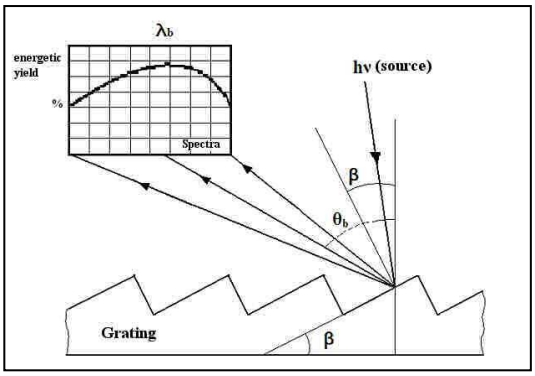

Figure 24. Dependence of energetic yield on diffracted light wavelength

Remaining wavelengths are diffracted with lower intensity in the range of 80-50 % depending in how far are from λ. (see fig. 24). Monochromator of Bologna instrument is equipped with a triple grating turret mounting:

- ruled grating 68x68 mm, 150 G/mm with Blaze wavelength 300 nm
- ruled grating 68x68 mm, 600 G/mm with Blaze wavelength 500 nm
- ruled grating 68x68 mm, 1200 G/mm with Blaze wavelength 300 nm

Software control allows the selection of appropriate grating or mirror depending on necessity. Is convenient to select the grating with λ of Blaze as close as possible to expected emission wavelength to maximize signal intensity. The selection of position 0 nm in monochromator is equivalent to mirror activation and all wavelength of the light source are reflected to exit slit. Monochromator has been provided already calibrated. The company performed calibration using standard emission lines of an Hg lamp.

Verification of monochromator calibration (May 30 2006)
Verification was made by comparing new instrument detected wavelength (fig. 25) with that of a standard fluorimeter (Cary Mod. Eclipse). Spectra were obtained by directly inserting different light sources into sample compartments. The spectras acquired with Spectra pro 2300i evidenced an higher signal to noise ratio; this was caused by the larger maximum allowed width of slits. Comparison (see tab.1) was based on six different wavelength (364-638 nm range) and three different light sources. Registered maximum wavelength difference was in 0.418-2.147 nm interval. Mint calibration was then considered satisfactory.

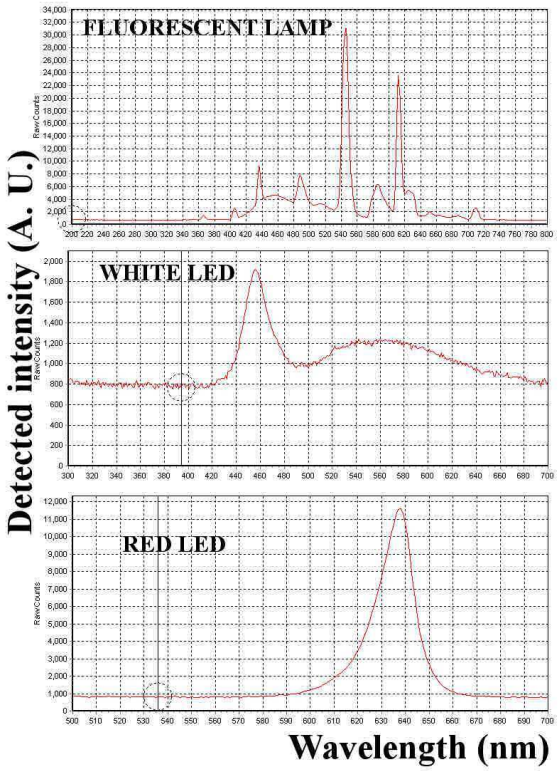

Figure 25. Emission spectra of three different commercial light sources obtained with Spectra Pro 2300i monochromator using silicon photodiode as detector. λ of Blaze: 500 nm

Wavelength (nm)	**Lamp WL1***	**Lamp WL2**	**Lamp WL3**	**Lamp WL4**	**White LED**	**Red LED**
Spectra pro 2300i	365.778	404.984	435.705	545.131	455.956	638.166
Cary Eclipse	364.483	403.563	435.287	546.552	456.552	640.313

Table 1. Comparison of detected emission wavelength of Acton spectra pro 2300 I and Cary Eclipse

*WL= Wavelength

2.6
Photodetectors

2.6.1
Types of detectors

PMT

Photomultiplier tubes (photomultipliers or PMTs for short) are extremely sensitive detectors of light in the ultraviolet, visible and near infrared. These detectors multiply the signal produced by incident light by as much as 108, from which single photons can be resolved. The combination of high gain, low noise, high frequency response and large area of collection have meant that these devices still find applications in nuclear and particle physics, astronomy, medical imaging and motion picture film scanning (telecine).

Photomultipliers are constructed from a glass vacuum tube which houses a photocathode, several dynodes, and an anode. (fig.26) Incident photons strike the photocathode material which is present as a thin deposit on the entry window of the device, with electrons being produced as a consequence of the photoelectric effect. These electrons are directed by the focusing electrode towards the electron multiplier, where electrons are multiplied by the process of secondary emission.

The electron multiplier consists of a number of electrodes, called dynodes. Each dynode is held at a more positive voltage than the previous one. The electrons leave the photocathode, having the energy of the incoming photon. As they move towards the first dynode they are accelerated by the electric field and arrive with much greater energy. On striking the first dynode, more low energy electrons are emitted and these, in turn, are accelerated toward the second dynode. The geometry of the dynode chain is such that a cascade occurs with an ever-increasing number of electrons being produced at each stage. Finally the anode is reached where the accumulation of charge results in a sharp current pulse indicating the arrival of a photon at the photocathode.

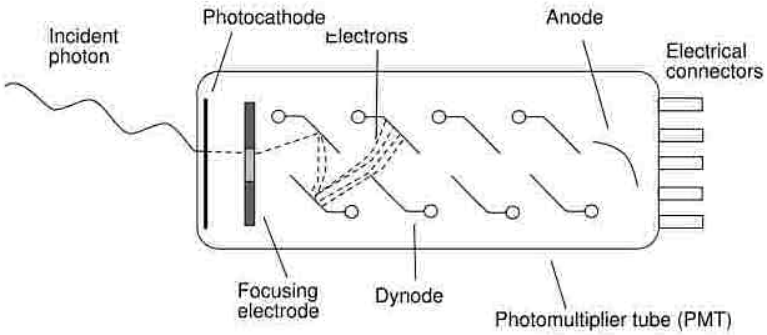

Figure 26. Scheme of Photomultiplier tube components and operation.

Photomultiplier noise originates from different phenomena :

1) Dark currents.
When no electromagnetic radiation is hitting photocathode some electrons are equally emitted for thermoionic effect. The result is a sinusoidal current. The mean value of that oscillations is called dark current and his intensity can be calculated by Richardson's equation:

$$I = AT^2 e^{(-e\Phi/kT)}$$

Where A is an empirical constant, k the Boltzmann constant, Φ the energy of electron extraction from photocathode and T absolute temperature.
From this statistical relation is clear that this type of noise can be reduced by lowering the detector temperature during measurement.
2) Light emission phenomena.
can be caused by four different effects:

A) Statistical noise.

This effect is due to statistical nature of photoemission and secondary emission process: is commonly called Schottky effect. Other signal fluctuations are caused by electron multiplier system. Fluctuations are increased because of the non homogeneity in electrons fly time between dynodes and secondary emission factor.

B) Surroundings light exposure.
Photomultiplier is an extremely sensitive detector for this reason even when high voltage is off exposure to day light causes photocathode emission with a subsequent increase of dark current. This increase can last from few seconds to several minutes depending on light intensity during exposure.

C) Magnetic field effect
Even a small magnetic field is sufficient to deviate electrons emitted by photocathode preventing to hit dynodes. For this reason PMT is normally carefully by a μ-metal screen to avoid possible signal interferences.

D) Thermal effects
In majority of photomultipliers, excluding dark currents, thermal effects are quite negligible. A modest temperature influence can also be observed in spectral sensitivity of cathodes.

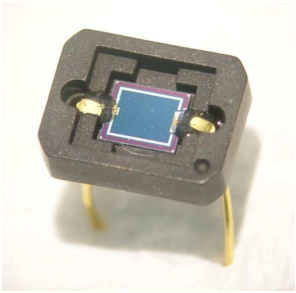

Fig 27. An example of photodiode detector

Photodiode

A photodiode (fig. 27) is a semiconductor diode that functions as a photodetector. Photodiodes are packaged with either a window or optical fibre connection, in order to let in the light to the sensitive part of the device.

A photodiode is a p-n junction. (see fig. 28) When light of sufficient photon energy strikes the diode, it excites an electron thereby creating a mobile electron and a positively charged electron hole. If the absorption occurs in the junction's depletion region, these carriers are swept from the junction by the built-in field of the depletion region, producing a photocurrent. A summary of materials used in p-n junctions is shown in tab. 2.

Photodiodes can be used under either zero bias (photovoltaic mode) or reverse bias (photoconductive mode). In zero bias, light falling on the diode causes a voltage to develop across the device, leading to a current in the forward bias direction. This is called the photovoltaic effect, and is the basis for solar cells in fact, a solar cell is just a large number of big, cheap photodiodes.

Diodes usually have extremely high resistance when reverse-biased. This resistance is reduced when light of an appropriate frequency shines on the junction. Hence, a reverse-biased diode can be used as a detector by monitoring the current running through it. Circuits based on this effect are more sensitive to light than ones based on the photovoltaic effect.

Fig 28. Scheme of a silicon p-n junction

Avalanche photodiodes have a similar structure, but they are operated with much higher reverse bias. This allows each photo-generated carrier to be

multiplied by avalanche breakdown, resulting in internal gain within the photodiode, which increases the effective responsivity of the device.

Material	Wavelength range (nm)
Silicon	190–1100
Germanium	800–1700
Indium gallium arsenide	800–2600

Table 2. Semicoductors commonly used in photodiodes with relative detection range

CCD (fig.29)

Charge-coupled device (CCD) is a light sensor, consisting of an integrated circuit containing an array of linked, or coupled, light-sensitive capacitors equivalent in principle to single photodiodes.

The photoelectric effect depicted in fig. 30 is fundamental to the operation of a CCD and photodiode. Atoms in a silicon crystal have electrons arranged in discrete energy bands. The lower energy band is Valence Band, the upper is the Conduction Band. Most of the electrons occupy the Valence band but can be excited into the conduction band by heating or by the absorption of a photons. The energy required for this transition is 1.26 eV. Once in this conduction band the electron is free to move about in the lattice of the silicon crystal. It leaves behind a "hole" in the valence band which acts like a positively charged carrier. In the absence of an external electric field the hole and electron will quickly re-combine and be lost. In a CCD an electric field is introduced to sweep these charge carriers apart and prevent recombination.

Thermally generated electrons are indistinguishable from photo-generated electrons. They constitute a noise source known as "Dark Current" and it is important that CCDs are kept cold to reduce their number.

Fig 29. An example of CCD light detector

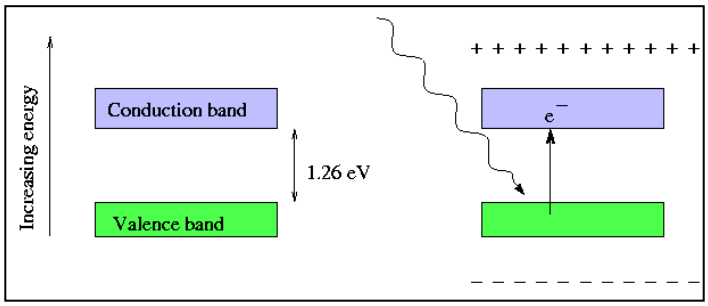

Figure 30. Scheme of photoelectrical effect on Silicon crystals with generation of a hole and an electron in a CCD pixel.

1.26eV corresponds to the energy of light with a wavelength of 1 micron. Beyond this wavelength silicon becomes transparent and CCDs constructed from silicon become insensitive.

CCD light detection is performed in a three step process:
(1) Exposure which converts light into an electronic charge at discrete sites called pixels;

(2) Charge transfer which moves the packets of charge within the silicon substrate;
(3) Charge to voltage conversion and output amplification.

Emission spectra is acquired when incident light, in the form of photons, falls on the array of pixels. In Austin setup ECL emission is diffracted by a grating reticle and a discrete small interval of wavelength (more or less 1 nm) is focused and accumulated in a single pixel column of CCD. The number of electrons collected at each pixel is linearly dependent on light level and exposure time. After appropriate exposure, the charge accumulated in each single CCD column is read and sent to software. The plot of accumulated light respect to position in CCD row will be the raw data of emission spectra. Last step is the already described calibration of column pixel number respect to the wavelength in nm using a standard spectra. Another interesting feature of CCD system is that can be also used for imaging . During ECL experiment the use of CCD imaging mode can be useful to understand from where the emission arise (Working or counter electrode) or to map light emission intensity into working electrode surface.

2.6.2
Acquisition of ECL spectra by CCD and PMT: a comparison

The acquisition of ECL spectra can be performed with different detectors.
To understand which one is more convenient in some practical conditions We need to consider some features of emitting species such as:

- Intensity of emission
- Time stability of emitting species
- Time stability of emission spectra

Considering the setup used in Bologna (monochromator and PMT) is clear that even considering losses due to monochromator expected sensitivity is higher with respect to a non amplified CCD. On the other hand is possible to collect only a single wavelength for each monochromator step. In the case of emitting species with time stable spectra and very weak emission intensity PMT is convenient respect to CCD in the sense of an higher signal on noise ratio. In the case of species which shows instead a fast emission decay or spectra shape change during experiment the use of CCD is the only possibility to succeed in registering it . CCD accumulating all wavelength at the same time, if emission is intense enough can easily register time limited emissions and time spectral transformations . In the same conditions PMT will register a mean of temporal evolution of the spectra, last stabilized spectra or nothing depending in the relative kinetics of data acquisition and time modification of emission.
For CCD and PMT can be written that:

$$t_{exp,CCD} = t_{acc}$$
$$t_{exp,PMT} = n\, t_{acc}$$

and easily follows that:

$$t_{exp,PMT} / t_{exp,CCD} = n$$

Where t_{exp} is the total time of the experiment and t_{acc} is the time for which each wavelength is accumulated and n is the number of monochromator steps. This means that temporal resolution of CCD is always n times that of PMT. On the other hand PMT-monochromator system sensitivity can be assumed as more or less 10-50 times higher with respect to CCD so signal on noise ratio will be better for this last detector. An important consideration is that PMT accumulation time for monochromator step cannot be shortened at will because ECL emission is pulsed and synchronization of data acquisition is not completely possible because of the frequent variations on the experimental

interval time between light impulses. Another possibility is to use relatively long potential impulses (e.g.1-2 s) and short accumulation time. In this case however ECL emission intensity shows a fast decay similar to that of current causing signal loss. For higher wavelegth (see section 1.3 for typical chronamperometry $t^{-1/2}$ current decay function). For this reasons It seemed not practically possible as one could think to compensate PMT lower temporal resolution with respect CCD with his higher sensitivity.

From previous considerations can be stated that:

- CCD is more convenient when ECL emission is relatively intense allowing also the tracking of spectra time modifications. CCD register a continue spectra even if emission is time impulsed.

- PMT is optimal when emission is time stable even of very low intensity.

Sensitivity and time resolution of CCD can be improved introducing amplified CCD (sensitivity close to that PMT) or streak cameras (temporal resolution of ps) that are however much more expensive setups respect to that considered here.

2.7

Software and acquisition conditions

When ECL signal is treated with SPECTRA HUB module and SPECTRA SENSE software (as described in setup number 1 in section 2.3) two different types of measurements can be performed: ECL signal vs. time (time based scan), ECL signal vs. wavelength (spectra acquisition). In this section basic adjustments to the software and instrument will be presented and relative effects discussed. It's important to remember that being emission electro generated (excitation methods: potential swept or impulse) light is always emitted discontinuously in time.

TIME BASED SCAN

With this operation method is possible to collect emission intensity vs. time of at specific wavelength or integrated in all spectra (position 0 of monochromator or detector placed inside darkbox as previously described). produced plot shows on x-axis the time and in y-axis the intensity expressed in arbitrary units (A. U.). Graphical interface for this type of acquisition that evidences adjustable parameters is reported in fig.31. In top left panel entitled "Intensity vs. time" three fundamental measurement parameter are specified: "Integration Time", "Interval" and "Data Points". "Integration time" parameter specifies the detector signal collection time, "Interval" specifies instead the time between two acquisition and must be equal or lower than Integration time. The combination of those two parameters allows synchronization of the detector with a pulsed signal with a pause between two subsequent emission. Considering that ECL intensity vs. time is similar to that of corresponding electrical current (see Cottrell equation section 1.3), the signal decay is very fast and occurs in a very short time.

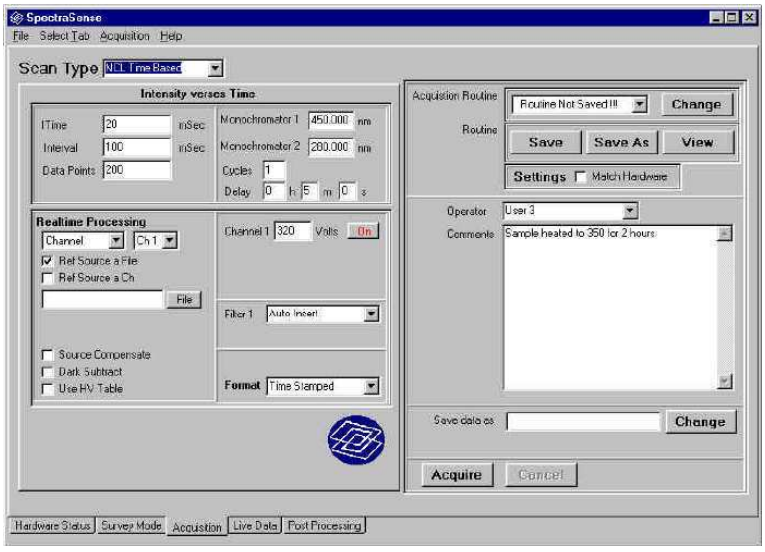

Figure 31. Graphical user interface of time based scan.

For this reason especially during chronoamperometric experiments "integration time" should be as short as possible and identical to "interval" to follow real emission transient. The instrument allow a minimal sample time of 5 ms (effective is about 10-20 ms due to onboard and software elaboration delays). "Data Points" is the number of collected experimental points. Multiplying "Data Points" for "Interval" one can obtain the total measurement duration. The monochromator position is selected by digitating wished value in "Monochromator 1" box. In the box "Cycles" on can specify how many times measurement must be repeated and the delay between measurements. In "Realtime processing" panel there is a "dark subtract" check box that can be used to subtract dark current measured prior to electrochemical excitation. "High Voltage" panel is used to specify PMT Voltage and to turn it on or off. At last "acquisition" panel is used to specify the file where data is saved and his format. The measurement starts when "Acquire" button is pressed.

SPECTRAL ACQUISITION SCAN

In this operation method ECL emission spectra is obtained registering detected intensity in function of wavelength. Graphical interface for this type of acquisition is reported in fig.32

In the left top panel "Monocromator 1" several monochromator parameters can be adjusted. It's possible specify starting and ending wavelength during scan and the "step" of increment in nm. By decreasing "step" paramenter the total experiment duration will increase accordingly because more points are collected. Another fundamental parameter is "ITime" e. g. detector integration time for each monochromator step. By increasing "ITime" the signal is accumulated for a longer time and thus is increased. On the other hand the dark current and noise are also increased. Itime can be set in 5 mS - 64 s range but dependently on PMT high voltage the maximum allowed value is normally lower. (i. e. If PMT high voltage is 1000 an accumulation of 6 s of the background signal is sufficient to saturate y-axis scale). The y-scale in both

time based and spectral acquisition reports signal as PMT of PD detected arbitrary units upon an intensity range of 0 to 1,000,000 A.U.. Depending on experimental conditions and studied compound PMT Voltage can be decreased to prevent detector saturation or increased to allow detection of low intensity emissions. A last important parameter is the box "read for points" which allows to specify how many time a single point must be read. If the value is greater than 1 saved data will contain a mean of the registered values with the benefit of a lower noise. The total experiment duration can be easily calculated by the expression:

$$t_{spectra}=((max_{WL}-min_{WL})/step)i_{time}n_{reads}$$

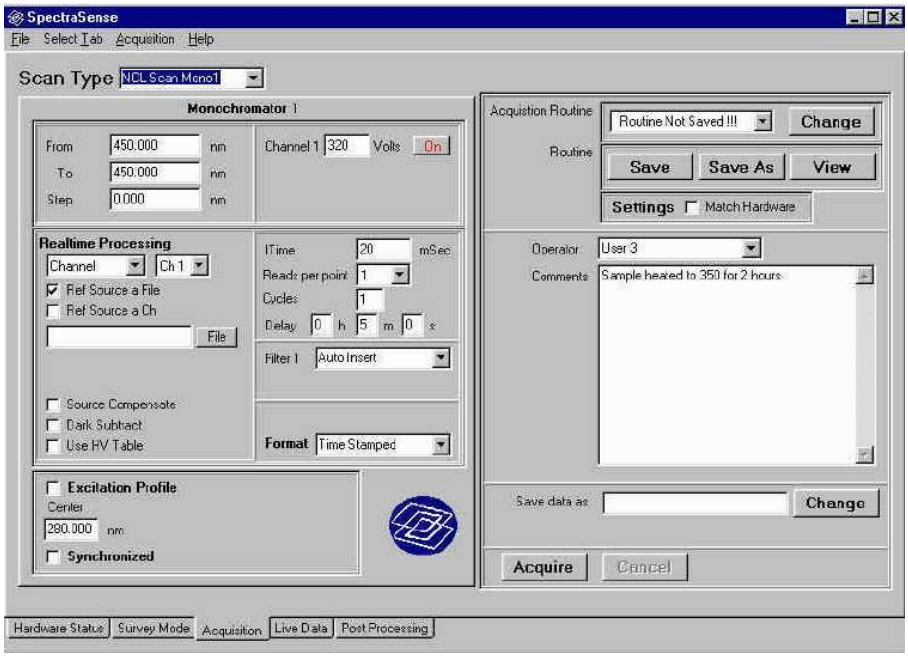

Figure 32. Graphical user interface for spectral acquisition.

Where $t_{spectra}$ is the total experiment duration, max_{WL} and min_{WL} are the maximum and minimum wavelength, *step* is the increase step of monochromator expressed in nm, n_{reads} the number of reads for each point and i_{time} the integration time. As can be seen from this formula each improvement on the spectra resolution and range is accompanied by an increase of the spectra collection time and necessarily of chemical modifications during electrolysis.

2.8

Theoretical model of ECL spectra acquisition.

First assumption is that We are using alternated chronoamperometric (CA) potential impulses to produce ECL. One step is at 0 V (vs. ref) and other at necessary reductive or oxidative potential. Normally the pulse width (p_w) is the same in all potential steps. Those conditions are encountered when ECL is produced in presence of a reductive or oxidative coreactant. The basic equation that expresses ECL intensity in function of time can be simply obtained from Cottrell equation (see section 1.3) by substituting current *i* with ECL time function $I_{ECL}(t)$ and adding a proportionality constant k_i:

$$I_{ECL}(t) = k_i \frac{FACD^{1/2}}{(\pi t)^{1/2}} \quad (1)$$

Where *F* is the Faraday's constant, *A* electrode area, *C* concentration of active species and *D* diffusion coefficient. Equation 1 has been written under the assumption that ECL intensity is linearly proportional to i which is not rigorously correct but is acceptable to build a model function. A more practical cell constant K_C can be obtained by combining different ones:

$$I_{ECL}(t) = \frac{K_C}{(t)^{1/2}} \quad (2)$$

where:

$$K_C = \frac{k_i FACD^{1/2}}{\pi^{1/2}} \tag{3}$$

At this point to reproduce a typical light emission discontinuous profile (see fig.2) a step function is necessary. Heaviside step function has two different forms:

$$H_n(x) = \frac{1+Sgn(x)}{2} \qquad \begin{cases} 0, & x<0 \\ n, & x=0 \\ 1, & x>0 \end{cases} \tag{4}$$

$$H(x) = \frac{1+Sgn(x)}{2} \qquad \begin{cases} 0, & x<0 \\ \frac{1}{2}, & x=0 \\ 1, & x>0 \end{cases} \tag{5}$$

By combining *H(x)* function with a periodic function, ECL emission intensity $I_{ECL}(t)$ can be expressed in following form:

$$I_{ECL}(t) = \frac{K}{t^{1/2}} \left(\frac{1+Sgn\left(\sin\left(\frac{\pi t}{2p_w} + \phi_0^t \right) \right)}{2} \right) \tag{6}$$

Where p_w is the CA impulse duration and $\varphi_0{}^t$ is the phase parameter in *t* space specific for each single measurement. Eq. 6 is valid under the assumption that I_{ECL} decay in successive impulses will continue from the intensity reached in

previous one. Another possibility is to assume that all impulses begin with the same I_{ECL} ;in this case $K/t^{1/2}$ must substituted in eq. 6 by:

$$\frac{K}{\left(t - \mathrm{int}(t / p_w)\, p_w\right)^{1/2}} \tag{7}$$

At this point ECL intensity registered by detector (I_{REG}) at a single wavelength λ is proportional to the product of PMT sensitivity S_{PMT} with I_{ECL} integrated over acquisition time t_c:

$$I_{REG}(\lambda) = \Phi(\lambda) \cdot \int_0^{t_C} S_{PMT}(t) \cdot I_{ECL}(t)dt \tag{8}$$

$\Phi(\lambda)$ function is introduced to take in account the dependence of emission intensity on λ and is the real spectra curve. $\Phi(\lambda)$ is normally a Gaussian or a peak function not dependent on time in the case of stable ECL emissions; for this reason has been put outside integral. S_{PMT} is for sure a constant respect to time so if we call it K_S We can write that:

$$\boxed{I_{REG}(\lambda) = K_S \cdot \Phi(\lambda) \int_0^{t_C} I_{ECL}(t)dt} \tag{9}$$

I_{REG} is an integral function which substantially depends on the overlapping between PMT detection time and ECL emission. If the signal is acquired when I_{ECL} is low or zero the integral and thus I_{REG} will tends to 0. This relation expresses the importance of temporal synchronization between signal acquisition and pulsed emission. Considering then that:

$$\lambda(t) = \lambda_0 + S_r \cdot t \tag{10}$$

where λ_0 is monochromator starting wavelength and S_r scan rate expressed in nm/s, easily follows:

$$t = \frac{\Delta\lambda}{S_r} \text{ where } \Delta\lambda = \lambda - \lambda_0 \tag{11}$$

and finally assuming for simplicity that λ_0=0 can be written:

$$t = \frac{\lambda}{S_r} \tag{12}$$

Let's consider now again eq. 9. By substituting $I_{ECL}(t)$ with explicit expression of eq. 6 We obtain that:

$$I_{REG}(\lambda) = K \cdot K_S \cdot \Phi(\lambda) \int_0^{t_C} \frac{1}{t^{1/2}} \cdot \left(\frac{1 + Sgn\left(\sin\left(\frac{\pi t}{2 p_w} + \phi_0^t \right) \right)}{2} \right) dt \tag{13}$$

By changing variable t into λ (eq.12) inside integral and under assumption that S_r is constant during measurement We obtain:

$$I_{REG}(\lambda) = \frac{K \cdot K_S \cdot \Phi(\lambda)}{S_r^{1/2}} \cdot \int_0^{\frac{\Delta\lambda}{S_r}} \frac{1}{\lambda^{1/2}} \cdot \left(\frac{1 + Sgn\left(\sin\left(\frac{\pi \cdot \lambda}{2 p_w \cdot S_r} + \phi_0^\lambda \right) \right)}{2} \right) d\lambda \tag{14}$$

Eq. 14 correlates directly ECL intensity with λ in the experimental conditions of monochromator-PMT setup. The ideal spectra is that expressed by the function $\Phi(\lambda)$ scaled by proportionality constants K, K_S (cell costant and PMT

sensitivity) and by a periodic step decaying function integrated respect to λ for the step $(\lambda-\lambda_0)/S_R$ which is a time implicit function. In this way analogously to eq. 13 the equation in λ space foresees the possibility of multiple impulses accumulation in a single wavelength measurement. An increase of S_r (scan rate) causes as expected a decrease of registered intensity and a period change in sinusoidal function. The pulse width p_W parameter is also an argument of sine and is correlated with I_{REG} period of oscillation. In our instrument S_r is not directly controllable but his value is mathematically correlated with that of $\Delta\lambda$ (MC step) and t_C (PMT acc. time) as shown in eq. 11; both this parameters are directly software adjustable. By numerically integrating eq. 14 is then possible to predict obtained spectra in given experimental conditions. Difficulties in real data reproduction arises from the fact the that experimental $I_{ECL}(t)$ function during the single step ($K/\lambda^{1/2}$ in eq. 14) can be stable (eq. 7), to evidence an intensity grow up after 0 V step or even having more than one maxima. If ECL is obtained by annihilation there is no more the 0 V potential step which is substituted by another emission peak of varied maximum intensity due to different time stability of electrogenerated cations and anions. To simulate this situation assuming for simplicity that ECL intensity is the same during oxidation and reduction is sufficient to put under absolute value the sine under Heaviside step function in eq. 13. Is also necessary to use the $I_{ECL}(t)$ function presented in eq.7. As can be easily understood real functions are not easy to manage analytically. Considering this, an empirical optimization of experimental parameters is often more convenient as shown in detail in next paragraph.

2.9
First tests and signal optimization

2.9.1
ECL spectra

Taking in account theoretical considerations of the previous paragraph is clear that differently to what happens with CCD an ECL spectra obtained with PMT as photodetector is of oscillating nature. A first series of tests has been performed with the new instrument by using the classical complex $Ru(bpy)_3^{2+}$ which gives a well known ECL spectra with maxima around 615-620 nm. Although CV can be used as switching voltage in following tests CA impulses are preferred for signal intensity maximization.

PMT Integration time effect

By using a solution 10^{-3} M of the complex and as switching potential 0.1 s oxidative and reductive alternate potential impulses a bright emission is easily observed. An orange disk of light can be seen by eye even in a lit room in correspondence of working electrode surface. Being excited state generated for cation-anion annihilation light is emitted in correspondence of cation and anion generation. The intensities of the two temporally separated emissions are never exactly coincident due to the unbalance between generated amount of cation and anion; another factor is the different temporal stability in solution of the two electrogenerated radicals. In experimental conditions used here (+1.5 and -1.5 V 0.1 potential impulses) from preliminary CA experiments cation resulted more stable and for this emission is more intense during reduction respect to oxidation. By keeping pulse width p_W constant PMT accumulation time t_C has been varied from 0.1 to 3 s. (see fig.33). As expected from eq. 13 ECL signal intensity increased and spectra become progressively continuous even if emission is pulsed. Considering in particular the case where t_C= 0.1 s depicted in fig.34 it is clear the presence of a “spike like” structure with frequent signal drops. This structure is due to the short integration time; when

t_C and p_w values are close the eq. 13 integral term depends randomly on φ_0^t which specifies from what temporal points of $I_{ECL}(t)$ spectra acquisition is started. If one single wavelength is collected during an emission peak the signal acquired will be intense, in case of emission tail medium and in case of pause close to 0. This variation of the signal is responsible of the "spiked" appearance of the spectra. By accurately observing fig.34 two domains with different density of lines are clearly visible. Those two regions are correlated to the different emission intensities during oxidation and reduction. This behaviour could be easily reproduced by introducing an $I_{ECL}(t)$ containing two peaks in eq. 13. This statement can be confirmed by observing fig. 33.b and 33.c (gear like structure). It is clear that increasing t_C to 1 and 2 s no more zero intensity signal is recorded but two different levels of emission continue to be observed. The difference between "cationic" and "anionic" emission become each time lower when t_C is increased. In fig. 33.d (t_C=3 s the $Ru(bpy)_3^{2+}$ spectra is completely continuous and no periodic signal oscillations are more present. By increasing integration interval (from 0 to t_C) in eq. 13 more and more emission peaks are collected and progressively the standard deviation between close λ integrations is lowered to negligible levels. The intensity oscillations due to irregularities on $I_{ECL}(t)$ period or to multiple time differed emission can be then statistically cancelled by increasing t_C upon time integration right to about 30 times p_W.

Monochromator Step effect

A series of two independent tests in same experimental conditions of previous paragraph have been performed by keeping costant t_C at 0.2 s and by varying $\Delta\lambda$ from 0.25 to 1 nm. (see fig. 35).

By comparing spectra (a) and (b) one can note that:

- ECL intensity is exactly the same in both spectra for all wavelength
- Spectra (b) shows a larger period of oscillation for $I_{REG}(\lambda)$.

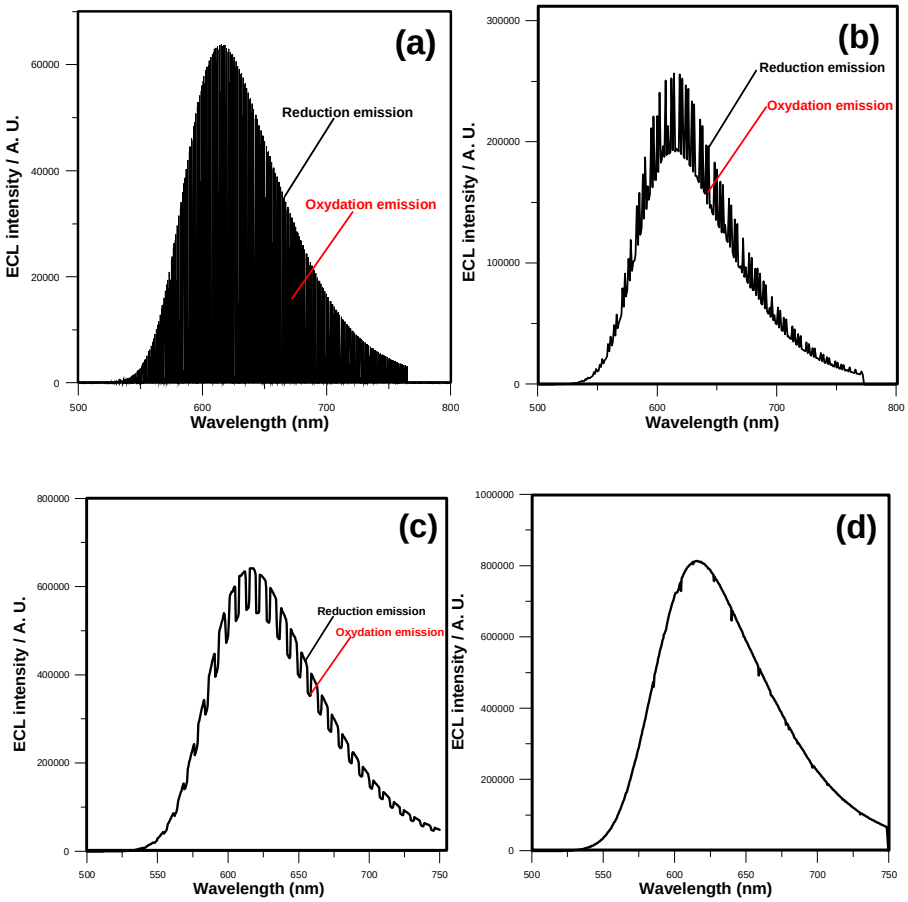

Figure 33. ECL spectra appearance for different PMT integration times(Itime) registered from a 10^{-3} M $Ru(bpy)_3^{2+}$ MeCN solution. Supporting electrolyte: $TBAPF_6$ 0.1 M; Emission mechanism: annihilation; Monocromator step: 0.25 nm; Switching method: 0.1 s CA impulses, E1 1.5V (I°Ox); E2 –1.5V (I°Red); PMT Voltage: 700. (a) Itime: 0.1 s; (b) Itime: 1 s; (c) Itime: 2 s; (d) Itime: 3 s.

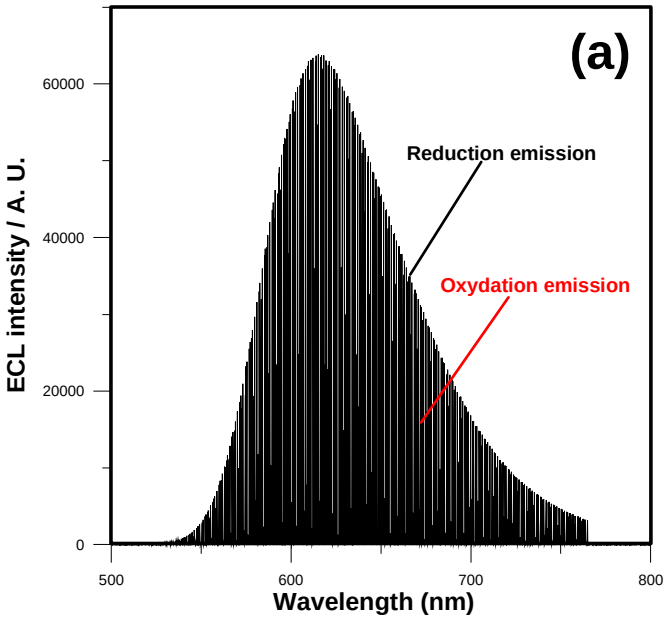

Figure 34. ECL spectra previously reported in figure 33.a is shown here with higher resolution. Two regions are clearly visible (one more dark and other more light) with the same emission maxima around 615 nm.

The fact that ECL intensity remains the same in two experiments easily follows from eq.13 because t_C is unchanged in integration interval.
About the second effect the oscillation period of $I_{REG}(\lambda)$ will depends on the argument of the sine in eq. 14 i. e. :

$$\frac{\pi \cdot \lambda}{2 p_w \cdot S_r} + \phi_0^{\lambda} \qquad (15)$$

Where φ_0^{λ} is the phase parameter in the λ space. Considering then eq.11 being t_C constant in the two experiments it follows that $\Delta\lambda$ *is* directly proportional to S_R. By increasing denominator of eq.15 the period of oscillation is

consequently increased. A similar effect can be obtained by increasing pulse width.

2.9.2
Light/current curves

Basic examples of this type of experimental curves, instrumental schemes and possible adjustments have been already introduced in sections 2.2 and 2.3. in this section will be reported a series of tests performed to check the correct operation of the new instrument under different conditions.

CV

Test were performed by using two different Ru complexes. $Ru(bpy)_3^{2+}$ was oxidized in presence of tripropylammine (NPr_3) and light/current curve was registered using a scan rate of 1 V/s. (fig. 36.a). The voltammetry at low scan rate is normally used as preliminary test to understand at which potential respect to reference electrode emission occurs. In this case being the NPr_3 in large excess respect to $Ru(bpy)_3^{2+}$ the potential of maximum emission was that of NPr_3 oxidation. (around + 1 V vs. Ag qref. electrode). Emission intensity was very high so that a 10^{-4} A/V sensitivity scale was used for PMT photocurrent amplification. The signal to noise ratio was good for i and ECL intensity.

A test in similar conditions using a lower efficiency dye, $Ru(bpy)_2(pyrtet)^+$, described and characterized in detail in next chapter, was performed to check system response to less intense emissions. By using the cation-anion annihilation mechanism emission has been detected only during reduction. (fig.36.b). An amplification factor of 10^{-6} A/V made the signal to noise ratio satisfactory. We can conclude that new instrument produced light/current vs potential curves of good quality similar to those obtained with Austin setup with both the considered dyes.

CA

light/current vs time curves have been obtained from the same $Ru(bpy)_3^{2+}$ used in CV by using fast CA impulses. During all test PMT was inserted directly into dark box close to electrode emitting surface. This test was important to check the reliability of the instrument from the point of view of sampling time. This feature was necessary because the previously described SPECTRA HUB module has been found to be too slow to follow ECL transient. By using AUTOLAB to collect signals is possible instead to sample i and ECL intensity until μs regime. Various CA tests were performed on $Ru(bpy)_3^{2+}$ by varying applied oxidative potential (+1 and +1.2 V vs Ag wire) and pulse width. (0,1 and 0.3 s). (fig. 37) . To cut out ECL signal high frequency noise and making the curve better looking has been found effective to use a sample time of 20 ms respect to lower values. Optimal amplification factor was of 10^{-5} A/V attenuated of 10 times which correspond to the range of CV. In this case however the maximum ECL intensity is higher of about one order of magnitude as expected from the higher current. CA is normally the switching method while collecting spectra; for this reason is important during preliminary CA to find the switching conditions that make ECL emission stable and of higher intensity at the same time. Comparing fig. 37.I and 37.II is evident than, using the same pulse width of 0.1 s a potential of +1.2 V is more performing than +1.0 V because stabilizes emission to higher intensities. Even if in CV the optimal potential was of +1 V at higher scan rates or during CA the effective potential applied is lower because of the higher cell resistance. An higher potential is therefore necessary to produce the same effect. Considering now experimental curves reported in fig 37.II (pulse width 0.1 s) and III (pulse width: 0.3 s) is clear that conditions in II are the optimal one. The fast time decay of ECL intensity makes short impulses more convenient. Finally can be said that new instrument succeeded in tracking ECL time transient during typical CA experiments and that a discrete reproducibility of light intensity was also observed.

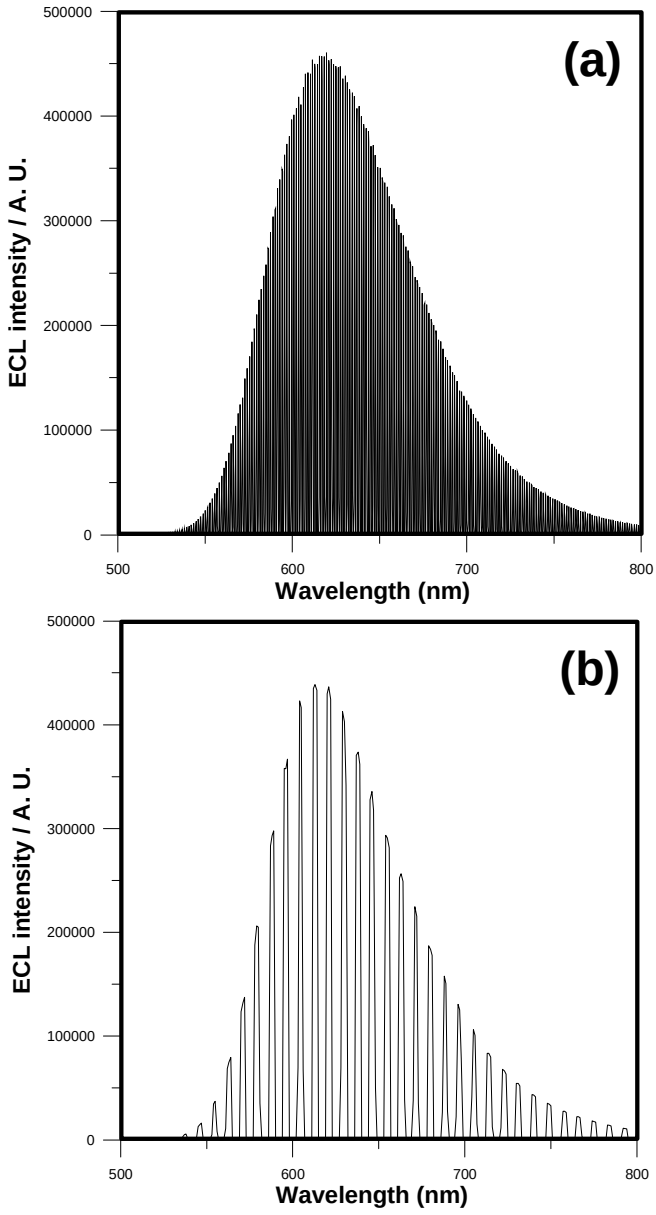

Figure 35. ECL spectra appearance for different monochromator step width at a fixed PMT integration time of 0.2 s. Experimental conditions are the same already described in fig. 33. (a) step width: 0.25 nm ; (b) step width: 1 nm.

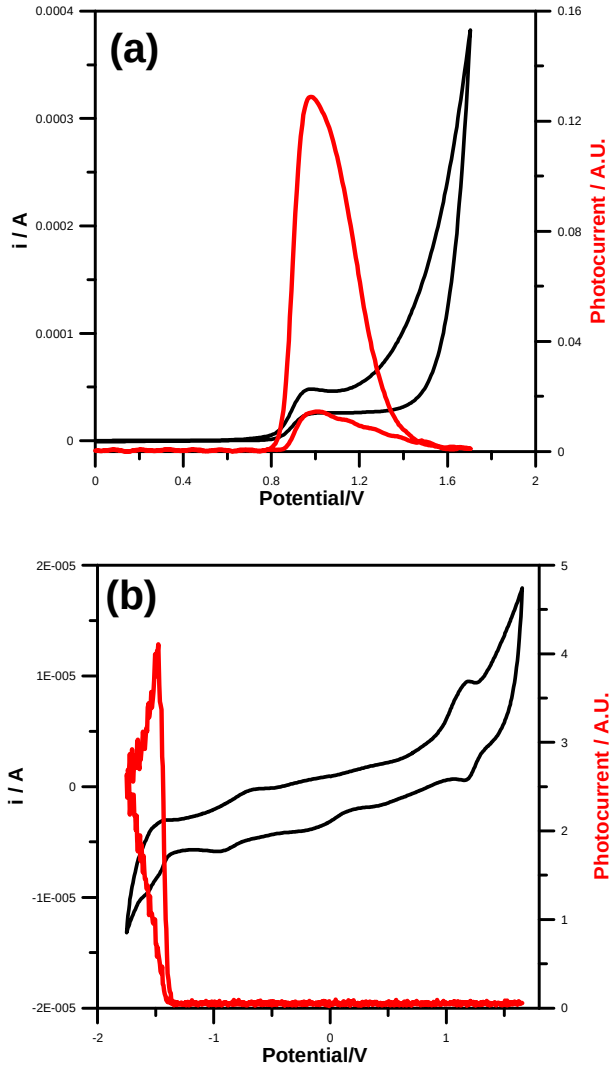

Figure 36. (a) Light current curve registered during CV from a 10^{-3} M MeCN solution of $Ru(bpy)_3^{2+}$ in presence of NPr_3 $3x10^{-2}$ M; supporting electrolyte: $TBAPF_6$ 0.1 M; scan rate: 1 V/s; PMT Voltage 750 V; Photocurrent amplification factor (PAF): 10^{-4} A/V not attenuated. (b) Light current curve registered during CV from a 10^{-3} M MeCN solution of Ru $(bpy)_2(pyztet)^{+*}$; mechanism: annihilation; supporting electrolyte: $TBAPF_6$ 0.1 M; scan rate: 1 V/s; PMT Voltage 750 V; PAF: 10^{-6} A/V not attenuated.

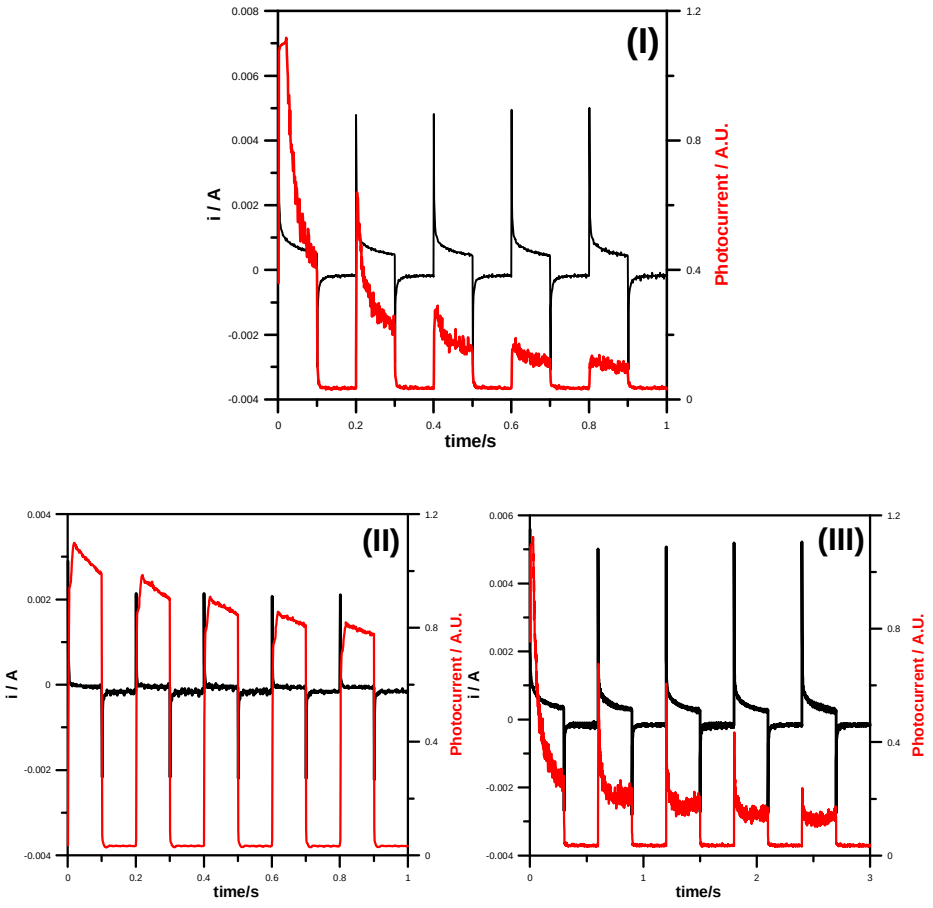

Figure 37. Light current curves registered during CA from a 10^{-3} M MeCN solution of $Ru(bpy)_3^{2+}$ in presence of NPr_3 $3x10^{-2}$ M; supporting electrolyte: $TBAPF_6$ 0.1 M; PMT voltage: 750; PAF: 10^{-5} A/V attenuated; sample time: 20 ms. (I) Potential program (PP): 0 V (1), +1.0 V(2), 0.1 s; (II) PP: 0 V (1), +1.2 V(2), 0.1 s; (III) PP: 0 V (1), +1.2 V(2), 0.3 s.

Appendix II: Electrochemical instrumentation and measurements in High vacuum conditions

Ultra-dry tetrahydrofuran, dichloromethane and tetrachloroethane are utilised as solvent due to the very large potential windows. The cell, containing the supporting electrolyte and the electroactive compound, is dried under vacuum at 370 K for at least 48 hours. Afterward the solvent is distilled by a trap-to-trap procedure into the electrochemical cell just before performing the electrochemical experiment. The pressure measured in the electrochemical cell prior to perform the trap-to-trap distillation of the solvent is typically around 1 × 10-5 mbar.

The one-compartment electrochemical cell is of airtight design, with high-vacuum glass stopcocks fitted with either Teflon or Kalrez (DuPont) O-rings, in order to prevent contamination by grease. The connections to the high-vacuum line and to the Schlenck containing the solvent is made by spherical joints fitted with Kalrez O-rings. Also the working electrode consists of a Pt disc ultramicroelectrode (with diameter of 125 μm and 25 μm), sealed in glass. The counter electrode consists of a platinum spiral and the quasi-reference electrode is a silver spiral. The quasi-reference electrode drift is negligible for the time required by a single experiment. Both the counter and the reference electrode are separated from the working electrode by ~ 0.5 cm. Further details about the electrochemical cell are described elsewhere.[5]

Potentials are measured with the ferrocene or decamethylferrocene standards and are always referred to saturated calomel electrode (SCE). $E_{1/2}$ values correspond to $(E_{pc}+E_{pa})/2$ from cyclic voltammetry (CV), whereas for irreversible processes the peak potential E_p is measured at 1 V/s. Ferrocene (decamethylferrocene) is also used as an internal standard for checking the electrochemical reversibility of a redox couple. Voltammograms are recorded with a custom made fast potentiostat[6] controlled by an AMEL model 568 function generator. Data acquisition is performed by a Nicolet model 3091 digital oscilloscope interfaced to a PC. The minimisation of ohmic drop is achieved through the positive feedback circuit implemented in the potentiostat.

References

[1] A. J. Bard, *Electrogenerated chemiluminescence*, Marcel Dekker, New York (2004).

[2] P. McCord, A. J. Bard, *J. Electroanal. Chem.* 318, 91 (1991).

[3] F. G. Gao, and A. J. Bard, *Chem. Mater*. 14, 3465 (2002).

[4] N. Tokel, A. J. Bard, *J. Am. Chem. Soc*. 94, 2862 (1972).

[5] M. Marcaccio, F. Paolucci, C. Paradisi, M. Carano, S. Soffia, C. Fontanesi, L. J. Yellowlees, S. Serroni, S. Campagna, V. Balzani, *J. Electroanal. Chem.* 532, 99 (2002).

[6] C. Amatore, C. Lefrou, *J. Electroanal. Chem.* 324, 33 (1992).

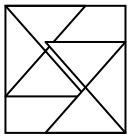

Chapter Three: new materials based on Ru

Nunc cognosco ex parte , tunc autem cognoscam, sicut et cognitus sum.
I Cor. 13, 12.

Since $Ru(bpy)_3^{2+}$ electrochemiluminescence (ECL) was discovered, photophysical properties of many Ru complexes have been investigated.[1] The intense emission of light generated by annihilation in organic solvents or in the presence of coreactant in water[2] has been extensively studied. The potential applications are correlated with the specific properties of the single compound. In organic light-emitting solid devices (OLED) tests, $Ru(bpy)_3^{2+}$ showed an intense orange emission with low applied voltages.[3-6] Molecules intended for light emitting solid devices require in general high quantum efficiencies, short response times, and high durability. Rutheniumtris(4,7-diphenyl-1,10-

phenanthroline) (normally called RuDPP or batophen) has been used as an oxygen sensor with fluorimetric detection in organic solvents and in supported silicon and xerogels films.[7] Ru(II) complexes interacting with DNA or other biomolecules often show a change in ECL intensity proportional to the concentration, and therefore, many analytical methods based on ECL have been developed.[2,8] In this chapter ECL emission properties of new sinthesized Ru(II) complexes containing tetrazolate group as a ligand are described. The new dyes have been tested under various experimental conditions in solution and solid state. The addition or removal of small groups around the tetrazolate moiety allowed us to study the effect in MLCT (metal-to-ligand charge transfer) transitions. The modification of ECL spectra is often remarkable even in relatively similar molecular structures. To detect biomolecules such as nucleic acids and proteins, the use as covalent labels[2] could be possible because of considerable quantum efficiency and red shift of some of the compounds with respect to $Ru(bpy)_3^{2+}$.

3.1
Complexes containing Tetrazolate based mono-coordinating ligands.

3.1.1.
Electrochemical Behaviour of selected Ligands and Complexes.

Before to perform ECL characterization of a new compound is of fundamental importance to understand what radical species can be generated electrochemically and energetic states involved. Without this basic information is not possible to give a correct interpretation of ECL emission spectra or of relative light/current curves. The behaviour and properties of some representative molecules and ligands behaving to the class of molecules studied has been thoroughly investigated in ultra clean conditions.[9] Selected compounds and chelating groups are shown in Fig. 1. Details on synthesis and structural characterization are out of the scope of this thesis therefore main

chemical reactions involved in new dyes preparation are summarized in fig.2, 3 and 4.

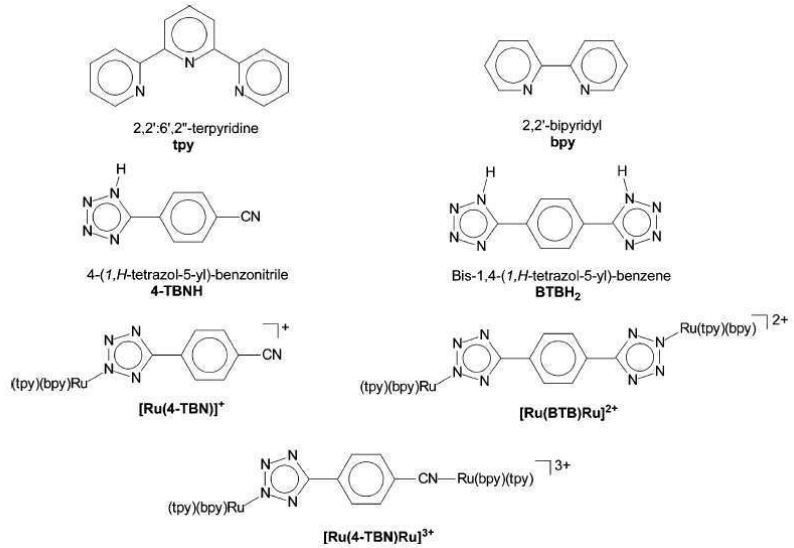

Figure 1. Structures and acronyms of compound and ligands investigated electrochemically in detail.

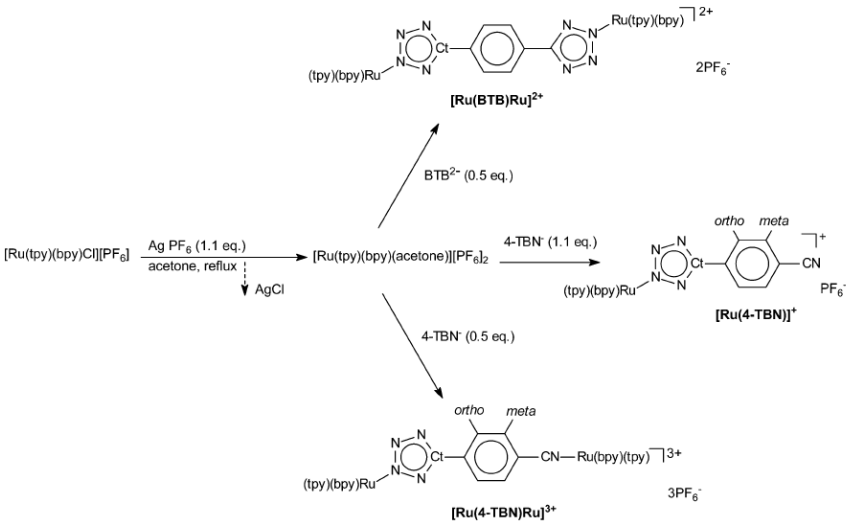

Figure 2. Scheme of the basic synthetic steps used to obtain the complexes introduced in fig.1.

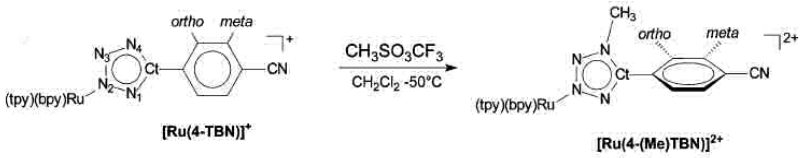

Figure 3. Reactions conditions for $[Ru(4\text{-}TBN)Ru]^{+}$ methylation.

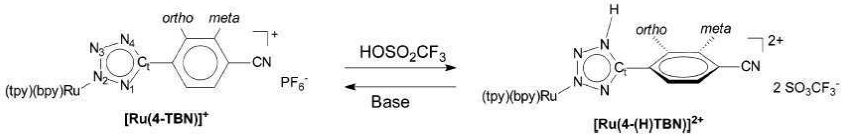

Figure 4. Scheme of chemical hydrogenation of $[Ru(4\text{-}TBN)Ru]^{+}$.

Uncoordinated Ligands. It is well established that the redox processes in Ru(II)-polypyridine complexes are mainly localized either on the metal center (oxidations) or on the ligands (reductions).[1,10,11] It is, therefore, of fundamental importance to know the electrochemical behavior of the uncoordinated ligands to understand the pattern of the ligand based redox series for the complexes. The electrochemistry of the uncoordinated ligand **bpy**[12] has been previously studied under the same experimental conditions used for this work. We investigated the redox behavior of the ligands 4-TBN and BTB, to our knowledge for the first time, either as their tetraphenylarsonium salts or N-protonated species, while tpy was reinvestigated in DMF under strictly aprotic conditions, both at room and low temperature.

4-TBN. The free ligand exists as the N-protonated species 4-TBNH and was investigated in ACN and DMF solutions both in its deprotonated form (i.e. 4-TBN) and as 4-TBNH. In acetonitrile the 4-TBNH shows two one-electron reductions but no oxidation process is observed up to + 2.5 V (vs SCE). Figure 5.a shows the CV of 4-TBNH, in DMF at 24 °C and a scan rate, *v*, of 1 V/s;

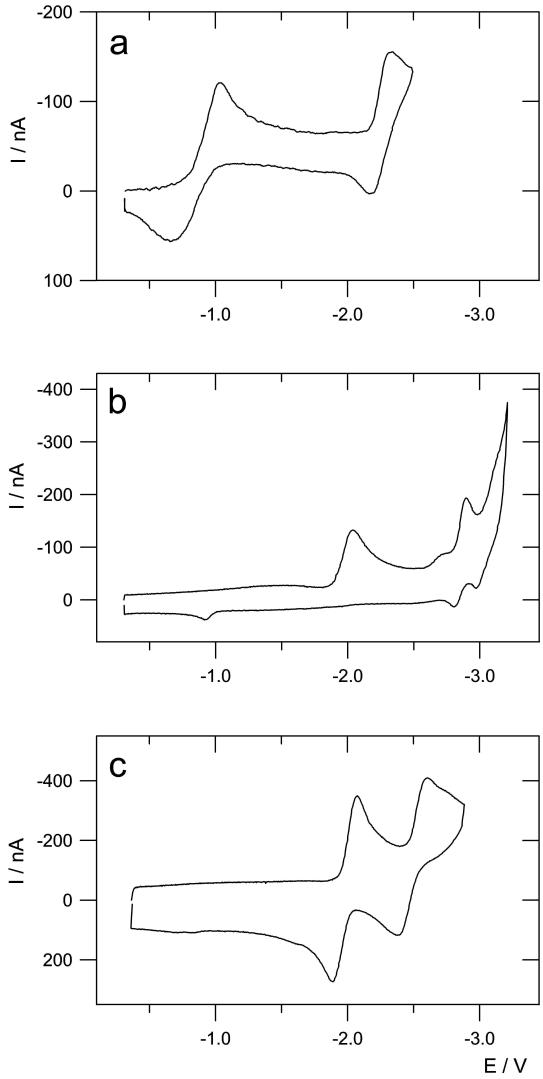

Figure 5 . Cyclic voltammetric curves of uncoordinated ligands. (a) 4-TBNH 1mM in a 0.05M TEATFB (Tetraethylammonium tetrafluoroborate)/DMF solution; Working Electrode Pt; T= 24°C; scan rate 1 V/s. (b) BTB 1 mM in a in a 0.05M TEATFB/DMF solution; Working Electrode Pt; T= 24°C; scan rate 10 V/s. (c) tpy 2 mM in a 0.07M TEATFB/DMF solution, working electrode Pt, T= -56°C , scan rate 100 V/s.

the first reduction wave exhibits some degree of electrochemical irreversibility, most likely due to internal rearrangements related to proton migration onto the nitrogens of the tetrazole ring, while the second reduction is Nernstian. The standard potentials of the processes are collected in Table 1, together with those of the other species.

BTB. The $BTBH_2$ ligand has been investigated as the deprotonated species (i.e. the BTB species) in DMF at room and low temperature. It shows three reductions: the first is completely irreversible even at 200 V/s while the further two processes are reversible. Although the third reduction occurs at the edge of the electrolyte/DMF discharge, it can still be observed as a reversible process. Figure 5.b shows the cyclic voltammetric curve of BTB at 24 °C and at 10 V/s. Just before the second voltammetric peak, there is a shoulder whose nature is still under investigation but is probably related to a species generated in a follow-up reaction.

tpy. The voltammetry of uncoordinated terpyridine, previously investigated,[13] shows a one-electron reduction process. It was reinvestigated in DMF, to compare it to the other ligands and complexes under the same strictly aprotic conditions, and it exhibits two reduction peaks both at room and low temperature. The first reduction is a one-electron Nernstian process while the second one-electron reduction shows chemical irreversibility at room temperature but becomes reversible at low temperature and at scan rates higher than 100 V/s. Figure 5.c shows the CV of tpy at -56 °C and 100 V/s. The $E_{1/2}$ values of the two processes are given in Table 1. The separation between them is 520 mV, and this value falls within the typical range (500-600 mV) for the electronic coupling energy[14] into the same orbital of polypyridyl ligands. The chemical follow-up reaction is probably a proton uptake process of the doubly reduced tpy with the solvent. This reaction is a rather fast process even at low temperature, and the voltammetric pattern is similar to other polypyridyl

ligands in the uncoordinated state[12] that are known to undergo fast protonation reactions in the doubly reduced state.

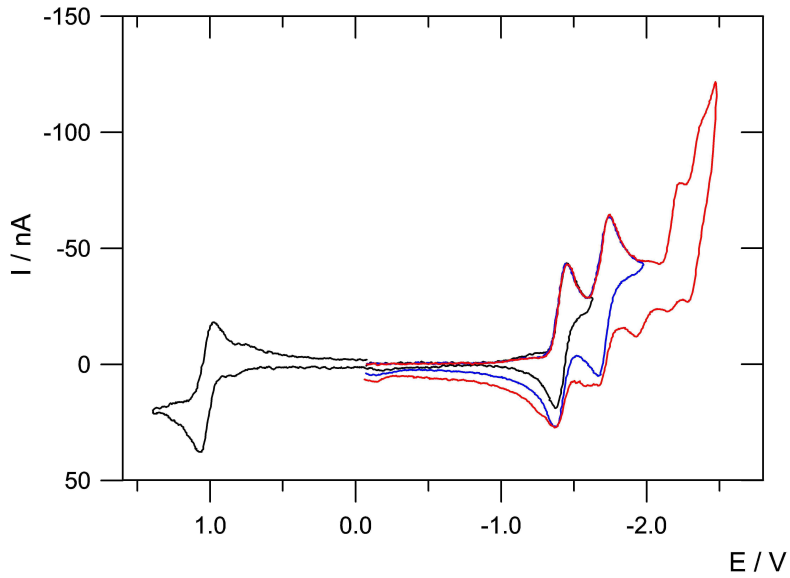

Figure 6 . Cyclic voltammetric curve for 1 mM mononuclear complex $[Ru(tpy)(bpy)(4BTN)]^+$ in a 0.06 M TBAH/ACN solution. Working electrode Pt, T= 25°C, scan rate=1 V/s.

Ruthenium Mono- and Dinuclear Complexes.

$[Ru(4\text{-}TBN)]^+$. Within the framework of the general strategy for the investigation of multinuclear species, showing a large number of redox processes, this species was studied since it represents a precursor or a model for the behavior of the dinuclear ones. The electrochemistry of the complex $[Ru\text{-}(4\text{-}TBN)]^+$ was investigated in ACN both at room temperature and at -45 °C. In both cases it shows four one-electron reduction processes and a one-electron oxidation. The first two reductions are completely reversible whereas the successive two are affected by chemical follow-up reactions. With increase of the sweep rate, the extent of the chemical irreversibility decreases, even though it still remains at 100 V/s. As a consequence of the chemical

irreversibility of the third process, an anodic peak appears on the reverse scan, at about -1.9 V (Figure 6). The chemical process associated with the third reduction probably involves protonation, either by the solvent or the electrolyte, of one of the tetrazolate nitrogens, whose basicity is increased when the other two ligands are reduced. The oxidation process appears chemically and electrochemically reversible at 1 V/s. As the scan rate is increased, the process reveals some degree of electrochemical irreversibility. The simulation of the cyclic voltammetric curve[15], comprising the oxidation and the first reduction wave, confirms that the oxidation is not a fully Nernstian process. A satisfactory agreement of the simulated curve with the experimental one is obtained when the heterogeneous constant k_h for the oxidation process is $4x10^{-2}$ cm/s and the electron-transfer coefficient R of the Butler-Volmer equation is 0.34. By contrast, the reduction process is satisfactorily simulated as a fast (diffusion-controlled) electron transfer. This can be understood on the basis of quantum molecular orbital calculations, carried out at DFT level[16], where it is shown that the HOMO spans over the metal centers and part of the bridging ligand, in particular on the tetrazolate ring (see the corresponding dinuclear species, Figure 9.a). The sluggishness of the electron transfer is therefore most probably associated with molecular rearrangement of the tetrazolate ligand, following the oxidation process. However, the reductions are centered onto the polypyridine ligands (vide infra), as also evidenced by the calculations, and these are intrinsically fast processes.

$[Ru(4\text{-}TBN)Ru]^{3+}$. On the basis of the behavior of the mononuclear species, which is one of the two constituent moieties of the complex $[Ru(4\text{-}TBN)Ru]^{3+}$, it is possible to rationalize the electrochemistry of the dinuclear species, whose cyclic voltammetric curve is shown in Figure 7. The bridging ligand can be considered as electronically asymmetric because the two coordinating nitrogens are chemically different: one belongs to the tetrazolyl ring and bears

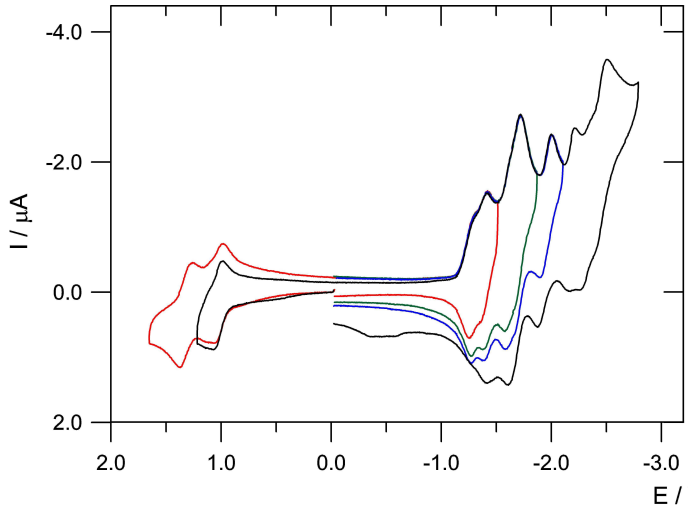

Figure 7 . Cyclic voltammetric curve of 1 mM of dinuclear complex $[Ru(4\text{-}TBN)Ru]^{3+}$ in 0.05 M TBAH/ACN solution. Working electrode Pt, T= 25°C, scan rate= 1 V/s.

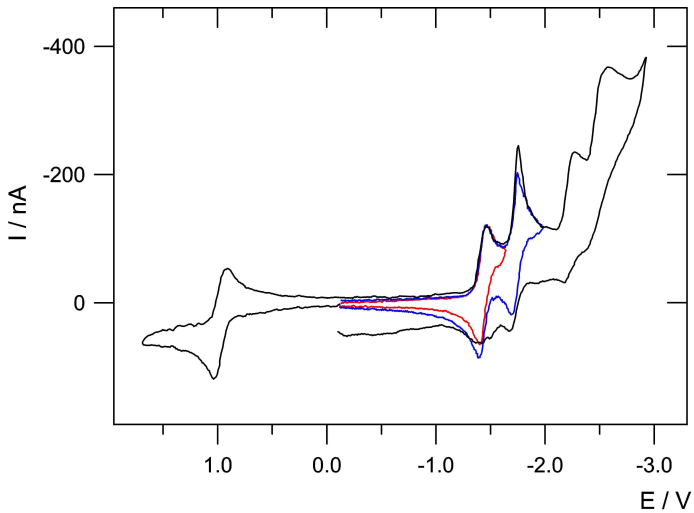

Figure 8 . Cyclic voltammetric curve of 1 mM of dinuclear complex $[Ru(BTB)Ru]^{2+}$ in 0.05 M TBAH/ACN solution. Working electrode Pt, T= 25°C, scan rate= 1 V/s.

a partial negative charge while the other can be considered to be a nitrile-N for its coordinating properties. The voltammetric curve shows five reduction peaks and two oxidation ones. Concerning the oxidations, the two peaks are both reversible one-electron processes, centered on the two Ru(II) centers. The sizable separation between the oxidations suggests a quite strong metal-metal bridge mediated interaction, but it could also be ascribed to the electronically asymmetric coordinating ends of the bridging ligands, giving rise to two nonequivalent ruthenium centers with different oxidation potentials. Probably this potential separation arises from an interplay of these two effects, with the second more important. A comparison of the $E_{1/2}$ potentials of the first oxidation of this dinuclear complex with that of the oxidation of the mononuclear precursor species $[Ru(4\text{-}TBN)]^{+}$ shows that the processes happen at the same value. Therefore the first oxidation of the dinuclear is centered on the ruthenium bound to tetrazolate moiety of the bridging ligand. A DFT calculation also supports this assignment of the oxidation processes to the HOMO mainly centered onto the ruthenium coordinated to tetrazole (Figure 9.a) and the second highest occupied MO onto the second metal center, coordinated to the nitrile end of the bridge.

$[Ru(BTB)Ru]^{2+}$. The voltammetric behavior of the dinuclear complex carrying the symmetric BTB bridging ligand is shown in Figure 8, and it consists of five voltammetric peaks: one in the oxidation region and the remaining in reduction. All the peaks are two-electron processes, as evidenced by chronoamperometric measurements. The electrochemical behavior is very similar to that of the mononuclear $[Ru(4TBN)]^{+}$ species which is, in fact, the building block of the dinuclear complex $[Ru(BTB)Ru]^{2+}$. The cyclic voltammetric curve shown in Figure 8 suggests that the first two reduction peaks are strongly affected by adsorption or precipitation phenomena. Moreover, the processes in the last two peaks are partially affected by chemical follow-up reactions. The electron-transfer processes in each of the voltammetric peaks are very close each other, and the evaluation of the $E_{1/2}$

values was carried out by digital simulation of the voltammetric curves. Accordingly, the two processes comprised in each peak have a separation in the range 30-60 mV (see Table 1), which is slightly larger than the separation due to the statistical factor for systems with very weakly interacting redox centers.[17] Thus, there is little delocalization across the BTB bridge, suggesting the same holds true for the 4-TBN-bridged species, as also indicated by DFT calculations. To understand the main localization of the reduction processes for the mono- and dinuclear complexes, the behaviour of the uncoordinated ligands must be taken into account, together with a comparison of the $E_{1/2}$ values of the corresponding processes for related complexes and results of the quantum molecular calculations. The reduction processes of the mononuclear species $[Ru(4\text{-}TBN)]^{+}$ can be assigned as follows: The first is attributed to tpy, since it is slightly easier to reduce than bpy, and hence, the subsequent reduction is centered onto bpy. The third process might be reasonably assigned to 4-TBN, and the last represents the second reduction (electron pairing into the same redox orbital) of the tpy. However, if the voltammetric curve (see also the $E_{1/2}$ values in Table 1) of the mononuclear is compared with those of the dinuclear species $[Ru(4\text{-}TBN)\text{-}Ru]^{3+}$ and $[Ru(BTB)Ru]^{2+}$, the last two processes of the mononuclear should be assigned to the second reduction onto tpy and bpy, respectively.

	oxidn $E_{1/2}$/V		redn $E_{1/2}$/V				
species	1	2	I	II	III	IV	V
tpy[a]			−1.98	−2.50			
4-TBNH[a,b]			−0.87	−2.24			
BTB[a]			−2.03[c]	−2.85	−3.05		
$[Ru(4\text{-}TBN)]^{+}$ [b]	1.02		−1.42	−1.71	−2.19	−2.34	
$[Ru(4\text{-}TBN)Ru]^{3+}$ [b]	1.02	1.32	−1.28	−1.63	−1.96	−2.19	−2.36
			−1.40	−1.70			−2.47
$[Ru(BTB)Ru]^{2+}$ [b]	1.01	1.03	−1.41	−1.71	−2.19	−2.45	
			−1.45	−1.74	−2.24	−2.52	

[a] TEATFB/DMF solution. [b] TBAH/ACN solution. [c] Cathodic peak potential.

Table 1. $E_{½}$ redox potentials (vs SCE) of the uncoordinated ligands, mono- and dinuclear Ruthenium complexes.

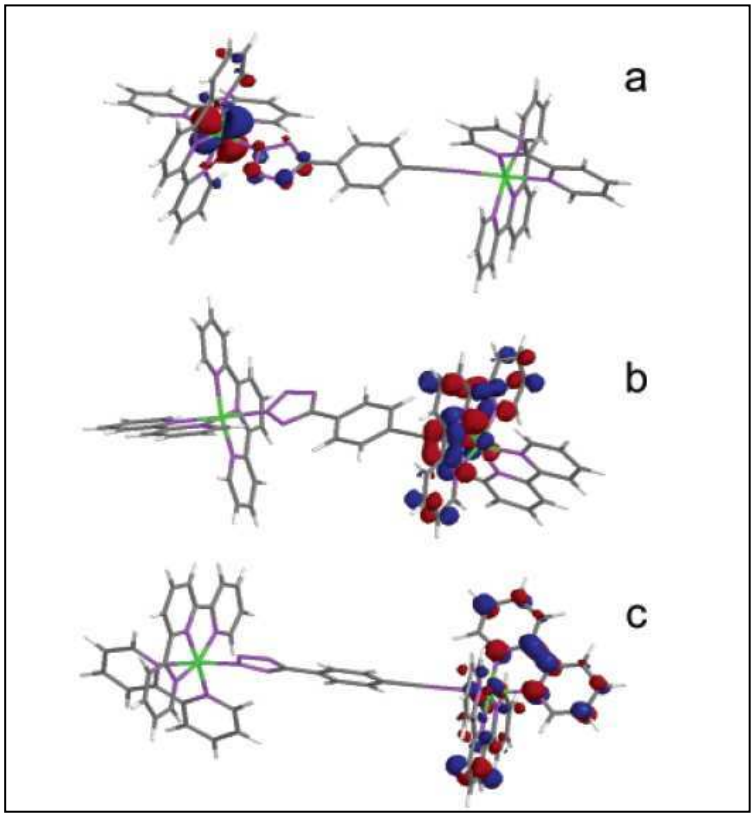

Figure 9. Molecular orbital surfaces of $[Ru(4\text{-}TBN)Ru]^{3+}$ showing the localization of relevant orbitals involved in the redox processes: (a) HOMO (first oxidation) mainly centered on the ruthenium coordinated to tetrazolate; (b) LUMO (first reduction) centered on the tpy; (c) third unoccupied MO (third reduction process) centered on bpy ligand.

Such an attribution is also supported by the separation between the first and the second set of peaks (i.e. between the second and third one), which reflects the energy of electron pairing into polypyridyl ligands. Thus the reduction centered onto 4-TBN is not observed since it is outside the negative limit of the useful potential window. On the basis of the assignments of reductions for $[Ru(4\text{-}TBN)]^{+}$, we can obtain those for $[Ru\text{-}(4\text{-}TBN)Ru]^{3+}$. The processes within the first two peaks are localized onto the two tpy's and the two bpy's. As expected, molecular orbital calculations indicated that the first reduction is localized on the tpy bound to ruthenium coordinated to the nitrile end of the 4-

TBN bridging ligand (Figure 9.b). Again, the first bpy to undergo reduction (i.e. the third one) is that coordinated to the ruthenium-nitrile moiety, as shown in Figure 9.c by the prevalent localization of the third unoccupied MO. The fifth reduction (i.e. the third peak) has a potential which does not match any process in the corresponding mononuclear species, and then it can be confidently attributed to the bridging ligand 4-TBN. The coordination to two metal centers shifts the unobservable process in the mononuclear to one occurring at less negative potentials, falling within the useful potential window. The process in the fourth peaks and the two in the fifth peak can be attributed as the second reduction of three out of four polypyridyl ligands (tpy and bpy), on the basis of the comparison of the $E_{1/2}$ values in Table 1. Finally, the localization of the reductions for the $[Ru\text{-}(BTB)Ru]^{2+}$ is quite straightforward comparing the CV curves and the potentials of processes. The first pair of two electron peaks represents the first reduction of the two tpy's and two bpy ligands. The last two peaks (four electrons) are the electron couplings onto the same redox orbital centered on each polypyridine.

3.1.2.
Photophysical and ECL properties

In the following paragraph photoluminescence (PL) and ECL characterization of six promising new complexes (Fig. 10) containing mono-coordinating tetrazolate group as ligand will be reported. Even if electrochemical behaviour of three over six dyes ($[Ru(4\text{-}TBN]^{+}$, $[Ru(4\text{-}TBN)Ru]^{3+}$ and $[Ru\text{-}(BTB)Ru]^{2+}$) in ultra "clean" conditions has been presented in previous paragraph considering that experimental conditions are varied a short section has been introduced to clarify experimental procedures . A recalculation of $E_{1/2}$ for for first oxidation and reduction processes was also necessary for all compounds to allow a direct comparison of ECL properties .

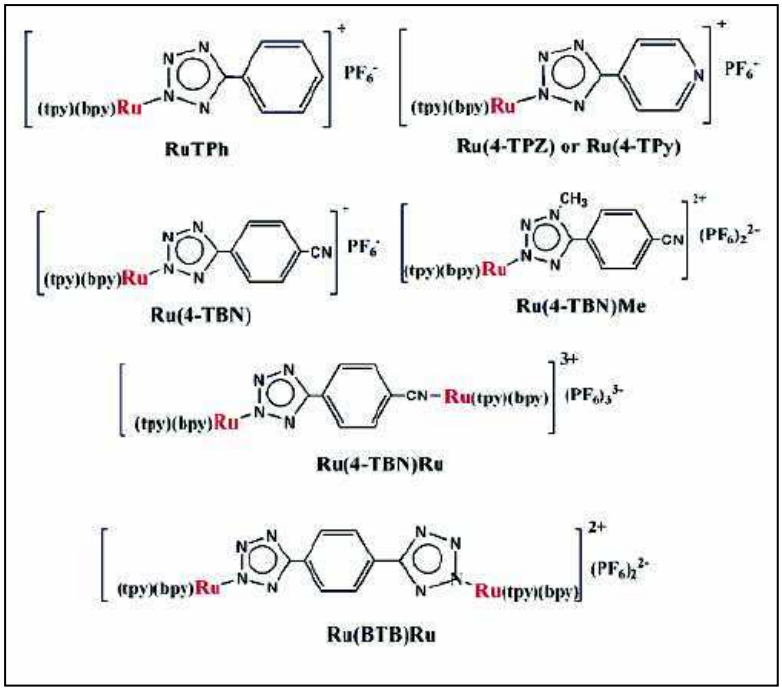

Figure 10. Structure and acronyms of the molecules which ECL emission properties are investigated.

The synthesis of the new cationic complexes Ru(TPh) and Ru(4-Tpy) has been performed by adopting the same two-step procedure showed in fig.2 and used with other complexes . This latter involved the preliminary chloride abstraction from the precursor species [Ru(tpy)(bpy)Cl][PF_6] followed by reaction with the desired tetrazolate ligand.

Experimental procedures

Electrochemistry and ECL. Cyclic voltammetry was carried out with a model 660 electrochemical workstation (CH Instruments, Austin, TX). Electrodes were polished with 0.05-μm alumina and then were ultrasonicated and thoroughly rinsed with Milli-Q water and acetone before each run. The quasi reference electrode was a coiled silver wire. A platinum disk (approximate

diameter 2 mm) was used as working electrode and a coiled Pt wire was used as an auxiliary electrode. The $E_{1/2}$ values for first reduction and oxidation are referred to SCE (saturated calomel electrode) and They have been calculated adding ferrocene as an internal standard. In ECL and electrochemical experiments acetonitrile (Fisher scientific HPLC grade) was used as received and 1 mM solution of the complex (as PF6- salt) was prepared with 0.1 M $TBAPF_6$ (Aldrich) as supporting electrolyte. Similar results were obtained with $TBABF_4$ (Aldrich). Before each ECL experiment, the sample was deaerated with Ar for 20 minutes in a specially made cell (see fig. 7 and 13 chapter 2). The exact concentration of oxygen in solution following deaeration was not measured. Preliminary potential cycling was performed systematically until a reproducible voltammogram between the first reduction and the first oxidation was obtained. The ECL signal during cyclic voltammetry was measured with a photomultiplier tube (PMT, Hamamatsu R4220p) placed on the side of the electrochemical cell. A voltage of 750 V was supplied to the PMT. A charge-coupled device (CCD) camera (Photometrics CH260) cooled below –135 °C interfaced to a personal computer was used to obtain ECL spectra. The camera was focused on the output of a grating spectrometer (Holographics, Inc.). Experimental setup in Austin has been described in detail in section 2.2. All ECL spectra have been recorded with a pulse width of 0.1 s and a 4 min exposure time.

Photoluminescence and lifetime. Photoluminescence (PL) measurements were performed with a Varian Cary Eclipse fluorimeter in acetonitrile (Fisher Scientific HPLC grade) with concentrations between 10^{-3} and 10^{-5} M. PL experiments were performed after 20 min degassing with Ar in a specially homemade O-ring sealed cell. (fig. 11) Samples were then progressively exposed to air to study oxygen sensitivity. Absorbance spectra were recorded by a Varian Cary 5 UV-vis-NIR spectrophotometer using the same sealed cell used for photoluminescence measurements in MeCN solutions. Lifetimes were measured in an air equilibrated sample using an IBH TCSPC model 5000 F (time correlated single photon counting) with a PMT detector (Applied

Voltage: 2150 V). The emission wavelength was selected by a computer-controlled monochromator. Two cut-offs (590 and 610 nm) were used during measurements. Lifetimes were then calculated by fitting the data with a single exponential decay function.

Figure 11. Homemade cuvette intended for fluorescence experiments in vacuum or degassed solutions.

Solid devices preparation. Light emitting solid devices were prepared as reported previously with $Ru(bpy)_3^{2+}$ by Bard and co-workers.[18,19] The inorganic thin layer was prepared on ITO glass (Delta Technologies, Ltd., 100 Ω, square) by spin coating from a MeCN solution (1-4 % w/v of complex). A small drop of In/Ga eutectic (from Aldrich) over the active layer, was used as counter electrode and connected to the reference electrode lead. Positive charge was injected through the underlying ITO glass used as working electrode (for a scheme see Fig. 5 of chapter 2). For Ru(4-TBN)Ru and Ru(4-TBN)Me complexes both spin coating and an alternative film deposition method were used: a few drops of an acetonitrile solution (0.1 up to 2 % w/v) were dried in air on ITO surface. In this way a thicker film could be obtained. Light intensity was measured using a photodiode positioned under the emitting thin layer as depicted in section 2.2.

Electrochemiluminescence.

The ECL spectra of a 1 mM Ar degassed acetonitrile solution of $Ru(bpy)_3(PF_6)_2$ obtained by direct annihilation between cation and anion has been taken as reference. The sample was run several times and the highest emission intensity was of 300,000 A.U. with maxima at 610 nm. Detailed voltammetric studies under ultra dry conditions ($MeCN/TBAPF_6$) have been reported in previous paragraph for Ru(4-TBN)Ru, Ru(BTB)Ru, and Ru(4-TBN). For the remaining three complexes and the reference $Ru(bpy)_3^{2+}$ the cyclic voltammetric curves in Ar degassed MeCN are showed in Figure 12. In the cyclic voltammetry experiments preliminary to ECL ones the complexes showed in general chemical reversibility in first oxidation and reduction wave (i_a/i_c very close to 1). If the scan was repeated for 100 cycles including only the first reduction and oxidation (scan rate 10 V/sec) no change in reversibility was observed. For all the complexes, including $Ru(bpy)_3^{2+}$, the presence of oxygen seriously affects the quality of reduction wave which becomes irreversible when the cell is air equilibrated (see Figure 12.b). Ru(4-TBN)Ru shows two reversible oxidation processes and two very close reduction waves assigned to weakly interacting Ru centers bridged by the asymmetric ligand as also stated in previous paragraph. Fluorescence, ECL and electrochemical data for all complexes and the reference one are summarized in Table 2. All molecules evidenced a smaller energy gap ($[E_{I,ox}-E_{I,red}]$, expressed in eV) with respect to the reference and the ECL maximum wavelength is always red shifted with respect to $Ru(bpy)_3^{2+}$. Upon changing the substituent, the emission shifts from 690 nm to 740 nm (see Table 2, Figure 13 and Figure 14). In general the ECL maxima are also red shifted from the corresponding PL by about 10-50 nm.

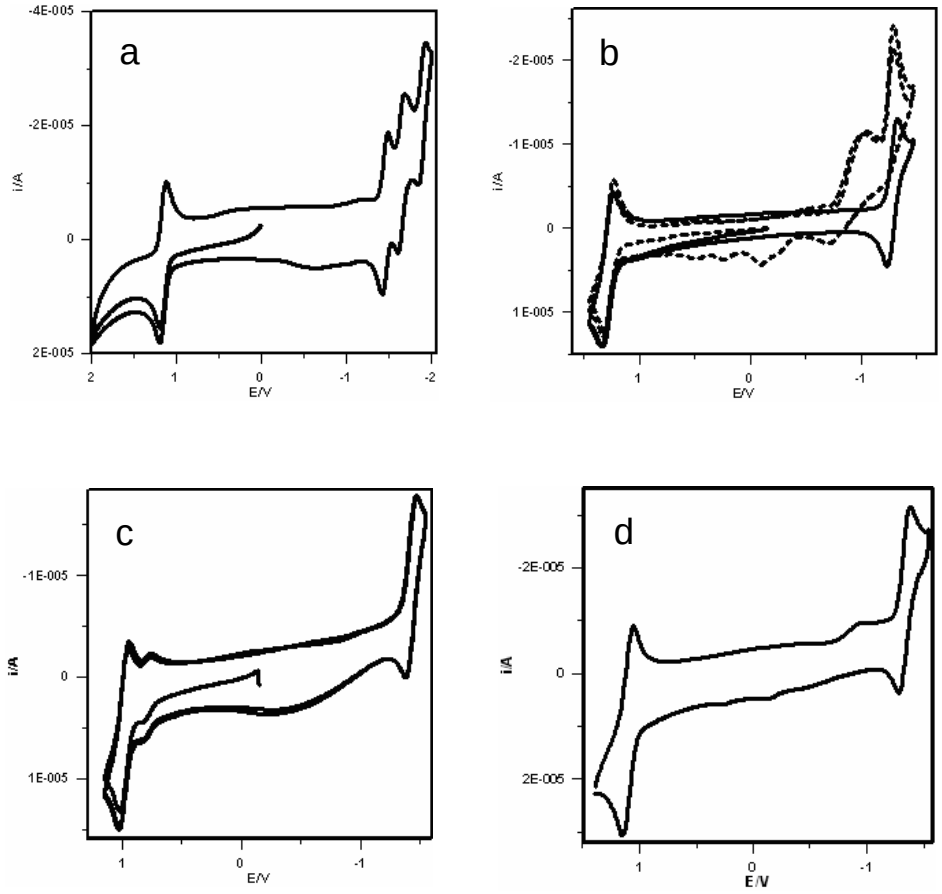

Figure 12. Cyclic voltammetric curves of 1 mM complexes in 0.1 M $TBAPF_6$/MeCN solution recorded with a 2 mm diameter Pt disk working electrode; T= 25 °C; scan rate 0.2 V/s. (a) $Ru(bpy)_3^{2+}$; (b) Ru(4-TBN)Me, air equilibrated (dashed line) and degassed (solid line) solution; (c) Ru(TPh). The small voltammetric wave at about 0.8 V is attributed to the oxidationprocess of the precursor species [Ru(tpy)(bpy)Cl]+, which is not luminescent; (d) Ru(TPy). In all voltammograms potential is referred to SCE.

compound	λ_{max},abs/nm (MLCT)	λ_{max},PL/nm	ϕ_{rel} (%)	E (I Ox.)/V (vs SCE)	E (I Red.)/V (vs SCE)	λ_{max},ECL/nm	most stable ion in ECL
$Ru(bpy)_3^{2+}$	455	630	100	+1.20	−1.48	610	anion
Ru(4-TPZ)	487	690	7.4	+1.12	−1.31	690	anion
Ru(4-TBN)Me	463	660	11.6	+1.25	−1.34	720	cation
Ru(4-TBN)	487	670, 700	5.7	+1.01	−1.42	730	anion
RuTPh	487	690	7.2	+1.03	−1.39	740	anion
Ru(BTB)Ru	487	690	9.0	+1.01	−1.39	700	cation
Ru(4TBN)Ru	460, 490	670, 700	15.3	+1.02	−1.35	690	anion

Table 2. PL, ECL and electrochemical data of the $Ru(bpy)_3^{2+}$ (reference compound) and the six complexes investigated. Energy gap can be estimated by the electrochemical data. The most stable ion was determined during ECL experiment comparing the relative light intensity during positive and negative potential pulse in chronoamperometry. φ_{rel}(%) is calculated taking $Ru(bpy)_3^{2+}$ as reference (100% efficiency).

ECL intensities for mononuclear compounds (see Figure 13) are lower than for $Ru(bpy)_3^{2+}$ but of the same order of magnitude. ECL spectra of the dinuclear complexes Ru(4-TBN)Ru and Ru(BTB)Ru with respect to $Ru(bpy)_3^{2+}$ under the same experimental conditions described above are shown in fig. 14. The relative ECL quantum efficiency for the six complexes are shown in Table 3. One of the two dinuclear Ru complexes, Ru(4-TBN)Ru, shows an emission about three times more intense than the reference one, which can be observed by naked eye in a dark room. The emission intensity can be tuned by simply including or not the second reduction and oxidation wave. The emission peak recorded by CCD is not symmetric; a tail at longer wavelength is clearly visible. The spectral resolution in the ECL experimental set-up does not allow one to clearly separate the lower energy shoulder as in PL experiments. Considering the four different mononuclear complexes the higher efficiency was for the ligands containing tetrazolate bound with pyridine and benzene. The introduction of the cyanide group in RuTPh (i.e. the species Ru(4-TBN)) causes a decrease of ECL intensity of about 75 %. When a methyl group is then inserted directly on the tetrazolate ring (Ru(4-TBN)Me) the intesity went back to higher values. Another interesting comparison is between Ru(4-TBN) and Ru(4-TBN)Ru.

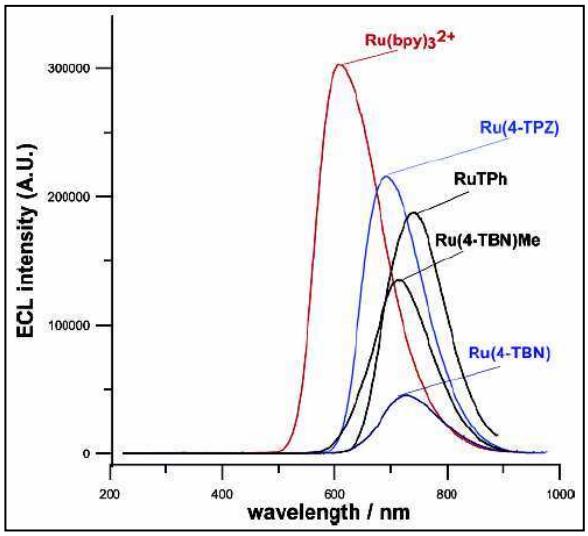

Figure 13. ECL emission spectra of the four mononuclear tetrazolate -based complexes, obtained by annihilation of one-electron oxidized and reduced forms. All ECL spectra were collected for 1 mM compound in 0.1 M TBAPF6/MeCN solution, T=25 °C and accumulation time 4 min.

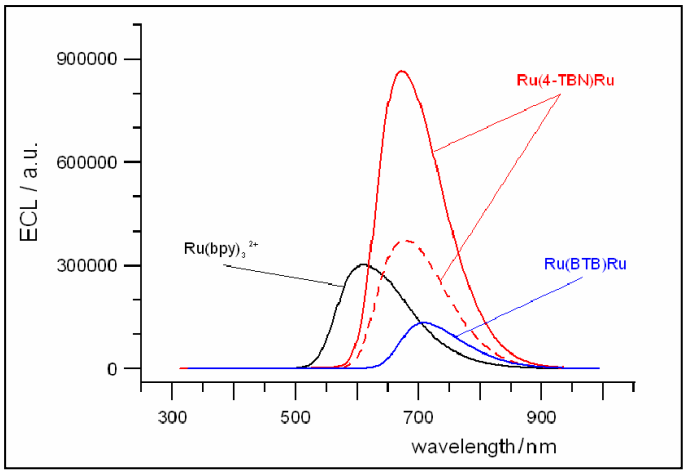

Figure 14. ECL spectra of the reference compound $Ru(bpy)_3^{2+}$ (black trace), Ru(BTB)Ru (blu trace) and Ru(4-TBN)Ru (red traces: dashed line spectrum obtained by annihilation of one-electron oxidized and reduced forms; solid line for the doubly oxidized and reduced forms of complex). All ECL spectra were collected for 1 mM compound in 0.1 M TBAPF6/MeCN solution, T=25 °C and accumulation time 4 min.

compound	max ECL intensity (A.U)	rECL-Int. (%)
Ru(4-TPZ)	227 869	75
Ru(4-TBN)Me	135 405	45
Ru(4-TBN)	45 625	15
RuTPh	187 232	62
Ru(BTB)Ru	134 928	45
Ru(4TBN)Ru[b]	372 410 (I Ox., I Red.)	120
	864 597 (II Ox., II Red)	290
$Ru(bpy)_3^{2+}$ (ref)	303 181	100

Table 3. Estimated Relative ECL Emission Efficiency of 1 mM Complex in 0.1 M $TBAPF_6$/MeCN Solution ($Ru(bpy)_3^{2+}$ Used as Reference)[a] Cycling the Potential between the $I_{Oxidation}$ and $I_{Reduction}$. [a]The relative ECL intensities (rECL-Int.) have been calculated by the formula: $rECL\text{-}Int.(\%) = 100*(I_{ECL,MAX}/I_{ECL,MAX,Ru(bpy)})$ [b] The potential has also been cycled between II Ox. and II Red.

The addition of a second Ru(bpy)(tpy) center causes an increase of ECL efficiency of six times. As stated above, the two Ru centers in Ru(4-TBN)Ru behave independently so the inclusion of the second oxidation and reduction localized on the second Ru center causes the ECL intensity to double. Considering the tetrazolate complex Ru(4-TBN)Ru with respect to $Ru(bpy)_3^{2+}$ PL relative quantum efficiency is 15.3 % (φ_{rel} in Table 2) and relative ECL is 123 % (rECL-Int in Table 3). The mismatching of photo- and electrochemiluminescence is necessarily correlated with processes prior to generation of the excited emitting state. The moderate presence of oxygen has been found to affect ECL efficiency of $Ru(bpy)_3^{2+}$ much more than the tetrazolate complexes suggesting the possibility to perform measurements under high vacuum conditions.

Photoluminescence and absorbance

Absorbance and air sensitivity. The absorbance and maximum emission wavelength of all complexes are shown in Table 2. All complexes (excluding Ru(4-TBN)Ru and Ru(4-TBN)) show, as expected, a single emission in MLCT region between 630 and 700 nm and a single absorbance maximum between 450 and 490 nm. The sensitivity to oxygen concentration is in general very low. Only Ru(4-TBN)Ru and Ru(4-TBN)Me have shown a decrease of

20-30% in maximum emission intensity when exposed to air, which is still very different from the sensitivity of the $Ru(DPP)_3$ tested under similar conditions.[7]

Broadened emission of Ru(4-TBN)Ru and relative lifetime. When the absorbance spectra of Ru(4-TBN)Ru and mononuclear Ru(4-TBN) in acetonitrile are compared (Figure 15) an additional absorbance peak appears at 460 nm in the MLCT region (Metal-to-Ligand Charge Transfer) in addition to the 490 nm peak present in both compounds. The two peaks at 460 and 490 nm are more visible in dichloromethane (DCM) than in MeCN (Figure 15). Both Ru(4-TBN)Ru and Ru(4-TBN) showed a broadened emission with respect to the other four compounds with a short wavelength difference between the maxima at 670 and 700 nm (Figure 16). The maximum intensity of both emissions of Ru(4-TBN)Ru is exactly twice the corresponding emissions of the mononuclear complex Ru(4-TBN). This can be explained in terms of the number of Ru centers that can emit from the single lower energy center. There is a clear increase of the intensity of the 700 nm emission with the concentration in Ru_1 and Ru_2 complexes (Figure 16). Temperature also affects the relative intensity of the second peak (Figure 17). In a 1 mM acetonitrile solution of Ru(4-TBN)Ru as the temperature is increased from 20 to 50 °C the emission band at 670 nm decreases more than that at 700 nm. There is no selectivity with the excitation wavelength on the 670 and 700 nm emission. At room temperature the two peaks seem to be thermally equilibrated and the emissions take place at similar rate. According to our results low temperature stabilizes the 670 emission and moderately high temperature the 700 nm emission (Figure 17). The presence of two thermally equilibrated emissions in the visible region has been recently reported for another mixed ligand Ru(II) complex; [20b] the two involved states were in that case the anthryl substituent triplet state and the complex lower energy ^{3}MLCT. In Ru(4-TBN)Ru the lifetimes of the 670 and 700 nm emissions for both mono

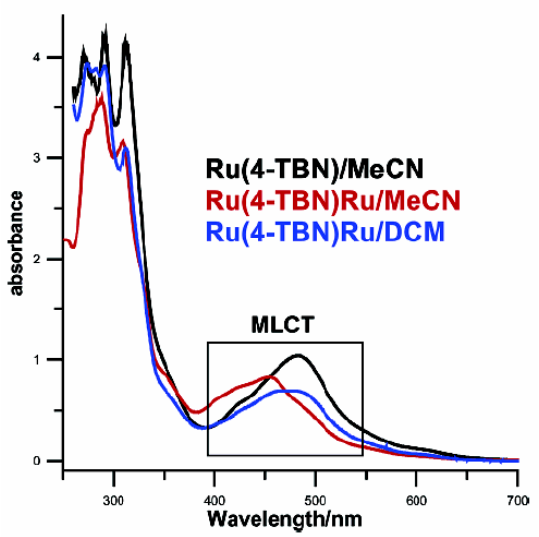

Figure 15 Absorbance spectra of 0.1 mM solutions of Ru(4-TBN)Ru (in acetonitrile and dichloromethane) and Ru(4-TBN) (acetonitrile only).

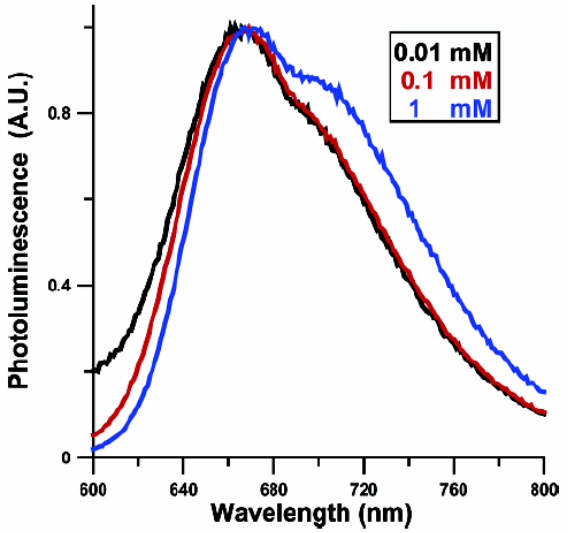

Figure 16 Concentration effect on the normalized intensity of the 700 nm emission of Ru(4-TBN)Ru in MeCN.

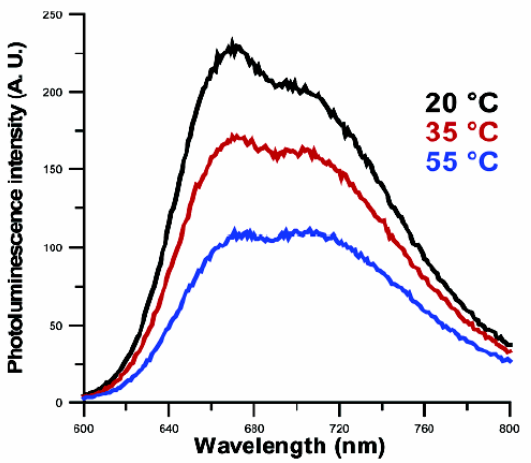

Figure 17 Effect of temperature on the emission band of 1 mM MeCN solution of Ru(4-TBN)Ru.

and dinuclear are similar (Table 4) which excludes the possibility of artifacts and distortions (low concentration conditions). Lifetimes measured on integrated spectra do not change significantly suggesting the similar nature of the two emissions. Considering that first two reductions were assigned to respectively the tpy and bpy ligand (see paragraph 3.1.1) and that both emissions are present even in the

Table 4. Lifetimes of the two complexes that evidenced broadened emission . The excitation

	Emission 670 nm	**Emission 710 nm**	**Full spectra emission**
Ru(4-TBN)Ru	**15.5 nS**	**15.8 nS**	**15.6 nS**
Ru(4-TBN)	**16.3 nS**	**15.8 nS**	**15.8 nS**

laser wavelength was 465 nm. Freshly prepared 10^{-5} M acetonitrile solutions were used. The cell was air equilibrated.

mononuclear compound It can be concluded that MLCT are localized on the same Ru center. In general Kasha's rule[20a] states that no multiple MLCT emissions are possible from the same Ru center but in the case of mixed ligands complexes one can sometime expect the presence of few MLCT states

with similar energies. The more reasonable explanation for the dual emission seems to be the presence of a vibrational structure in the emission from the tpy-Ru MLCT or alternatively from bpy-Ru MLCT transition. Further and more detailed studies on the photophysics are necessary to thorougly understand this broadened emission.

3.1.3

Solid device tests.

Solid devices based on the reference compound. $Ru(bpy)_3^{2+}$, were first prepared using the same method as reported earlier.[18-19] If observed under an optical microscope the inorganic thin layer on ITO surface appears yellow and homogeneous. The steady state current was small and stable up to 2.25 V suggesting the absence of pinholes and the good quality of the coverage. The maximum light intensity was estimated to be 1.75 $\mu W/mm^2$ and easily visible in the daylight. The $Ru(bpy)_3(ClO4)_2$ solubility in acetonitrile is about 40 mg/mL. For four out of the six complexes (excluding Ru(4-TBN)Ru and Ru(4-TBN)Me) pinholes and short circuit effects could not be avoided and the emission was very weak (two orders of magnitude less intense) compared to $Ru(bpy)^{2+}$. This is due to the low solubility in acetonitrile and to the successive crystallization on the ITO surface that prevent the formation of an homogeneous film. Changing the solvent (DCM, acetone) or drying a deposited drop from a lower concentration solution, did not improve the emission intensity.

Ru(4-TBN)Ru .The solubility was 4% w/v in acetonitrile. Using spin coating, precipitation and crystallization on ITO surface resulted in a inhomogeneous film with pinholes. No steady-state emission was reached and a maximum light intensity of about 0.6 $\mu W/mm^2$ was measured (applied potential 4 V; red-orange light was observed by naked eye). Reproducibility was not good due to pinholes distribution in the sample. Different attempts were made: spin coating at lower speeds (400, 300, 200, 100 rpm), for shorter times (1 min, 30 s, 15 s), and using lower concentrations (4, 3, 2, 1 % w/v). However, the film

properties did not change. The steady state emission was reached when a 4% acetonitrile solution was dried on an ITO substrate (Figure 18). The film thickness increased from the previously- estimated values of 100-200 nm to 500-1000 nm showing iridescence. The durability was improved but the response time (30 minutes reaching the maximum intensity) and the maximum intensity (about 0.05 μW/mm2 at 4 V) strongly decreased as compared with spin coated film. The behaviour was similar to that observed for $Ru(bpy)_3^{2+}$ when the device was prepared and operated in a dry box.[6] The $Ru(bpy)_3^{2+}$ gave a crystalline insulating and iridescent film when a drop from a similar solution was dried. An explanation of this behaviour is the increased time necessary to cross the diffusion layer and the higher amount of solvent molecules retained by tetrazolate-based complexes as compared to $Ru(bpy)_3^{2+}$. This could also explain the reversible memory effect of potential conditioning on response times (Figure 19).

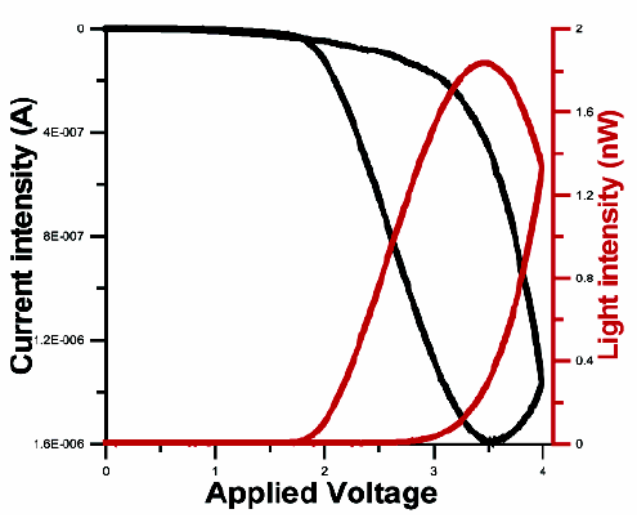

Figure 18. Light/current/potential curves of a solid device prepared by drying a drop of 4% w/v acetonitrile solution of Ru(4-TBN)Ru.

By waiting for some minutes after the switching off of the activation potential of the device, the response time increased again due to the thermal disorder effect on the double layer generated by the voltage application in a previous

operation. In this thick, but still conductive, film the kinetics are slowed and a continuous decrease of open circuit current is observed after operation.

Ru(4-TBNMe). Solid devices have been prepared and an intensity of 0.1 $\mu W/mm^2$ was obtained. With a applied potential of 5 V the emission spectrum was recorded using the previously described CCD camera setup. The maximum was in the NIR region at 780 nm. Comparing emission spectra of the same compound in solution and in solid films a red shift is often observed due to modification of interactions between molecules in condensed structures.[21] The solubility in acetonitrile is much lower than that of Ru(4-TBN)Ru and the active film was prepared by drying a drop of a 0.4% w/v solution. The film is still crystalline and affected by pinholes. The response time was about ten times lower than for $Ru(bpy)_3^{2+}$ but faster than that for Ru(4-TBN)Ru. The film structure withstood, and the emission continued to be observed, up to 10 V; the response time progressively increased whereas the durability decreased. A reversible memory effect in response times was again observed.

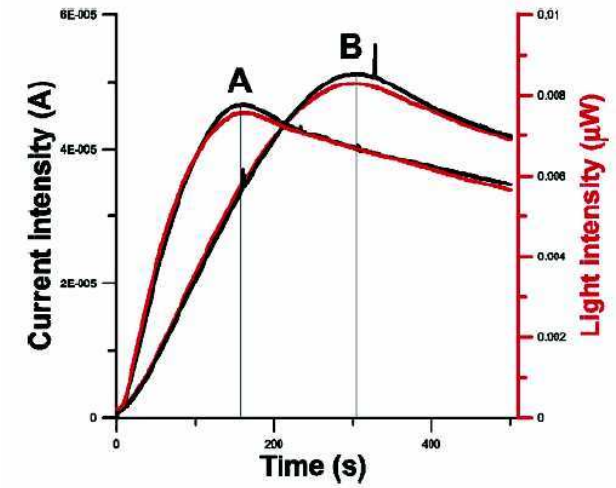

Figure 19. Light/current/time curves obtained applying 5 V switching potential in successive 500 s experiments on a Ru(4-TBN)Ru based solid device. Thickness of the active film approximately 1 µm. (A) Second subsequent run; (B) second run after a pause of 5 min.

3.1.4

Notes on this first series of compounds.

The measurements performed in this sections showed the possibility of altering the ECL emission wavelength by changing the groups around the tetrazolate ligand. In general, for this class of compounds, the energy gap is lower and the emissions are red-shifted with respect to $Ru(bpy)_3^{2+}$. The fact that emission is shifted in IR region is important for application in biological matrixes where a background emission is often present in UV-VIS region. From this point of view should be interesting to build ECL labelling agents based in those new complexes. (especially Ru(4-TBN)Me). In degassed acetonitrile solutions, Ru(4-TBN)Ru showed a surprisingly intense ECL emission, suggesting the use of Ru(4-TBN)Ru for the preparation of light emitting solid devices, which show emission intensity comparable to that of $Ru(bpy)_3^{2+}$ based devices. In addition, Ru(4-TBN)Me can be also considered as a luminophore for the design of NIR (780 nm) light emitting solid devices.

3.2
Complexes containing tetrazolate based bis-coordinating ligands.

Considering the promising results obtained in previous paragraph another series of compounds containing tetrazolate based ligands has been taken in consideration (fig.20). The relatively small structural differences between the three complexes are evidenced using the red colour. In general all dyes are octahedral and contain two bis-chelating 2-2'bipyridil (bpy) and one bis-chelating tetrazole based ligand. Ru(pyr-tet) contains a pyridine functionalized in position 2 with tetrazolate ring, Ru(pyr-tet)Me is the same complex methylated on nitrogen 2 of tetrazolate and at the end Ru(pyz-tet) contains tetrazolate ring bound with pos. 2 of pyrazine.

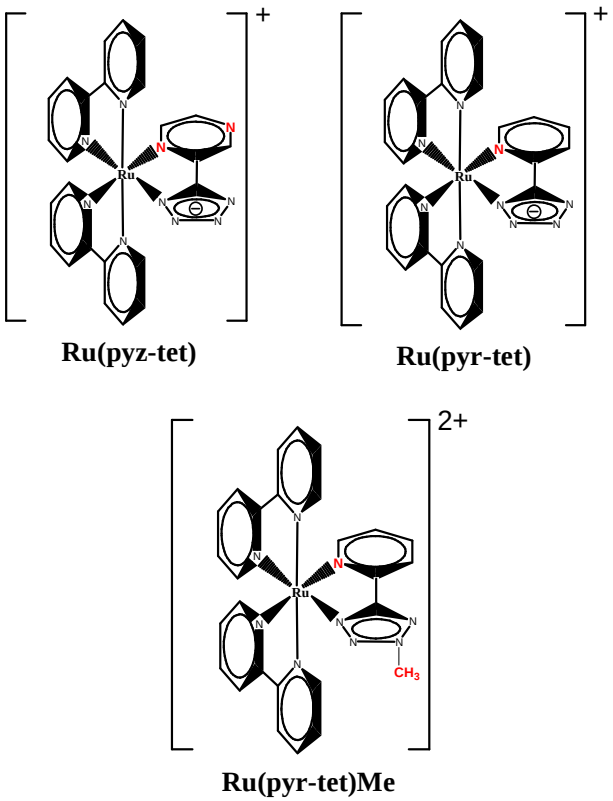

Figure 20. Structures and acronyms of the complexes object of this section.

pyr-tet and pyz-tet ligands are negatively charged and overall complex charge is +1. Ru(pyr-tet)Me is doubly positively charged because methylated tetrazole is neutral (see fig.3). One of the substantial differences from previously analyzed molecules is that each Ru is doubly coordinated by tetrazolate ligand. A paper reporting synthetic procedures and structural characterization is in preparation. Those new dyes were selected as candidates for ECL investigations because of pretty high quantum efficiency during preliminary fluorescence measurements. Together with the classical scope of ECL efficiency improvement in organic solvents, one of the objectives was also the understanding of tetrazolate protonation effect on ECL intensity. In the section 3.2.2. after ECL charaterization in acetonitrile the complex Ru(pyr-tet) has been successfully tested in a aqueous buffer and air equilibrated cell. Those features allowed to make an ECL titration with calf thymus DNA (ct-DNA). This experiments, described in the last paragraph of this chapter, were necessary to understand the type of interaction of the complex with DNA double helix.

3.2.1

Electrochemical properties.

Cyclic voltammetric curves were registered for all complexes in the previously described ultra dry conditions (see appendix chapt. 2). The $E_{1/2}$ for reduction and oxidation processes, referred to SCE are reported in table 5.

	Ox $E_{1/2}$ (V)	**Red $E_{1/2}$(V)**				
	1	**I**	**II**	**III**	**IV**	**V**
Ru(pyr-tet)[a]	+1.23*	-1.28	-1.60	-2.30	-2.55	
Ru(pyz-tet)[a]	+1.25*	-1.45	-1.75	-2.14	-2.68	-3.03*
Ru(pyr-tet)Me[b]	+1.27*	-1.19	-1.36	-1.69	-1.81	-2.29*

Table 5. Oxidation and reduction potentials of the complexes containing bi-coordinating tetrazolate based ligands. Potential is referred to SCE. All processes are assumed to be monoelectronic.

[a]Solvent: ultradry THF. [b]Solvent: ultradry DMF. *The process was only partially reversible.

As stated above redox processes in Ru(II)-polypyridine complexes are mainly localized either on the metal center (oxidations) or on the ligands (reductions).[1,10,11] In those measurements ultra dry DMF and THF were used to focus on reductive processes. Because of the limited potential window in oxidation the relative $E_{1/2}$ was calculated from partially irreversible processes due to overlapping of the process with solvent oxidative discharge. As expected however $E_{1/2}$ for I oxidation process didn't change much by varying the complex. This potential was not substantially shifted from the values observed in MeCN and aqueous solutions during ECL generation . (see for comparison tab. 5 and fig. 27). It is then clear then that the only oxidation process and HOMO is localized on Ru centre for all the dyes. Let's consider now the reductive voltammetric curves of Ru(pyr-tet) and Ru(pyr-tet)Me reported in fig. 21 and 22. It's useful to compare that curves with that of $[Ru(4\text{-}TBN)]^+$ (fig. 6). The succession of the peaks appears to be analogous: two close peaks a gap and other two peaks even more close one another. By taking then in account the previously reported speculations on $[Ru(4\text{-}TBN)]^+$ reductions assignments (par. 3.1.1), based on DFT molecular orbital calculations and in a accurate comparison between single ligand and overall complex voltammetry We can conclude that:

1) reduction peaks namely I and II can be associated with monoelectronic reduction of first and second bpy ligand.
2) Reduction peaks labelled III and IV are related to electron pairing in the same single MO previously reduced .

The last assignment is confirmed by the fact that $E_{1/2,III}$-$E_{1/2,I}$ is approximately equal to $E_{1/2,IV}$-$E_{1/2,II}$ and value is in the range of electron pairing energy in polypiridine ligands. The most expanded potential scale in Ru(pyr-tet) voltammetry is justified by the higher electrical resistance caused by

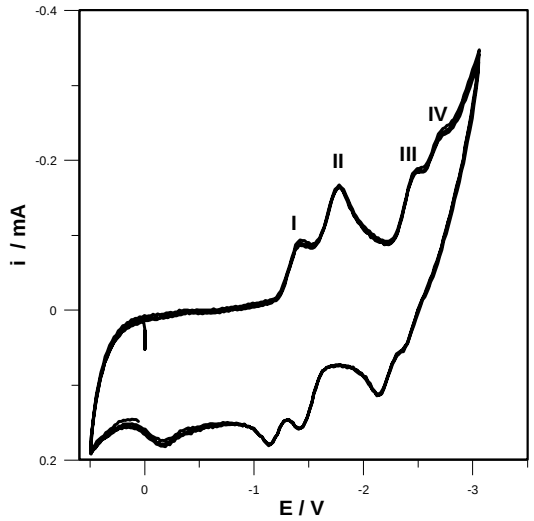

Figure 21. Cyclic voltammetric curve of a 10^{-3} M Ru(pyr-tet) THF solution; Supporting electrolyte: $TBAPF_6$ 0.1 M; THF; Scan rate: 10 V/s; T= 25 °C, Working electrode: Pt disk of 125 μm diameter (UME). Potentials are referred to SCE.

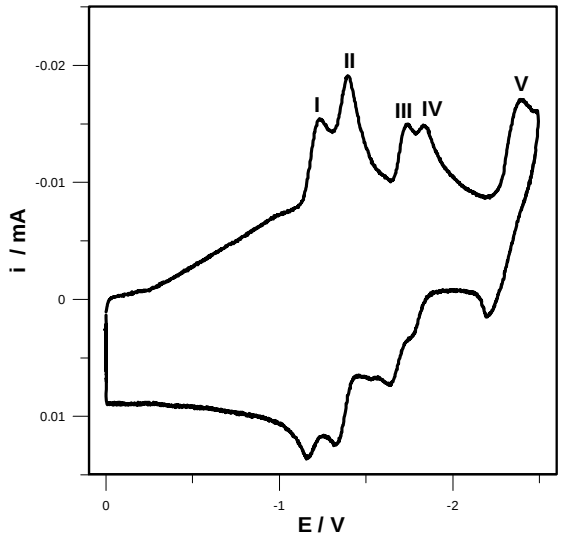

Figure 22. Cyclic voltammetric curve of a 10^{-3} M Ru(pyr-tet)Me DMF solution; Supporting electrolyte: $TBAPF_6$ 0.1 M; ; Scan rate: 1 V/s; T= -60 °C; Working electrode: Pt disk of 125 μm diameter (UME). Potentials are referred to SCE.

increased scan rate respect to that of Ru(pyr-tet)Me. For this last compound a fifth reduction (label V in fig. 22) has been observed and is probably associated to an higher energy unoccupied MO localized on tetrazolate ligand. The unusual fact that first four reductions are localized in only 2 out 3 electroactive ligands can be justified assuming that electron rich pyr-tet and (pyr-tet)Me unoccupied MO lie at higher level respect to that of bpy and his electron coupling energy. In the case of Ru(pyr-tet)Me contrarily to Ru(pyr-tet) the third and especially fourth reduction process looks as partially irreversible. A different assignation of voltammetric reduction peaks can be hypothesized for the complex Ru(pyz-tet) (fig. 23) assuming that bpy ligand is more hard to reduce with respect to pyz-tet because two Nitrogen are present

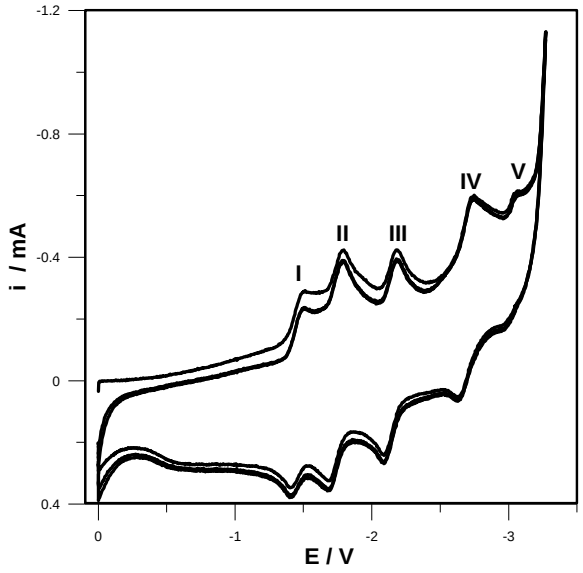

Figure 23. Cyclic voltammetric curve of a 10^{-3} M Ru(pyz-tet) THF solution; Supporting electrolyte: $TBAPF_6$ 0.1 M; THF; Scan rate: 10 V/s; T= 25 °C; Working electrode: Pt disk of 125 μm diameter (UME). Potentials are referred to SCE.

in his ring. Accordingly reduction I should be localized on pyz-tet ligand, the following two on single bpy ligands (II, III). The following two reductions can be reasonably assigned to electron coupling on pyz-tet and bpy ligand respectively (IV,V). A summary of the reduction assignments is shown in fig. 24. More investigations (i.e. voltammetries of the ligands pyr-tet, pyz-tet and pyr-tet-Me that are currently unavailable for stability problems) are however necessary to understand in major detail those higher reduction states.

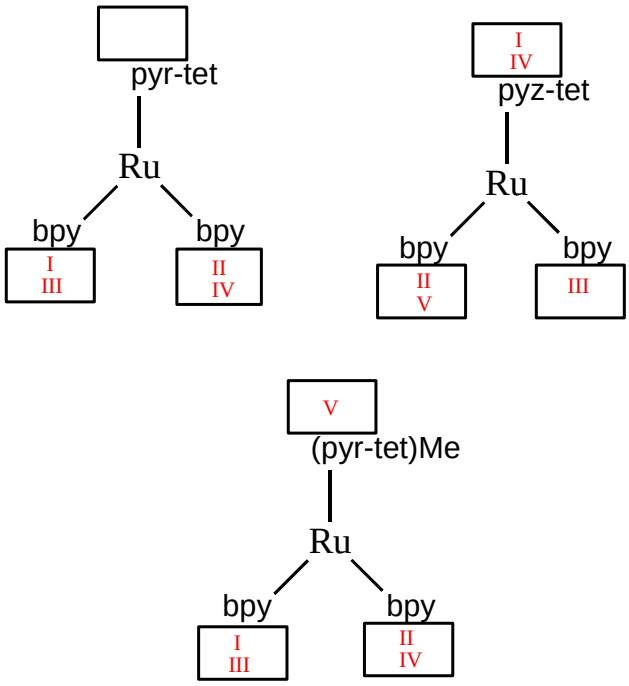

Figure 24. Scheme of localization of reduction processes into Ru(pyr-tet), Ru(pyr-tet)Me and Ru(pyz-tet) complexes.

3.2.2. Emission properties in organic solvents.

Fluorescence.

Similarly to the previous series of compounds, preliminary photophysical investigations are necessary to readily understand what MLCT states could be populated electrochemically. In fig. 25 are shown emission spectras of $Ru(bpy)_3^{2+}$, Ru(pyr-tet) and Ru(pyz-tet) recorded from 10^{-4} M MeCN air equilibrated solutions. The MLCT energy in absorbance spectra (not shown) is very similar for all complexes (around 450 nm); exact value is evidenced in fig. 25 as exciting wavelength. At this point fluorescence quantum efficiency $\phi_{rel,PL}$ of the new dyes is calculated taking that of $Ru(bpy)_3^{2+}$ as 100 % and assumed as:

$$\phi_{rel,PL} = \frac{I_{PL}(Ru(bpy)_2 X)}{I_{PL}(Ru(bpy)_3)} \cdot 100$$

It's clear that $\phi_{rel,PL}$ of Ru(pyr-tet) is about one order of magnitude higher than that of Ru(pyz-tet). On the other hand Ru(pyr-tet) quantum efficiency is not far from that of the standard (more or less 1/3). An explanation of the great difference between quantum efficiency of the new dyes can be given by taking in account the previously discussed LUMO and HOMO assignements (section 3.2.1). The fundamental aspect to consider could be the LUMO localization which should be the same MO populated in MLCT excited state generation. The LUMO of Ru(pyr-tet) is the long living bpy MO as in $Ru(bpy)_3^{2+}$; considering Ru(pyztet) the MO of pyz-tet ligand is that at lower energy and his shorter life time is probably caused by the presence of two nitrogen atoms. Life time measurements on the complexes and on the single tetrazolate ligands could definitely confirm this hypothesis. The maximum emission wavelength is very close to that of $Ru(bpy)_3^{2+}$ for both complexes. The effect of methylation (Ru(pyr-tet)Me) on Ru(pyr-tet) emission spectra is shown in fig. 26. $\phi_{rel,PL}$ for Ru(pyr-tet)Me is approximately 1/3 of that of the pristine

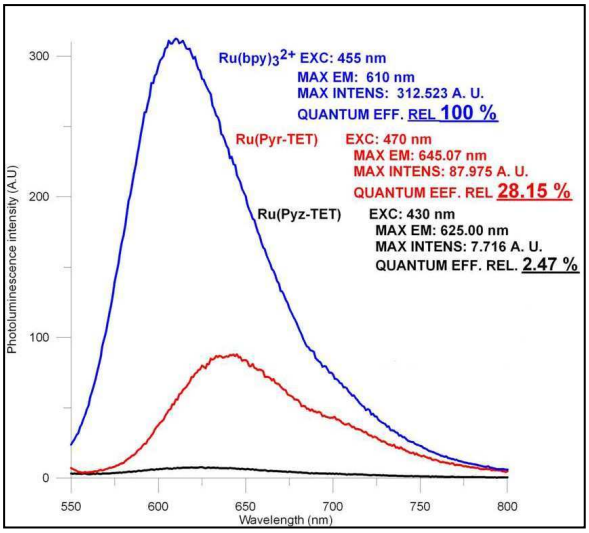

Figure 25. Fluorescence spectra of MeCN 10^{-4} M solutions of $Ru(bpy)_3^{2+}$, Ru(pyr-tet) and Ru(pyz-tet). Maximum absorbance MLCT band was used as excitation wavelength. Cell was air equilibrated.

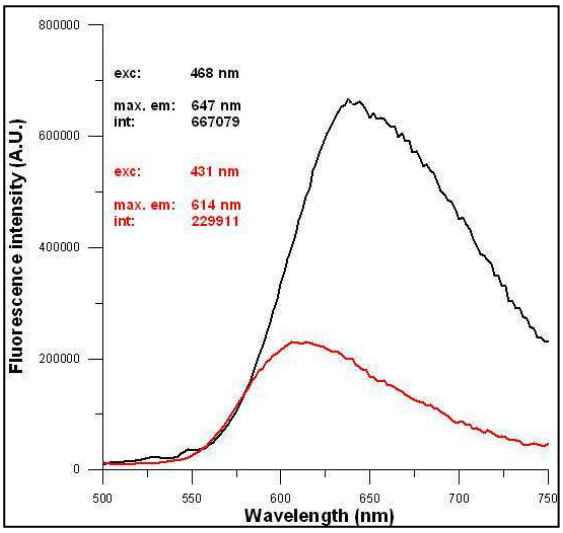

Figure 26. Fluorescence spectra of MeCN 10^{-5} M solutions Ru(pyr-tet) (Black line) and Ru(pyr-tet)Me (Red line). Maximum absorbance MLCT band was used as excitation wavelength. Cell was Ar degassed.

complex and his maxima blue shifted of about 30 nm reflecting exciting wavelength shift. This effect could be explained by considering the partial contribution to the LUMO of the higher energy (pyr-tet)Me MO which is probably more consistent than that of pyr-tet. Some of the consequences on the LUMO are the higher energy (lower emission wavelength) and a slightly lower life time (lower efficiency). The absolute quantum efficiency can be then easily calculating by considering that $Ru(bpy)_3^{2+}$ estimated efficiency is 4.2 %.

Electrochemiluminescence.

Even if voltammetric characterization introduced in section 3.2.1 has been performed in ultra dry THF or DMF, electrochemical stability of the new complexes allowed satisfactory ECL emissions also in conventional solvents by simplifying sample preparation. The use of bottle quality MeCN in Ar degassed cell was sufficient to obtain voltammetric curves that showed one oxidative (1) and two reductive reversible processes (I, II) for all complexes. The i_a/i_c value is close to 1 for all processes. As example a typical voltammetry registered from a Ru(pyr-tet) MeCN solution has been reported in fig. 27.

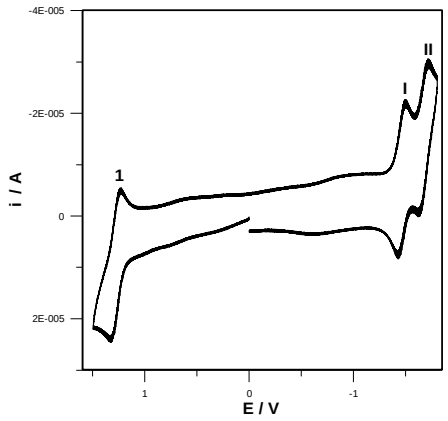

Figure 27. Cyclic voltammetry of a 10^{-3} M MeCN solution of Ru(pyr-tet). The solvent is used as received (bottle quality) and the sample is degassed with Ar for 10 minutes using ECL electrochemical cell previously introduced in fig. 13 of chapter 2 . Supporting electrolyte: $TBAPF_6$ 0.1 M. Working electrode: Platinum disk of 2 mm diameter. Potential is referred to SCE.

The remaining complexes Ru(pyr-tet)Me and Ru(pyz-tet) voltammetric curves registered in the same conditions are very similar to that shown in fig. 27. All the dyes are energy sufficient (i. e. $\Delta E = E_{1/2,I}-E_{1/2,1} \geq Energy_{MLCT}$ expressed in eV) to populate electrochemically the MLCT states with ΔE of around 2.5 eV lower than that of $Ru(bpy)_3^{2+}$ (2.68 eV). Preliminary light/current/potential curves (CV) and light/current/time curves (CHRONO) were systematically recorded for each complex to check out the emission time stability and to optimize experimental conditions for successive spectra acquisitions. The preliminary tests suggested that the best exciting method were alternated 0.1 s potential steps at respectively 1 oxidation and I reduction potential.

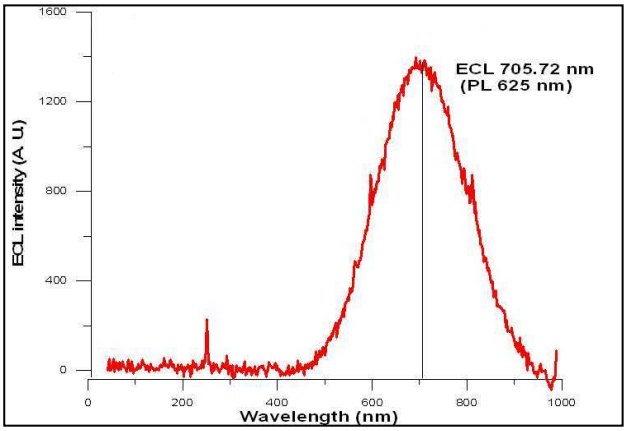

Figure 28. ECL spectra of Ru(pyz-tet) 10^{-3} M MeCN solution. Supporting electrolyte: $TBAPF_6$ 0.1 M. Emission mechanism: anion-cation direct annihilation. Switching potential: +1.65 V (I Ox.) 0.1 s impulses alternated with – 1.35 V (I Red.) 0.1 s impulses. CCD accumulation time: 4 min. Cell was Ar degassed for 10 minutes.

Ru(pyz-tet).

Emission ECL spectra registered by 4 minutes CCD accumulation is reported in fig. 28. By taking $Ru(bpy)_3^{2+}$ as a standard the already definited rECL-Int. is of 0.43 % which is about five smaller respect to fluorescence efficiency ($\phi_{rel,PL}$ of 2.47 %). ECL low emission intensity could be explained considering that pyz-tet localized MLCT state is short lived with respect to

that of bpy. The inclusion of the second reduction causes no change in emission intensity because of process partial irreversibility that produces and electrode filming product. Maximum emission wavelength is interestingly red shifted in the NIR region (705 nm). Red shifts like this are often observed in ECL for different reasons. In this case the relatively great red shift from fluorescence (~80 nm) is probably related with molecular rearrangements or chemical modifications during excited state formation that could also justify the decreased efficiency. No excimer formation has been ever reported and seems possible for such octahedral complexes.

Ru(pyr-tet).

As expected from preliminary fluorescence characterization, this dye evidenced an extraordinary intense ECL emission. The light emitted at the working electrode disk was well visible by eye even in a lit room as happens with $Ru(bpy)_3^{2+}$. The emission spectrum is reported in fig. 29. The maximum wavelength is very close to that observed in fluorescence ($\Delta\lambda \sim 5$ nm) and being around 640 nm is red shifted respect to $Ru(bpy)_3^{2+}$ of about 30 nm. The fact that $\Delta\lambda$ is so small contrarily to Ru(pyz-tet) suggests that populated MLCT state is exactly the same of fluorescence evidencing the dye stability during oxidative and reductive potential steps. rECL-Int is estimated to be of 243 % so apparently the new dyes emits more than the standard . The discrepancy between rECL-Int and $\phi_{rel,PL}$ could be explained in terms of difference between diffusion coefficients and to the ratio of formation of quenching products at the electrode. Another delicate aspect is the standardization of oxygen concentration after Ar degassing. As in the case of the previous series of complexes the concentration of oxygen has not been measured prior to ECL measurements so that small differences in O_2 concentration can affect relative emission intensities. To improve the reproducibility of ECL intensity It will be possible to perform measurements in ultra dry conditions (see section 2.4 “high vacuum cell”) were the oxygen concentration is equally very close to 0 for the new studied complex and the

standard (10^{-5} bar of internal pressure). What can be said is that Ru(pyr-tet) has the scarce property to have ECL intensity very similar to that of $Ru(bpy)_3^{2+}$ and an exceptional electrochemical stability in cation-anion annihilation. The inclusion of the second reduction causes an emission intensity drift of about 2.5 times (fig. 29) with maxima at the same wavelength. The simpler explanation is that a partial irreversibility on second reduction causes filming products at the electrodes. This way the emitting surface is reduced and an amount of generated radical anion is not producing excited state causing an ECL intensity decrease.

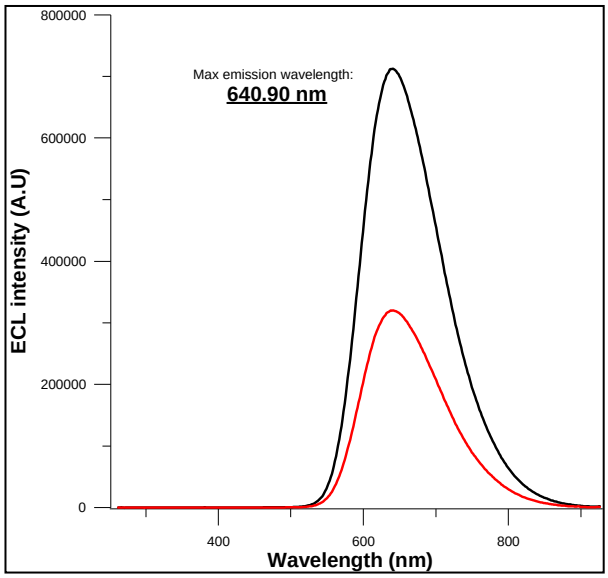

Figure 29. ECL spectra of Ru(pyr-tet) 10^{-3} M MeCN solution. Supporting electrolyte: $TBAPF_6$ 0.1 M. Emission mechanism: anion-cation direct annihilation. CCD accumulation time: 4 min. Cell was Ar degassed for 10 minutes. Switching potential: **(black line)** +1.55 V (I Ox.) 0.1 s impulses alternated with – 1.6 V (I Red.) 0.1 s impulses; **(red line)** +1.5 V (I Ox.) 0.1 s impulses alternated with – 1.9 (II Red.) V 0.1 s impulses

Ru(pyr-tet)Me.

Emission spectra of the methylated form of Ru(pyr-tet) has been tested in MeCN using anion-cation annihilation. Emission profiles are shown in fig. 30.

Unlike happens in fluorescence that is blue shifted of about 35 nm ECL maxima is exactly coincident with that of Ru(pyr-tet) at about 645 nm. Considering that rECL-Int is 51 % and $\phi_{rel,PL}$ 9.6 % the behaviour is the same already described for Ru(pyr-tet) with both PL and ECL intensity attenuated of about 3-4 times. The introduction of the methyl group causes thus a decrease of ECL intensity and populated MLCT is unexpectedly identical to that of Ru(pyr-tet).

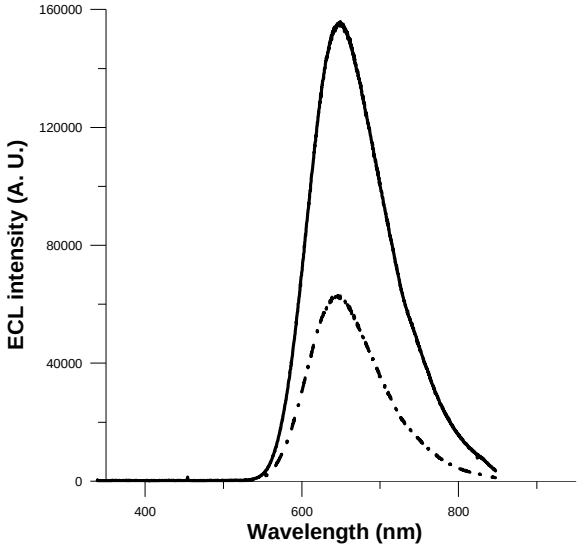

Figure 30. ECL spectra of Ru(pyr-tet)Me 10^{-3} M MeCN solution. Supporting electrolyte: $TBAPF_6$ 0.1 M. Samples were Ar degassed for 10 minutes. CCD accumulation time: 4 min. (**Solid line**) switching potential: +1.5 V (I Ox.) 0.1 s impulses alternated with – 1.65 V (I Red.) 0.1 s impulses Emission mechanism: anion-cation direct annihilation. (**Dotted line**) switching potential: +1.2 V (potential of max. ECL intensity) 0.1 s impulses alternated with 0 V 0.1 s impulses; Emission mechanism: oxidation in presence of NPr_3 added at $3x10^{-2}$ M concentration .

ECL in presence of NPr_3

Considering the reversibility and time stability evidenced in first oxidative process an excess of the oxydative coreactant NPr_3 (conc. $3x10^{-2}$ M) has been added in the same MeCN solutions used previously in cation-anion annihilation tests to check emission properties. Emission maxima showed no shift whereas intensity was in general lower than that obtained with

annihilation method. The causes of the decrease were essentially two: (i) the formation of filming products at the electrode promoted by the ammine electro-generated radicals; (ii) the progressive coreactant consumption. ECL spectra of Ru(pyr-tet)Me by employing the two different mechanisms are shown in fig. 30. An intensity decrease of about 2.5 times respect to annihilation is observed when ECL spectra is collected in presence of NPr_3 for Ru(pyr-tet) and Ru(pyr-tet)Me. In the case of Ru(pyz-tet) the addiction of NPr_3 caused a complete disappearance of ECL signal due to some fast filming reaction. ECL and photophysical properties in MeCN are summarized for all dyes in table 6.

Compound	MLCT[a]		$\varphi_{rel,PL}$	λ_{ECL}/nm	rECL-Int C-A*	rECL-Int NPr_3**
	λ_{abs}/nm	λ_{PL}/nm				
Ru(pyz-tet)	**430.3**	**625.1**	**2.5 %**	**705.3**	**0.4**	**-**
Ru(pyr-tet)	**468.4**	**645.3**	**28.1 %**	**640.9**	**243.2 %**	**107.0 %**
Ru(pyr-tet)Me	**431.7**	**614.5**	**9.6 %**	**645.2**	**51.4 %**	**19.9 %**

Table 6. Summary of photophysical and ECL emission properties in Ar degassed MeCN.

[a] Fluorescence from air equilibrated MeCN 10-5 M solutions.

* C-A= cation-anion annihilation in Ar degassed MeCN solution. [Ru]=10^{-3} M; [$TBAPF_6$]=0.1 M.

**NPr_3= oxidation in presence of NPr_3 $3x10^{-2}$ M.

3.2.3. Dependence on protonation of ECL intensity.

The presence of three lone pairs into negatively charged tetrazolate ring makes the complex Ru(pyr-tet) to behave as a nucleofilic molecule. As already showed in fig. 3 and 4 this reactivity can be exploited to add a proton or a methyl into tetrazolate ring in presence of a strong acid (triflic). In this section the effect of Ru(pyr-tet) protonation on ECL emission is investigated. The reagent employed to add protons is a strong organic acid that is assumed as completely dissociated: CF_3COOH. The reaction scheme depicted in fig. 31 evidences that in principle three possible protonation sites are present in Ru(pyr-tet).

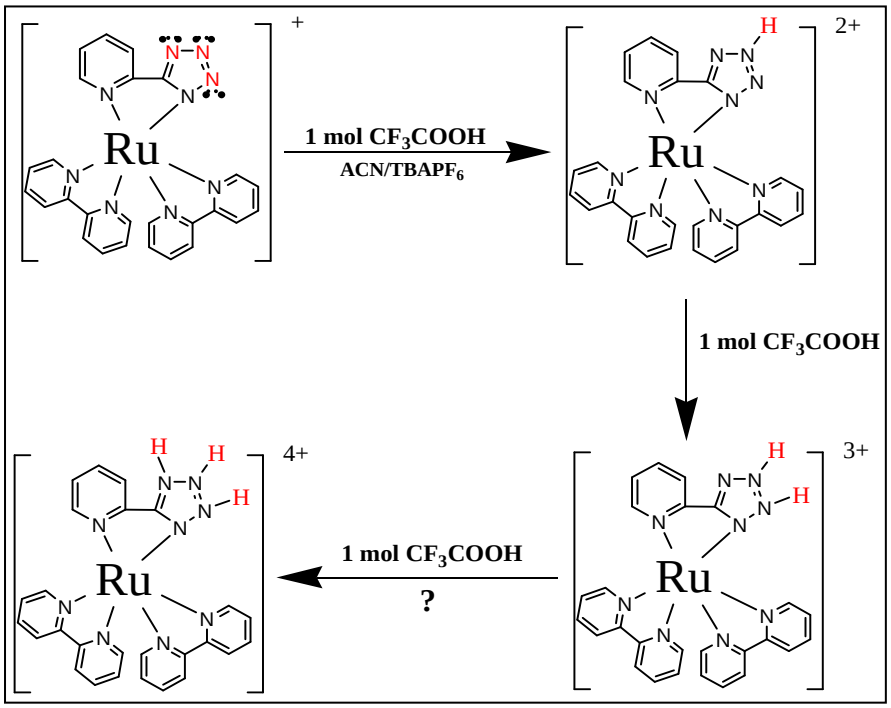

Figure 31. Scheme of hypothetic successive protonation steps in Ru(pyr-tet) tetrazolate based ligand.

The positive charge increment in combination with steric effects on the three lone pairs allows however a single protonation step. Protonation seems possible only in position 2 respect to tetrazolate coordinating nitrogen. In this series of experiments the mechanism employed to produce ECL is again the cation-anion annihilation in MeCN /$TBAPF_6$ solutions at same concentrations used for complex basic characterization. Considering that in Ru(pyr-tet)Me the nitrogen which is expected to add a proton in Ru(pyr-tet) is protected by a methyl group this compound has been taken as a non reacting model. The modification of cyclic voltammetric curves and ECL emissions are compared to study the effect of acid addiction and to verify the occurrence of protonation.

CV

Trifluoro-acetic acid has been employed in electrochemical and ECL experiments because in absence of protons excess is expected to be stable in oxidation and reduction. Few μL of MeCN concentrated solution were prepared from glass sealed phial to minimize water contamination. The appropriate equivalent amount of reactant was then accurately introduced by micropipette into electrochemical cell.

Ru(pyr-tet)Me

Let's consider first the behaviour of the model system Ru(pyr-tet)Me introduced in fig. 32. The voltammetry of a 1 mM CF_3COOH MeCN solution shows unexpectedly a reversible peak at about -0.5 V vs Ag which is associated with protons reduction and successive re-oxidation. This behaviour can be understood if We assume that only atomic hydrogen is generated and adsorbed in the surface of Pt working electrode. The fact that Ag wire is not a true reference electrode (a potential drift is expected upon strong acid addiction) is not a problem because both hydrogen associated peaks and complex I Ox. and I Red. can be used ad internal standard to shift potentials to appropriate values and to make appropriate curves overlapping. By comparing the CV curve of the pristine complex with that obtained after addiction of 1 and 2 equivalents of acid it's clear that the last ones are a simple combination of the Ru(pyr-tet)Me and CF_3COOH voltammetries. This fact is a clear evidence of non-interaction between the acid protons and the complex that continue to behave independently after addiction.

Ru(pyr-tet)

If We look now at the results of analogous experiments performed on Ru(pyr-tet) showed in fig. 33 It's immediately clear that voltammetries obtained after acid addiction are not a simple linear combination of that of the complex and of the acid. Two features can be pointed out: (i) a catalytic effect of Ru(pyr-

tet) in molecular hydrogen evolution is present; (ii) potentials of oxidation and reduction processes of the complex are substantially unchanged .

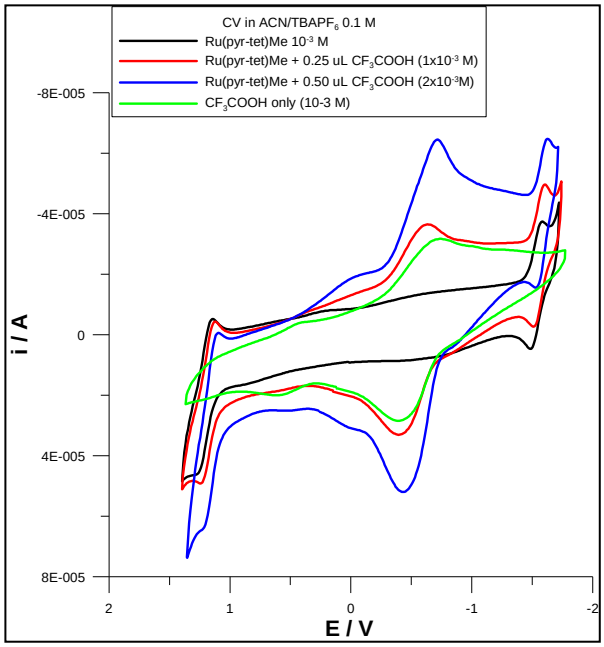

Figure 32. Voltammetric curve of Ru(pyr-tet)Me (black line) is compared with that of CF_3COOH (green) in the same experimental conditions. The cyclic voltammeties of Ru(pyr-tet)Me after addiction of 1 (red line) and 2 (blue) equivalents of acid are also reported to evidence experimental curve modifications.

(i) By comparing fig. 32 with fig. 33 It's clear that irreversible peak at about 0 V vs Ag It's the same associated with proton reduction and re-oxydation observed in fig. 32 (two short distanced peaks are present even in CF_3COOH voltammetry). Like in previous complex electrical current is proportional to the added equivalents of acid; this is a clear evidence that no proton is consumed by reaction with Ru(pyr-tet) and H^+ continues to behave as free species. Even if protonation did not occurred tetrazolate localized lone pairs show a catalytic effect on H^+ electrochemical reduction process. In the case of Ru(pyr-tet) in fact proton reduction is clearly irreversible probably because

molecular H_2 is formed and H can no more be re-oxidized. An hypothetic mechanism is shown in fig. 34 involving a temporary hydrogenation of tetrazolate ring.

(ii) By observing fig. 33 It is clear that the complex first oxidation and first two reductions remain at the same potential before and after acid addiction. The distance between first reduction and first oxidation is consequently constant and the fact that second reduction is more evident in the curve where 3 equivalents of protons were added is due to a small difference on applied potential limit. Those observations seem to confirm that no protonation has occurred in these experimental conditions.

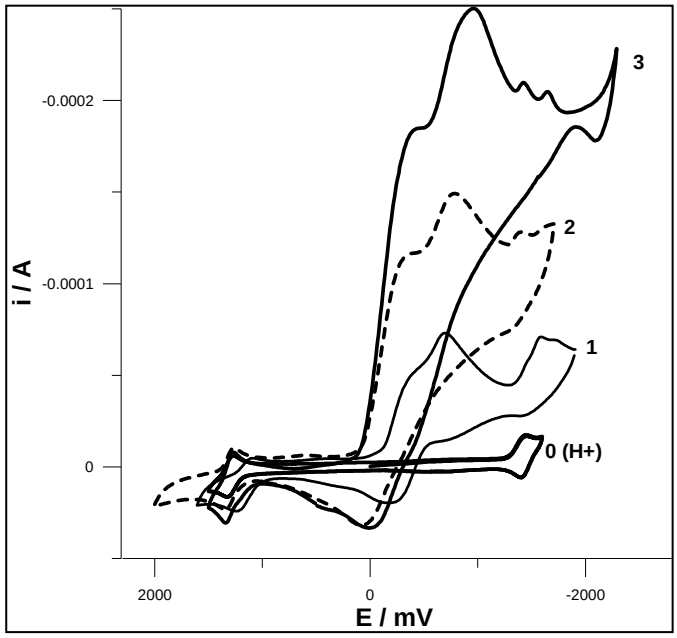

Figure 33. Modification of cyclic voltammetric curve of a 10^{-3} M MeCN solution of Ru(pyr-tet) upon addiction of 1, 2, 3 and 4 equivalents of CF_3COOH. Supporting electrolyte: $TBAPF_6$ 0.1 M. Scan rate: 1 V/s.

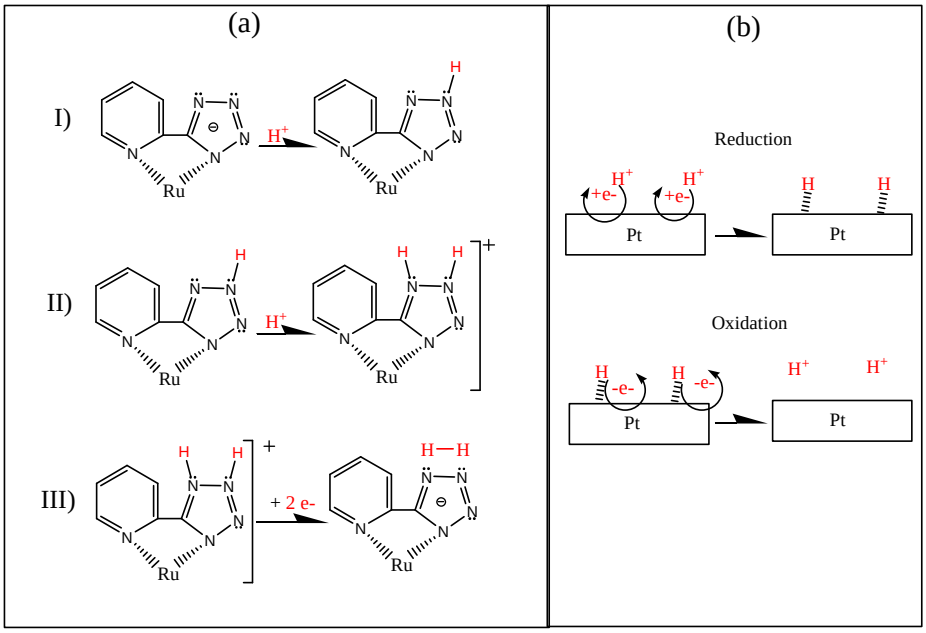

Figure 34. (a) An hypothetic mechanism of the catalytic effect of Ru(pyr-tet) on reduction of acid protons to H_2 . The key feature is the proximity of the temporarily hydrogenated N atoms into tetrazolate ring. (b) Reversible protons reduction into Pt electrode surface. Electro-generated H atoms are adsorbed into metal surface without recombination. In the case of Ru(pyr-tet)Me two adjacent lone pairs are not disposable as in Ru(pyr-tet).

ECL

ECL experiments are not significant to confirm that hydrogenation of Ru(pyr-tet) occurred. There is in fact no substantial difference in emission intensity decay from Ru(pyr-tet)Me (fig. 35) and Ru(pyr-tet) (fig. 36) which is fundamentally caused by the excess protons. Considering first the compound Ru(pyr-tet)Me light/time curve have been registered after that 0 (black line), 1 (red line) and 2 (blue line) equivalents of acid have been added. It's important to notice that potential applied was that necessary to include first reduction and oxidation which values varied in successive experiments upon acid addiction because of quasi reference electrode drift. The emission during reduction almost completely disappeared when an equivalent of acid was added whereas emission during oxidation decreased much less. By adding a second equivalent

the maximum intensity during oxidation was reduced to ¼ of initial and integrated emission during oxidation was estimated to be around 1/50 of the initial value. A much faster time decay of the emission is also evident in presence of acid. The effects of proton presence are different: (i) Having a reduction potential lower than the complex they decrease the amount of generated radical anion. (ii) They can combine with electrogenerated anion more fast (higher diffusion coefficient) than cation so signal is obtained in a competitive regime only during oxidation when a great amount of complex radical cation is generated. The proton negative effect on ECL intensity can be

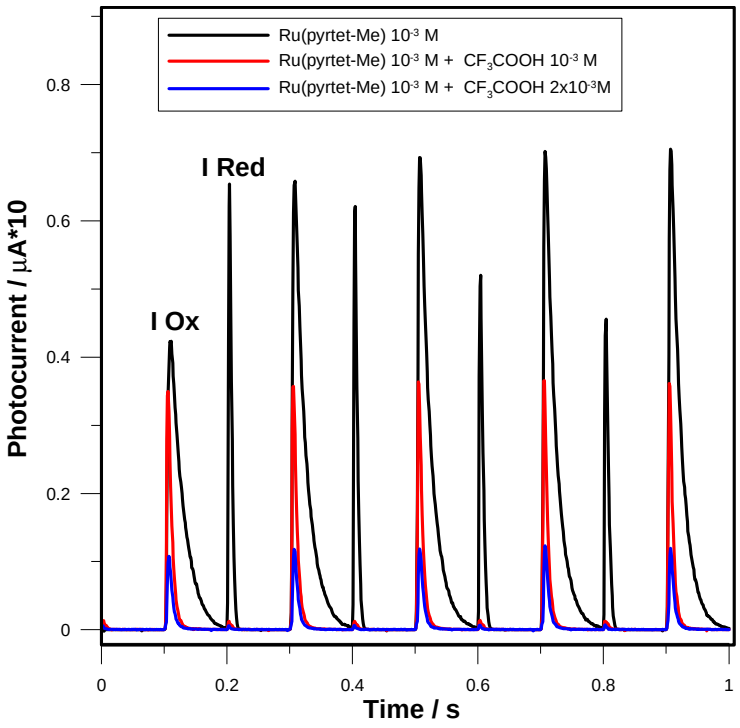

Figure 35. Light/time curves registered from a MeCN 10^{-3} M solution of Ru(pyr-tet)Me in the same experimental conditions described in fig.30. Switching method: positive potential impulse of 0.1 s including I Ox. of the complex and 0.1 s negative potential impulse including I red. Mechanism: cation-anion annihilation

schematized as follows:

1) $Ru(pyr\text{-}tet)Me + e^- \longrightarrow Ru(pyr\text{-}tet)Me^{\bullet -}$

2) $Ru(pyr\text{-}tet)Me - e^- \longrightarrow Ru(pyr\text{-}tet)Me^{\bullet +}$

3) $Ru(pyr\text{-}tet)Me^{\bullet -} + Ru(pyr\text{-}tet)Me^{\bullet +} \longrightarrow Ru(pyr\text{-}tet)Me^{*} + Ru(pyr\text{-}tet)Me$

1) $H^+ + e^- \longrightarrow H$

2) $H - e^- \longrightarrow H^+$

3) $Ru(pyr\text{-}tet)Me^{\bullet -} + H^+ \longrightarrow Ru(pyr\text{-}tet)Me + H$

where the reactions with the same number are in competition. Red colour is used to point out electron transfers involving H^+ and the black Ru(pyr-tet)Me processes. Finally considering fig. 36 It's clear that a similar negative effect of protons is evident also in Ru(pyr- tet) which in principle is even more hard

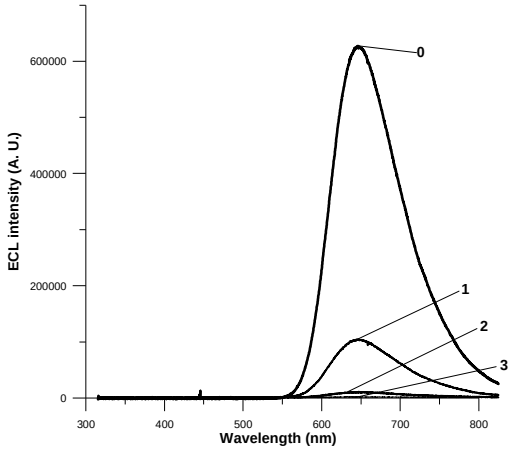

Figure 36. Ru(pyr-tet) ECL spectra in presence of 0, 1, 2 and 3 equivalents of CF_3COOH. CCD accumulation time: 4 minutes. Potential program is the same described in fig. 35. The spectra is registered from a 10^{-3} M MeCN containing 0.1 M $TBAPPF_6$ as supporting electrolyte. The cell was Ar degassed for 10 min before each run.

to reduce because of the possible coordination of two hydrogen atoms at once. There is no shift on maximum emission wavelength when acid is added but only a clear decrease of intensity of about 60 times. This result is in agreement with previous conclusions that Ru(pyr-tet) is still not protonated.

3.2.4 ECL of Ru(pyr-tet) in buffered aqueous solution.

The bright ECL emission of Ru(pyr-tet) in MeCN solution together with his discrete solubility in water suggested the possibility to perform ECL tests in aqueous conditions. These measurements were necessary to check the complex readability to biological assays because practical experimental conditions are air equilibrated aqueous buffers. This series of tests was also an occasion to compare the performance and emission features of $Ru(bpy)_3^{2+}$ with that of the tetrazolate based more efficient dye. The delicate aspect of ECL quantitative measurement was taken in account by using the square geometry cell and trying to find the conditions in which ECL was higher and stable at the same time. ECL was obtained by oxidation in presence of NPr_3 in a 0.1 M phosphate buffer solution (PBS) at pH 7.5 the value at which coreactant activity is maximum according to Leland.[23] The concentration of the ammine, considering that his effect on ECL intensity is known to be linear, was equal to solubility at pH 7.5 to maximize emission intensity ($3x10^{-2}$ M).[23] A preliminary comparison of emission features has been performed by using a true reference electrode. (fig. 37). As expected the light/potential curve has two maxima for all dyes the first in correspondence of NPr_3 oxidation and the second when Ru complex is oxidised. Because NPr_3 is in large excess respect to Ru the first maxima is much more intense than the second. Potentials of oxidation of NPr_3 and Ru complexes can be thus estimated from light/potential curves. NPr_3 is oxidised at + 0.84 V (1), $Ru(bpy)_3^{2+}$ at +1.18 V (2) and Ru(pyr-tet) at + 1.39 V (3) vs Ag/AgCl. Ru(pyr-tet) has an higher oxidation potential respect to $Ru(bpy)_3^{2+}$. Has been however
empirically found that to obtain an higher intensity and reproducible signal is convenient to include only NPr_3 oxydation during ECL experiments. For this

reason the two dyes are equivalent from this point of view. If fig. 37 is carefully observed is also evident that the Ru(pyr-tet) emission peak in correspondence of NPr_3 oxidation is broader than that of $Ru(bpy)_3^{2+}$. This feature is for sure a benefit of Ru(pyr-tet). In a successive series of tests the maximum intensity of emission was carefully compared. By employing bottle quality NPr_3 ECL maximum intensity detected from Ru(pyr-tet) was of 8 times higher than that of $Ru(bpy)_3^{2+}$. (not shown) Being the value of relative emission intensity far from $\phi_{rel,PL}$ the presence of impurity in the ammine was a possible explanation.

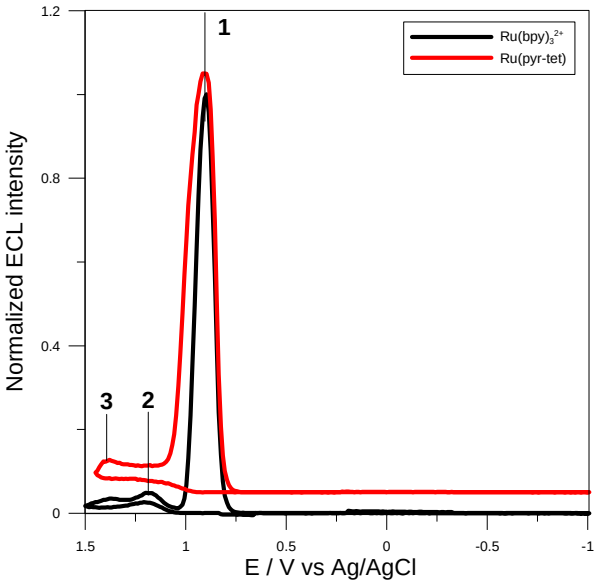

Figure 37. Comparison of the light/potential curves of $Ru(bpy)_3^{2+}$ and Ru(pyr-tet). Supporting electrolyte: phosphate buffer solution (PBS) 0.1 M (pH 7.5). ECL mechanism: oxidation in presence of NPr_3 ($3x10^{-2}$ M). Switching method: Cyclic voltammetry. Scan rate: 0.2 V/s. The cell is that with square geometry introduced in chapter 2. Working and two symmetrical counter electrodes are Au foils inserted into rigid Teflon support and pressed by a three holes mask. (see section 2.4). Working electrode exposed Au disk was of the approximated diameter of 3 mm. Potentials are referred to Ag/AgCl electrode.

As a matter of fact tetrazolate based dye has proved to be more robust in presence of impurities than $Ru(bpy)_3^{2+}$. The NPr_3 was at this point purified by distillation and a yellowish highly fluorescent fraction was separated indicating the presence of oxidation products.

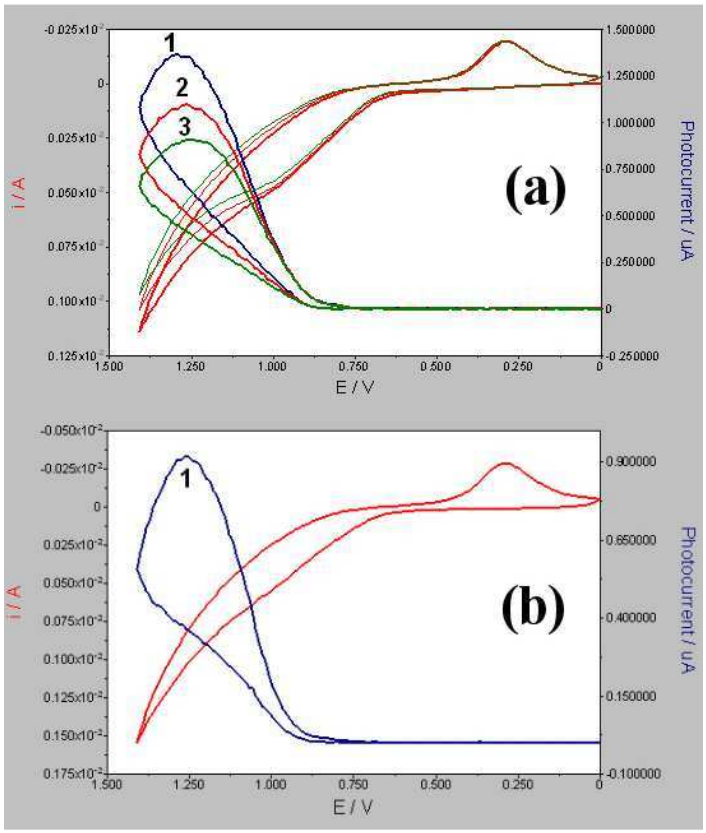

Figure 38. Light/current/potential curves registered during cyclic voltammetries in aqueous 10^{-5} M solutions of the complex: (a) Ru(pyr-tet); (b) $Ru(bpy)_3^{2+}$. Potential is swept from 0 V to that of maximum ECL intensity (+1.35 V). Experimental conditions are identical to that described in fig. 37 but a quasi reference Ag wire has been employed for the sake of simplicity. NPr_3 was purified for distillation and preserved under Ar.

The distilled NPr_3 (perfectly clear) was preserved under Ar to avoid oxidation in air. By using this purified NPr_3 the performances of the two complexes has been again compared: first effect was a general increase of signal of about 10 times respect to previous measurements. In fig. 38 is shown that Ru(pyr-tet) has a maximum intensity of 1.4 μA of photocurrent vs. the 0.9 μA of the standard. A relatively slow scan rate of 0.2 V/sec is used to minimize emission intensity decay upon cycles (see fig. 38.a). The factor that causes ECL maximum intensity decrement when scan is repeated is the formation of filming products at the electrode (see appendix for an overview of the causes and possible cleaning methods) which is proportional to current and thus to scan rate.

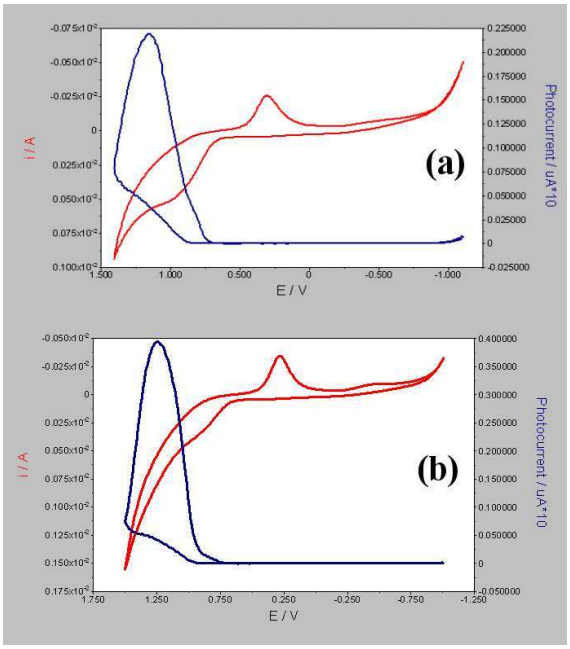

Figure 39. Light/current/potential curves registered during cyclic voltammetries in aqueous 10^{-5} M solutions of the complex by using a cathodic working electrode cleaning. (a) Ru(pyr-tet); (b) $Ru(bpy)_3^{2+}$. Potential is swept from 0 V to maximum ECL intensity (+1.35 V). and then to -1 V. Experimental conditions are the same described in previous fig. 38. NPr_3 was purified for distillation and preserved under Ar. Potentials are referred to Ag wire.

This effect can be easily avoided by inserting a cathodic cleaning swept (-1 V). When negative potentials are reached in water molecular hydrogen is generated at the working electrode detaching the films eventually adsorbed. This cleaning effect is clearly evidenced in fig. 39 where the $Ru(bpy)_3^{2+}$ intensity is increased of 40 times and that of Ru(pyr-tet) of 16 times. In these conditions moreover the ECL intensity is constant for repeated scans and the max. ECL intensity of the standard is higher than that of Ru(pyr-tet) (40 vs 22.5 μA). The ECL emission maxima for the two complexes was found identical in water and MeCN solution.

Many complexes whose exhibit a good ECL efficiency in organic solvents show a very weak emission in aqueous air equilibrated solutions. In these experiments has been found that the new complex Ru(pyr-tet) has an ECL emission intensity similar to the standard also in presence of water and air. The new dye seems to produce less filming products than $Ru(bpy)_3^{2+}$ when NPr_3 impurities are present. Light emitted at the working electrode is still clearly visible by eye in a dark room even at a Ru concentration of 10^{-5} M. The rare properties of this new complex allow to test his interaction with DNA by ECL and fluorescence titration. The new molecule is also very promising in the field of ECL labels for immuno-assays.

3.3.
Studies of interaction with DNA of Ru(pyr-tet) and Ru(pyr-tet)Me

3.3.1.
Introduction.

DNA structure

DNA is a high molecular weight polymer of 2'-deoxyribonucleoside-5'-monophophates[24]. Sequential linkage of the deoxyribonucleosides occurs via condensation of the 5'-phosphate group with the 3'-OH of the next deoxyribonucleoside in the chain. Each unit possesses a purine (adenine (A) or

guanine (G)) or pyrimidine (thymine (T) or cytosine (C)) at the 1 position of the deoxyribose ring. The base is attached to the sugar via the 9-N of the purine or the 1-N of the pyrimidine. Hydrogen bonds between the bases on two anti-parallel chains results in the familiar, double stranded, complementary base pairing of DNA. Calf thymus DNA, the nucleic acid used in this section, is composed of 40 % G-C base pairs and 60 % A-T base pairs.[24] The polymer exists as the common B-form helix (fig. 12 of chapt. 1), in typical electrolytes which has a repeat unit of 10.5 base pairs per helical turn (helical pitch = 34 Å; i. e., ca. 3.4 Å per base pair) and a diameter of 20 Å.[25] The planes of the hydrogen-bonded base pairs are roughly perpendicular to the major axis of the helix.

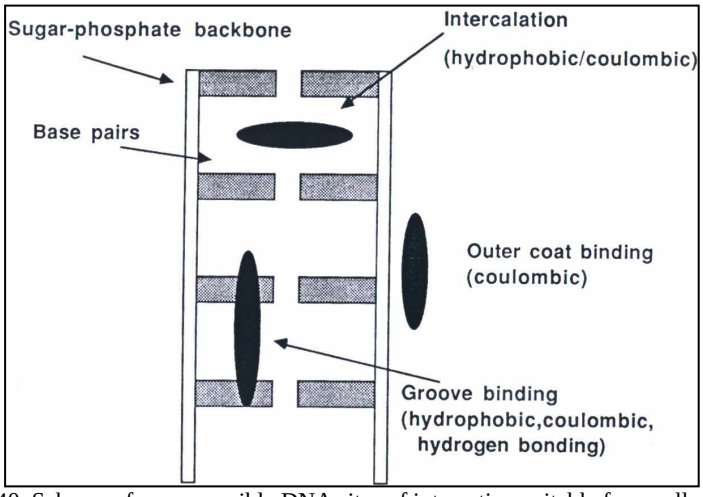

Figure 40. Scheme of some possible DNA sites of interaction suitable for small molecules.

Interactions of small molecules with DNA

The structural features of DNA provide for several distinct types of interactions with small molecules. The first two types are simple electrostatic interactions and coordinative interactions, for example between DNA and divalent metal ions such as Zn^{2+}, Pb^{2+} and Cu^{2+}. Electrostatic binding of cations to the anionic sugar-phosphate backbone of DNA or coordination of these ions to suitable sites involving nitrogens on the bases has been reviewed

in detail.[26] Binding of simple metal ions can have profound effect of the structure and function of DNA. The conformation of the helix, the energy required to separate the double-stranded form and the ability of DNA to participate in normal biochemical functions can all be affected upon metallation. For example, Ni^{2+} can produce DNA protein crosslink, which compromise the fidelity of DNA transcription, ultimately resulting in carcinogenesis.[27] A third fundamental interaction is intercalation. Insertion of small, planar, aromatic species between adjacent base pairs of DNA is usually accompanied by an electrostatic binding component, in addiction of a hydrophobic one for the nonbonding interaction between the intercalator and bases. The double helix of B-DNA possesses a large major groove and a shallower, narrower minor groove,[25] into which various drugs may insert themselves (groove binding). This fourth major type of interaction (often occurring in conjunction with intercalative, electrostatic and hydrogen-bonding interactions) is illustrated by several types of antibiotics and anti-cancer agents. e. g. actinomycin (intercalation, major groove binding)[28] and netropsin (minor groove binding)[29]. The fundamental types of interactions are summarized in fig. 40.

Inorganic complexes interacting with DNA

The existence of small complexes that bind and react at specific sequences or sites is important to understand how to target DNA with specificity. These mechanisms lead not only to novel chemotherapeutics but also to the synthesis of new molecules reliable for highly sensitive diagnostic tools. Stable, inert, and water-soluble complexes containing spectroscopically active metal centers are extremely valuable as probes of biological systems. Intercalators are small molecules that contain a planar aromatic heterocyclic functionality which can insert and stack between the base pairs.[30] First series of complexes that were reported to bind DNA for intercalation were Pt(II) planar molecules containing an aromatic heterocyclic ligand.[31] In following years has been found that increasing the surface area for intercalative stacking by a complex leads to a substantial increase in binding affinity. As a result, metallointercalators which

contain an extended heterocyclic ligand can provide effective tools to probe nucleic acids.[32-35] By inserting and stacking between the base pairs, octahedral complexes containing the 9,10-phenanthrenequinone diimine (phi) or dipyridol[3,2-a:2',3'-c]phenazine (dppz) ligand provided predictable, stable anchors in the major groove with a known orientation of all the functionalities on the metal complex established with respect to the DNA duplex. (fig. 41)

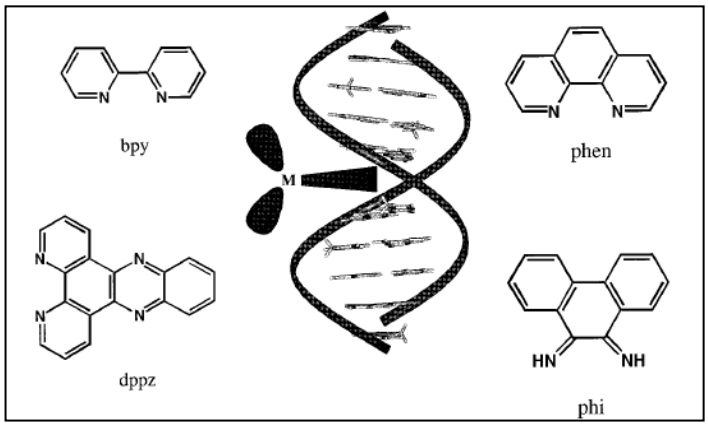

Figure 41. Ancillary ligands (bpy and phen, not intercalating) and a single intercalating ligand (dppz or phi) need to be present in the same complex to obtain an effective DNA probe. In the centre of figure is depicted a molecule of complex intercalated into DNA major groove.

$[Ru(phen)_2(dppz)]^{2+}$ do not luminesce in aqueous solutions due to the ability of water to deactivate the excited state through hydrogen bonding with the intercalating ligands.[36-38]Interestingly, upon introduction of B-form, double-helical DNA to an aqueous solution, photoluminescence is observed,[36] reflecting the shielding of the intercalating ligand from bulk solvent. (fig. 42). For $[Ru(phen)_2(dppz)]^{2+}$ bound to DNA the excited-state lifetime is approximately 200 ns, whereas free in aqueous solution is only 200 ps.[38] This light switch effect is quite remarkable and provides the basis for a valuable photophysical probe of nucleic acids. $[Ru(phen)_2(PHEHAT)]^{2+}$ is also a light switch but displayed a lower quantum efficiency increase when bound to DNA

respect to $[Ru(phen)_2(dppz)]^{2+}$.[39] Some Ru complexes show decreased luminescence bound to DNA as a result of electron transfer quenching, the majority showed no increase or only a slight increase. The photophysics and photochemistry of many Ru and Os complexes in presence of DNA has been the subject of a recent review.[40]

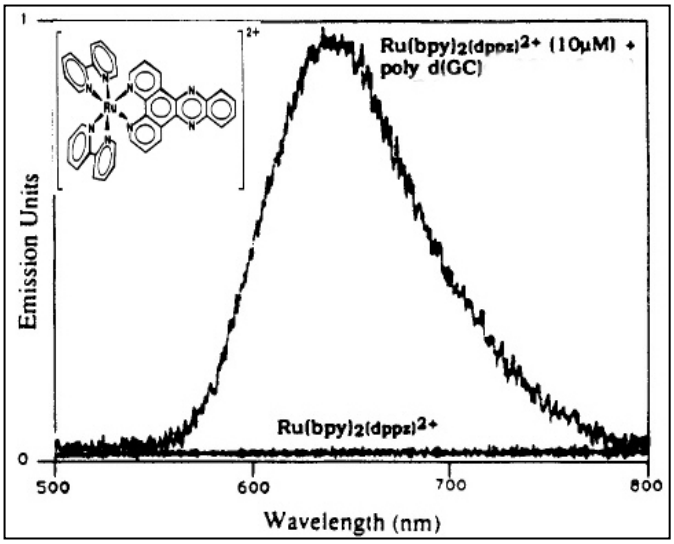

Figure 42. Steady-state emission spectra of $Ru(bpy)_2(dppz)^{2+}$ (10 pM) in the absence and presence of B-form double-helical nucleic acids. In each case in the absence of polynucleotide, only the base-line spectrum, the same level of emission as detected with pure solvent, is obtained for the ruthenium complex in 50 mM NaCl/5 mM Tris, pH 7.0, at 25 °C.

The emission intensity of the ruthenium(II) complexes is modified considerably on increasing the DNA concentration in the medium, as illustrated in the case of $Ru(bpy)_n(TAP)_{3-n}^{2+}$ in fig 43. Interestingly, two types of behaviour are observed for these series: if the complex contains less than two oxidizing TAP ligands, the emission increases with increasing DNA concentration, whereas if the complex contains two or three TAP the emission is quenched indicating that the most oxidizing complexes in the excited state are quenched by DNA. In the case of luminescence enhancement, the

complexes are protected by the DNA double helix. In contrast for complexes containing at least two π-acceptor ligands the ^{3}MLCT states are quenched by the nucleobases.

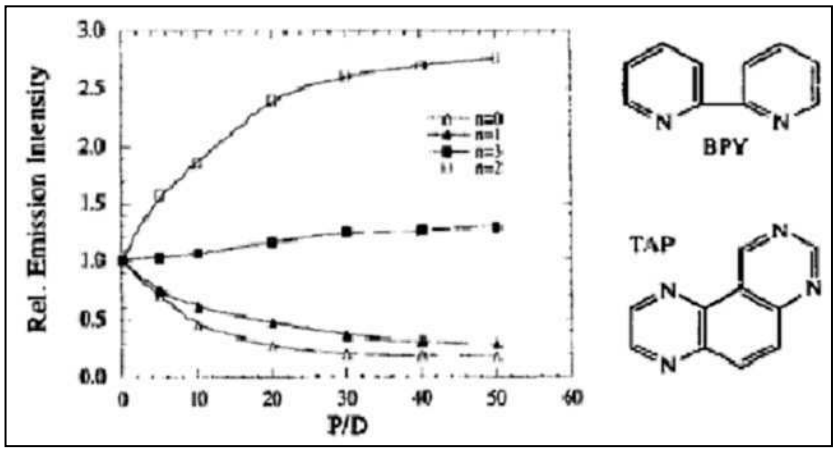

Figure 43. Effect of increasing ratio of DNA (P/D = nucleotide phosphate conc./ [Ru]) in the emission intensity of the complexes at constant concentration for $Ru(bpy)_n(TAP)_{3-n}^{2+}$, n= 0, 1, 2, 3.

The systematic introduction of variations into dppz ligand on $[Ru(phen)_2(dppz)]^{2+}$ did not lead to improvements in sensitivity to aqueous quenching of luminescence so that new compounds cannot be accurately described as "light switch". Replacement of the ruthenium with osmium as the central metal ion causes the luminescence observed for Ru(II) with a maximum of 620 nm to red-shift to 738 nm.[41] This compound can be used as a red-emitting luminescent reporter of DNA presence. $[Co(phen)_2(dppz)]^{3+}$ has also been synthesized . This analogue binds to DNA with high affinity and is able to cleave DNA when photoirradiated.[42] Finally $[Re(CO)_3(py)$- $(dppz)]^+$ has been proven to have the same light switch effect as complex containing Ru(II).[43] This complex is capable of tightly bind calf thymus DNA and when irradiated to cause DNA damage. [44] In the following sections the interaction with DNA of Ru(pyr-tet) and Ru(pyr-tet)Me has been tested trying different experimental techniques. The interesting new feature of the tetrazolate based

ligands is the presence of unreacted lone pairs localized in a negatively charged heterocyclic ring which behaviour in presence of DNA has previously never been investigated.

3.3.2
Cyclic voltammetric titration of DNA.

The use of electrochemical investigations to study metallointercalation agents in presence of double strand DNA allowed to provide informations about interactions with both the reduced and oxidised form of the metal.[45] In fig. 44 is shown as an example the cyclic voltammetry of $Co(phen)_3^{3+}$ in presence and in absence of an excess of calf thymus DNA. The presence of nucleic acid causes the peak currents of the CV waves of oxidation and reduction to diminish considerably.

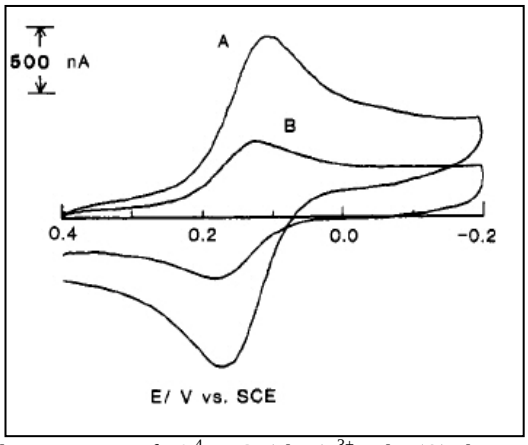

Figure 44. Cyclic voltammograms of 10^{-4} M $Co(phen)_3^{3+}$ in the (A) absence and (B) presence of 5.0 mM nucleotide phosphate (NP). Scan rate, 100 mV/s. Supporting electrolyte: 50 mM NaC1/5 mM Tris pH 7.1. [Adapted from ref. 45].

Additionally, the peak potentials E_{pc} and E_{pa}, both shifted to more positive values. In the following fig. 45 is shown that by adding a non interacting complex ($Mo(CN)_8^{4-}$) his oxidation potential and electrical currents did not changed after DNA addiction. This second experiment showed that the

decrease of i_{pc} for the complex $Co(phen)_3^{3+}$ is not due to an increase of solution viscosity but to the binding with the large and slowing diffusing DNA molecule.

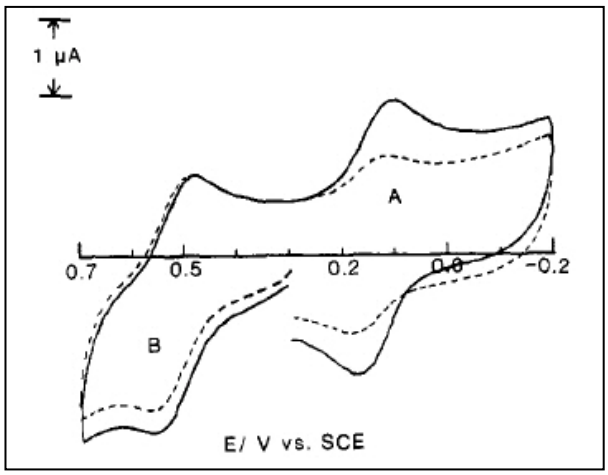

Figure 45. Cyclic voltammetry of a mixture of $Co(phen)_3^{3+}$ (redox couple A, $1.1x10^{-4}$ M) and $Mo(CN)_8^{4-}$(redox couple B, $1.1x10^{-4}$ M), in the absence (solid curve) and the presence (dashed curve) of 5.45 mM NP. Sweep rate, 100 mV/s. Scan initiated at +0.30 V vs SCE. [adapted from ref. 45].

If We define *R*= [NP]/[Ru] where [NP] is the molar nucleotide phosphate concentration the total current i_t at any R is:

$$i_t = B[D_f^{1/2} C_f + D_b^{1/2} C_b]$$

where B= 2.69 x 10^5 $n^{3/2} A \nu^{1/2}$ for CV of a Nerstian wave at 25 ° C. C_b is related to the total metal added, C_t governed by binding of chelate by DNA by

$$C_b = \{b - (b^2 - 2K^2 C_t [NP]/n_S)^{1/2}\}/2K$$
$$b = 1 + KC_T + K[NP]/2n_S$$

where K is the intrinsic binding costant, n_S is the number of pairs required to bind a molecule of complex. (Binding site). This model is valid for noncooperative, non-specific binding and a single discrete binding site for each complex molecule . A similar treatment can be used to deal with more complicated situations. (Mc Ghee Von Hippel model)[46] A regression analysis of the electrochemical data by using this model yield for $Co(phen)_3^{3+}$: K= 5.8 x 10^3, n_s= 6.7, D_f/D_b= 40. It's important to notice the great decrement of diffusion coefficient that follows interaction with DNA. By considering this effect the contribution of the bound fraction can be usually neglected when i_t is calculated.

The cyclic voltammetry was not practically usable to study interactions with DNA of Ru(pyr-tet) and Ru(pyr-tet)Me because of the relatively low water solubility (~10^{-4} M) that prevented from the clear observation of any electrochemical process of the complex. The use differential scan techniques, introduced to shut down the disturbing high capacitive and background currents, did not improved significantly the situation. A similar behaviour has been found for $Ru(bpy)_3^{2+}$.

3.3.3
Fluorimetric DNA titration.

Fluorescence emission has been successfully used, from the early stages, to study the interaction with DNA of many organometallic complexes.[40] The simplicity of sample preparation and the signal reproducibility permits to easily obtain titration curves reporting fluorescence intensity in function of R as already shown in fig. 43.

DNA solution preparation

A 0.1 M phosphate buffer solution (PBS) was first prepared using equimolar quantities of Na_2HPO_4 and KH_2PO_4 in millipore water. The pH was adjusted to 7.5 using concentrated H_3PO_4 or NaOH 3 M. 10 mL of Calf thymus DNA solution (from Sigma Aldrich, pellets) of the approximate concentration of 1

mg/mL was prepared in PBS. Previously described DNA solution was gently inverted for 12 h using a rotating mixer (FALC Mod. F205) maintaining the approximate temperature of 5 °C. The following day the strands not dissolved were praised or mechanically eliminated by tweezers in order to obtain an homogeneous solution. A sample of the solution was diluted of 30 times with PBS and the absorbance spectra was registered three times to ensure his homogeneity.

The nucleotide phosphate [NP] concentration was determinated using the Beer's law dividing the absorbance intensity registered at 260 nm by the assumed ε_{260} = 6600 $L \cdot cm^{-1} \cdot mol^{-1}$.[47] Another interesting parameter to check the quality of DNA sample is the ratio Abs_{260}/Abs_{280}=r. If r is higher than 1.7 the grade of contamination with proteins is considered acceptable. In the DNA solution used for PL and ECL titration experiments was found that [NP] = 1.3 mM and r = 1.85.

Sample preparation and titration curves

50 μM solutions of Ru(pyr-tet) and Ru(pyr-tet)Me were prepared in the same buffer used previously for DNA. Different amount of DNA were then added by obtaining six different solutions with R= 1, 5, 10, 30 and 80. At the same time six equivalent DNA solutions were prepared in PBS 0.1 M/pH 7.5 buffer with R= 0, 1, 5, 10, 30, 80 in absence of Ru complexes. These solutions have been ran first using 468 nm as exciting wavelength. (Ru(pyr-tet) MLCT maxima). The fact that no difference was detected in background emission intensity by varying R was a proof that scattering was not significantly affected by viscosity increasing DNA concentration. The titration fluorescence curves obtained for the complexes Ru(pyr-tet) and Ru(pyr-tet)Me are reported in fig. 46. I(R)/I(0) is the ratio between fluorescence max. intensity at a certain R and max. intensity in absence of DNA. The value I(R)/I(0) has been normalized on Ru concentration considering that Ru complex is diluted from added DNA solution. The linearity of fluorescence intensity vs. [Ru] as been assumed considering the low concentration conditions of the experiments.

The titrations curves reported in fig. 46 have been obtained by mediating the results of three different independent tests for each complex. By considering that standard deviation of I(R)/I(0) is of ± 0.19 for Ru(pyr-tet) and of ± 0.37 for Ru(pyr-tet)Me one can easily conclude that there is in fact no fluorescence intensity dependence on DNA concentration. In the case of Ru(pyr-tet)Me a small effect similar to that observed for $Ru(bpy)_3^{2+}$ (fig. 43) seems however to be present.

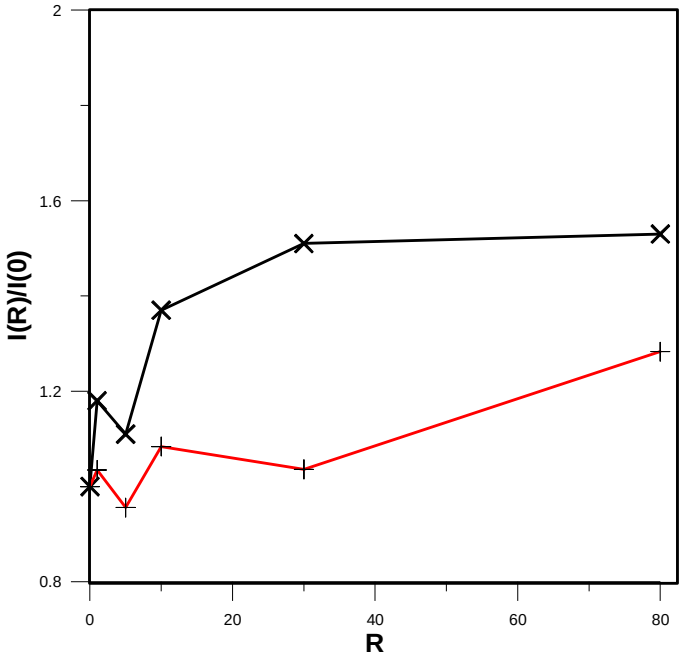

Figure 46. Fluorescence DNA titration of a 50 μM solution of Ru(pyr-tet) (red line) and Ru(pyr-tet)Me (black line). Experiments were performed in PBS 0.1 M/pH 7.5.

As expected from tetrazolate based ligands compact structure an efficient intercalation into DNA base pairs was not evidenced from titration curves. A weak electrostatic interaction with the DNA sugar backbone could be although present. It's important to remember moreover that as discussed above the

majority of the complexes interacting with DNA show no sensible change of fluorescence intensity in his presence. (sect. 3.3.1.)

3.3.4

ECL DNA titration.

DNA titration by using ECL signal is more complicated than correspondent fluorescence experiments. Some delicate questions are the ECL signal reproducibility and the accurate standardization of electrodes cleaning procedure. ECL DNA titration of Tris(1,10-phenanthroline)ruthenium(II) and of Tris(2,2'-bipyridine)osmium(II) have been reported by Bard and co-workers by using IGEN commercial ORIGEN analyzer[47,48] , the flow cell system introduced in fig. 11 of chapter 1. From ECL titration curves analogously to voltammetric approach binding constant K and binding size n_s can be normally calculated by regression analysis using the classical McGhee and von Hippel model.[47] If C_t is total concentration of emitting species, C_b the concentration bound to DNA and C_f the free one it's clear that $C_t=C_b+C_f$ and $X_b=C_b/C_t$. Under the assumption that only free metal complex contribute to ECL can be written that:

$$\frac{I(R)}{I(0)}=\left\{\frac{RC_tK}{2}\left[1-2n_s(X_b/R)\right]\times\left[\frac{1-2n_s(X_b/R)}{1-2(n_s-1)(X_b/R)}\right]^{s-1}+1\right\}^{-1}$$

which is exactly the equation to be regressed to find the values of K and n_s .

Sample preparation and experimental conditions

Electrochemical cell employed was the previously described square geometry cell (fig. 17 chapt. 2) . Working electrode was an Au foil disc of the approximate diameter of 3 mm. The two counter electrodes, positioned symmetrically on the left and right side of working electrode were two Au

discs of 2 mm diameter. The reference electrode was an Ag/AgCl electrode. A photomultiplier tube, biased at 750 V and placed in front of cell, completely including emitting electrode surface was used as light detector. For ECL measurements 5 sets of freshly prepared solutions with R= 0, 1, 5 , 30 and 80 were used for Ru(pyr-tet) and Ru(pyr-tet)Me. The composition of solutions was exactly the same of those employed in previous fluorescence experiments except for the presence of $3x10^{-2}$ M NPr_3 added in the base solution (R=0). The switching method was cyclic voltammetry. After a chronoamperometric step of 1 minute at – 1.0 V vs Ag/AgCl cyclic voltammetry was performed at 0.2 V/s from 0 V to + 1.0 V. The maximum ECL intensity detected was taken as signal and mediated over 5 independent identical samples. The CA step was necessary to clean carefully the electrode from eventual films prior to run the measurement. Other conditions are substantially those obtained during Ru(pyr-tet) ECL optimization experiments described in sect. 3.2.4.

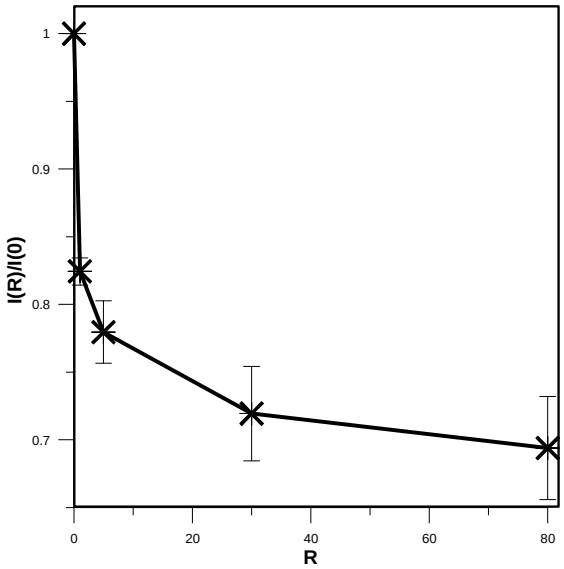

Figure 47. ECL Normalized titration curve of Ru(pyr-tet)Me (50 μM) with calf thymus DNA. Plotted signal is the ECL maximum intensity mediated on 5 independent samples. Experiment is performed after a preliminary cathodic working electrode cleaning (-1 V vs. Ag/AgCl) by

oxidising in presence of NPr_3 $3x10^{-2}$ M (max potential + 1.0 V). Scan rate: 0.2 V/s. Supporting electrolyte: PBS 0.1 M at pH 7.5.

After each run the cell and the electrodes were carefully washed with acetone, sonicated for one minute in Millipore water, washed again with water and acetone and carefully dried prior to the introduction of next sample.

Preliminary results and discussion

The calf thymus DNA titration curves of Ru(pyr-tet)Me and Ru(pyr-tet) are reported respectively in figures 47 and 48. The I(R)/I(0) value has been normalized on [Ru] as was made for fluorescence experiments to take in account the progressive dilution of the complex by increasing R. It's also important to notice that the ratio $[NPr_3]/[Ru]$ is constant respect to R with a large excess of the ammine. In the case of Ru(pyr-tet)Me (fig. 47) I(R)/I(0) decreases when DNA concentration increases. This behaviour is that observed for Tris(1,10-phenanthroline)ruthenium(II) and of Tris(2,2'-bipyridine)osmium(II) [47,48] but in the present case the data cannot be regressed by the classical McGhee and von Hippel model discussed above. The decrease of ECL intensity is related to the drift of the complex diffusion coefficient when is in associated form (see 3.3.1). The complex bond to DNA is practically no more generating ECL because cannot reach the electrode surface. The Ru(pyr-tet) behaviour on the other hand is completely unexpected showing an I(R)/I(0) almost linearly proportional to R . Considering that Ru(pyr-tet) fluorescence intensity has not evidenced any increment in presence of DNA this complex would be in contrast with previously published complexes. The drift of diffusion coefficient cannot be compensated in this case by quantum efficiency increase and for this reason is completely incompatible also with McGhee and von Hippel model. By watching the error bars in titration curve of Ru(pyr-tet) however It's evident that the standard deviation σ of I(R)/I(0) is increasing with R. Considering that I(R)/I(0)-I(R+1)/I(0) is often lower than $0.5 \cdot \sigma$ one can be statistically confident at 50 % that ECL increase is real but there is the 50 % of probability that ECL is constant respect to R and what is observed is a simple variation inside

population. For those reasons ECL titration experiments need to be repeated by trying to solve reproducibility problems. Preliminary data indicated however a substantially different behaviour in Ru(pyr-tet) and Ru(pyr-tet)Me that could be caused by the residual reactivity of Ru(pyr-tet). This aspect will be object of future investigations by the new flow cell system that has been thought as an improvement tool of ECL titrations.

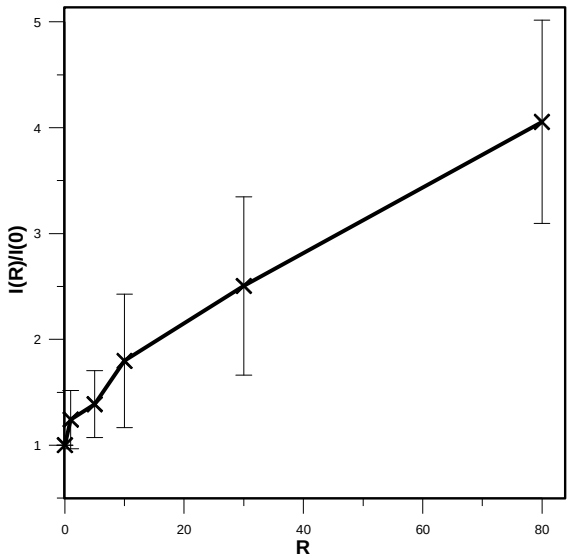

Figure 48. ECL normalized titration curve of Ru(pyr-tet) (50 μM) with calf thymus DNA. Experimental conditions are identical to those previously described in fig. 47.

Appendix III: filming reactions and electrode cleaning techniques.

If We consider a typical system where ECL is generated by simultaneous oxidation of a Ru(II) complex and NPr_3 the following processes have to be taken in account:

Oxidations at working electrode

1a) **Ru(II) - e^- → Ru(III)$^\bullet$**

1b) **NPr_3 - e^- → $NPr_3^{\cdot+}$**

Collateral reaction of generated species

2a) **Ru(III)$^\bullet$ + NPr_3 impurities → Filming products**

2b) **Ru(III)$^\bullet$ + H_2O → Filming products**

Excited species generation and light emission

3) **Ru(III)$^\bullet$ + $NPr_3^{\cdot+}$ → Ru(II)***

4) **Ru(II)* → Ru(II) + light**
(Step governed by fluorescence quantum efficiency)

1a), 1b), 3) and 4) are very fast electron transfers and radicalic reactions. 2a) and 2b) are slow and can cause discrepancies between PL and ECL efficiency by reducing the amount of Ru(III) in 3). The use of pure NPr_3 is fundamental to avoid absorption layers at working electrode. Negative secondary effect of adsorption films are: (i) decrease of working electrode oxidizing surface and total charge injected; (ii) decrease of emitting surface and consequently of total emitted light .
The film adsorbed on electrode surface can be soluble on not soluble. In the first case a time t is necessary to diffuse away and the secondary effects are time limited causing also a longer ECL response time. In this case solution stirring could help to shorten the film diffusion time. If produced film are not soluble they need to be removed. Some possible methods are:

- Cathodic H_2 bubbling by applying negative potentials to aqueous solutions.

- Use of rotating disk electrode where diffusion layer is continuously renewed and solution stirred.

- Use of UME (ultra micro electrodes) where with spherical diffusion steady state is reached faster than in “macro” electrodes .

- Mechanical film removal by alumina, diamond paste or sonication.

- Washing with acid and basic solutions.

The formation of filming products can alter observed relative ECL efficiency between complexes especially if adsorbed layer is formed with different equilibrium constants and kinetics.

References

[1] V. Balzani, F. Scandola, *Supramolecular Photochemistry*; Ellis Horwood: Chichester, U.K., (1991); (b) V. Balzani, A. Juris, *Coord. Chem. Rev*., 211, 97 (2001); (c) P. Sauvage, J. P. Collin, J. Chambron, S. Guillerez, C. Coudret, V. Balzani, F. Barigelletti, L. De Cola, L. Flamigni, *Chem. Rev*. , 94, 993 (1994). (d) A. Juris, V. Balzani, F. Barigelletti, S. Campagna, P. Belser, A. von Zelewsky, *Coord. Chem. Rev.*, 84, 85 (1988). (e) V. Balzani, A. Juris, M. Venturi, S. Campagna , S. Serroni, *Acc. Chem. Res.*, 31, 26 (1998). (f) C. A. Slate, D. R. Striplin, J. A. Moss, P. Chen, B. W. Erickson, T. J. Meyer, J. *Am. Chem. Soc*., 120, 4885 (1998). (g) Y. –Z. Hu, S. Tsukiji, S. Shinkai, S. Oishi, J. Hamachi, *J. Am. Chem. Soc*., 122, 241 (2000).

[2] (a) A. J. Bard, *Electrogenerated chemiluminescence*; Marcel Dekker: New York, (2004). (b) M. M. Richter, *Chem. Rev.*, 104, 3003 (2004) .

[3] (a) F. G. Gao, A. J. Bard, *J. Am. Chem. Soc.*, 122, 7426 (2000). (b) A. Wu, D. Yoo, J. K. Lee, M. F. Rubner, *J. Am. Chem. Soc.*, 121, 4883 (1999). (c) H. Rudmann, M. F. Rubner, *J. Appl. Phys.*, 90, 4338 (2001). (d) J. Kido, M. Kimura, K. Nagai, *Science*, 267, 1332 (1995).

[4] M. Buda, G. Kalyuzhny, A. J. Bard, *J. Am. Chem. Soc.*, 124, 6090 (2002).

[5] F. G. Gao, A. J. Bard, *Chem. Mater*., *14*, 3465 (2002).

[6] G. Kalyuzhny, M. Buda, J. McNeil, P. Barbara, A. J. Bard, *J. Am. Chem. Soc.*, 125, 6272 (2003).

[7] R. M. Bukowski, R. Ciriminna, M. Pagliaro, F. V. Bright, *Anal.Chem*., 77, 2670 (2005).

[8] (a) W. Miao, A. J. Bard, *Anal. Chem.*, 76, 5379 (2004). (b) W. Miao, A. J. Bard, *Anal. Chem*., 75, 5825 (2003).

[9] For experimental details on electrochemical measurements in high vacuum conditions using ultra dry solvents please refer to chapter 2 appendix.

[10] (a) V. Balzani, A. Juris, M. Venturi, S. Campagna, S. Serroni, *Chem. Rev*., 96, 759 (1996). (b) G. R. Newkome, A. K. Patri, E. Holder, U. S. Schubert, *Eur. J. Org. Chem*., 235 (2004). (c) E. A. Medlycott, G. S. Hanan, *Chem. Soc. Rev*., 34, 133 (2005). (d) H. Hofmeier, U. S. Schubert, *Chem. Soc. Rev*., 33, 373 (2004). (e) R. Zong, R. P. Thummel, *Am. Chem. Soc*., 126, 10800 (2004). (f) S. D. Bergman, I. Golberg, A. Barbieri, F. Barigelletti, M. Kol, *Inorg. Chem*., 43, 2355 (2004) and references therein.

[11] M. Marcaccio, F. Paolucci, C. Paradisi, S. Roffia, C. Fontanesi, L. J. Yellowlees, S. Serroni, S. Campagna, G. Denti, V. Balzani, *J. Am. Chem. Soc.*, 121, 10081 (1999).

[12] (a) S. Roffia, R. Casadei, F. Paolucci, C Paradisi, C. A. Bignozzi, F. Scandola. J. *Electroanal. Chem.* , 302, 157 (1991). (b) S. Roffia, M. Marcaccio, C. Paradisi, F. Paolucci, V. Balzani, G. Denti, S. Serroni, S. Campagna, *Inorg. Chem*., 32, 3003 (1993).

[13] T. Saji, S. Aoyagui, *J. Electroanal. Chem.*, 58, 401 (1975).

[14] (a) M. G. Teixeira, S. Roffia, C. A. Bignozzi, C. Paradisi and F. Paolucci, *J. Electroanal. Chem.*, 345, 243 (1993). (b) M. Marcaccio, F. Paolucci, C. Paradisi, M. Carano, S. Roffia, C. Fontanesi, L. J. Yellowlees, S. Serroni, S.Campagna, V. Balzani, *J. Electroanal. Chem.*, 532, 99 (2002) and references therein.

[15] Digital simulation of the cyclic voltammetric curves was carried out either by Antigona (the same home made software used for data acquisition) or DigiSim 3.0.

[16] The theoretical calculations at different levels of theory have been used, applying density functional theory (DFT) only in gas phase. Preliminary validation of the model for this class of complexes was carried out by performing geometry optimization (using B3LYP, BP86 and MPW1PW91 functionals, with either 3-21G* on all the atoms or 6-31G* with effective core potential for ruthenium (i) double zeta LanL2DZ and (ii) LACVP* basis set) and it showed that good and reliable results are obtained with BP86/3-21G*, in reproducing the experimental geometry within a maximum average deviation of 0.03 Å for the bond lengths. All calculations were performed using Gaussiano 98 or Spartan 02 software package.

[17] J. B. Flanagan, S. Margel, A. J. Bard, F. C. Anson, *J. Am. Chem. Soc.*, 100, 4248 (1978).

[18] (a) F. G. Gao, A. J. Bard, *J. Am. Chem. Soc.*, 122, 7426 (2000). (b) A. Wu, D. Yoo, J. K. Lee, M. F. Rubner, *J. Am. Chem. Soc.*, 121, 4883 (1999). (c) H. Rudmann, M. F. Rubner, *J. Appl. Phys.*, 90, 4338 (2001). (d) J. Kido, M. Kimura; K. Nagai, *Science*, 267, 1332 (1995).

[19] M. Buda, G. Kalyuzhny, A.J. Bard, *J. Am. Chem. Soc.*, 124, 6090 (2002).

[20] (a) M. Kasha, *Faraday Soc. Discuss.*, 9, 14 (1950). (b) J. Wang, E. A. Medlycott, G. S. Hanan, F. Loiseau, S. Campagna, *Inorg. Chim. Acta*, 360, 876 (2007).

[21] M. Surin, E. Hennebicq, C. Ego, D. Marsitzky, A. C. Grimsdale, K. Mullen, J.-L Bredas, R. Lazzaroni, P Leclere, *Chem. Mater.*, 16, 994 (2004).

[22] I. K. Jae, S. Ik-Soo , K. Hasuck and L. Jin-Kyu, *J. Am. Chem. Soc.*, 127, 1614 (2005).

[23] J. K. Leland, M. J. Powell, *J. Electrochem. Soc.* 137, 3127 (1990).

[24] J. N. Davidson, *The Biochemistry of Nucleic Acids*, 6th ed., Methuen Press: London (1969).

[25] A. Rich, *Proc. R. A. Welch Found. Conf. Chem. Res.*, Welch Foundation: Houston, 29 (1985).

[26] I. Bertini, C. Luchinat, *Structure and Motion: Membranes, Proteins and Nucleic Acids*, Adenine Press: N. Y., pp. 293-329, (1985).

[27] M. Costa, J. D. Heck, *Adv. Inorg. Biochem.*, 6, 285 (1985).

[28] L. A. Marky, J. G. Snyder, D. P. Remeta, K. J. Breslauer, *J. Biomol. Struct. Dyn.*, 1,487 (1983).

[29] J. H. Griffin, P. B. Dervan, *J. Am. Chem. Soc.*, 108, 5008 (1986).

[30] L. S. Lerman, *J. Mol. Biol.*, 3, 18 (1961).

[31] K. W. Jennette, S. J. Lippard, G. A. Vassiliades, W. R. Bauer, *Proc. Natl. Acad. Sci. U.S.A.*, 71, 3839 (1974).

[32] A. M. Pyle, J. K. Barton, *Progress in Inorganic Chemistry: Bioinorganic Chemistry*, S. J. Lippard Ed., John Wiley & Sons: N. Y., 38,413 (1990).

[33] T. W. Johann, J. K. Barton, *Philos. Trans. R. Soc.*, 354, 299 (1996).

[34] C. S. Chow, J. K. Barton, *Methods Enzymol.*, 212, 219 (1992).

[35] C. J. Murphy, J. K. Barton, *Methods Enzymol.*, 226,576 (1993).

[36] A. E. Friedman, J. –C. Chambron, J. –P. Sauvage, N. J. Turro, J. K. Barton, *J. Am. Chem. Soc.*, 112, 4960 (1990).

[37] C. Turro, S. H. Bossmann, Y. Jenkins, J. K. Barton, N. J. Turro, *J. Am. Chem. Soc.*, 117, 9026 (1995).

[38] E. J. C. Olson, D. Hu, A. Hormann, A. M. Jonkman, M. R. Arkin, E. D. A. Stemp, J. K. Barton, P. F. Barbara, *J. Am. Chem. Soc.*, 119, 11458 (1997).

[39] C. Moucheron, A. Kirsch-De MesMaeker, S. Choua, *Inorg. Chem.*, 36, 584 (1997).

[40] C. Moucheron, A. Kirsch-De MesMaeker, J. M. kelly, *J. Photochem. and Photobiol. B: Biology*, 40, 91 (1997).

[41] R. E. Holmlin, J. K. Barton, *Inorg. Chem.*, 34, 7 (1995).

[42] S. Arounaguiri, B. G. Maiya, *Inorg. Chem.*, 35, 4267 (1996).

[43] H. D. Stoeffler, N. B. Thornton, S. L. Ternkin, K. S. Schanze, *J. Am. Chem. Soc.*, 117, 7119 (1995).

[44] V. W. -W. Yam, K. K. –W Lo, K. –K. Cheung, R. Y. –C. Kong *Chem. Soc. Dalton. Trans.*, 3, 2067 (1997).

[45] M. T. Carter, A. J. Bard, *J. Am. Chem. Soc.*, 109, 7528 (1987).

[46] J. D. McGhee, P. H. Von Hippel, *J. Mol Biol.*, 86, 469 (1974).

[47] M. T. Carter, A. J. Bard, *Biocon. Chem.*, 2, 257 (1990).

[48] M. Rodriguez and A. J. Bard, *Anal. Chem*., 62, 2658 (1990).

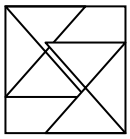

Chapter four: new materials based on Ir

Melius est dare quam accipere

Recently it was found that, among many possible metal/ligand combinations, orthometalated iridium(III) complexes[1] shown an interesting combination of photophysical and electrochemical properties, which makes them very promising materials for the electricity-to-light conversion in the ECL reactions.[2-8]

In this chapter the results of ECL and electrochemical characterization of new and already poublished orthometalated iridium(III) complexes is introduced and discussed. Differently to the chapter 3 new ECL Bologna instrument has

been used in ECL measurements. The only exception was $Ir(pq)_2acac$ that was instead ran with A. J. Bard experimental setup in Austin.

4.1
Reference ECL emitting Ir(III) complexes

4.1.1
$Ir(bpy)_3^{3+}$

$Ir(bpy)_3^{3+}$ (fig.1) is a ionic complex first synthesized about 30 years ago.[9,10] Electrochemistry[11], photophysical properties and spectroelectrochemistry have been already thoroughly investigated and reported.[10,12] To the best of our knowledge however ECL investigations have not be published; considering the high fluorescence efficiency (max. wavelength 510 nm) and the expected water solubility, the complex appeared to us as a promising blu shifted ECL label.

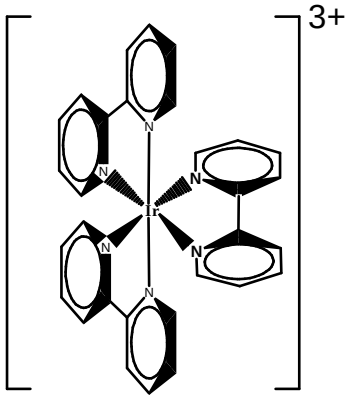

Figure 1. Structure of $Ir(bpy)_3^{3+}$. The compound was provided by Cyanagen s.r l. as a chloride salt.

Electrochemistry

Cyclic voltammetric curve obtained in ultra pure MeCN[11] is shown in fig. 2; the corresponding half wave potentials are summarized in table 1. The cyclic

voltammetry registered before ECL experiments (MeCN not purified) was very similar to that of fig 2. Only the first three reduction processes and Ir(III) centred irreversible oxidation were visible because the presence of water impurities in media reduced the solvent useful potential window.

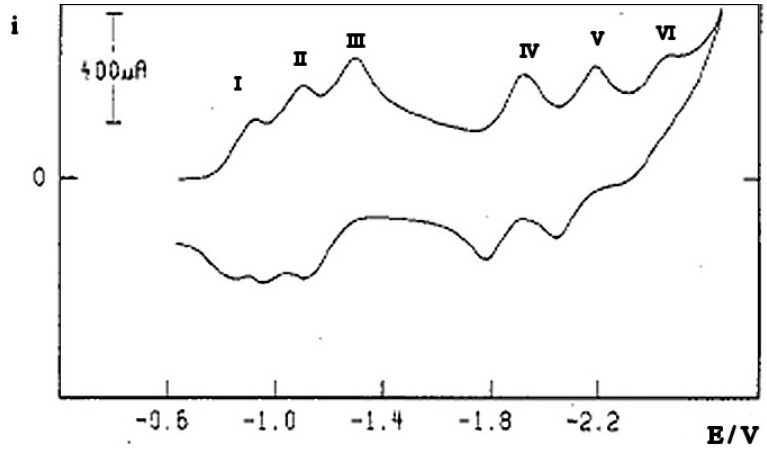

Figure 2. Cyclic voltammogram of 4 x 10^{-4} M MeCN solution of $Ir(bpy)_3^{3+}$; scan rate: 9 V/s. Supporting electrolyte: 0.1 tetraethylammonium perchlorate. Potentials are referred to SCE. [Adapted from ref. 11]

1 Oxidation	I reduction	II reduction	III reduction	IV reduction	V reduction	VI reduction
+2.124 V (irrev)	**-0.829 V**	**-0.998 V**	**-1.224 V**	**-1.843 V**	**-2.097**	**-2.371 V**

Table 1: $E_{1/2}$ of reductive and oxidative processes of $Ir(bpy)_3^{3+}$ vs SCE calculated at a scanrate of 100 V/s. [From ref. 11]

Photoluminescence and absorbance

By using the MLCT band around 370 nm (fig. 3) as exciting wavelength an intense emission spectra has been collected from MeCN solutions. (fig. 4) The relative fluorescence efficiency respect to $Ru(bpy)_3^{2+}$ is about 90 %. Maximum emission wavelength is in the green region (510 nm) as previously reported in literature for similar compounds.[10] Moreover an emission shoulder around 600

nm is visible in the spectra. Emission intensity didn't change sensibly in presence and absence of air. The emission spectra registered in aqueous solution is very similar to that in MeCN. The solubility in aqueous media is however much lower than that in organic solvents.

ECL emission and potential switch effect.

As expected from first oxidation irreversibility only a weak fast disappearing emission was produced by anion-cation direct annihilation**.** The oxidation in presence of the coreactant NPr_3 in MeCN solutions resulted instead in a bright ECL emission well visible by eye also in a lit room. (fig. 5).

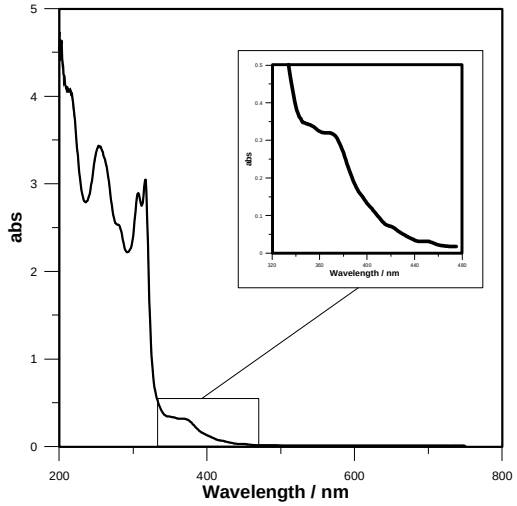

Figure 3. Absorbance spectra of a 10^{-5} M $Ir(bpy)_3Cl_3$ aqueous solution. MLCT and ILCT regions are not clearly separated as reported for similar species.[10] There is no substantial shift on absorbance wavelengths by using MeCN as solvent. Experiments have been ran by using a 10 mm standard quartz cuvette.

Unexpectedly the ECL emission maxima (613 nm) was very close to that of $Ru(bpy)_3^{2+}$. The populated state is probably that corresponding to the shoulder (600 nm) previously observed on fluorescence which was very close to this wavelength. Interesting then if first oxidation of $Ir(bpy)_3Cl_3$ is included (oxidative step potential > 2.2 V vs Ag) a clear shoulder around 500 nm appears in ECL emission spectra. (fig. 5) This can be explained by considering

the 2 possible pathways by which excited state is obtained in presence of NPr_3:

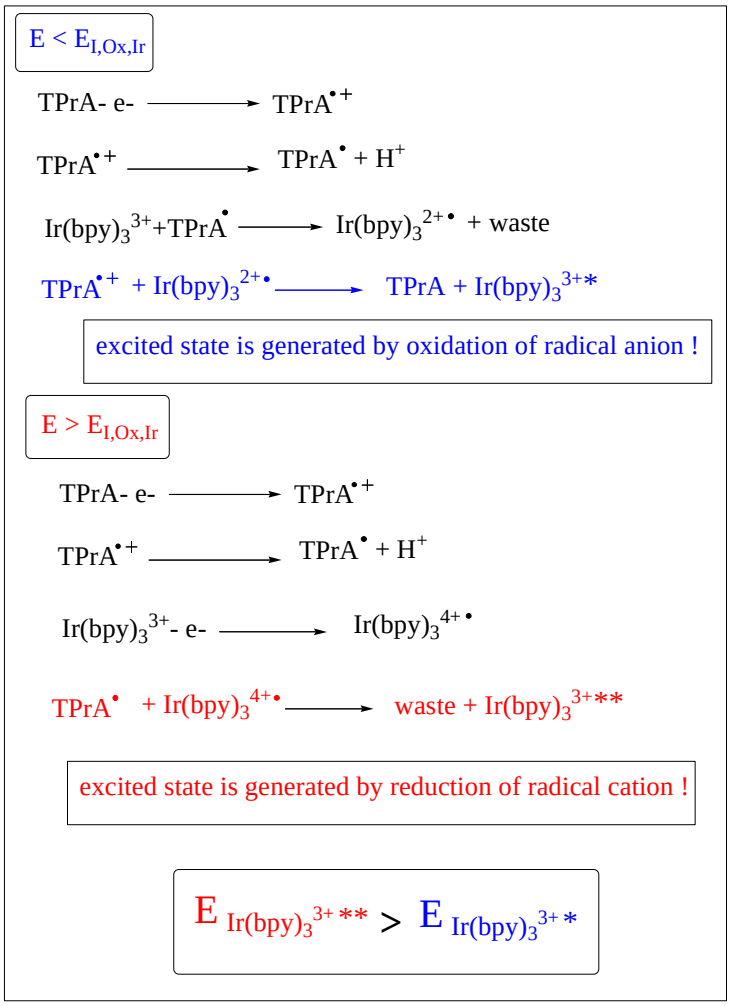

One can then reasonably suppose that two different excited states are generated by varying potential. Considering that fluorescence spectra of $Ir(bpy)_3^{3+}$ has two different emission maxima in the case of generated $Ir(bpy)_3^{3+*}$ only the lower state is populated whereas when $Ir(bpy)_3^{3+**}$ is

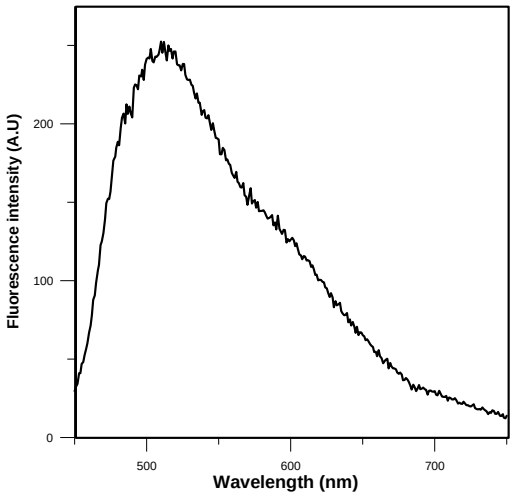

Figure 4. Fluorescence spectra of an Ar degassed 10^{-5} M $Ir(bpy)_3Cl_3$ MeCN solution. Exciting wavelength was of 400 nm. Maximum is at 510 nm with a shoulder around 600 nm.

produced both emission are present in ECL spectra. One could also think that dual emission is due to the presence of an emitting impurity with a lower oxidation potential respect to $Ir(bpy)_3^{3+}$. Respect to Ru(II) complexes where normally MLCT and IL (interligand) transitions are clearly energetically separated in the case of Ir(III) complexes they tends to be much closer and frequently not distinguishable one another. As consequence the presence of multiple peaks and shoulders in the visible region of fluorescence spectra is common.[8,10, 13] . The presence of impurities of more spontaneously formed $Ir(bpy)_2X$ complexes would not change significantly the potential of first oxidation (around +2.3-2.5 V vs SCE) or emission spectra maxima (similarly close to 500 nm).[10,11] Moreover, by observing the voltammetry of our sample of $Ir(bpy)_3^{3+}$ no clear oxidative processes are visible before to reach his proper irreversible process. Considering these aspects the presence of a "potential switch effect" on 500 nm ECL emission is highly probable.

In water ECL emission in presence of NPr_3 completely disappeared. The aqueous media is often sufficient to quench almost completely the fluorescence of many compounds.

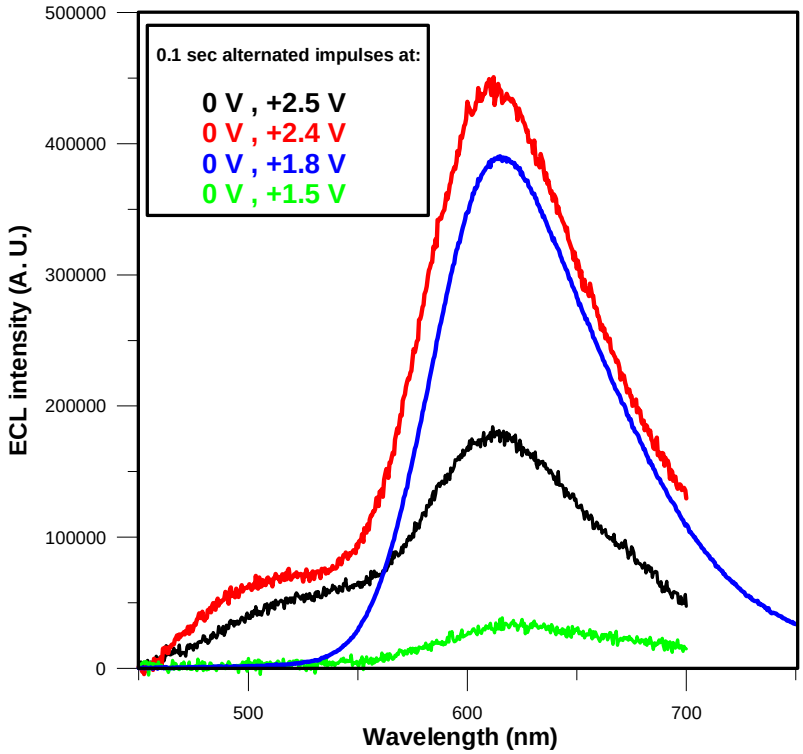

Figure 5. ECL emission spectra of $Ir(bpy)_3Cl_3$ 10^{-3} M MeCN solution by varying the potential of oxidative step. Supporting electrolyte: 0.1 M $TBAPF_6$. Switching method: CA; conditions are specified in the figure inset. ECL mechanism: oxidation in presence of $3x10^{-2}$ M NPr_3. PMT voltage: 1000 V. ITime: 4 s. Monochr. step: 0.5 nm. Potentials are vs. Ag wire.

By considering however that in this case fluorescence is still present a different quenching mechanism needs to be invoked. A possible cause could be the addition of water to the complex coordination sphere during carbocation electrochemical generation. Maybe the presence of chloride anions could also produce some negative effect. Further investigations in aqueous media are however necessary to thoroughly understand the complete disappearance of ECL signal.

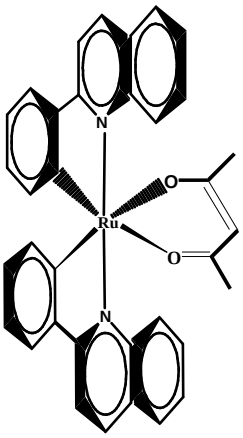

Figure 6. Structure of $Ir(pq)_2acac$. The neutral compound was provided by Cyanagen s.r l.

4.1.2

$Ir(pq)_2acac$

Recently, already existing organometallic materials used in OLED (organic light emitting devices) such as Alq_3[14] and cyclometalated Ir(III) complexes[3,4,6,7] have been studied as new ECL reagents. Since these materials have high PL efficiencies compared to the low PL efficiency of $Ru\text{-}(bpy)_3^{2+}$ (Φ_{PL}= 0.042), some ECL studies on annihilations of self-radical and cross-radical ions have been carried out.[3,4,6] The attention on $Ir(pq)_2acac$ was attracted from a recent paper claiming that the ECL intensity was 77 times higher than that of $Ru(bpy)_3^{2+}$ in $MeCN/NPr_3$ conditions.[15] An aspect unclear in this article was the big mismatching between relative fluorescence (2.5) and ECL (77) quantum efficiency. An unexpected choice was then the use of NPr_3 in MeCN instead of water if the testing was finalized to the use of the dye as a bio-sensor. For these reasons the compound has been synthesised according to the literature procedure[15] and ECL and fluorescence tests have been repeated.

Electrochemistry

By operating in high vacuum conditions (see chapt. 2 appendix for further details) cyclic voltammetric curves have been registered using ultra dry

tetrahydrofurane (THF) as solvent. The results of electrochemical investigations are reported in fig. 7 and the corresponding half wave potentials are summarized in table 2. At low temperature (T= -60 °C) a single reversible oxidation wave (marked as 1) and two reversible reduction processes (I, II) were evidenced (fig. 7.a). If the scan is repeated at room temperature by cycling potential around second reduction his partial irreversibility is clearly observed in the progressive decrease of re-oxidation wave (inset fig. 7.a). A similar partial irreversibility is present at room temperature in the oxidation process. The voltammetric curve reported in fig 7.b evidences the following reductive processes marked as III and IV . These peaks falls close to the limit of solvent discharge and are not clearly definited. For this reasons for the reduction processes marked as III and IV the relative $E_{1/2}$ has not been calculated.

1 Oxidation	I reduction	II reduction
+ 0.98 V (partially irreversible)	**- 1.77 V**	**- 1.94 V (partially irreversible)**

Table 2: $E_{1/2}$ of reductive and oxidative processes of $Ir(pq)_2(acac)$ vs SCE calculated at a scanrate of 1 V/s. T= 25 °C.

If cyclic voltammetry is performed at room temperature using bottle quality MeCN as solvent (e. g. the conditions used in the following ECL experiments) a reversible reductive process and an oxidative one is still present; the $E_{1/2}$ values are very close to those reported in tab. 2. By repeating the scan the oxidation process becomes progressively irreversible; the cause is the probable formation of filming products on electrode surface.

Fluorescence and absorbance

The absorbance spectra of $Ir(pq)_2(acac)$ registered in MeCN is reported in fig. 8. MLCT region has a complicated structure of peaks as happens with many Ir(III) based dyes.[10]

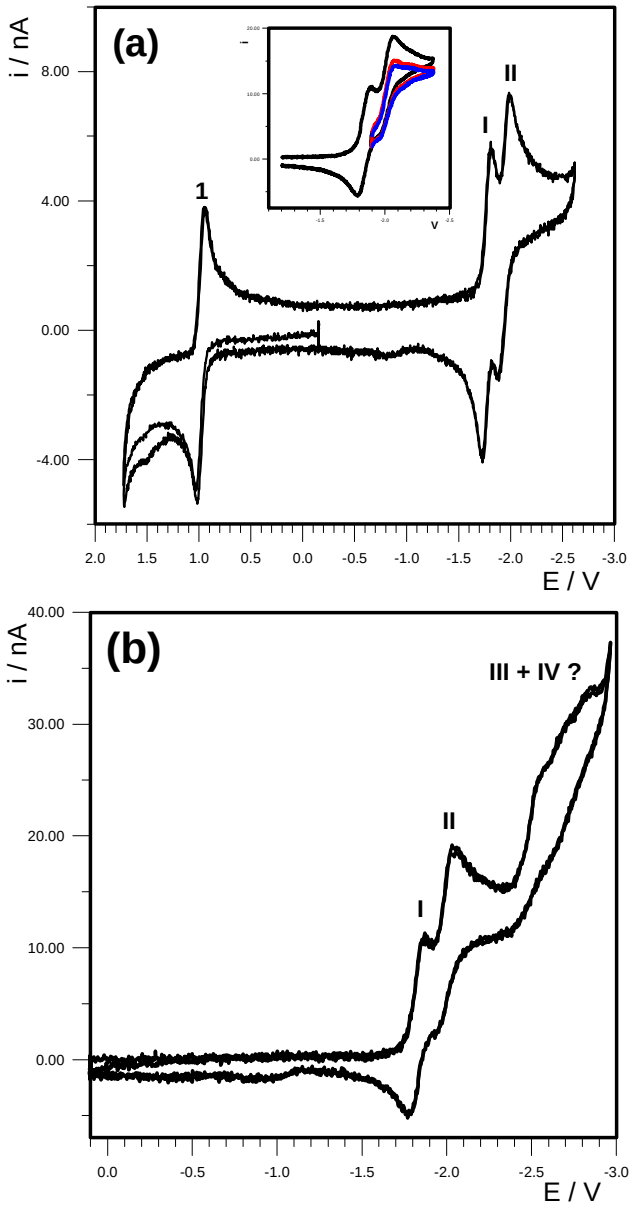

Figure 7. Voltammetric curves of $5x10^{-4}$ M THF solutions of $Ir(pq)_2(acac)$. Supporting electrolyte: 0.1 M $TBAPF_6$. Working electrode: Pt 50 μm UME. (a) T= - 60 °C, scanrate: 1 V/s . (b) (and (a) inset) T= 25 °C, scanrate: 1 V/s. Potentials are referred to SCE.

By using the higher intensity MLCT band as exciting wavelength the emission properties of $Ru(bpy)_3^{2+}$ and $Ir(pq)_2(acac)$ have been carefully compared. (fig. 9). If the fluorescence measurement is performed in Ar degassed cell the relative PL fluorescence efficiency of Ir complex is 2.37 times higher that of $Ru(bpy)_3^{2+}$. This is in excellent agreement with the recently published value of 2.38.[15] If however experiment is repeated in air equilibrated cell the relative fluorescence is close to 1 (0.96).

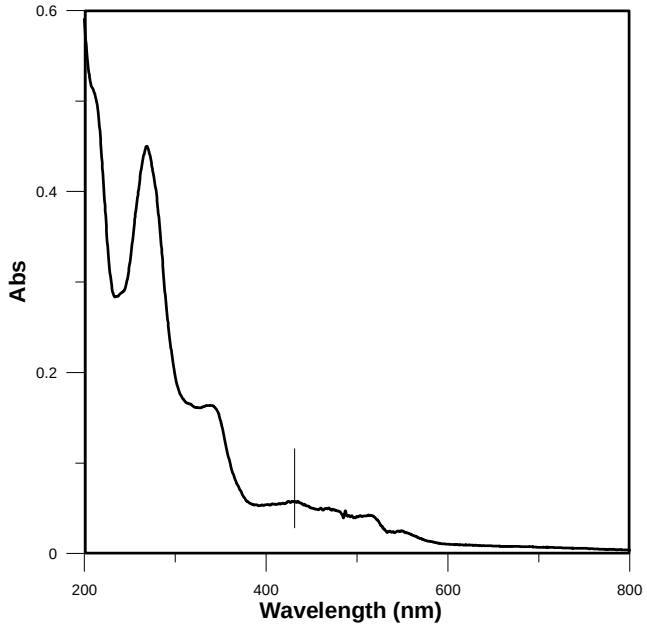

Figure 8. Absorbance spectra of a 10^{-5} M $Ir(pq)_2$acac MeCN solution.

This as a matter of fact demonstrates that the $Ir(pq)_2(acac)$ complex (1/10 of initial intensity) is more sensitive to oxygen quenching than $Ru(bpy)_3^{2+}$ (reduction to ¼ of initial intensity).

ECL comparison

To verify the relative ECL intensity of $Ir(pq)_2(acac)$ and $Ru(bpy)_3^{2+}$ two identical 10^{-3} M MeCN solutions were prepared with an excess of NPr_3 ($3x10^{-2}$

M). All the comparison experiments were ran in the square geometry cell discussed in section 2.4 to improve reproducibility. To confirm the results different types of investigations were performed. In the first series (fig. 10) light/current/potential curves have been registered during slow cyclic voltammetries (scan rate = 0.5 V/s). In the second series the ECL emission spectra was collected accumulating simultaneously all wavelength during chronoamperometric oxidative impulses. (fig. 11)

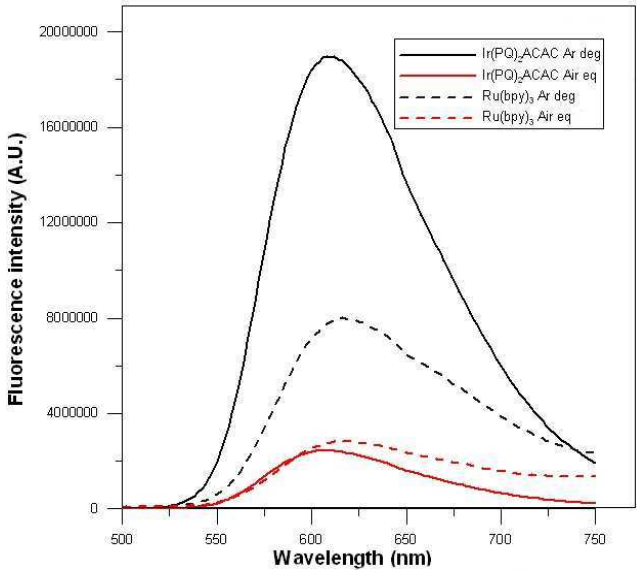

Figure 9. Fluorescence spectra of 10^{-5} M $Ir(pq)_2acac$ and $Ru(bpy)_3^{2+}$ MeCN solutions. Exciting wavelength was 430 nm for $Ir(pq)_2acac$ and 460 nm for $Ru(bpy)_3^{2+}$. Experiment were ran in either Ar degassed (Legend: Ar deg) and air equilibrated (Legend: Air eq) cell to compare the relative oxygen sensitivity.

From the light/current curves reported in fig. 10 can be easily calculated that the maximum ECL intensity of $Ir(pq)_2(acac)$ is 2.17 times that of $Ru(bpy)_3^{2+}$. This value is very close to the relative fluorescence efficiency. The maximum potential applied was that necessary to oxidize the complex and NPr_3. Considering that $E_{1/2,IOx}$ of $Ir(pq)_2(acac)$ is +0.98 V vs SCE and that of $Ru(bpy)_3^{2+}$ +1.20 V[16] the first emits at a lower applied potential. If the curves

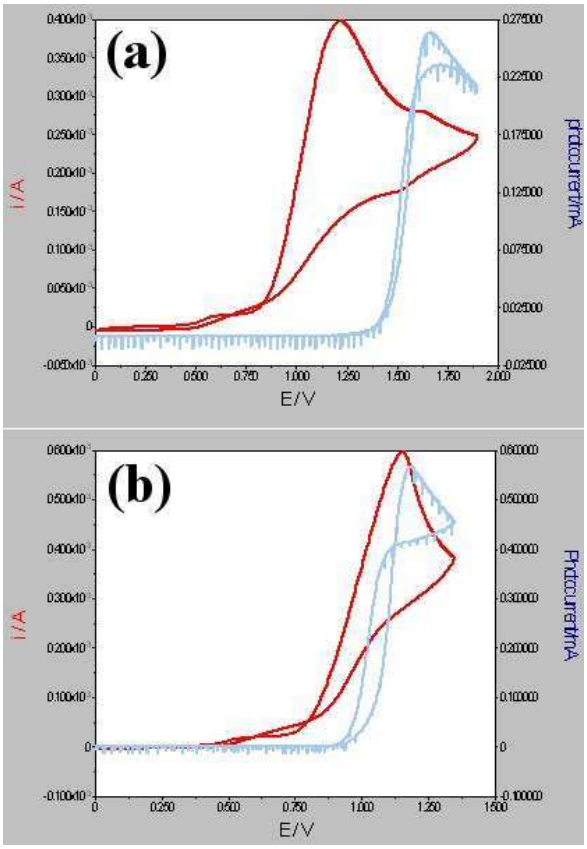

Figure 10. Comparison of the light/current/potential curve of $Ru(bpy)_3^{2+}$(a) and $Ir(pq)_2$(acac) (b). ECL was generated from 10^{-3} M MeCN solutions in presence of $3x10^{-2}$ M NPr_3. Supporting electrolyte: 0.1 M $TBAPF_6$. Switching method: cyclic voltammetry. Scanrate: 0.5 V/s. ECL signal was registered by applying 750 V to a PMT positioned in front of emitting electrode. Potentials are referred to Ag wire.

10.a and 10.b are compared It's clear that the irreversible peak of NPr_3 oxidation is in the same position. This process can be assumed as an internal standard. (~ +0.9 V vs SCE). During these experiments light was emitted only when NPr_3 and the complex radical cation were simultaneously produced. Consequently ECL emission peak was very close to NPr_3 oxidation for $Ir(pq)_2$acac because his I Ox. potential is practically coincident with that of the

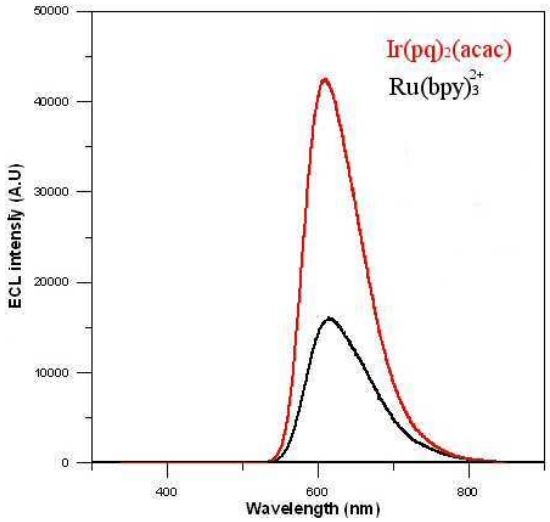

Figure 11. Comparison of ECL spectra of $Ru(bpy)_3^{2+}$ and $Ir(pq)_2(acac)$. Emission was collected from 10^{-3} M MeCN solutions in presence of $3x10^{-2}$ M NPr_3. Supporting electrolyte: 0.1 M $TBAPF_6$. Switching method: chronoamperometry. Potential program: a single 0.1 s impulse at +1.6 V vs. Ag. CCD* accumulation time: 0.3 s. *A new CCD has been used. (Acton Research Mod. SPEC-10). The sensitivity was about 5 times that of the old one already described in sect. 2.2.

ammine. $Ru(bpy)_3^{2+}$ emitted instead at an higher potential (+0.34 V) with respect to NPr_3 oxidation peak. The higher ECL efficiency of Ir complex was confirmed by comparing the single impulse emission spectra. (fig. 11) Maximum ECL intensity of Ir dye is 2.64 times that of $Ru(bpy)_3^{2+}$. If ECl signal is integrated on wavelengths the total light emitted by $Ir(pq)_2(acac)$ is more than 3 times that of Ru dye. We can thus conclude ECL emitting intensity of $Ir(pq)_2(acac)$ is 2.5 times that of $Ru(bpy)_3^{2+}$ a value as expected very close to that of relative fluorescence efficiency. This value is completely different from that of 77 measured in the reference paper! The mission maxima were practically coincident for the two complexes. ($\lambda_{max,Ru(bpy)3}$ =621 nm; $\lambda_{max,\ Ir(pq)2(acac)}$= 618 nm)

ECL by annihilation

An attempt was made to generate ECL by cation-anion direct annihilation in Ar degassed MeCN/$TBAPF_6$ solution. Initially the emission was intense enough to be seen by eye. After few cycles the emission completely disappeared and at the same time I Ox process became irreversible in CV. Using the same bottle quality Ar degassed solvent, containing thus the same amount of water impurities, $Ru(bpy)_3^{2+}$ produced a very intense and time stable emission. This behaviour seem to confirm taking in account previous fluorescence results that $Ir(pq)_2(acac)$ is sensitive to O_2 and water quenching. Another possible explanation is the relatively rapid formation of filming products at the working electrode during oxidation (see electrochemical characterization) that is avoided in presence of the fast radicalic reactions promoted by NPr_3.

Water solubility

$Ir(pq)_2(acac)$ is completely insoluble in water. Sonication, annealing , pH change to acid and basic values did not prevented his complete crystallization and the absence absorbance bands. This behaviour, easily predictable from the absence of charge in the molecule, unrewarding of interesting photophysical and ECL properties is not consistent with the use as DNA or proteins labelling agent. There are however many different possible strategies to solve the solubility problem such as: introduction of peripheral polar groups into the ligands, use as dopant into nanoparticles, synthesis of nanocrystals , suspension with surfactants, etc.

4.2
Ir(III) tetrazolate based complexes

4.2.1
Structures

The compounds investigated in this section are mono- and dinuclear Ir(III) complexes containing mixed tetrazolate and polypiridyl ligands. The Ir(III) and previously discussed Ru(II) complexes containing tetrazolate moiety have been synthesised by A. Palazzi's group in the Bologna faculty of industrial chemistry. The relative chemical structures and acronyms are reported in the following figure 12. The complexes Ir(pyz-tet), Ir(pyr-tet)Br and and Ir_2(2,3-btp) contains the negatively charged ligands: 2-(tetrazol-5-yl)-pyrazine (charge= -1), 2-(tetrazol-5-yl),5-Br-pyridine (-1), 2-(phenyl)-pyridine (-1) and bis-2,3-(tetrazol-5-yl)-pyrazine (-2) . The positive charge of the central metal atom (+3) is completely neutralized in each complex. As consequence all compounds are soluble in organic solvents such as MeCN and dichloromethane (DCM) but completely insoluble in water as $Ir(pq)_2(acac)$.

4.2.2
Electrochemistry: results and discussion

Electrochemical investigations on mono- and dinuclear Ir(III) complexes have been performed in different experimental conditions. In the following paragraphs the results are reported.

Ir(pyr-tet)Br

Electrochemical behaviour of Ir(pyr-tet)Br is shown in fig. 13. The voltammetric curve of the first two reduction processes at room temperature, shows monoelectronic electron transfers. First process is completely

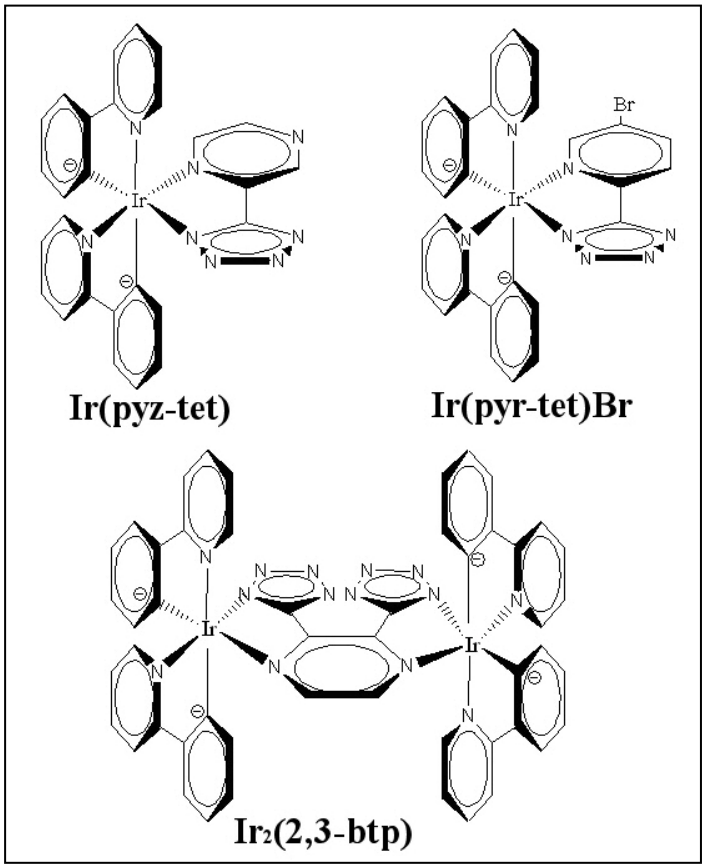

Figure 12. Structure and acronyms of the Ir(III) complexes investigated in this section.

irreversible with a cathodic peak potential of -1.74 V vs. SCE and the second can be considered as reversible. By analyzing voltammetric curve the irreversibility of the first process appears to be at the same time of electrochemical and chemical nature. To understand thoroughly electron transfer processes simulation has been performed. The software employed , called Antigona, has been developed in our lab by Dr. Loic Mottier to simulate voltammetric experiments. The equations which govern the diffusion to the electrode and kinetic processes are solved in function of the parameters of experimental curve. By a best fitting procedure simulated and real data is

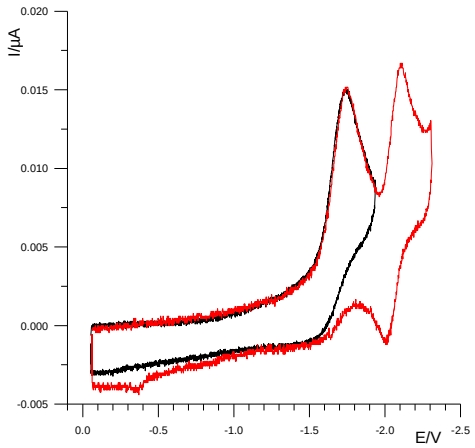

Figure 13. Voltammetric curves of a Ir(pyr-tet)Br 1 mM THF solution. Supporting electrolyte: 80 mM $TBAPF_6$. Working electrode: 10 µm Pt disk. T= 25 °C. Scanrate: 10 V/s.

compared to determine electron transfer constant, standard potential of the irreversible processes and the kinetic constants of the chemical process coupled with redox processes. In the figure 14 the simulated CV (red curve) is in good agreement with experimental one (black curve).

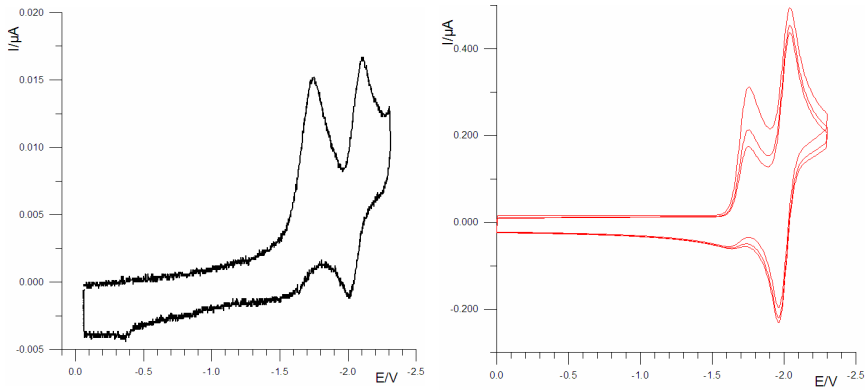

Figure 14. Cyclic voltammetric curves of a 1 mM Ir(pyr-tet)Br THF solution. Experimental conditions are identical to those reported in fig. 13. Experimental curve on the left is compared with simulated one on the right.

Simulation has been ran under the assumption that the mechanism is of ECE (electrochemical-chemical-electrochemical) type as schematized below. When the complex is reduced a chemical reaction will follow from the electro-generated species. The final product of this chemical follow up is himself reduced. In the following kinetic scheme A indicates the initial species (i. e. Ir(pyr-tet)Br) and B the reaction product obtained from A^-.

$$A + e^- \xrightarrow{E^0_{Red,A}} A^-$$

$$A^- \underset{K_b}{\overset{K_f}{\rightleftharpoons}} B$$

$$B + e^- \xrightarrow{E^0_{Red,B}} B^-$$

As discussed previously for Ru(II) complexes being the nature of ligands heteroaromatics the reductions are normally localized on ligands and oxidations on metallic centres. By taking as reference the behaviour of similar species, first reduction is expected to be localized on the (pyr-tet)Br ligand where the presence of the bromine makes the LUMO energy lower. Many old dated papers report that the electrochemical reduction of halogenated aromatic compounds often results in the halogen extraction which is released in solution in his anionic form. In the present case is highly probable that the reaction coupled with first reduction is the Br^- extraction and that B in the above scheme is the complex Ir(pyr-tet). The potential of reduction of Ir(pyr-tet) is more negative than that of halogenated analogue so the second process observed in CV (fig. 13) could be the reversible reduction of B . From simulation the first reduction process resulted as a slow electron transfer (k_h=0.1 cm/s and α=0.3). The chemical follow up has been found to be fast and irreversible ($K_f >> K_b$). By extending the voltammetric scansion to more negative potentials (fig. 15) two further mono-electronic processes are evidenced probably localized in the phenyl-pyridine ligands. Regarding oxidation a mono-electronic process can be noted around +1.38 V not far from solvent discharge. In this case the process should be attributed to Ir but considering the polypyridinic nature of the ligands It's also probable that

oxidation involves a HOMO with a partial contribution of the (pyr-tet) ligand as was found by DFT calculations for Ru(II) analogue complexes. (see section 3.1.1)

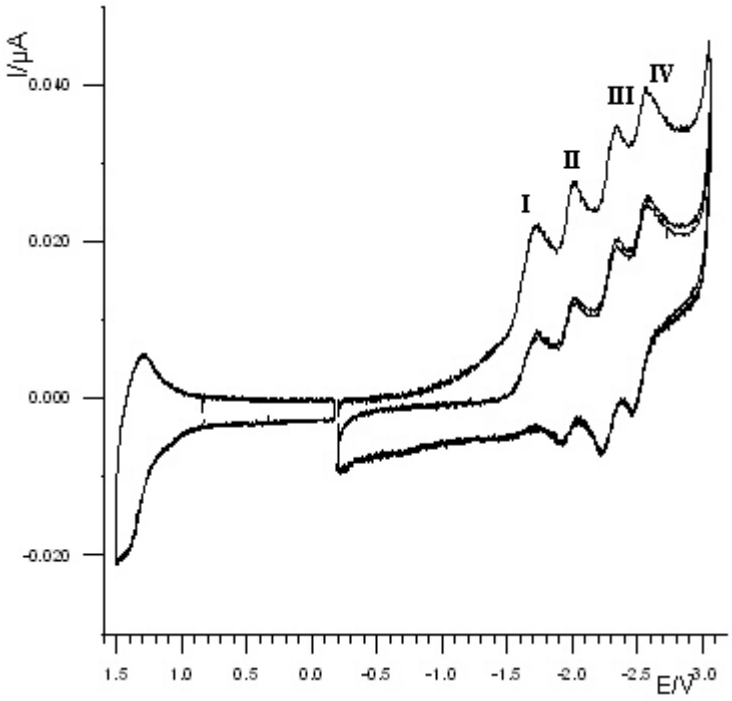

Figure 15. Voltammetric curves of a Ir(pyr-tet)Br 1 mM THF solution. Supporting electrolyte: 80 mM $TBAPF_6$. Working electrode: 10 μm Pt disk. T= 25 °C. Scanrate: 50 V/s.

The simulation of voltammetric curve extended to all reduction processes, reported in fig. 16, confirms the attribution of the remaining two reversible processes. Voltammetric measurements at low temperature (-60 °C) show that I reduction process, relative to the Br^- extraction, unrewarding of the kinetics slow down is still irreversible. Second reduction process didn't changed significantly whereas the remaining processes observed at room temperature were no more clear and confused with solvent discharge. (fig. 17).

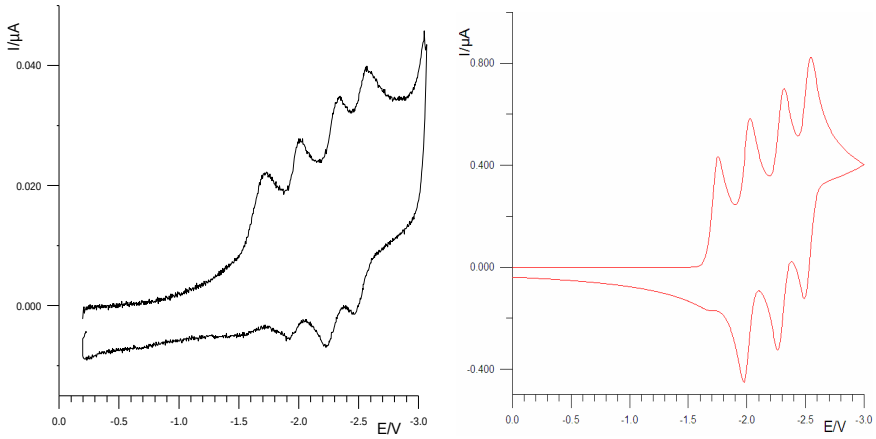

Figure 16. . Cyclic voltammetric curves of a 1 mM Ir(pyr-tet)Br THF solution. Experimental conditions are identical to those reported in fig. 13. Experimental curve on the left is compared with simulated one on the right.

From these observations first reduction can be definitely assigned to the breakage of the Br-pyridine bond. Even if THF is not a suitable solvent at these potentials a mono-electronic reversible oxidation process was observed at low temperature; his potential has been found to be + 1.23 V vs. SCE.

Ir(pyz-tet)

The structure of this complex is very close to that of analogue compound discussed in previous paragraph; for this reason similar electronic properties are expected. Consequently the CV of the two complexes are compared in order to assign redox processes. Looking in the reductions region, a first mono-electronic reversible process is present with an $E_{1/2}$ of -1.44 V vs. SCE. By examining electronic properties of the two different types of ligand present in coordination sphere (i.e. the presence of two nitrogen atoms in pyrazine ring), first reduction is expected to be localized in pyz-tet ligand.

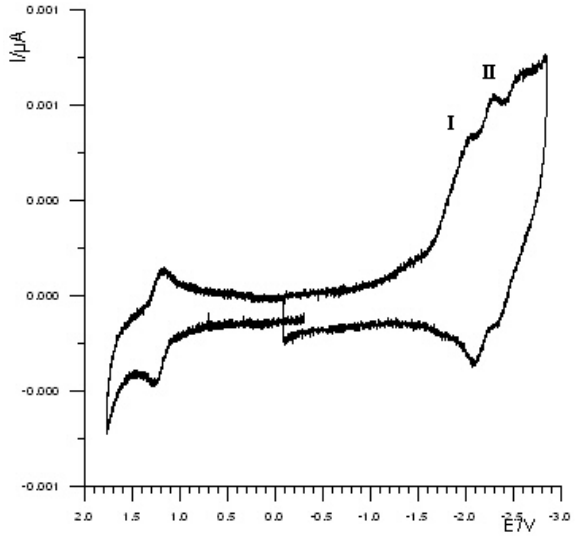

Figure 17. Voltammetric curves of a Ir(pyr-tet)Br 1 mM THF solution. Supporting electrolyte: 80 mM $TBAPF_6$. Working electrode: 10 µm Pt disk. T= -60 °C. Scanrate: 20 V/s.

At more negative potentials, (respectively -2.25 and -2.50 V) a second and third reduction process is present. Second reduction is reversible but the last voltammetric peak (fig. 18) is affected by a splitting that can be attributed to a partial chemically originated irreversibility. As a matter of fact by repeating measurement at low temperature this feature completely disappears. (fig 19). It's interesting to note (see tab.3) that III and IV reduction process of Ir(pyr-tet)Br fall at potential nearly identical to Ir(pyz-tet) II and II reduction. This is a clear indication that II and IV reduction are centred on the two phenyl-pyridine ligands. Moreover, the comparison of the cyclic voltammetries evidences the different number of redox processes due to the presence of a chemical reactivity caused by the alogen substitution in Ir(pyr-tet)Br.

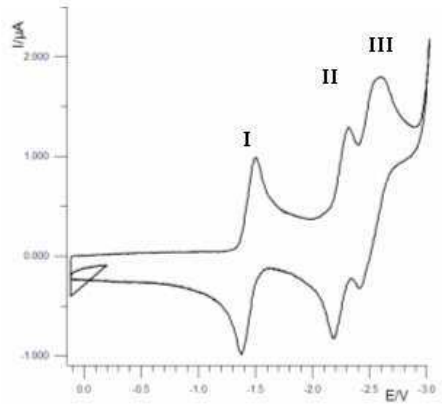

Figure 18. Voltammetric curves of a Ir(pyz-tet) 1 mM THF solution. Supporting electrolyte: 80 mM $TBAPF_6$. Working electrode: 50 µm Pt disk. T= 25 °C. Scanrate: 1 V/s.

In the region of positive potentials no process was evicenced before solvent discharge at room temperature. (fig.20). On the other hand by observing the cyclic voltammetry registered at low temperature (T= -60 °C) three reversible reduction processes and a single oxidation one were clearly present. (fig. 19). The $E_{1/2}$ for the reversible oxidation process, not present at room temperature, was found to be +1.33 V vs. SCE.

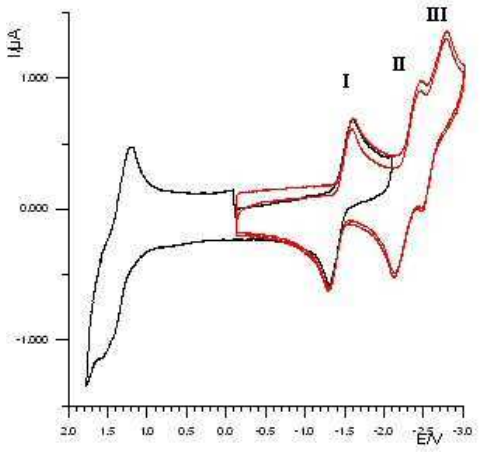

Figure 19. Voltammetric curves of a Ir(pyz-tet) 1 mM THF solution. Supporting electrolyte: 80 mM $TBAPF_6$. Working electrode: 50 µm Pt disk. T= -60 °C. Scanrate: 10 V/s.

Ir_2(2,3-btp)

The cyclic voltammetry showing reductive processes is reported in fig. 21. A first mono-electronic reduction process is present at -1.17 V vs. SCE; the second one, irreversible and nono-electronic falls at -2.13 V. By analyzing the CV curve the irreversibility of the II reduction has been found to be of electrochemical and chemical nature at the same time. The chemical follow up reaction is supposed to be a conformational modification that leads to an irreversible isomerization. In the following fig. 22 the CV has been registered in the same experimental conditions by increasing scan rate. It can be noted that second reduction is still irreversible whereas for the last two reductive processes (marked III and IV) resolution of the peaks improved. The simulated curve, reported then in fig. 23, was in good agreement with experimental one. On the basis of previous considerations the following mechanism is proposed :

$$A + e^- \xrightarrow{E^0_{Red,A}} A^-$$

$$A^- + e^- \xrightarrow{E^0_{Red,A^-}} A^{2-}$$

$$A^{2-} \underset{K_b}{\overset{K_f}{\rightleftharpoons}} B^{2-}$$

$$B^{2-} + e^- \xrightarrow{E^0_{Red,B2-}} B^{3-}$$

$$B^{3-} + e^- \xrightarrow{E^0_{Red,B3-}} B^{4-}$$

$$B^{4-} + e^- \xrightarrow{E^0_{Red,B4-}} B^{5-}$$

In this scheme A is identified as the pristine complex Ir_2(2,3-btp) that is doubly reduced. The product of second reduction A^{2-} is not kinetically stable and is rapidly converted to B^{2-} that is then reduced in following steps. Regarding the nature of chemical process, a conformational change in the doubly reduced form of the complex can be reasonably hypothesized. The simulation allowed

calculating and correctly assigning all observed reduction processes that are summarized in table 3.

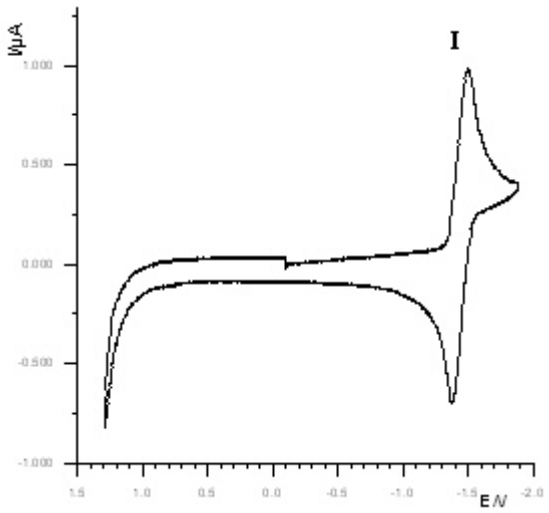

Figure 20. Voltammetric curves of a Ir(pyz-tet) 1 mM THF solution. Supporting electrolyte: 80 mM $TBAPF_6$. Working electrode: 50 μm Pt disk. T= 25 °C. Scanrate: 1 V/s.

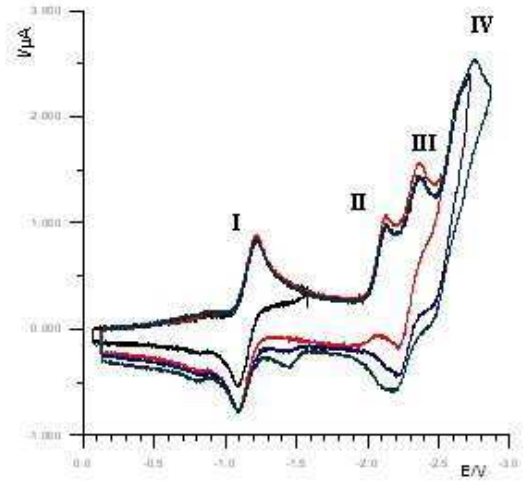

Figure 21. Voltammetric curves of a Ir_2(2,3-btp) 1 mM THF solution. Supporting electrolyte: 80 mM $TBAPF_6$. Working electrode: 50 μm Pt disk. T= 25 °C. Scanrate: 1 V/s.

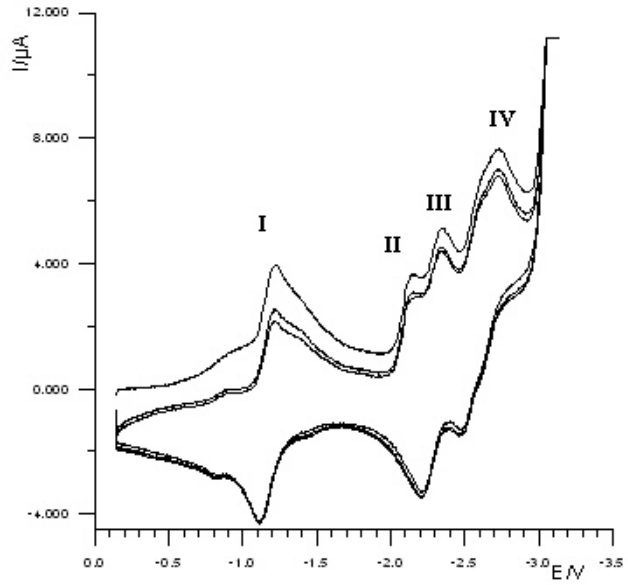

Figure 22. Voltammetric curves of a Ir_2(2,3-btp) 1 mM THF solution. Supporting electrolyte: 80 mM $TBAPF_6$. Working electrode: 50 µm Pt disk. T= 25 °C. Scanrate: 10 V/s.

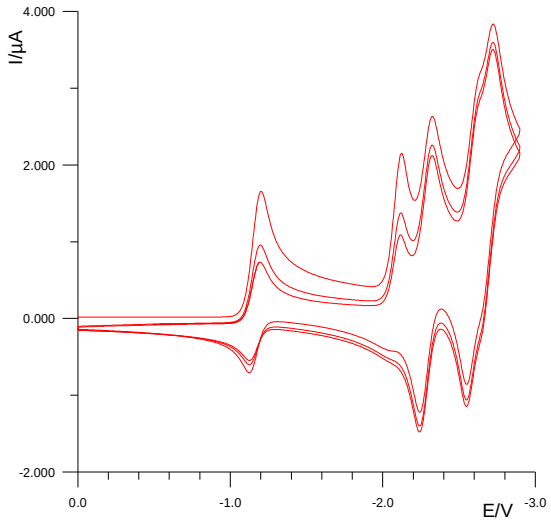

Figure 23. Simulated Voltammetric curves of a Ir_2(2,3-btp) 1 mM THF solution in the same conditions of experimental one reported in fig. 22

Oxidation processes of Ir_2(2,3-btp) were studied in the same experimental conditions previously described for reduction but by using a different solvent. The use of ultra dry DCM allowed exploring positive potentials region avoiding the problem of solvent discharge. Two irreversible oxidative peaks have been found at +1.06 V and +1.23 V vs SCE in this media. The measurements evidenced oxidation processes that reasonably can not be considered completely localized on metallic centre because a substantial contribute to LUMO is expected from the tetrazolate based bridging ligand. The oxidation processes localized exclusively on Ir(III) are supposed to be instead at higher potentials. Electrochemical data of the investigated Ir(III) complexes is summarized in table 3.

	T (°C)	1	I	II	III	IV
Ir(pyr-tet)Br	+25	1.38	-1.74**	-2.00	-2.29	-2.52
	-60	1.23	-2.04**	-2.20	-	-
Ir(pyz-tet)	+25	-	-1.41	-2.25	-2.50	-
	-60	1.33	-1.45	-2.3	-2.64	-
Ir_2(2,3-btp)	+25	1.23** 1.06**	-1.16	-2.13**	-2.29	-2.60 -2.72

Table 3. Summary of $E_{1/2}$ * of reductive (I, II, III, IV) and oxidative (1) processes for investigated Ir(III) tetrazolate complexes.

* potentials are referred to SCE.

** $E = E_P$ (peak potential calculated by simulation)

4.2.3
Photophysical and ECL properties.

After electrochemical investigations spectroscopic properties of the Ir(III) compounds have been carefully studied. The measurement of absorbance and photo-induced light emission are normally performed before to test electrochemiluminescence in order to make the ECL data more understandable. The $Ru(bpy)_3^{2+}$ has been taken again as fluorescence and ECL standard for his electrochemical stability and bright luminescence.

UV-VIS absorbance

Absorbance spectrum provides useful information on the energetic levels involved in excited state generation. For this reason, MLCT bands, the ones associated with light emission in the visible region are of particular interest. In fig. 24 are reported absorbance spectra of the three Ir(III) complexes. Three different colours are used to indicate Ru(pyz-tet), Ru(pyr-tet)Br and Ir_2(2,3-btp). All complexes show the following three separate bands in decreasing energy order: ILCT or $\pi^* \leftarrow \pi$ (inter-ligand charge transfer), LMCT (ligand to metal charge transfer) and MLCT (metal to ligand charge transfer). The maximum intensity MLCT band is close to 400 nm for all complexes. Ir_2(2,3-btp) shows an higher ε in MLCT region respect to mononuclear complexes because two metal-ligand chromoforic centres are present in a single molecule resulting in an higher light absorption.

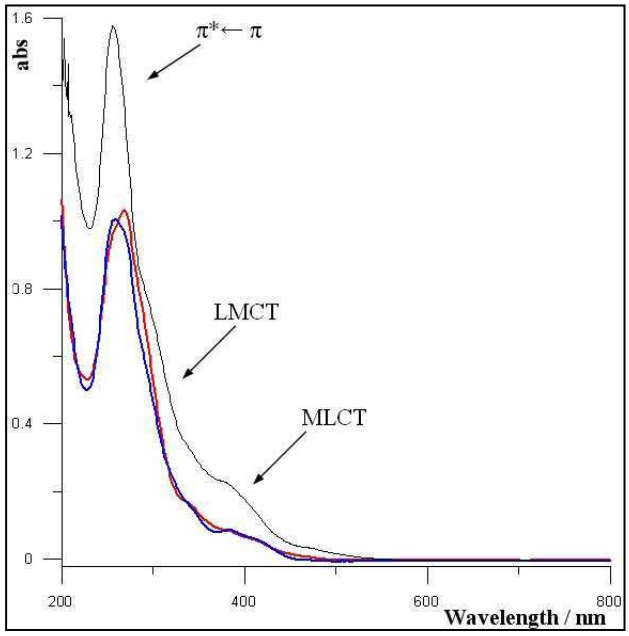

Figure 24. Absorbance spectra of 0.02 mM MeCN solutions of Ir(III) complex. Blue line: Ir(pyr-tet)Br; red line: Ir(pyz-tet); black line: Ir_2(2,3-btp). Samples were Ar degassed .

The Absorbance maxima registered in MLCT region for the different Ir(III) complexes are summarized in tab. 4

	λ/nm	**Abs**
Ir(pyr-tet)Br	380	0.088
Ir(pyz-tet)	383	0.084
Ir_2(2,3-btp)	381	0.227

Table 4. Summary of MLCT absorbance bands of Ir(III) complexes. Solvent: MeCN. T= 25 °C.

The LMCT band, not very pronounced is typical of Ir complexes. There is not an equivalent band in the spectra of $Ru(bpy)_3^{2+}$ how can be noted from fig.25.

Around 270 nm, the intense absorbance peaks structure present in every metallorganic complex is caused by the typical $\pi^* \leftarrow \pi$ transitions (ILCT).

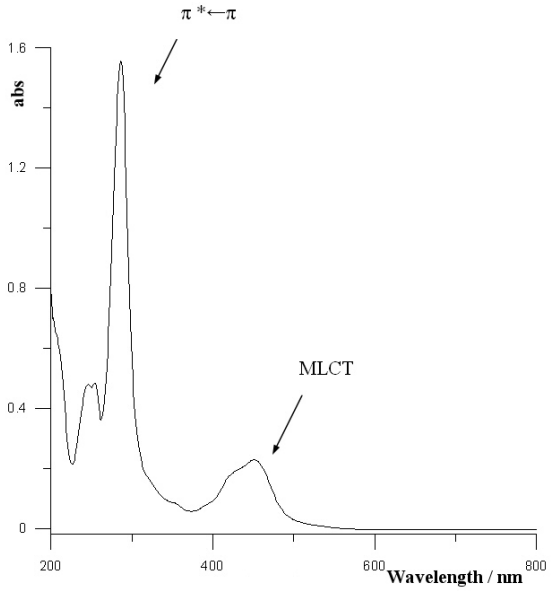

Figure 25. Absorbance spectra of a 0.02 mM solution of $Ru(bpy)_3(ClO_4)_2$ registered at 25 °C.

Photoluminescence

The study of emission spectra, preliminar to ECL analysis, It's useful to estimate the maximum emission intensity and the relative wavelength. In figure 26 are reported the emission spectra of all Ir(III) complexes compared with that of the standard collected in the same experimental conditions. The exciting wavelength is that with the maximum absorbance in MLCT region.

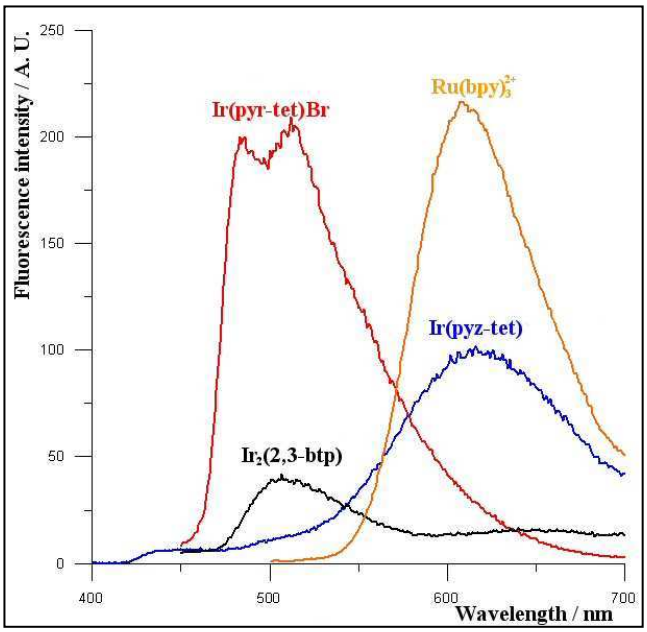

Figure 26. Comparison of emission spectra of Ir(III) complexes and the standard. Photoluminescence was registered from a 0.02 mM MeCN solutions of the complex. Wavelengths of excitation are those previously reported in tab. 4. For $Ru(bpy)_3^{2+}$ λ_{exc} was 460 nm. Cell was air degassed for 5 minutes.

The results of fluorescence investigations are reported in table 5. The emission spectra of Ir(pyr-tet)Br evidences two maxima, respectively at 486 and 510 nm, with an intensity almost identical to that of $Ru(bpy)_3^{2+}$. In general for the Kasha's rule[17] multiple MLCT emissions are forbidden, in the case however of mixed ligand, the presence of different MLCT levels with similar energies could result in a dual emission. Another possible explanation could be the presence of a vibrational structure in the MLCT band that could also explains the asymmetricity of emission peak. Similar emission phenomena have been reported for some Ir(III) and Ru(II) complexes.[18,19] Anyway, to understand the real nature of dual emission more detailed photophysical investigation should be necessary as in the case of Ru(pyr-tet) (see section 3.1.2).

Another interesting feature of Ir(pyr-tet)Br is the blue shift of his emission of about 100 nm with respect to $Ru(bpy)_3^{2+}$. The causes of this higher energy emission can be substantially two: (i) the presence of Ir as central atom instead of Ru; (ii) the presence of a halogen atom bound with pyridinic ring. A recent work showed that increasing the fluorination of a pyridine ligand in a cyclometallated Ir(III) complex a widening of the HOMO-LUMO gap occurs leading generally to a blue shift in emission.[20] By taking in account this paper Ir(pyrtet-Br) shows as expected a fluorescence blue shift of 100 nm induced by the introduction of a Br in meta position[21] respect to coordinating N in the pyr-tet ligand pyridine. This effect can be definitely confirmed by testing fluorescence of Ir(pyr-tet) where no halogen atom is present. The synthesis of Ir(pyr-tet) is actually in progress.

	λ_{exc}/nm	$\lambda_{max,PL}$/nm	Emission intensity/A.U.
Ir(pyr-tet)Br	383	486 510	199 209
Ir(pyz-tet)	338	618	100
Ir_2 (2,3-btp)	381	509	28
$Ru(bpy)_3(ClO_4)_2$	451	609	216

Table 5. Summary of photoluminescence properties of 0.02 mM MeCN solutions of the Ir(III) complexes and standard. Emission in IR-VIS region is obtained by populating MLCT bands. Solutions were Ar degassed.

In fig. 26 the fluorescence spectra of Ir(pyz-tet) is indicated by a blue line. The maximum is very close to that of $Ru(bpy)_3^{2+}$ and the relative intensity around 50 %. In this case the pyz-tet LUMO lies at a lower energy respect to that of (pyr-tet)Br and fluorescence is observed at the same wavelength of $Ru(bpy)_3^{2+}$. The fig. 26 black curve is the spectra of dinuclear complex with emission

maximum at 509 nm and an approximate relative efficiency of 10 % respect to $Ru(bpy)_3^{2+}$. As observed for Ru(pyr-tet)Br an interesting blue shift of about 100 nm is present.

Last test was the evaluation of sensitivity to air that was found pretty small for all compounds except the dinuclear one. Figure 27 shows the emission spectra of Ir_2(2,3-btp) before and after degassation. The emission peak at 509 nm is surprisingly completely quenched in presence of air. This feature is promising for the set-up of an high sensitivity oxygen sensor based on fluorescence.

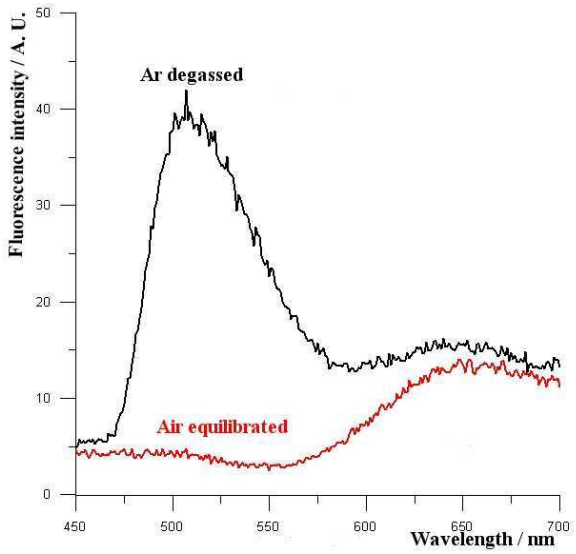

Figure 27. Emission spectra of a 0.02 mM solution of Ir_2(2,3-btp) in degassed* (black curve) and air equilibrated cell (red curve).* Cell was degassed by Ar flow for 5 minutes.

Electrochemiluminescence

Ir(pyr-tet)Br

As previously reported fluorescence maximum is an intense band made of two peaks at 510 and 486 nm. On the other hand in electrochemical investigations has been found a reversible oxidation process ($E_{1/2}$=+1.38 V vs. SCE)) and an

irreversible first reduction (E_p=-1.74 V). It's important to remember that when Ir(pyr-tet)Br is reduced the corresponding complex without the halogen atom (Ir(pyr-tet) is electro-generated. In figure 28 is shown ECL emission in function of time during a cyclic voltammetry. It's important to note that the time is here an implicit function of the applied potential because the last one is continuously varied at the constant 1 V/s scan rate. The cyclic voltammetry included proper complex first reduction (I Red) and his first oxidation process to study the ECL emission obtained by cation-anion direct annihilation. The ECL signal is zero until I Ox. or I Red potential is reached where sharp peaks of emitted light are registered. In figure 28 the light emission peak registered during oxidation (positive potentials) is labelled "Ox" and the one in correspondence of reduction (negative potentials) "Red".

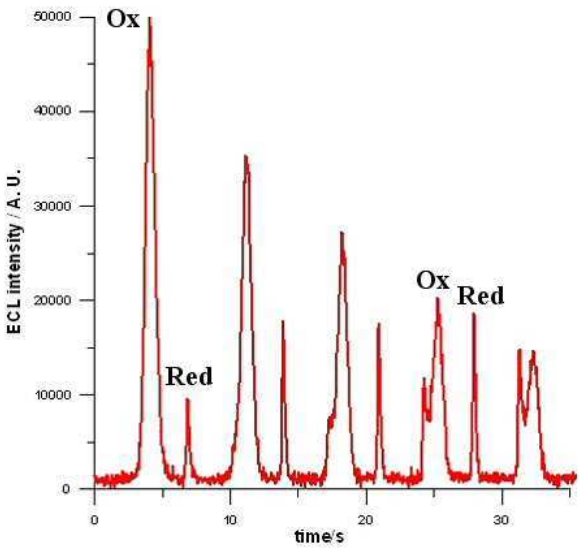

Figure 28. ECL emission in function of time during repeated CV cycles on a Ir(pyr-tet)Br 0.5 mM MeCN solution. Supporting electrolyte: 0.1 M $TBAPF_6$. Scan rate: 1 V/s. Potential program: E_1= +1.35 V (I Ox), E_2=-1.62 V (I Red.). Solution was Ar degassed for 5 minutes. ECL mechanism: cation-anion direct annihilation. PMT bias: 1000 V. ITime: 10 ms. Sample time: 35 mS.

The time interval between a “Red” peak and the following “Ox” is higher of that between a “Ox” peak and following “Red” because the absolute value of the maximum negative potential reached is higher than positive one and the scan rate is constant. The time at which first emission is observed is not significant because the beginning of electrochemical experiment and light acquisition are not accurately synchronized in “time based scan” as happens in light/current/time curves. Light is then emitted when a sufficient amount of electro-generated positive radicals meets the corresponding negatively radical anions obtained during reduction.

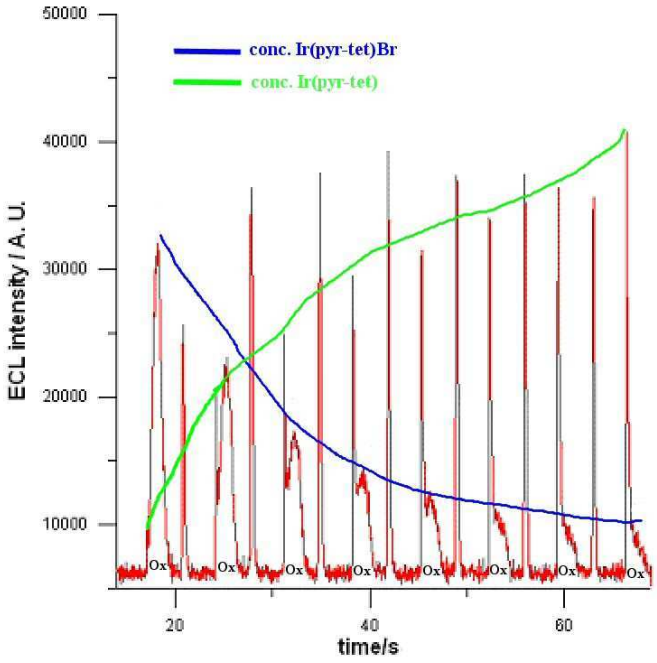

Figure 29. ECL emission in function of time during repeated CV cycles on a Ir(pyr-tet)Br 0.5 mM MeCN solution: following cycles. In this graph the electrochemically induced conversion of Ir(pyr-tet)Br in Ir(pyr-tet) + Br_2 is well visible by observing the transformation of the 2 emission peaks registered during oxidisation. Experimental conditions were exactly the same described in fig. 28.

By comparing the “Ox” light peaks with “Red” ones It’s clear that the first are in general of higher intensity. The explanation is that during reduction a big

amount of injected electrons are used in halogen extraction from Ir(pyr-tet)Br and thus generated anions have a very short life time and lower possibilities to produce excited states. The intensity of “Ox” peak is fast decaying in time whereas “Red” peak reaches pretty quickly steady state. Surprisingly the “Ox” light peak, initially single ,progressively splits in two separate peaks both registered during reduction. The second peak, initially just a shoulder, is anticipated in potential (i.e. time) respect to the one obtained from the beginning. In the figure 29 the following cycles of the same experiment are presented. By observing accurately the two emission peaks obtained during oxidation It’s clear that an electrolysis of one minute in these experimental conditions is sufficient to convert almost completely Ir(pyr-tet)Br complex in the analogue Ir(pyr-tet) which oxidation potential is probably anticipated (see fig.30). The fact that emission during reduction results in a single peak is due to fact that the electrogenerated Ir(pyr-tet) is reduced to higher potentials respect to Ir(pyr-tet)Br (see sect. 4.2.2) so the radical anion of the latter complex should not be generated in these experiments.

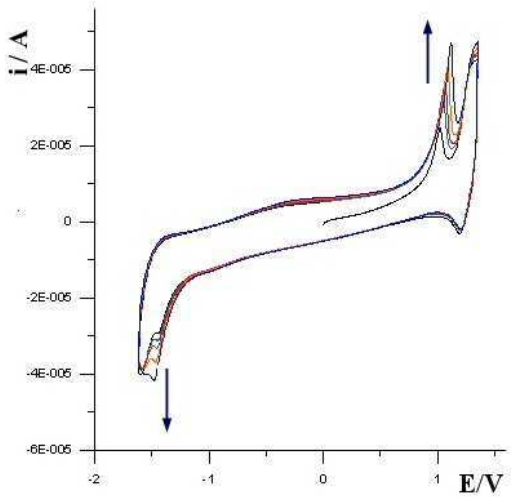

Figure 30.Cyclic voltammetric curves of a 1 mM Ir(pyr-tet)Br MeCN solution. Supporting electrolyte: 80 mM $TBAPF_6$. Working electrode: Pt disc electrode of 3 mm diameter. Scan rate 1 V/s. T = 25 °C. Potentials are reported vs. Ag wire.

From the point of view of concentrations profiles, if We assume that ECL intensity of a species is proportional to its concentration in diffusion layer, It's a clear experimental evidence that during electrolysis while Ir(pyr-tet)Br ECL peak is decreasing in intensity (blue line of fig. 29) Ir(pyr-tet) one (green line) is correspondingly increasing. On the other hand the summation of the intensities of the two ECL "Ox" peaks is approximately constant as expected for a conversion reaction. Putting together previous considerations the following mechanism can be proposed:

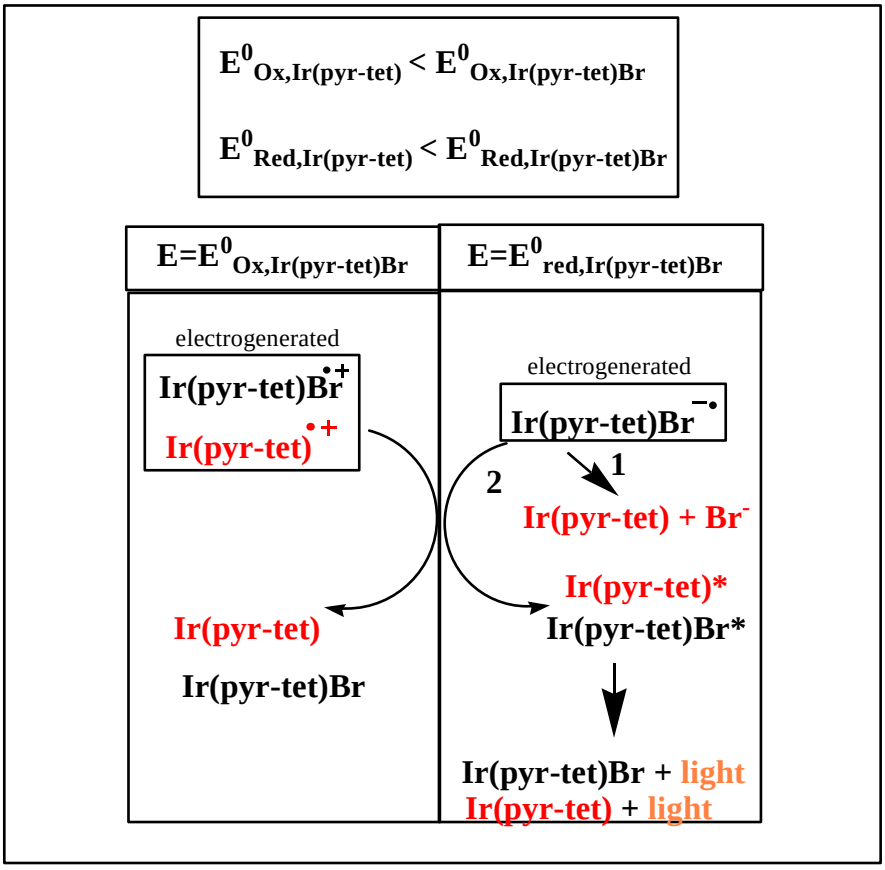

By taking in consideration this scheme is clear that an ECL emission peak is expected to be observed at the potential (or implicitily at the time) where at least one over the three reactive radical species is electro-generated. As

predicted by the model thus, in the present case the emission peaks are three: one in correspondence of Ir(pyr-tet) oxidation, another in correspondence of Ir(pyr-tet)Br oxidation and the last in correspondence of Ir(pyr-tet)Br reduction. Those three limiting cases, depicted in the following scheme justify the fact that two ECL emission peaks are observed during oxidation and only one during reduction.

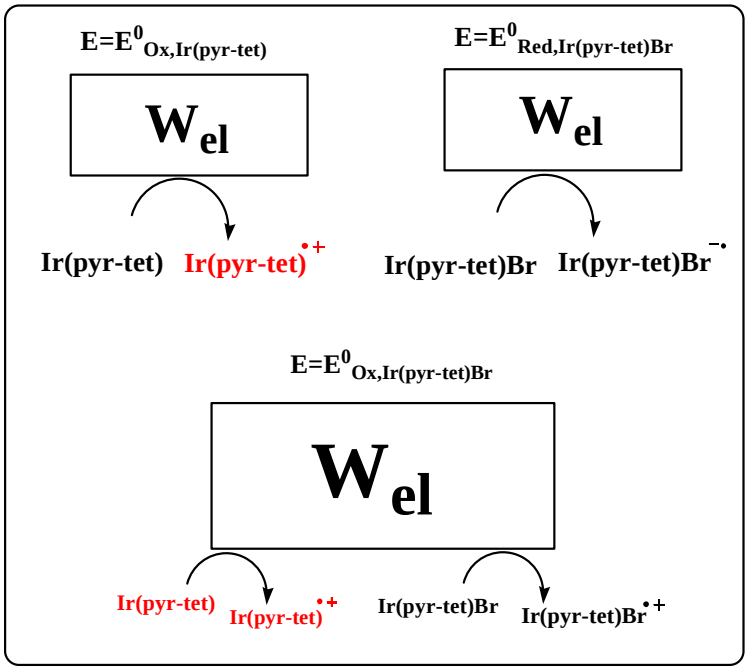

To justify the assumption that Ir(pyr-tet) is more easily oxidized than Ir(pyr-tet)Br the cyclic voltammetric curves registered during ECL measurements are reported in fig. 30. It can be easily noted that an irreversible peak, not present in the first scansion, appears around + 1 V (vs. Ag) and progressively increases by repeating scansions. This voltammetric peak, observed contemporaneously to ECL shoulder appearance, has been considered as an oxidative process of the freshly electrogenerated Ir(pyr-tet). When the Ir(pyr-tet) complex will be available the potentials of electrochemical processes will be carefully compared in this experimental conditions to confirm the interpretation.

These results demonstrated the practical possibility to study by ECL the kinetics of chemical processes coupled with electron transfers in the cases where reactant and product are light emitters.

By using annihilation mechanism ECL intensity and time stability of the emission was not sufficient to allow spectra collection. Considering the irreversibility of first reduction of Ir(pyr-tet)Br and the subsequent electro-induced reactions to obtain a more stable and intense signal the use of a oxidative coreactant has been found convenient. For these reasons by oxidizing in presence of NPr_3 (max potential~ $E_{Ox,NPr3}$) the emission resulted much more intense than that obtained previously by annihilation. (fig. 31). The signal is due to fast radicalic reactions involving oxidation products of NPr_3 and the complex radical cation producing excited state. If at this point the experiment is repeated by reaching the oxidation potential of the complex as expected a second ECL emission peak of lower intensity appears. (fig. 32).

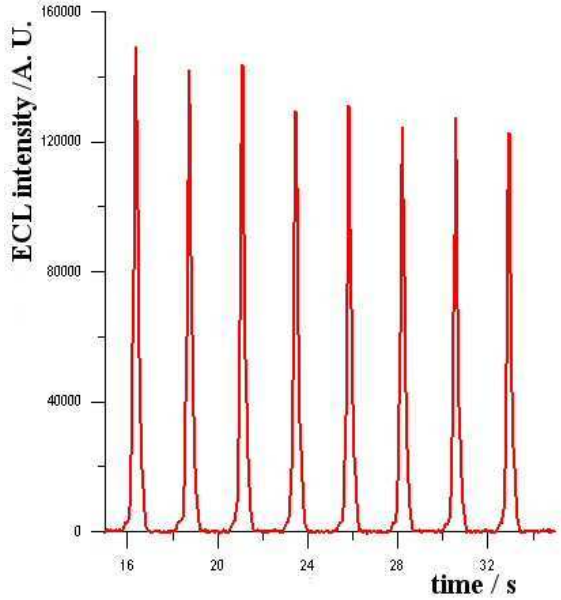

Figure 31. ECL emission in function of time during repeated CV cycles on a Ir(pyr-tet)Br 0.5 mM MeCN solution. Supporting electrolyte: 0.1 M $TBAPF_6$. Scan rate: 1 V/s. Potential program: E_1= 0 V, E_2=+1.1 V (I Ox of NPr_3). ECL mechanism: oxidation in presence of NPr_3($3x10^{-2}$ M). PMT bias: 1000 V. ITime: 10 ms. Sample time: 35 mS.

The two mechanisms of excited state generation in presence of the ammine producing the different peaks have been already discussed in detail in section 4.1.

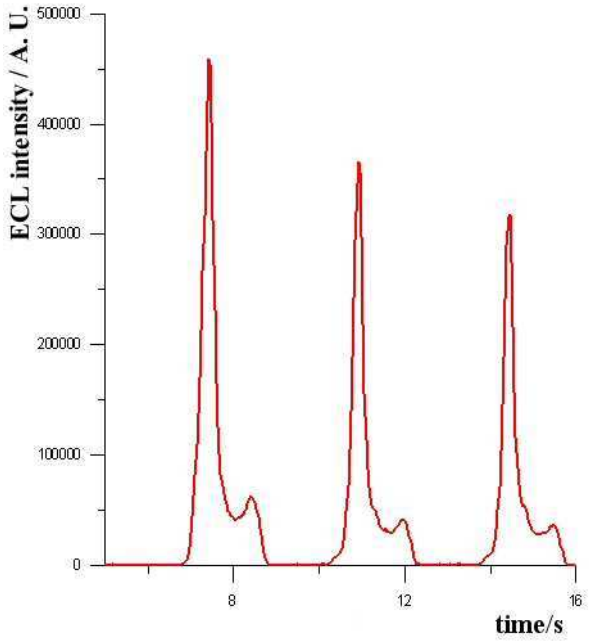

Figure 32. ECL emission in function of time during repeated CV cycles on a Ir(pyr-tet)Br 0.5 mM MeCN solution. Supporting electrolyte: 0.1 M $TBAPF_6$. Scan rate: 1 V/s. Potential program: E_1= 0 V, E_2=+1.4 V (I Ox of the complex). ECL mechanism: oxidation in presence of NPr_3 ($3x10^{-2}$ M). PMT bias: 1000 V. ITime: 10 ms. Sample time: 35 mS.

The fact that the second ECL peak, corresponding to the complex oxidation, is less intense than first (NPr_3 oxidation) is substantially a consequence of the molar excess of the coreactant with respect to Ir. The fact that emission in the presence of coreactant was stable in time is a further confirmation that the new peak appeared during oxidation in annihilation experiments was caused by an electro-generated new molecule produced during reduction.

ECL signal obtained in these conditions was intense enough to allow spectra registration that is reported in fig. 33. The maximum of emission was at 510 nm, the same value obtained in photoluminescence experiments; this fact

confirms that excited state is the same populated in fluorescence spectra. The structure of the peaks and the general aspect of the spectra is very similar to that obtained by photo-excitation , however signal to noise ratio is lower.

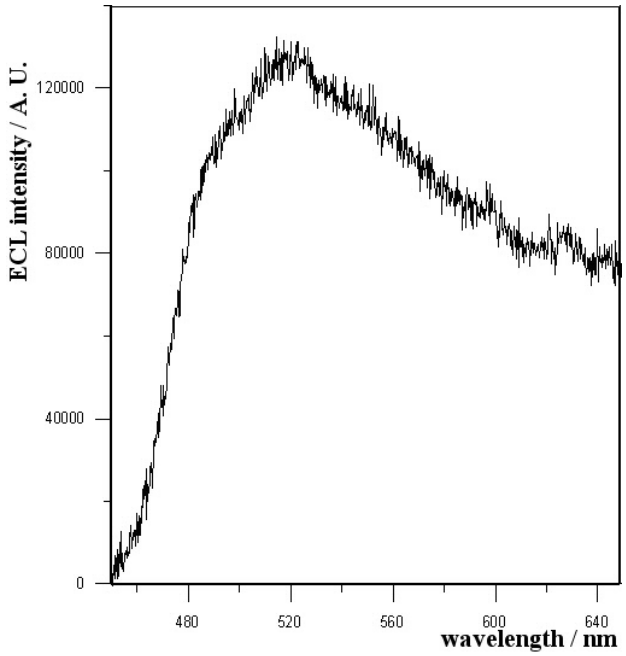

Figure 33. ECL spectra obtained from a Ir(pyr-tet)Br 0.5 mM MeCN solution. Supporting electrolyte: 0.1 M $TBAPF_6$. Switching method: chronoamperometry. Potential program: E_1= 0 V , 1 s; E_2=+1.1 V, 1 s. ECL mechanism: oxidation in presence of NPr_3($3x10^{-2}$ M). PMT bias: 1000 V. ITime: 5 s. MCStep: 0.25 nm.

Ir(pyz-tet)

The complex Ir(pyz-tet), as already reported, shows an intense fluorescence spectra with maximum around 618 nm. Differently from previous electrochemical investigations, if the cyclic voltammetry is performed in bottle quality MeCN the compound evidences a reversible first oxidation process. In fig. 34 is reported a cyclic voltammetric curve showing mono-electronic and reversible first oxidation and reduction processes.

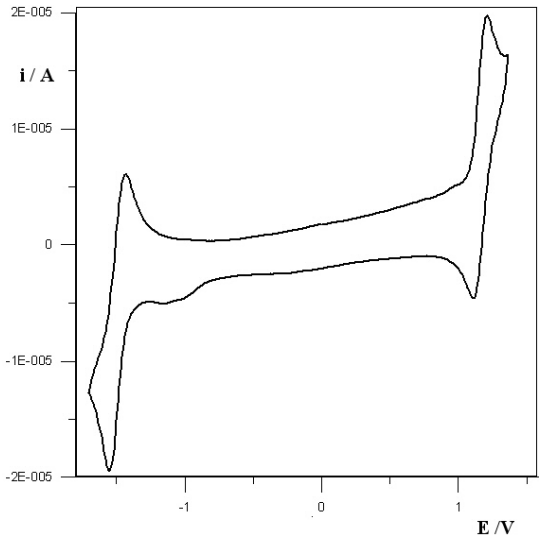

Figure 34.Cyclic voltammetric curves of a 0.5 mM Ir(pyz-tet) MeCN solution. Supporting electrolyte: 40 mM $TBAPF_6$. Working electrode: Pt disc electrode of 3 mm diameter. Scan rate 1 V/s. T = 25 °C. Potentials are reported vs. Ag wire.

The stability of electrochemical processes allows the generation of ECL by annihilation.(fig.35). Two different light signals are present: one instable of medium intensity during negative potential steps and another stable of low intensity during positive potential steps. This behaviour suggests that probably the cation has a higher life time respect to anion being the emission during reduction more intense. The instability of ECL emission during negative potential steps seems to be caused by the formation of filming product at the electrode slowly diffusing away. The intensity of ECL emission obtained by cation-anion direct annihilation was not intense enough to register ECL spectra. The coreactant NPr_3 was then introduced to increase signal intensity. In fig. 36 as example is reported a typical cyclic voltammetry registered in presence of the ammine. Due to the large excess of NPr_3 the only plain electrochemical processes are the first and second ammine irreversible oxidation.

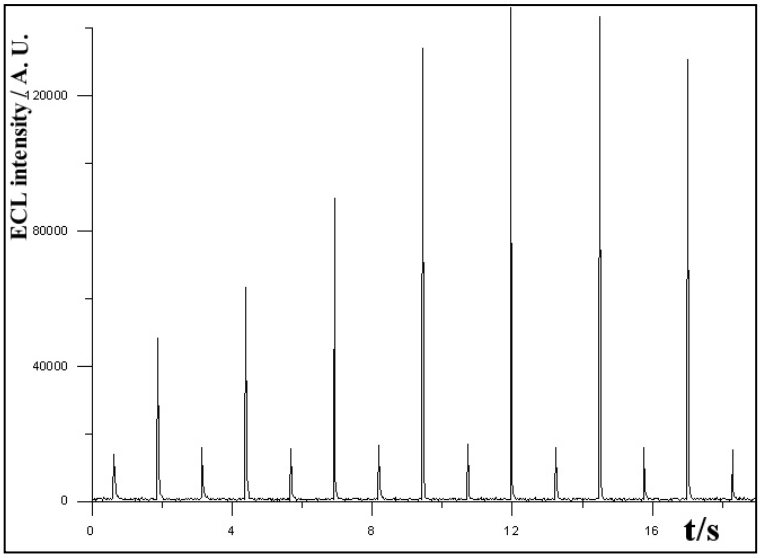

Figure 35. ECL emission in function of time during repeated CV cycles on a Ir(pyz-tet) 0.5 mM MeCN solution. Supporting electrolyte: 0.1 M $TBAPF_6$. Switching method: triple step chronoamperometry. Potential program: E_1= +1.35 V (I Ox), E_2= 0 V, 0.5 s; E_3= -1.25 V (I Red.), 0.5 s. Solution was Ar degassed for 5 minutes. ECL mechanism: cation-anion direct annihilation. PMT bias: 1000 V. ITime: 10 ms. Sample time: 35 mS.

In fig. 37 is reported the ECL emission in function of time when a large excess of NPr_3 is present. As observed and discussed for Ir(pyr-tet)Br two separate ECL emission peaks, corresponding to different potentials, were evidenced. In this case however the two emissions were unexpectedly of the same intensity and the potential necessary to get an acceptable signal was surprisingly high (+3 V vs. Ag). There is not a clear reason that justify the necessity of a so positive potential; one explanation can be the difficulty to generate a sufficient amount of Ir(pyz-tet)* at lower potentials because of secondary reactions of the electro-generated radical cations which the ammine. Anyway the emission is intense enough to get a well resolved ECL spectrum. (fig. 38). The maximum (610 nm) is very close to that of fluorescence and can be concluded that in photo- and electro-generated luminescence the same excited state is populated.

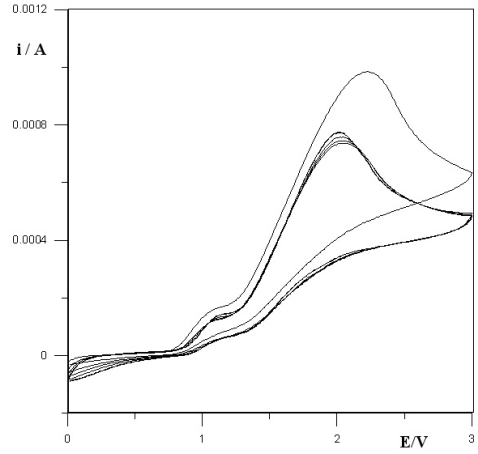

Figure 36.Cyclic voltammetric curves of a 0.25 mM Ir(pyz-tet) MeCN solution containing $3x10^{-2}$ M NPr_3. Supporting electrolyte: 40 mM $TBAPF_6$. Working electrode: Pt disc electrode of 3 mm diameter. Scan rate 1 V/s. T = 25 °C. Potentials are reported vs. Ag wire.

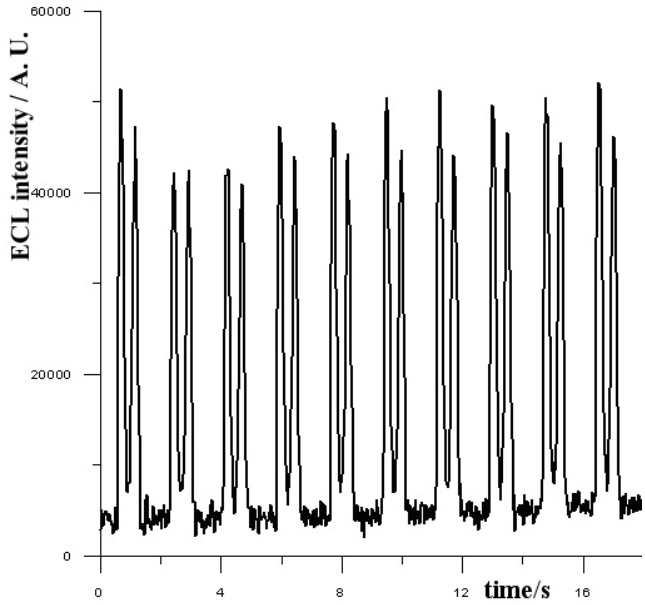

Figure 37. ECL emission in function of time during repeated CV cycles on a Ir(pyz-tet) 0.25 mM MeCN solution. Supporting electrolyte: 0.1 M $TBAPF_6$. Scan rate: 5 V/s. Potential program: E_1= 0 V, E_2=+3.5 V. ECL mechanism: oxidation in presence of NPr_3 ($3x10^{-2}$ M). PMT bias: 1000 V. ITime: 10 ms. Sample time: 35 mS.

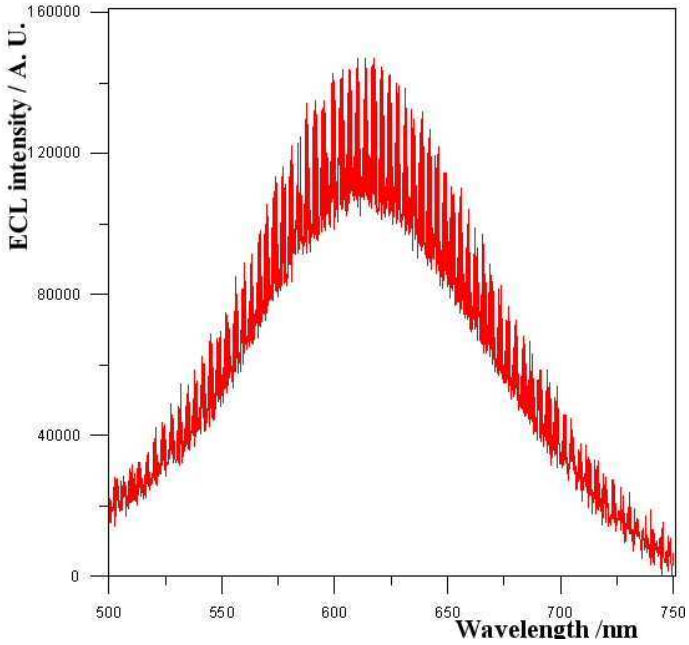

Figure 38. ECL spectra obtained from a Ir(pyz-tet) 0.25 mM MeCN solution. Supporting electrolyte: 0.1 M $TBAPF_6$. Switching method: chronoamperometry. Potential program: E_1= 0 V , 0.5 s; E_2=+3.0 V, 1000 ms. ECL mechanism: oxidation in presence of NPr_3($3x10^{-2}$ M). PMT bias: 1000 V. ITime: 2 s. MCStep: 0.25 nm.

Ir_2(2,3-btp)

As for Ir(pyr-tet)Br the fluorescence of this complex was blue shifted respect to $Ru(bpy)_3^{2+}$ of about 100 nm (max. 509 nm) and his efficiency pretty low (~10 % of the standard). From the point of view of electrochemical properties the first reduction is stable and reversible ($E_{1/2}$ = 1.16 V) whereas first oxidation is irreversible (E_p=1.06 V). In figure 39 is reported the ECL emission in function of time during a cation-anion annihilation experiment. The generated signal is pretty weak but apparently time stable. An attempt of spectral acquisition failed probably because ECL intensity is not sufficient. Another probable explanation considering the irreversibility of the first oxidation process is the slow formation of a quencher or filming products that

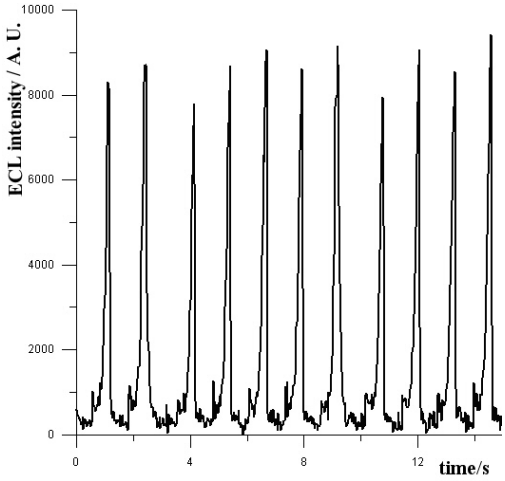

Figure 39. ECL emission in function of time during repeated CV cycles on a Ir_2(2,3-btp) 1 mM MeCN solution. Supporting electrolyte: 0.1 M $TBAPF_6$. Switching method: double step chronoamperometry. Potential program: E_1= +1.53 V (I Ox), 0.5 s; E_2= -1.28 V (I Red.), 0.5 s. Solution was Ar degassed for 5 minutes. ECL mechanism: cation-anion direct annihilation. PMT bias: 1000 V. ITime: 10 ms. Sample time: 35 mS. Potentials are referred to Ag wire.

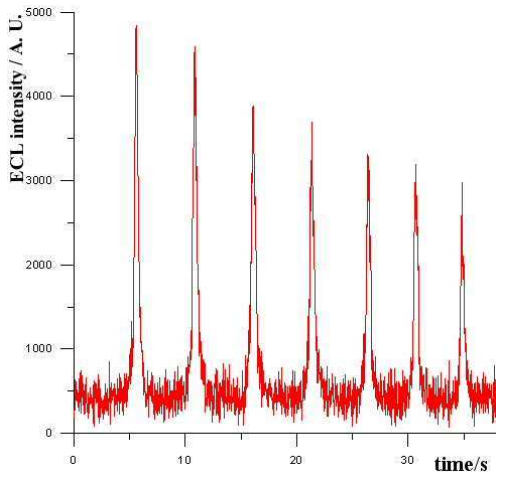

Figure 40. ECL emission in function of time during repeated CV cycles on a Ir_2(2,3-btp) 0.5 mM MeCN solution. Supporting electrolyte: 0.04 M $TBAPF_6$. Scan rate: 1 V/s. Potential program: E_1= 0 V, E_2= -2.5 V. ECL mechanism: reduction in presence of $(NH_4)_2S_2O_8$ (40 mM). PMT bias: 1000 V. ITime: 10 ms. Sample time: 35 mS. Potentials are referred to Ag wire.

was not evidenced during time based experiments because of short electrolysis time. Considering that in the complex evidences an irreversible Ox. and a reversible I Red. the coreactant $(NH_4)_2S_2O_8$ has been added to try improvement of ECL emission intensity. The resulting ECL vs. time plot is reportes in fig. 40. The signal is unfortunately of low intensity, not reproducible and fast decreasing. This behaviour did not allowed the aquisition of ECL spectra.

References

[1] M. Dixon, J.-P. Collin, J.-P. Sauvage, L. Flamigni, S. Eucinas, F.Barigelletti, *Chem. Soc. Rev*. 29, 385 (2000).

[2] K. Nishimura, Y. Hamada, T. Tsujioka, K. Shibata, T. Fuyuki, *Jpn. J. Appl. Phys.*, 40, 945 (2001).

[3] E. M. Gross, N. R. Amstrong, R. M. Wightman, *J. Electrochem. Soc*.149, 137 (2002).

[4] D. Bruce, M.M. Richter, *Anal. Chem.* 74, 1340 (2002).

[5] C. Cole, B. D. Muegge, M. M. Richter, *Anal. Chem.* 75, 601 (2003).

[6] A. Kapturkiewicz, G. Angulo, *Dalton Trans.*, 3907 (2003).

[7] B. D. Muegge, M. M. Richter, *Anal. Chem.*, 76, 73 (2004).

[8] A. Kapturkiewicz, T.-M. Chen, I. R. Laskar, J. Nowacki, *Electrochem. Commun*. 6, 827 (2004).

[9] W. C. M. Flynn, J. N. Demas, *J. Am. Chem. Soc*., 96, 1959 (1974).

[10] R. J. Watts, J. S. Harrington, and J. Van Houten, *J. Am. Chem. Soc.*, 99, 2179 (1977).

[11] J. L. Kahl, K. W. Hanck and K. DeArmond, *J. Phys. Chem*, 82, 540 (1978).

[12] V. T. Coombe, G. A. Heath, A. MacKenzie and L. J. Yellowlees, *Inorg. Chem.*, 23 (1984).

[13] A. Kapturkiewicz, J. Nowacki, P. Borowicz, *Electrochim. Acta*., 50, 3395 (2005).

[14] E. M. Gross, J. D. Anderson, A. F. Slaterbeck, S. Thayumanavan, S. Barlow, Y. Zhang, S. R. Marder, H. K. Hall, M. F. Nabor, J. –F. Wang, E. A. Mash, N. R. Armstrong, R. M. Wightman, *J. Am. Chem. Soc.*, 122, 4972 (2000).

[15] J. I. Kim, I. -S Shin, H. Kim, J –K Lee, *J. Am. Chem. Soc.*, (Communication), 127, 1614 (2005).

[16] The $E_{1/2}$ for I Ox. and I Red of $Ru(bpy)_3^{2+}$was previously calculated in the same solvent in section 3.1.2.

[17] M. Kasha, *Faraday Soc. Discuss.*, 9,14 (1950).

[18] E. Krausz, *Inorg. Chem.*,32, 4053 (1993).

[19] E. C. Glazer, D. Magde, Y.Tor, *J. Am. Chem. Soc*., (Communication),127, 4190 (2005).

[20] K. Dedeian, J. Shi, N. Shepherd, E. Forsythe, D. C. Morton, *Inorg. Chem.*,(Communication), 44, 4445 (2005).

[21] P. Coppo, E. A. Plummer and L. De Cola, *Chem. Comm.*, 1774 (2004).

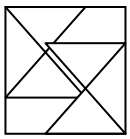

Chapter Five: ECL on chip

In rebus dubis plurimum est audacia

In commercial ECL analyzers (see appendix) a decrease of signal reproducibility after long time of operation is often observed. This problem is caused by the progressive degradation of emitting metal surfaces. A possible strategy to avoid this effect is the introduction as working electrode of mono-use gold sputtered silicon wafers. In a first series of experiments different geometrical properties of the chip containing both working and counter electrode have been modulated to find the best configuration. The second step was then the chip chemical functionalization to include the ECL emitting

label. The obtained device has been used to study the reliability of the ECL system for the detection of a generic probe-target coupling reaction.

5.1
ECL chip structure and preparation

Gold electrodes have been prepared by Olivetti I-Jet s. p. a. by using fabrication procedures proper to microelectronics. Suitable electrode geometries have been obtained through a photolithographic procedure by using appropriate contact masks.

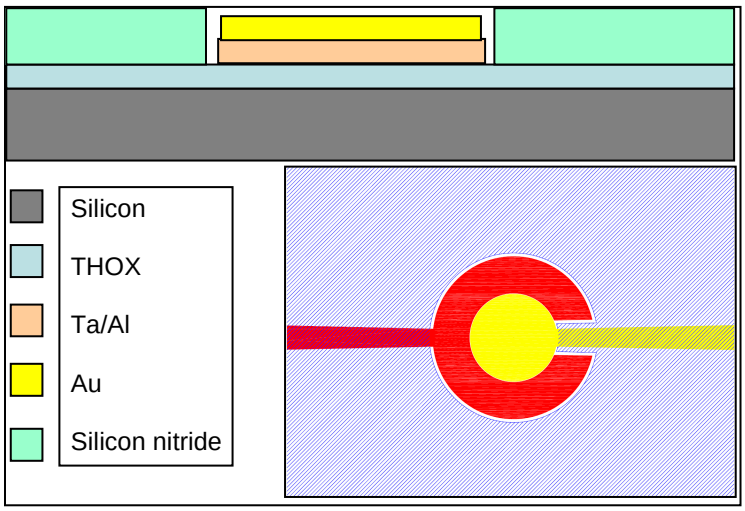

Figure 1. Materials and layers of ECL chips.

Gold electrodes were fabricated by either evaporation or sputtering of gold onto standard 6” silicon wafers. To get a perfect electrical insulation between gold and silicon substrate, the latter was covered by a thermally-grown silicon oxide (THOX) thin film. In order to improve the adhesion of the gold film onto the substrate, an “adhesion promoting” underlayer of Ti, Cr or Ta/Al alloy was firstly deposited onto the SiO_2 surface. Finally, an insulating overlayer of SiO_2 or Si_3N_4 was deposited to cover the metallic contacts thus obtaining a better definition of the active surface area. (see the overall scheme

reported in fig. 1). Two-electrode (working (W) and counter electrode (C)) configurations, using various geometries (i.e. squares, circles or stars), areas (diameters: 0.5-1-2 mm), and inter-electrode gaps (5-30-300 micrometers) were combined onto the same wafer, obtaining ca. 100 electrodes on each wafer. Furthermore, various thicknesses of the gold coating have been tried.

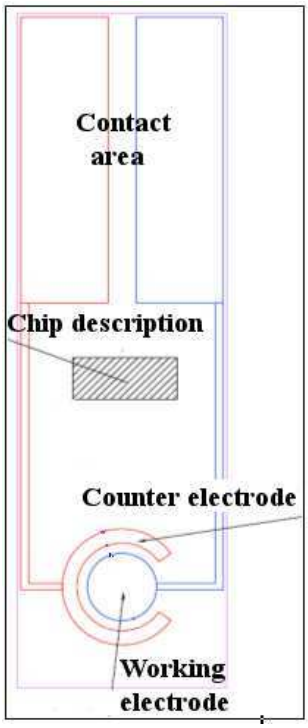

Figure 2. General setup of a circular geometry ECL chip electrode.

In the chip description area is specified the geometry (EC stands for Circular, EQ for square and ES for star shaped), the dimension of working electrode in μm and the distance between counter and working in the same unit. (e. g. EQ_500_30 means that the electrode is squarewith side of 500 μm and W-C distance of 5 μm). Before to run the chip proper characterization some basic

verifications has been carried on. The proper electrical insulation of the chip was verified with scanning electrochemical microscopy (SECM) technique. (fig.3) During the scansion when the tip is on a conductive area the registered current increases whereas in presence of an insulating substrate decreases rapidly. This way the conductive area of the chip has been mapped (red region in fig. 3) and has been verified that the chip was correctly prepared.

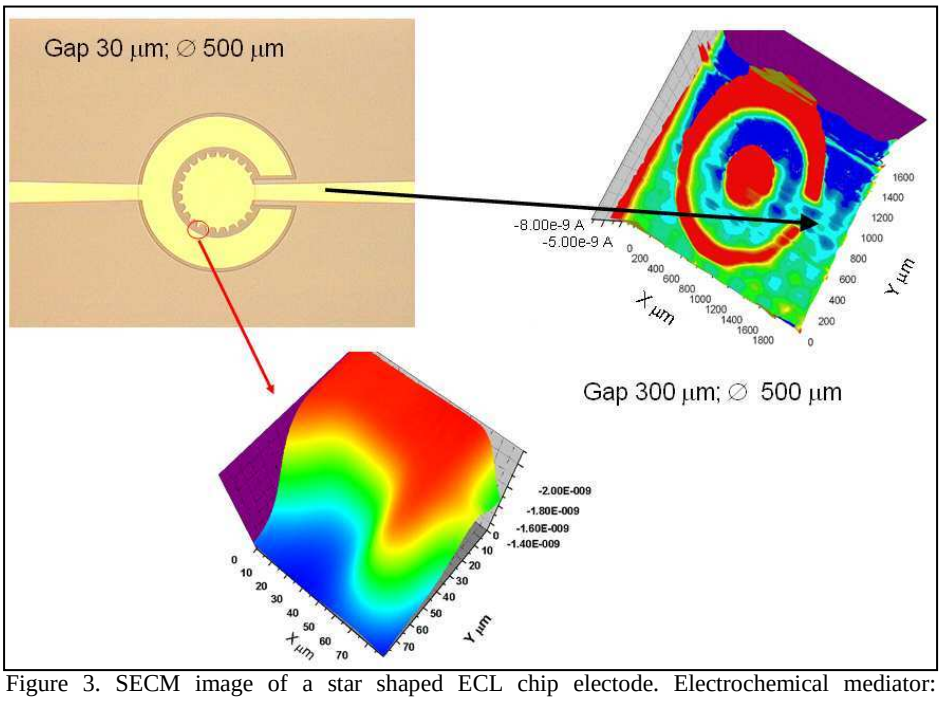

Figure 3. SECM image of a star shaped ECL chip electode. Electrochemical mediator: Ferrocene-OH. Supporting electrolyte: KNO_3 100 mM.

Another simple test consisted in the verification of the effective separation of W and C when the distance was minimal (5 μm) by observation under optical microscope (fig. 4). Also from this point of view the chip was considered satisfactory.

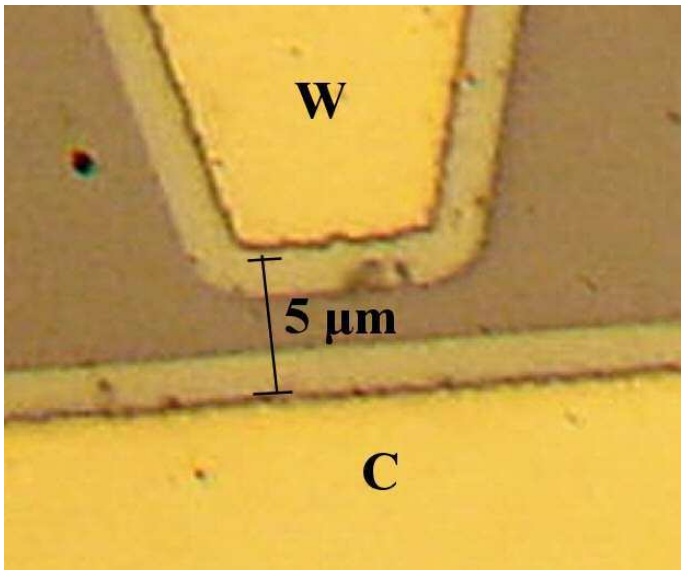

Figure 4: Optical microscope image of a 5 µm W-C gap. The grey region around electrodes is the Ta/Al underlayer of the approximate width of 1 µm.

5.2
Experimental procedures

Electrochemistry and electrochemiluminescence

Cyclic voltammetry and ECL was carried out with an AUTOLAB electrochemical station (Ecochemie, Holland) and previously introduced ECL Bologna setup. The silicon chips were used as counter and working electrode. In both cyclic voltammetric (CV) and ECL experiments a homemade compact glass cell and a Teflon chip holder was used (fig. 5). This cell was previously described in major detail in section 2.4; one of his benefits is that contacts are made without soldering the chip. The Quasi Reference electrode, an Ag wire, can be inserted directly in the back of the Teflon holder. Prior to each

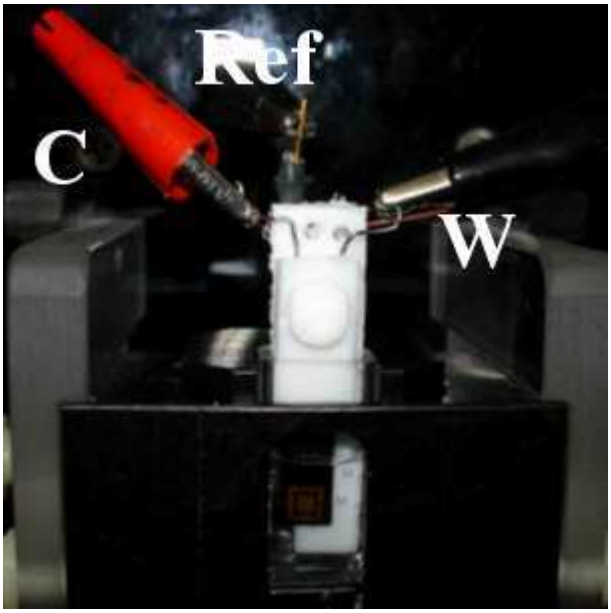

Figure 5. The cell and the chip holder used in ECL and CV experiments (side view).

experiment cell and CHIP holder were immersed in a concentrated KOH EtOH/H2O 1:1 solution for 10 minutes then washed with water, rinsed with a concentrated HCl solution, sonicated and finally washed with water and acetone. The chips were immersed for 5 minutes in piranha solution (H_2O_2 / H_2SO_4 1:3 v:v) before each experiment then sonicated and washed with water and acetone. The CHIP electrodes modified by SAM were washed with water and EtOH after functionalization and prior to each measurement to ensure the absence of adsorbed or free $Ru(bpy)_3^{2+}$ from marked reactants. Quasi reference Ag electrode was polished with 0.05-μm alumina and then was sonicated and thoroughly rinsed with Milli-Q water and acetone before each run. For electrochemical and ECL experiments a phosphate buffer solution (PBS) was prepared using equimolar quantities of Na_2HPO_4 and KH_2PO_4 . The concentration of PBS was 0.1 M and pH was adjusted to 7.5 using concentrated H_3PO_4 or a 3 M solution of NaOH. The optimization of the buffer solution in ECL commercial analyzers in discussed in the appendix. Tripropylammine (NPr_3 or TPA) was added as coreactant in concentration of

$3x10^{-2}$ M (the maximum soluble amount at this pH) . ECL was generated by a single oxidation step of the Ru complex and TPA. The ECL signal during cyclic voltammetry was measured with a photomultiplier tube (PMT, Hamamatsu R4220p) placed few millimetres in front of the CHIP working electrode inside a darkbox including completely the surface of working electrode .

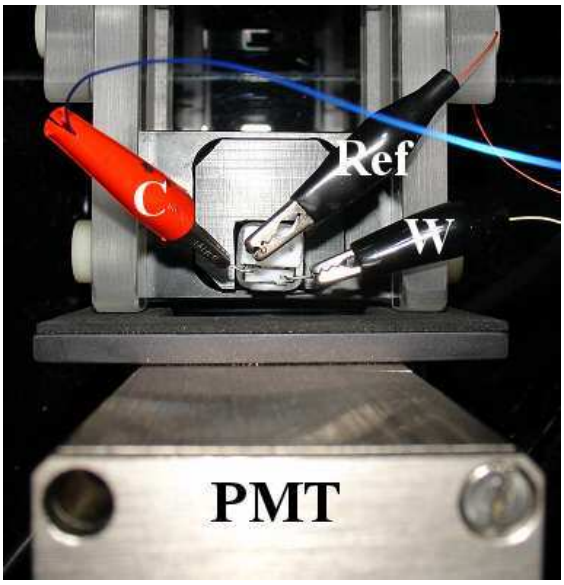

Figure 6. The setup used during ECL experiments.(top view). The PMT is placed just in front of the chip.

A voltage of 1000 V was supplied to the PMT. ECL spectra has been recorded inserting the same PMT in a dual exit monochromator (ACTON RESEARCH mod. spectra pro 2300i). Fotocurrent detected at PMT was accumulated for 3 to 5 seconds depending on emission intensity, for each step of monocromator. Monochromator in and out slits were fixed to the maximum value of 3 mm. Experimental setup for detection of integrated ECL emission is summarized in fig.6.

Photoluminescence

Photoluminescence (PL) measurements were performed with a Varian (mod. Cary Eclipse) fluorimeter equipped with solid sample holder. The experimental setup (fig. 7) allowed to focus exciting laser into working electrode. The presence of light at the PMT was checked, before each test, registering the spectra of the source partially reflected by the gold surface of the CHIP.

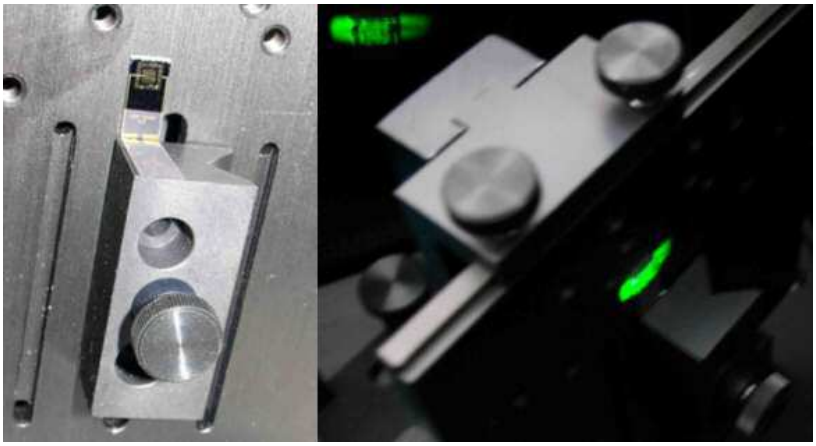

Figure 7. The solid sample holder and experimental setup used in fluorescence experiments.

5.3

Chip weak points.

Sensitivity to basic solutions

When the chip is washed with an highly basic solutions the Al/Ta underlayer is etched. From the previous homogeneous grey colour an iridescent oxide film is clearly visible on the underlayer with a standard optical microscope. (fig. 8)

As consequence ECL signal tends to decrease of about 10-100 times depending on the amount of oxide present. On the other hand no changes were observed in the chip after washing with an highly acidic piranha solution. Silicon and silicon nitride layers showed in general no sensitivity to acid and basic solutions.

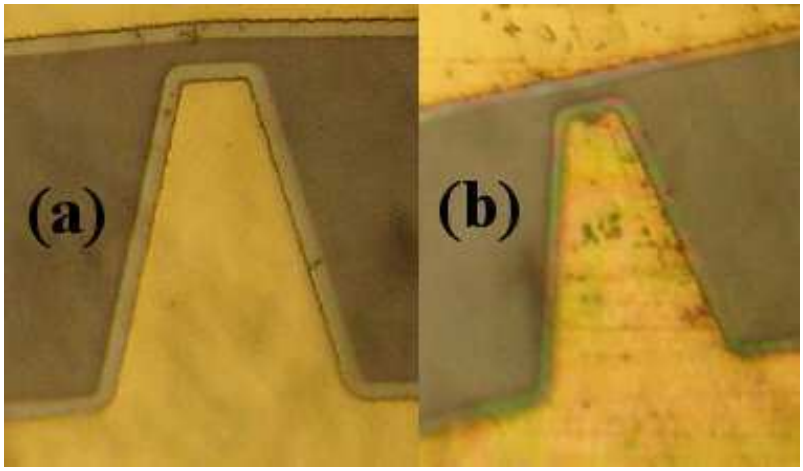

Figure 8. Optical microscope image of ECL electrode before (a) and after (b) treatment with 3 M NaOH solution.

Corrosion of the edges

In square geometry electrodes if the electrical current passing trough is higher than 10 mA a corrosion and detaching of the Al/Ta layer together with Au one is clearly observed (fig. 9). The effect is more visible at the corners because of the higher current density. For this reason when using square geometry electrodes It should be better to run cyclic voltammetries at a scan rate lower than 10 V/s. A similar effect has never been observed for circular and star shaped electrodes probably because of current density homogeneity on the edges . For a better understanding of the phenomena the system could be simulated by using appropriate boundary conditions.

Formation of a quenching film

If after an ECL run, a chip is observed under optical microscope a brown film is present on the working electrode surface. (see fig. 10). After a water rinse, to remove the $Ru(bpy)_3^{2+}$ crystals, by watching the chip under the fluorescence microscope has been found that this film is not fluorescent. The

amount of filming product is higher in the regions of higher current density (i.e. at the edges). In the case of the lower W-C distance chip (5 μm), when a sufficient current is passed, the electrogenerated film can bridge the two electrodes. The effect of the two electrodes junction is a short circuit revealing the conductive nature of the film. In the future It should be interesting to study the exact composition of this film to understand if the underlayer play a role in his formation. If It is not the case this film could help in understanding what molecule is the quencher and possibly the responsible of $Ru(bpy)_3^{2+}$ time emission decay. As recently reported in fact, the $Ru(bpy)_2(H_2O)_2^{2+}$ formed from the reaction between $Ru(bpy)_3^{2+}$ and H_2O could be the quencher of his solid state emission[1] but this hypothesis has still not confirmed.

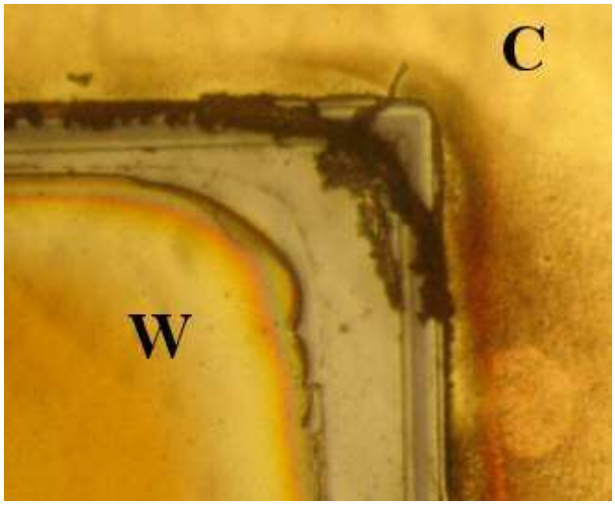

Figure 9. Corrosion and detachment of gold layer with high current density (> 10 mA)

Absence of a true reference electrode

If an external Ag wire is used as a reference electrode the resistance of the cell greatly decreases with respect to the case where It was not present and the potential scale appears to be expanded. (fig 11). It's also important to consider the use of a true reference electrode (for example Ag/AgCl) to exclude the possibility of potential drift that can occur with quasi reference electrodes.

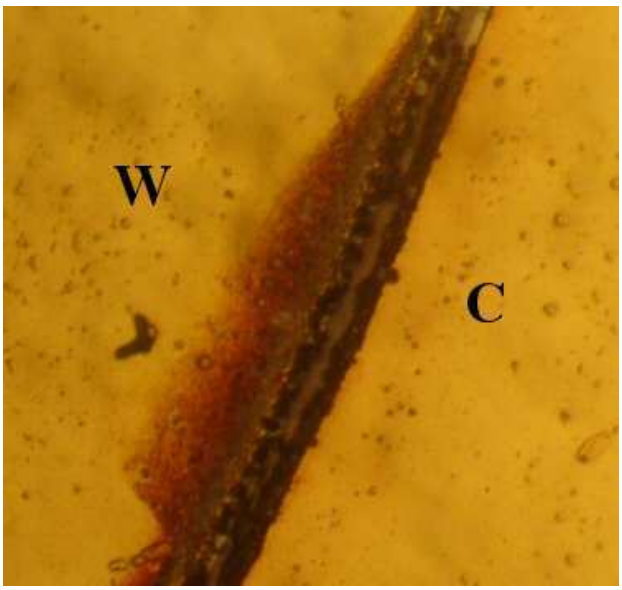

Figure 10. Optical microscope image of the brown filming product deposited in the region between working and counter electrode.

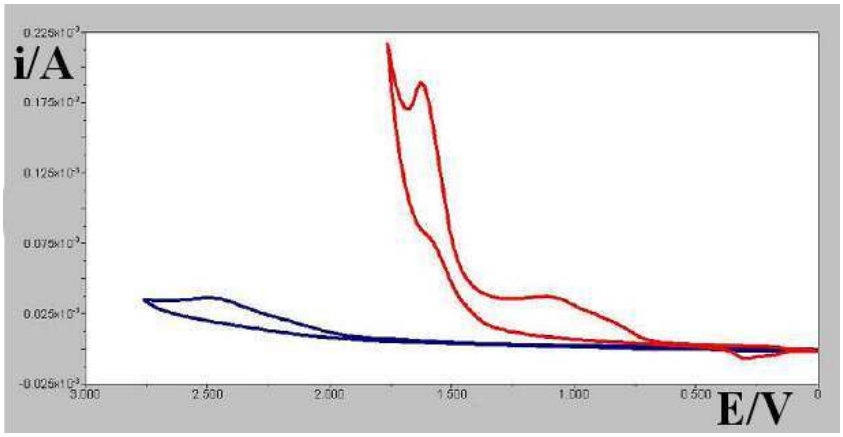

Figure 11. Effect of the quasi reference electrode presence (red curve) and absence (blue curve) on the shape of the cyclic voltammetry registered from a EQ_500_300 chip. Solution: $Ru(bpy)_3^{2+}$ 10^{-4} M/ NPr_3 $3x10^{-2}$ M. Supporting electrolyte: PBS 0.1 M at pH 7.5.

5.4
ECL Reproducibility tests on the chip

5.4.1
Structure of the tests

During these measurements two different compounds have been tested separately: the new tetrazolate based Ru(pyr-tet) and the standard $Ru(bpy)_3^{2+}$. Four independent measurements have been performed according to the following scheme for each complex:

Copy 1 of the chip
-Chip washing[2]
1) test 1 on solution 1 (Ru + NPr_3 in PBS)
-washing
2) test 2 with solution 1

Copy 2 of the chip, change of solution
-washing
3) test 1 with solution 2
-washing
4) test 2 with solution 2

Each measurement has been repeated 5 times without chip washing to check signal stability. From the collected data the following information can be thus obtained by statistical analysis:

- Chip reproducibility: on the first use of the chip, on two successive usages
- Comparison of relative ECL emission intensity of Ru(pyr-tet) and $Ru(bpy)_3^{2+}$.

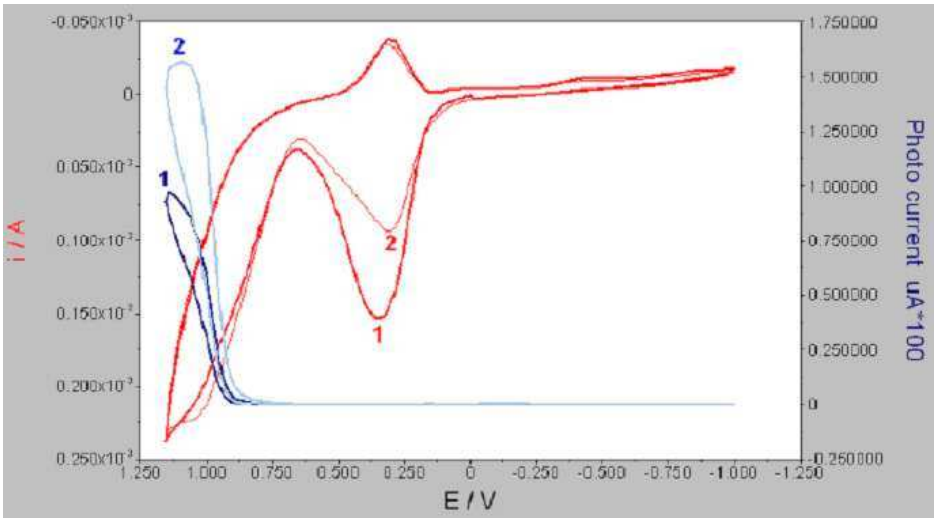

Figure 12. Effect of cleaning cathodic step in ECL and CV curve of a $Ru(bpy)_3^{2+}$ 10^{-4} M/NPr_3 3x 10^{-2} M solution. Chip: EQ_2000_30. Supporting electrolyte: PBS 0.1 M at pH 7.5. Scan rate: 0.5 V/s. PMT bias: 750 V. Potentials are vs. Ag wire.

Specific experimental conditions

During the reproducibility test measurements a solution with [Ru]= 10^{-4} M was prepared by using $Ru(bpy)_3(PF)_2$ triply crystallized from acetone or chromatographically highly purified Ru(pyr-tet). The oxidative coreactant NPr_3 ,added at a concentration of 3x10^{-2} M ,was previously purified by distillation and preserved under Ar to avoid oxidation in air. The switching method was cyclic voltammetry (scan rate: 0.5 V/s). The potential program was E_1= 1.2 V, E_2= -1.0 V vs. Ag. By using the NPr_3 irreversible oxidation as internal potential reference no sensible drift of the quasi reference Ag wire was observed. As consequence the max. ECL intensity was reached during all the tests. The typical light/current/potential curve profile during a measurement is shown in fig. 12. The effect of H_2 evolution, when negative potential is reached between first and second scan, is an ECL intensity increase and a decrease of the current triangular peak around +0.3 V. In the following scans usually no more modifications of the light/current/potential curve were

observed. The emission maximum intensity measured during three successive CV cycles has been thus taken as ECL signal. It's important to specify that during solutions preparation the accuracies were of ± 0.1 ml in volumetric measurements and ± 0.05 mg in weigh.

5.4.2

Results and discussion

During the tests the chips displayed a very bright eye visible emission in correspondence of the positively biased electrode surface (fig.13). The emitting area appeared of an homogeneous orange colour. The results of chip reproducibility studies on $Ru(bpy)_3^{2+}$ and Ru(pyr-tet) are reported in table 1. For each of the four measurement are specified the ECL intensities (I_{ECL}) registered during the relative 5 tests. The mean value and standard deviation has been calculated for each set of tests.

Ru(pyr-tet) and $Ru(bpy)_3^{2+}$ relative emission intensity

The $I_{ECLRu(pyr\text{-}tet)}$ /$I_{ECL,Ru(bpy)}$ value mediated on all measurements has been found to be of 8.60 %. This value is much lower than that obtained by square cell (56 % in sect. 3.2.4) and far from fluorescence relative quantum efficiency in air (28 % sect. 3.2.2). This results evidences as ECL relative emission intensity depends on experimental conditions that consequently need to be carefully fixed. The ECL intensity dependence on diffusion coefficient and electrolysis conditions could be eliminated by definiting it as follows:

$$E_{ECL,n} = \frac{\int_{V_i}^{V_f} I_{ECL}(V)dV}{\int_{V_i}^{V_f} i(V)dV}$$

where $E_{ECL,n}$ is the normalized ECL intensity and (V_i,V_f) is the interval of

potential where emission occurs. Another simpler definition could be:

$$E_{ECL,n} = \frac{I_{ECL,\max}}{i_{ECL,\max}}$$

where the ECL intensity is normalized respect to the current ($i_{ECL,max}$) in the single point of the maximum. A practical problem in this approach is the fact that during experiments the light was measured in arbitrary units which depend on experimental conditions (i.e. PMT voltage, PMT sensitivity, slits aperture, electrode area etc…) that varied from square to chip cell setup. The measurement of absolute emitted light should be made by photon counting that is not currently available in Bologna setup.[3] The current normalization was not used here for simplicity but will be implemented in future investigations when an accurate calculation of ECL efficiency is necessary. This set of measurements confirmed that Ru(pyr-tet) has an ECL emission intensity very similar to that of $Ru(bpy)_3^{2+}$.

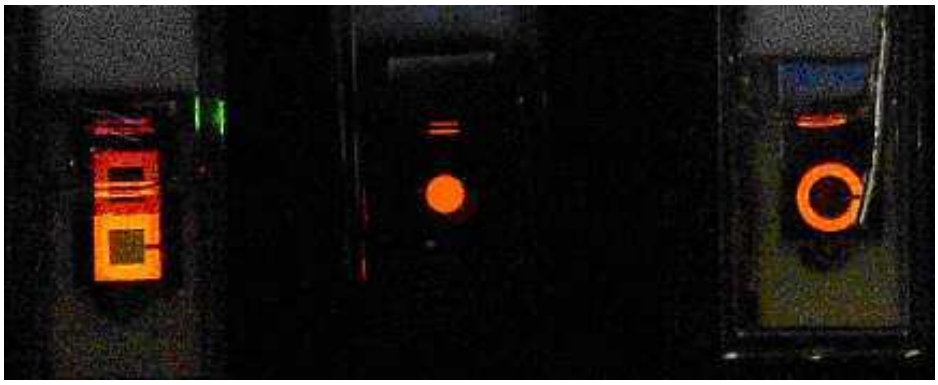

Figure 13. Photographic images of ECL emission from a 0.1 mM $Ru(bpy)_3^{2+}$/ $3x10^{-2}$ M NPr3 solution. Supporting electrolyte: 0.1 M PBS at pH 7.5. From the left to right: EQ_2000_5, EC_2000_5 and again EC_2000_5 chip electrode. ECL emission appears homogeneous in all working electrode surface. These images show the possibility to invert the counter with working electrode by retaining the emission.

ECL decrease for repeated chip usage

From tab. 1 is clear that when a chip is used a second time with the same solution after a washing step a decrease of ECL intensity is observed for both complexes. This is due to a thin film formation at working electrode (sect. 5.4) and to his surface modification during operation. The decrease of ECL signal cannot be caused by NPr_3 consumption because of his large excess. Considering the mean value of five tests the following I_{ECL} decreases from first to second chip usage have been calculated:

Chip 1	**Decrease (%)**
$Ru(bpy)_3^{2+}$	-14.0
Ru(pyr-tet)	-20.9
Chip 2	
$Ru(bpy)_3^{2+}$	-13.1
Ru(pyr-tet)	-25.9
General	
$Ru(bpy)_3^{2+}$	-13.6
Ru(pyr-tet)	-23.4

The decrease is a bit lower for $Ru(bpy)_3^{2+}$; the decrease was very similar in the two copies of the chip.

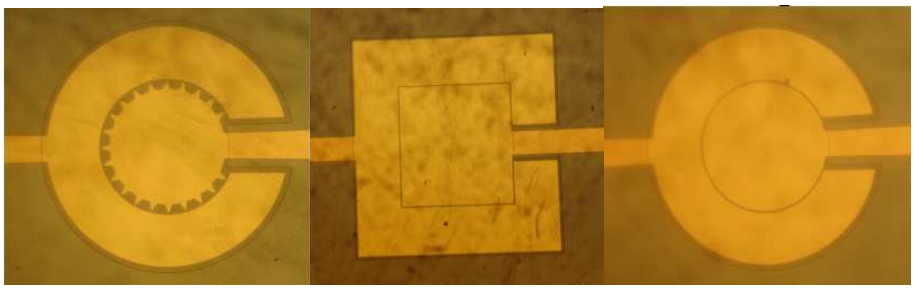

Figure 14. Optical microscope image of the three different geometries of the working electrode. From left to right: ES_2000_5, EQ_2000_5 and EC_2000_5 chip electrodes. The gold areas covered by the insulating film in the left and right side appears as reddish.

	Chip 1 Sol 1	*Mean*		*Std. Dev.*		Chip 1 Sol 2	*Mean*		*Std. Dev.*		Chip 2 Sol 1	*Mean*		*Std. Dev.*		Chip 2 Sol 2	*Mean*		*Std. Dev.*	
Test Number	1	2	3	4	5	1	2	3	4	5	1	2	3	4	5	1	2	3	4	5
$Ru(bpy)_3^{2+}$	92.5	93.5	91.4	92.3	92.5	78.4	77.3	79.1	80.0	79.5	101.9	102.9	92.0	89.8	100.3	84.8	85.4	85.0	83.7	84.1
Summary		92.44		0.75			78.86		1.05			97.38		2.70			84.6		0.69	
Ru(pyr-tet)	8.2	9.1	8.9	9.0	8.9	6.8	6.8	7.1	7.1	7.1	8.4	8.6	8.4	8.4	8.3	6.3	6.0	6.1	6.4	6.4
Summary		8.82		0.36			6.98		0.16			8.42		0.11			6.24		0.18	

Table 1. Summary of the data collected in ES_2000_5 chip reproducibility tests. The measured value is ECL intensity expressed in arbitrary units. (20 µA/V current scale) .

Chip reproducibility

The inter-chip reproducibility was estimated by % standard deviation between values measured in two identical copies of the chip. The following values were calculated:

FIRST USAGE	
$Ru(bpy)_3^{2+}$	
Chip 1	92.44 A. U.
Chip 2	97.38 A. U.
Reproduc.	**± 3.6 %**
Ru(pyr-tet)	
Chip 1	8.82 A. U.
Chip 2	8.42 A. U.
Reproduc.	**±3.28**
SECOND USAGE	
$Ru(bpy)_3^{2+}$	
Chip 1	78.86 A. U.
Chip 2	84.60 A. U.
Reproduc.	**±4.97 %**
Ru(pyr-tet)	
Chip 1	6.98 A. U.
Chip 2	6.24 A. U.
Reproduc.	**±7.92 %**
MEAN REPRODUC.	
$Ru(bpy)_3^{2+}$	**±4.29 %**
Ru(pyr-tet)	**±5.60 %**

The reproducibility obtained in ECL measurement by using chip electrodes is in general very good (±5 %). Respect to initial one of ± 3% in second usage is lowered to ±5-7 %. This values suggests the suitability of the chips to ECL quantitative measurements.

5.5
Chip geometry optimization

5.5.1
Structure of the tests

This series of measurements was made to maximize ECL signal by varying the chip electrode geometry (fig. 14). As already introduced three different geometrical aspect of the chips were modulated:

- working electrode shape: square (EQ) , circular (EC) and star shaped (ES)
- dimension of W: 500, 1000 and 2000 μm
- W-C distance: 5, 30 and 300 μm.

Considering all the degrees of freedom the system to be maximized can be mathematically represented with a three index array of total 27 elements.
Assuming however that ECL signal is reasonably proportional to the electrode area, is convenient to study only the chips with dimension of 2 mm. This way the resulting two indexes matrix of configurations can be written as:

EQ_5 EQ_30 EQ_300
EC_5 EC_30 EC_300
ES_5 ES_30 ES_300

Where the column number represents the W-C distance in μm and the row the shape. For each element of this matrix, by using $Ru(bpy)_3^{2+}$ as emitting complex, a set of five ECL intensity measurements has been performed. The experimental conditions were identical to those described in sect. 5.5.1 except for geometry variation. From the final matrix of ECL intensities, containing the mean of the 5 equivalent experiments, will be determined the best combination of the varied parameters.

Configuration	test 1	test 2	test 3	test 4	test 5
ES_5	101.90	102.90	92.00	89.78	100.31
ES_30	90.24	95.49	93.29	96.20	97.32
ES_300	82.70	97.93	108.61	116.03	117.61
EQ_5	178.50	207.61	199.68	197.72	197.33
EQ_30	167.05	154.85	169.83	168.34	167.48
EQ_300	130.37	147.64	150.21	151.55	152.53
EC_5	131.07	133.45	126.25	125.40	127.23
EC_30	84.20	93.75	98.21	100.43	101.59
EC_300	103.27	105.99	104.86	108.55	108.73

Table 2. ECL emission intensity (A. U.) by varying chip configuration parameters. The photocurrent was in the range of 20 μA/V. Each test was repeated five times. ECL emission was generated by oxidizing a 0.1 mM $Ru(bpy)_3^{2+}$/ $3x10^{-2}$ M NPr3 solution. Supporting electrolyte: 0.1 M PBS at pH 7.5. Switching method: Cyclic voltammetry. Scan rate: 0.5 V/s. Potential program: E_1= +1.2 V, E_2=- 1.0 V vs Ag.

5.5.2

Results and discussions

The following matrix contains the ECL intensities calculated as mean values of the five tests for the different W-C distances and geometries; the corresponding raw data is reported in table 2.

	5	30	300
EQ	**196.16 ± 10.71**	**165.50 ± 6.05**	**146.46 ± 9.17**
EC	**128.68 ± 3.43**	**95.63 ± 7.06**	**106.28 ± 2.36**
ES	**97.37± 6.03**	**94.50 ± 2.8**	**104.57 ± 14.49**

The mean values of max. electrical current measured during the same experiments are reported in the following matrix where i_{max} is expressed in A.

	5	30	300
EQ	**$2.17x10^{-4}$**	**$2.15x10^{-4}$**	**$2.17x10^{-4}$**
EC	**$2.62\ x10^{-4}$**	**$1.57x10^{-4}$**	**$1.66x10^{-4}$**
ES	**$1.37x10^{-4}$**	**$1.49x10^{-4}$**	**$1.62x10^{-4}$**

For all geometries the emission intensity appeared as homogeneous in all working electrode surface (see fig. 13). The inversion of W with C didn't changed this feature. This consideration confirmed the previous hypothesis that total ECL intensity is a linear function of the electrode area.

The ECL emission in ES electrodes evidenced no dependence on W-C distance. From fig. 8 and 13 is clear however that in this geometry the minimum distance of 5 μm is reached only in the "star" tips whereas for remaining electrode edges is only of 50 μm. As a matter of fact EC geometry, where W-C distance is constant, showed a 25 % of signal increase by lowering it from 30 μm to 5 μm. The positive effect of the short W-C distance is definitely confirmed by EQ geometry. The values of light and current intensity of the square geometry need to be divided for 1.27 prior to comparison with EC and ES, the approximated electrode area ratio (4/3.14). By comparing EQ with EC geometry it's clear that even with 30 μm W-C distance there is an increase of normalized light emission of about 30 % with the same current. This behaviour evidence a positive effect of the square geometry on the circular one. By decreasing the W-C distance to 5 μm in EQ geometry the

normalized ECL intensity is increased of about 20 % as was for EC geometry (25 %). By summarizing two effects on ECL intensity seem to be present:

I) an increasing effect of the square geometry respect to the circular one at constant current (+30 %)

II) a positive effect of the lower 5 μm W-C gap at constant current (+20 %).

For these reasons the best configuration was found to EQ_2000_5 where the two effects were combined.

Future chips improvements
Taking in account the results of optimization tests the following modifications will be done in the improved version of the chip:

- reduction of W-C distance to 3 μm
- reduction of underlayer protrusion (currently 1 μm) to gain space
- the reference electrode will be included (Ag/AgCl)
- it will be investigated the possibility to realise a MEA (Multi-Electrode Array) version of the chip.

5.6
ECL annihilation emission in water
As previously reported[4] using short distanced (2 μm) interdigitated electrodes is possible to generate ECL from aqueous $Ru(bpy)_3^{2+}$ solutions even in absence of supporting electrolyte. Thanks to the short W-C distance if the complex was simply oxidised the radical cation generated at the anode (W) can annihilate with radical anion contemporaneously produced at the cathode.(see fig. 15) A similar experiment was tried by using chips with the minimal W-C distance (5 μm) to understand if the previously observed

increase of ECL intensity in short distanced electrodes was caused by this effect.

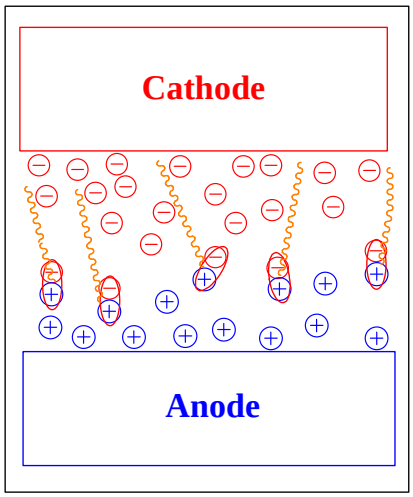

Figure 15. Scheme of direct annihilation between electro-generated radical cation and anion for short inter-electrodes distances. Anion and cation are both generated by biasing positively the working electrode without the need of a reduction. The position where emission occurs depends on the ions relative mobility.

Experiment I

A $Ru(bpy)_3^{2+}$ 10^{-4} M aqueous solution was prepared by using Millipore ultra pure water without adding supporting electrolyte. During a cyclic voltammetry in correspondence of the complex oxidation, a weak ECL emission was detected (fig. 16). The photocurrent range was of three orders of magnitude lower than that employed in presence of NPr_3. (nA/V instead of μA/V). If the ring like chip electrode is used as working (fig. 16) the maximum ECL intensity increased of about 3.5 times, more than the relative area increase of about 2.5 . This effect was reproduced in several tests with both EQ and EC electrodes.

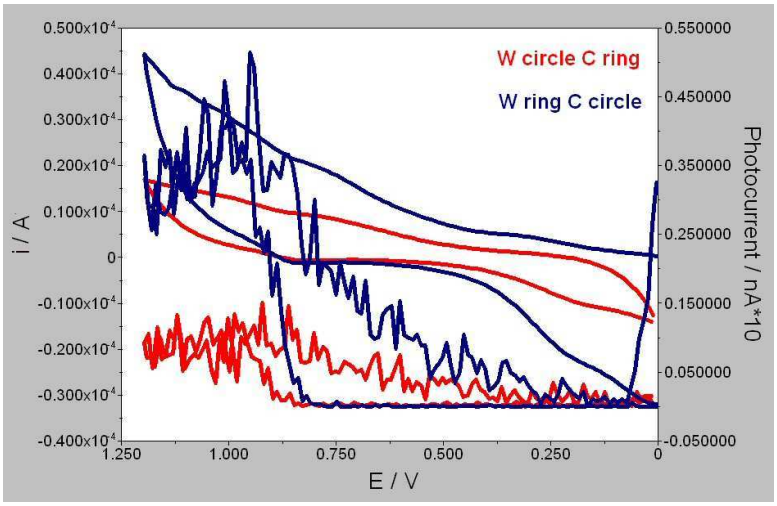

Figure 16. Light/current/potential curves registered from a 10^{-4} M $Ru(bpy)_3^{2+}$ aqueous solution by using a EC_2000_5 chips as working and counter electrode and an Ag wire as reference. No supporting electrolyte was added. Switching method: Cyclic voltammetry. Potential program: E_1= 0 V, E_2= +1.2 V. Scan rate: 0.5 V/s.

Experiment II

The $Ru(bpy)_3^{2+}$ 10^{-4} M solution was prepared this time in PBS 0.1 M. By oxidizing up to + 1.1 V vs. Ag the maximum ECL intensity increased of about one order of magnitude respect to experiment I, similarly to the current increment consequent to electrolyte addition. (fig. 17.a). Considering the low intensity of these emissions, two orders of magnitude less intense than that in presence of NPr_3, can be excluded that the annihilation contribution is the responsible of previously observed ECL increase in short distanced electrodes. By oxidizing up to + 1.5 V (fig 17.b) the ECL peak around 1 V remains of the same intensity but a new peak appears at about + 0.1 V vs Ag an order of magnitude more intense than previous. Such positive potentials seem not to be reached in presence of NPr_3 and cannot thus be used to explain the previously discussed effect. The double emission was reproducible with different chip configurations. It's not clear if the ECL emission at +0.1 V is localized on W or in C consequently an image of the weakly emitting chip will be captured in future by an amplified CCD camera. The emission at +0.1 V was not observed

if the potential was stopped at more positive values during reverse scan. The emission appeared then not to be a time delayed effect but could be the consequence of the generation of a small amount of radical anion immediately annihilating with the previously generated short-distance radical cations.

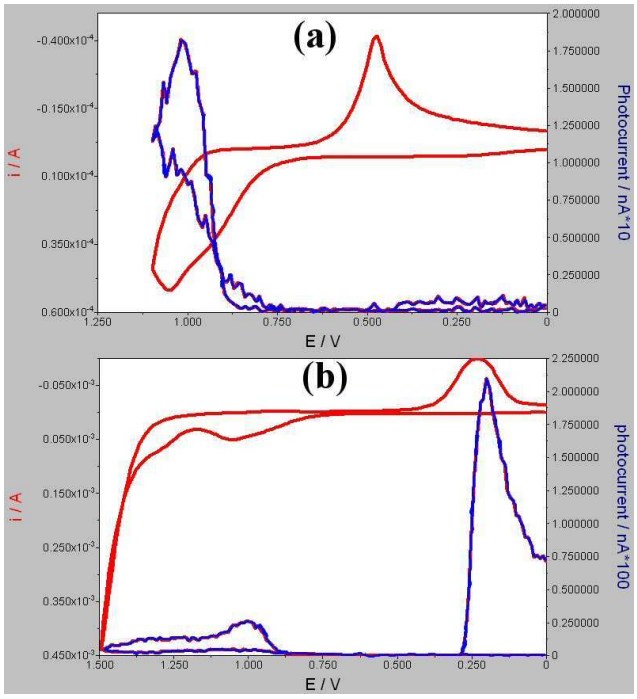

Figure 17. Light/current/potential curves registered from a 10^{-4} M $Ru(bpy)_3^{2+}$ aqueous solution by using a EC_2000_5 chips as working and counter electrode and an Ag wire as reference. Supporting electrolyte: 0.1 PBS at pH 7.5. Switching method: Cyclic voltammetry. Potential program: (a) E_1= 0 V, E_2= +1.1 V; (b) E_1= 0 V, E_2= +1.5 V. Scan rate: 0.5 V/s.

5.7
ECL on functionalized chips

The study of ECL emission from functionalized electrodes containing self assembled monolayers (SAM) of $Ru(bpy)_3^{2+}$ labelled surfactants has been previously reported by Bard e coworkers.[5,6] In general ECL emission has been observed for different working electrode materials such as Gold and Indium

Tin Oxide (ITO). The ECL signal was found to be about 100-1000 times more intense in ITO with respect to Au. The presence of a metallic surface in the proximity of emitting complex causes the complete quenching of photo-excited emission so that photoluminescence for such kind of solid film can be obtained only on insulating substrates. The same quenching effect is present in ECL but the different mechanism of excited state generation, involving charged species, makes the radiative decay possible and competitive with the metallic quenching pathway. The use of lipoic acid is a relatively new method[7] to prepare the SAM; previous studies evidenced also the discrete electrochemical stability of the molecule during reductive and oxidative processes[8]. The chips functionalization process and the acronyms of involved species are summarized in figure 18. Here we show how ECL detection can be pratically used to confirm the presence of an addiction product on a SAM where the most conventional fluorescence detection is not working. The employed method has been found to be fast, easy and inexpensive especially if compared with more sophisticated techniques such as SIMS or MALDI.

5.7.1

Synthesis and purification of the ECL label Rubpy-NH_2

(bis(2,2'-bipyridine)[4-(4'-methyl-2,2'-bipyridine) butylamine] Ruthenium(II) diperchlorate)

Starting materials: 4,4'-dimethyl-2,2'-bipyridine, Li diisopropylamine, 1,3 bromopropane, Potassium Phthalimide (Aldrich), Hydraziniumhydroxid (Merck), $RuCl_3x3H_2O$ (Fluka).

Step 1: synthesis of 4-(4-bromobutyl)-4'-methyl-2,2'-bipyridine (a).

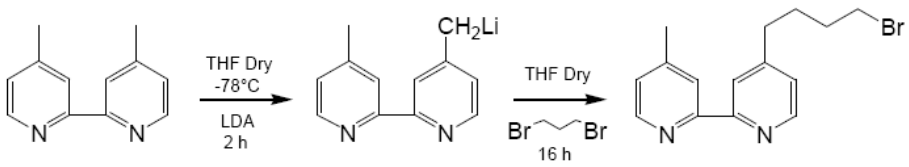

Under Argon atmosphere 10.81 g of 4,4'-dimethyl-2,2'-bipyridine (58.67 mmol) were dissolved in THF dry (259 mL) to form a colourless solution. The solution was cooled to -78°C and Li diisopropylamine (30 mL of 1.8 M solution, 54.06 mmol) were slowly added (1 mL/min) by means of a dropping funnel. A dark red milky solution formed. The solution was kept stirring at -78°C for 2 hours, then 1,3 dibromopropane (59 mL, 10 eq) was added dropwise. The dark solution was kept stirring in the dry ice bath overnight, letting slowly reach room temperature. 50 mL of brine were added in the flask and a white precipitate formed. The mixture was then poured in a separatory funnel and 100 mL additional brine were added. Two extractions with dichloromethane (150 mL each) were performed. The organic phase was dried and the solvent evaporated under reduced pressure. A distillation was performed in order to get rid of large excess of 1,3 dibromopropane.
The obtained brown oil was kept in fridge for 1 day and a white precipitate formed. Filtration was performed (gouch, por. 4) and the white-grey solid retained on the filter was washed with few mL of cold diethylether. The eluted brown solution was evaporated under reduced pressure to obtain 15.03 g of brown oil (crude product). The oil was loaded on a silica chromatographic column (7x12 cm) and elution was performed with cyclohexane:ethylacetate 2:1. The chromatographic process was monitored with TLC (silica with fluorescent indicator, cyclohexane:ethylacetate 2:1) and a developing solution of $(NH_4)_2Fe(SO_4)_2$. The fractions containing the spot with rf=0.3 (which forms a purple spot with the developing solution) were collected and evaporated under reduced pressure. 9.88 g of yellowish oil were obtained (product, Yield=55%).

NMR analysis (400MHz, $CDCl_3$, 25°C) showed: 1.81-1.95 (m, 4H, CH_2-CH_2); 2.43 (s, 3H, CH_3); 2.72 (t, 2H, CH_2bpy); 3.42 (t, 2H, CH_2Br); 7.11-7.14 (m, 2H, aromatics); 8.22-8.25 (m, 2H, aromatics); 8.52-8.58 (m, 2H, aromatics).

Step 2: synthesis of 4-(4-phthalimidobutyl)-4'-methyl-2,2'-bipyridine (b).

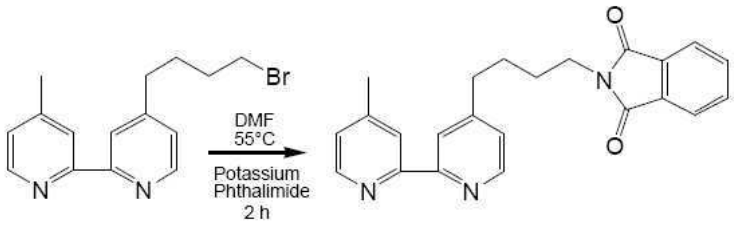

1.82 g of Potassium phthalimide (9.83 mmol) were dissolved in 30 mL of DMF. A solution of 3 g of (a) (9.83 mmol) in 10 mL DMF was prepared (dissolved with gentle heating) and added to the first solution. 5 additional mL of DMF were user to wash the becker and added to the solution. The pale red mixture was heated to 55°C and kept stirring for 2 hours. After cooling to room temperature 90 mL of distilled water were added in the flask. The solution was extracted three times with dichloromethane (60 mL each time) and the organic phase washed with 45 mL of NaOH 0.2 M and subsequently with 30 mL of distilled water. After drying and evaporating the solvent under reduced pressure 3.69 g of brown oil were obtained. The oil was loaded on a silica chromatographic column (6x12 cm) and elution performed with toluene:ethylacetate 1:1 solution. The chromatographic process was monitored with TLC (silica with fluorescent indicator, toluene:ethylacetate 1:1 solution) and a developing solution of $(NH_4)_2Fe(SO_4)_2$. Fractions with spot at rf=0.54 (some of them contained also a spot at rf=0.68) were collected and evaporated under reduced pressure. A waxy, yellowish solid was obtained. Addition of cyclohexane (10 mL) and ethylacetate (1 mL) produced a fine white solid which was filtered (gouch, por. 3) and washed with cyclohexane. The white solid obtained was then used to form a milky solution with acetone (350 mL) and ethanol (3 mL). The suspension was kept in fridge overnight, then evaporated under reduced pressure. Cyclohexane and a small amount of ethylacetate were added to form a suspension which was kept in fridge for two

days. Filtration was then performed (gouch, por. 3) and 1.60 g of white solid product were obtained (Yield = 44%).

Step 3: synthesis of 4-(4-aminobutyl)-4'-methyl-2,2'-bipyridine (c).

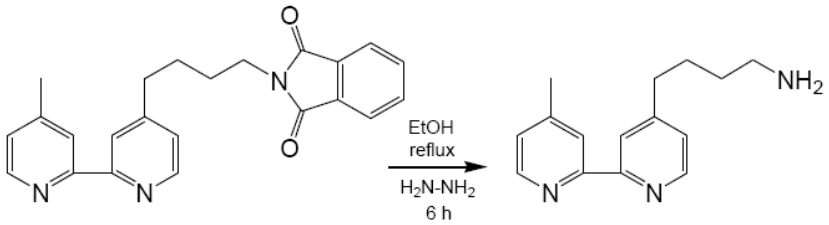

1.60 g of (b) (4.31 mmol) and ethanol 96° (48 mL) were added in a flask to obtain a milky suspension. Hydraziniumhydroxid 80% solution (287 uL, 1.1 eq) was added and the mixture was kept stirring and refluxing for 6 hours. A clear yellowish solution formed. The solution was reduced under reduced pressure to few mL (yellow-brown oil) and added to 160 mL of brine to form a cloudy solution. Three extractions with dichloromethane (150 mL each) were performed and the organic phase was then dried and evaporated under reduced pressure. 0.99 g of yellow-brown oil were obtained (product, Yield = 95%).

Step 4: synthesis of bis(2,2'-bipyridine)Ruthenium(II) dichloride dihydrate (d).

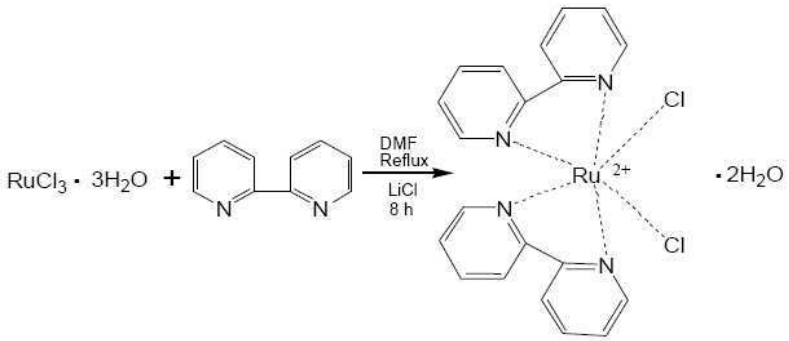

Under Argon atmosphere $RuCl_3x3H_2O$ (5.08 g, 19.43 mmol), 2,2'-bipyridine (6.10 g, 2.01 eq) and LiCl (5.53 g, 6.71 eq) were dissolved in degased DMF

(37 mL). A black solution formed. The solution was kept stirring and refluxing for 8 hours. After few minutes cooling (not yet room temperature) 160 mL acetone were added in the flask and the solution kept in fridge overnight. Filtration was then performed (gouch, pro. 4) and the dark solid on the filter was washed with distilled water (200 mL), let dry on the gouch for 1 hour, washed with diethilether and let dry on the gouch overnight. 5.1 g of dark powder were collected (product, Yield=50%).

Step 5: Synthesis of bis(2,2'-bipyridine)[4-(4'-methyl-2,2'-bipyridine)butylamine] Ruthenium(II)diperchlorate (Rubpy-NH_2).

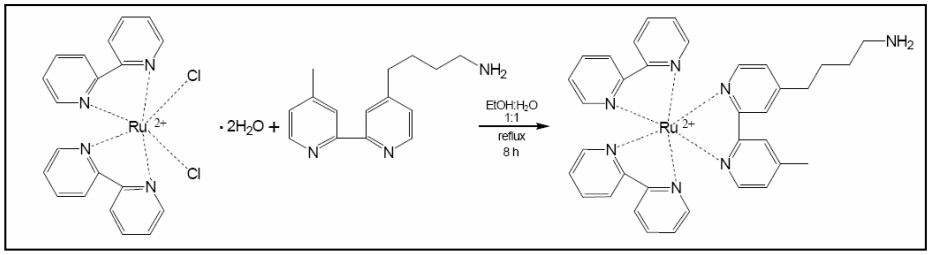

Under Argon atmosphere (c) (583 mg, 2.42 mmol) and (d) (1.05 g, 2.01 mmol) were dissolved in 100 mL of ethanol:H_2O 1:1 solution. A black solution formed. The solution was kept stirring and refluxing for 8 hours. Orange reflections showed up in the solution. Upon cooling the solvent was reduced under reduced pressure to about 15 mL. Cationic exchange chromatography was then carried out using a Sephadex SP25 resin in a 2.5x20 cm column. Elution was performed with distilled water until almost transparent elution was achieved. Then the eluent solution was switched to NaCl 0.25 M to elute the dark band on the top of the column. The ionic strength was raised during elution up to NaCl 2 M to elute completely the orange product. The main orange-red fraction was reduced under reduced pressure to a volume of about 100 mL. 1 mL of HCl 37% and 4 mL of $NaClO_4$ 5 M solution were added a the solution became cloudy and a dark gunk precipitated. Heating with phon dissolved the precipitate and the hot solution was poured in a new flask. The

solution was kept at room temperature overnight then 3 additional mL of $NaClO_4$ 5 M solution were added to induce precipitation. The mixture was kept in fridge overnight and a oily precipitate on flask's wall formed. Vigorous scratching with spatula and sonication at 60°C turned the precipitate in a fine powder. Filtration was then performed (gouch, por. 4) and the orange product on the filter was washed with few drop of icy water. 945 mg of orange-red solid were obtained (Rubpy-NH_2).

5.7.2
Electrodes functionalization

Chemicals and materials

Lipoic acid from Aldrich (≥99%), EDC (1-ethyl-3-(3-dimethylaminopropyl) carbodiimide hydrochloride, triethylamine, ethanol, dichloromethane, H_2SO_4 (98%), hydrogen peroxide (30%), dimethylformamide from Fluka, were used without further purification. Ultrapure 18 MΩ/cm water was obtained by a Milli-Q (Millipore) system. Rubpy-NH_2 and lipoic acid NHS (where NHS is N-hydroxysuccinimmide) were obtained from Cyanagen s.r.l. The glassware used during the electrodes functionalization was cleaned with freshly prepared Piraña solution (98% H_2SO_4 /30% H_2O_2, 7/3, v/v).

TOF-SIMS (Time Of Flight Secondary Ion Mass Spectrometry) setup

The features and experimental setup are summarized in fig. 18

Preparative procedures of ECL gold electrodes

Two strategies were investigated for the preparation of the self assembled lipoic acid monolayers carrying the ECL active probe Rubpy-NH_2. In the first method the coupling product between Rubpy-NH_2 and lipoic acid NHS ester was synthesized and used without further purification to form the monolayer. (scheme 1)

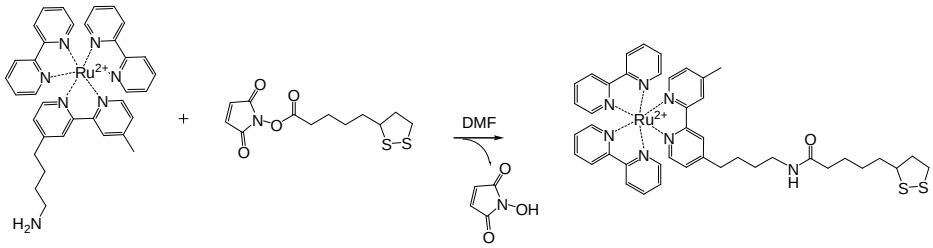

scheme 1

As second method we carried out the coupling of the ECL active moiety Rubpy-NH_2 with lipoic acid's SAMs on gold electrodes (scheme 2).

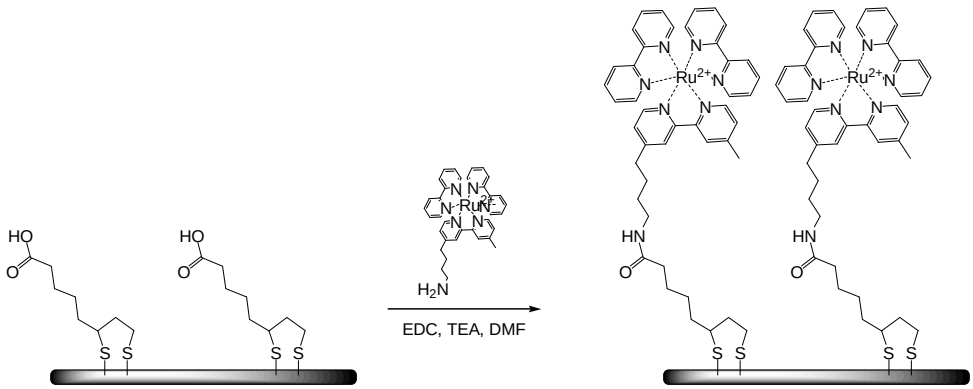

Scheme 2

TOF-SIMS characterization (see below the details) showed that a slightly higher compactness of the SAMs on samples electrodes was reached with the strategy showed in scheme 2. For this reason we describe in detail only the former method that is also simpler from a synthetic point of view. The gold coated silicon electrodes where cleaned at room temperature using freshly prepared Piraña solution for 3-5 min., thoroughly washed with water, ethanol and then dried with a flow of N_2. Electrodes were soaked for 20h in 4mL vials containing a stirred 1.1mM lipoic acid ethanolic solution. A discrete amount of Acetic acid (10% v/v) was added to optimize the SAM deposition according to

well established methods.[9] The chips were then thoroughly washed with ethanol, water and dried under vacuum. The coupling with the active ECL probe was performed in the same way using a DMF solution of Rubpy-NH_2, triethylamine (1.6mM each) and EDC (6.4 mM). After 20h the electrodes were washed with ethanol, water and the dried with N_2.

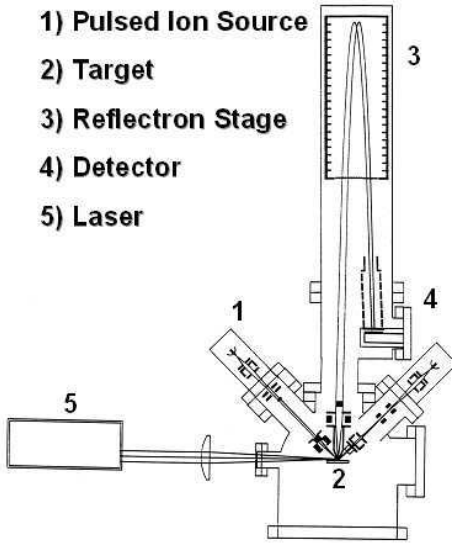

FEATURES

•Primary Source: Ions ($^{69}Ga^+$; $^{133}Cs^+$; Ar^+); Electrons; Photons..

•High Sensitivity and parallel detection: Transmission: 20÷60% for atomic species >50% for molecular species

•Mass Resolution: 8000 @ 28 amu; >10000 @ high mass

•High Mass Range: not limited by the instrument

•Charge compensation: by low energy electrons (10-30eV)

•Lateral Resolution: microprobe mode with 0.1 µm resolution

•Sample stage and load lock both equipped with N_2(l) cooling stage for frozen samples

Figure 18. Scheme and features of the TOF-SIMS system used in chip structural characterization.

SIMS-TOF analysis on functionalized chips

The ionic fragments of interest generated from functionalized chips are summarized in table 3. In fig. 19 are reported the TOF images for an ECL electrode functionalized by only the lipoic acid SAM. The concentration of a single fragment is spatially monitored in each image and is higher when the colour becomes lighter (from red to yellow).

Image number	fragment	Mass/Dalton
1	**96Ru**	95.9090
2	**98Ru**	97.9070
3	**99Ru**	98.9075
4	**100Ru**	99.9062
5	**101Ru**	100.9074
6	**102Ru**	101.9062
7	**104Ru**	103.9071
8	**107Ag**	106.9052
9	**C_10H_9N_2**	157.0849
10	**Au**	196.9649
11	**Group205**	205.0793
12	**C_8H_13O_2S_2**	205.0795
13	**C_8H_13O_2S_2**	206.0898
14	**Unknown256**	256.2715
15	**Group257**	256.8235
16	**Group290**	289.9254
17	**Group308**	307.6464
18	**Unknown312**	312.3390

Table 3. Fragments generated during SIMS-TOF experiments

Images 12 (Mass=205) and 13 (Mass=206) represent the presence of lipoic acid on gold surface.

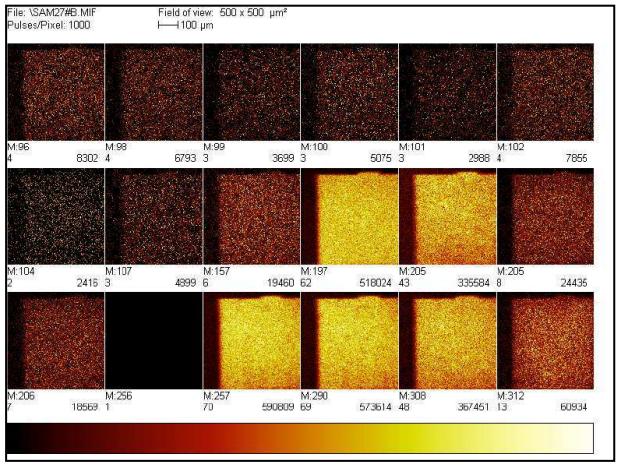

Figure 19. SIMS-TOF images of the chips functionalized with a lipoic acid SAM.

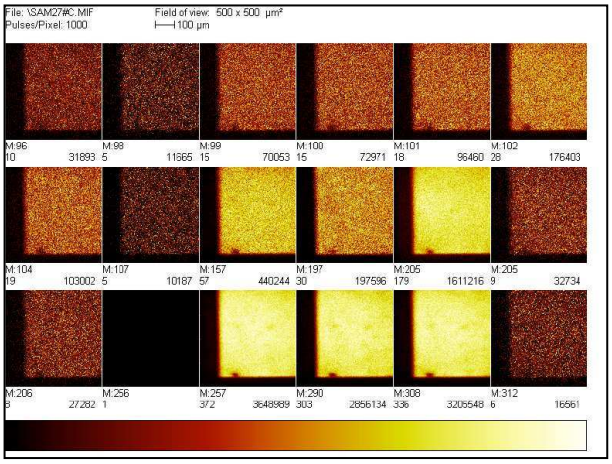

Figure 20. SIMS-TOF images of the chips functionalized with scheme 1.

TOF-SIMS images for an ECL electrode functionalized in one step using the coupling product between Rubpy-NH_2 and lipoic acid NHS ester are reported in fig. 20. Images 1-7 (Mass= 96-104) represent the presence of Ru(II) isotopes. The total concentration of Ru can be thus obtained by summating these low intensity seven slides. Images 12 (Mass= 205) and 13 (Mass = 206) illustrate the presence of lipoic acid on gold surface.

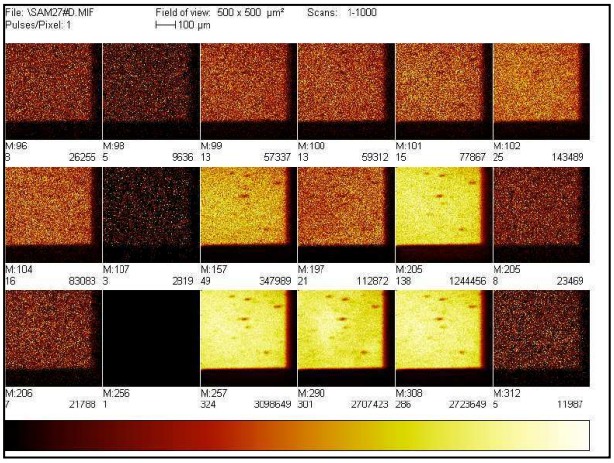

Figure 21. SIMS-TOF images of the chips functionalized with scheme 2.

Finally TOF-SIMS images for an ECL electrode functionalized in two steps using the coupling reaction between Rubpy-NH_2 and lipoic acid SAM is presented in fig. 21. Images 1-7 (Mass=96-104) represent the presence of Ru(II) isotopes. Images 12 (Mass=205) and 13 (Mass=206) illustrate the presence of lipoic acid on gold surface. Image 10 (Mass= 197) represent the Au. The intensity in this case is slightly lower that in the second set of images. This probably indicates the higher density of the SAM obtained in the two step respect to the one step method.

5.7.3

Photoluminescence

Different copies of the chip were fixed carefully into the solid sample holder as shown in fig. 7. The excitation laser wavelength was of 460 nm, the MLCT absorbance maxima of $Ru(bpy)_3^{2+}$. The partially reflected source was eliminated using a cutoff filter for wavelengths under 550 nm. No difference was registered in the emission of the chip functionalized with SAM and Rubpy-NH_2(CHIP-bpy) with respect to the non functionalized one. No difference was evidenced between the chips prepared by one and two steps reaction scheme. As expected the quenching caused by Au electrodes surfaces prevented the radiative pathway of decay.

5.7.4

Electrochemistry and ECL.

A cyclic voltammetry was first ran for each sample in order to check if the cell contacts were good and then repeated for 10 cycles to check reproducibility and stability of the obtained curve. The potential was swept from 0 to 1.5 V (vs Ag wire) at 1 V/s. To oxidize NPr_3 is known to be necessary in this conditions a potential in the range of + 0.8-1 V. Because a drift of ±100-200 mV of the quasi reference electrode could sometimes occur, to be sure to oxidize the ammine a maximum potential of 1.5 V has been reached A series

of 4 successive tests including CV (fig. 22) and the ECL (fig. 23) were performed in different conditions in order to check the presence of the coupling reaction and to ensure that emission was due to the $Ru(bpy)_3^{2+}$ contained in the SAM. The test number 1 and 2 (fig. 22 and 23) were ran with well polished blank chips (e. g. not functionalized) in PBS 0.1 M and PBS/NPr_3 solution to exclude the possibility of an ECL background emission from buffer and NPr_3; this tests were necessary in consideration of the low concentration of $Ru(bpy)_3^{2+}$ at the electrode in functionalized chips. In the test 1 cyclic voltammetry showed a stable resistive behaviour and no ECL emission was observed at all. In the experiment 2 the current increased of an

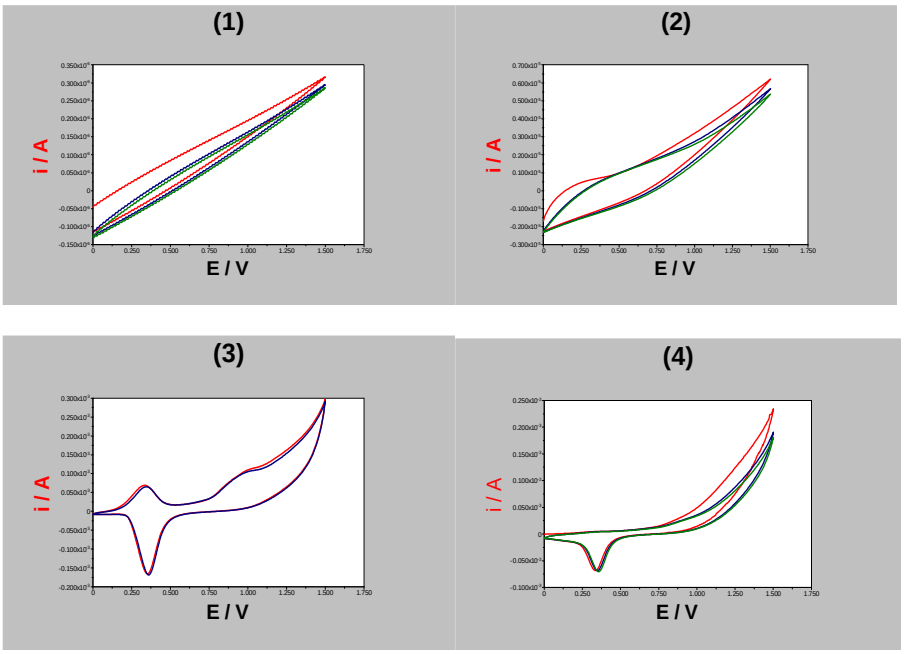

Figure 22. Cyclic voltammetries registered using a qRef Ag wire electrode. Scan rate 1 V/sec. T= 20 °C. Cell was air equilibrated. (1) chip without SAM in 0.1 PBS at pH 7.5; (2) chip without SAM in 0.1 PBS (pH 7.5) and NPr_3 $3x10^{-2}$ M; (3) CHIP-bpy in 0.1 PBS (pH 7.5) and NPr_3 $3x10^{-2}$ M; (4) CHIP without SAM in 0.1 PBS (pH 7.5) and NPr_3 $3x10^{-2}$ M using the same solution used previously in test 3.

order of magnitude with respect to the first and a progressive decrease of the oxidation current of NPr_3 was observed for repeated swept as expected; this was due to the consumption of the ammine during his irreversible oxidation. In the test 3 a CHIP-bpy was introduced in the PBS/NPr_3 solution. Two well visible SAM de-adsorption peaks[10] appeared from second cycle at about +0.3 V and + 1.0 V vs. Ag on direct scan; an adsorption peak appeared in reverse scan around + 0.3 V with the typical triangular shape. During test 3 a discretely intense ECL emission was detected. Emission slowly decreased by time as

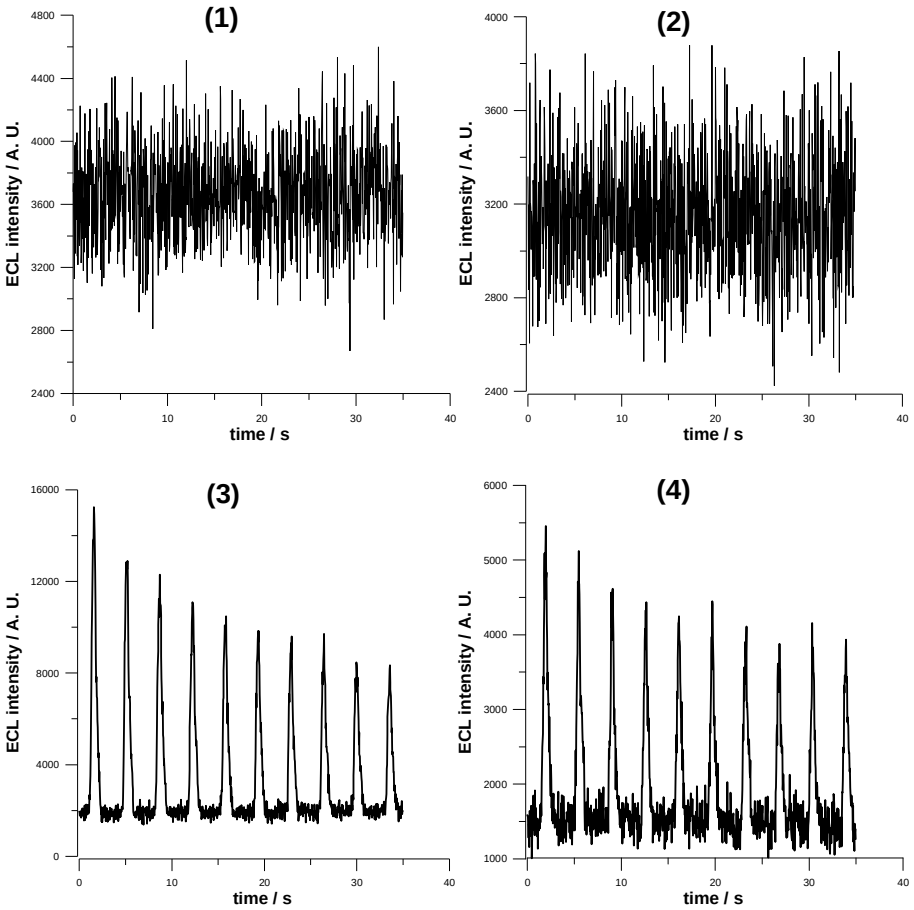

Figure 23. Integrated ECL intensity vs time registered during the cyclic voltammetries reported in fig. 22. The PMT voltage was of 1000 V with an integration time of 10 ms.

intensity of the adsorption peaks increased. ECL spectra was registered in the same conditions and his maximum was found at 620 nm (fig. 24) compatible with that of $Ru(bpy)_3^{2+}$ emission in solution. Normally when the dye is in a SAM or in solid state a red shift of about 30-60 nm is reported.[5,6] The experiment 3 confirmed the presence of the dye on the CHIP-bpy functionalized CHIP. The experiment 4 has been performed introducing again in solution the blank chip in the same solution used in test 3. Both CV and ECL changed completely from previous test 2 and were similar to that of test 3 suggesting that the $Ru(bpy)_3^{2+}$ based surfactant was released in solution causing ECL emission and the adsorption peaks in cyclic voltammetry. The same series of four tests were performed using chip functionalized with the one step reaction where LipAc and Rubpy-NH_2 were inserted at the same time. The results were identical to those of the CHIP-bpy obtained by two separated reactions.

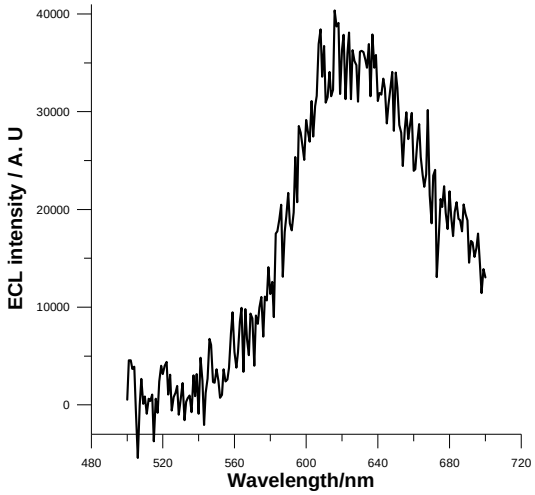

Figure 24. ECL spectra of CHIP-bpy emission in a 0.1 M PBS and NPr_3 $3x10^{-2}$ M solution at pH 7.5 (conditions of test 3). Switching method: chronoamperometry. Potential program: E_1= +0 V , t_1=100 ms ; E_2=+1.3 ,t_2=100 ms (Potentials are vs. qRef Ag wire) . T= 20 °C. The cell was air equilibrated. The PMT integration time was of 5 s.

ECL experiments suggested again that the $Ru(bpy)_3^{2+}$ marked product was present on electrode surface and that the SAM was detached from the chip during electrolysis. ECL measurements have been reproduced with three different copies of the chip for each preparation method.

5.7.5
Conclusions

This series of experiments showed the possibility to detect the occurrence of a coupling reaction on a SAM active site using a fast, simple and economic method based on ECL. This approach could also be used to check the SAM stability during electrolysis.

Appendix V: assay solution composition in commercial ECL analyzers.[11]

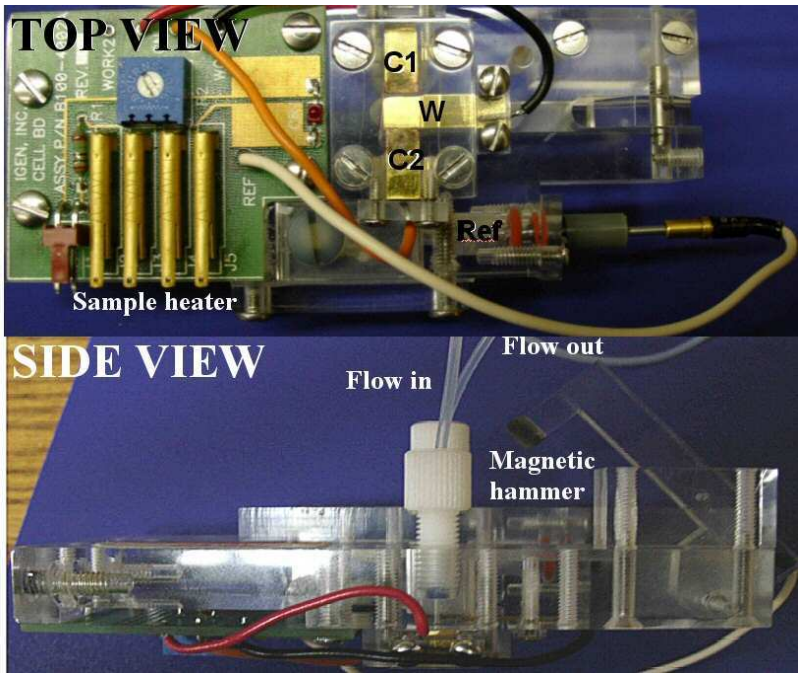

Figure 25. Top and side view of the electrochemical cell of ORIGEN ECL analyzer. This type of flow cell, built in the early '90, was intended for immuno-assays tests with magnetic beads as carriers.

To make ECL technique suitable for clinical analysis the use of an electrochemical flow cell (fig. 25) must be combined with an appropriate formulation of assay buffers because his composition can efficiently affect the ECL intensity, sensitivity, selectivity and stability. This appendix regards then the fundamental aspects of optimizing the formulation of assay buffers. The use of NPr_3 coreactant, as previously introduced in sect. 4.1 involves the intermediacy of a dissociative chemical reaction following the initial electron transfer step to generate a highly active intermediate. The assay buffer solution provides an appropriate environment for the ECL process, and the existing of biological species as well.

The formulation of the IGEN inc. assay buffer is summarized as following:

Component	**Concentration**	**Function**
NPr_3	0.1 M	Source of ECL intermediate
KH_2PO_4	0.2 M	pH buffer, supporting electrolyte
NaN_3	7.7 mM	preservative, ECL signal enhancer
NaCl	50μM	ECL signal enhancer
Triton-100	0.05 % (in volume)	surfactant, electrode surface condition improvement (good wetting agent)
Tween-20	0.05 % (in volume)	surfactant, electrode surface condition improvement

Obviously, NPr_3 is the most important species in above formula. A small amount of NaN_3 is also important in the assay buffer. Its basic function is preservative. Note than N_3^- also can be oxidized to a strong reducing radical N_3, which will enhance ECL signal about 10-20 %. On the other hand, has been found that a small amount of NaCl (3-20 mM) added to the buffer can enhance the ECL intensity by a factor of 3-6 times.

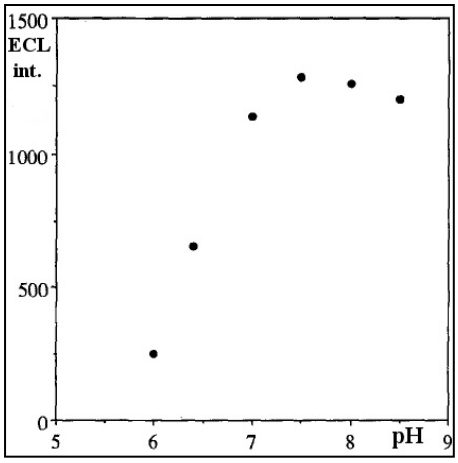

Figure 26. The pH dependence of ECL intensity using 0.10M NPr_3 and 10^{-9} M $Ru(bpy)_3^{2+}$. The signal is corrected for background. [Adapted from ref. 13]

This enhancement may be due to the specific adsorption of chloride at Au and Pt electrode surfaces. Another explanation could be that chloride was oxidized to

chlorine; chlorine or ClO^- (Cl_2 dissolved in H_2O to produce ClO^-) would catalyze ECL reaction. It is interesting to note that Br^- and F^- have a similar ECL enhancement effect in the same conditions.[12] The solution pH is another important factor for assay buffer formulation. The pK_a of $H_2PO_4^-$ is about 7 and $H_2PO_4^-$ can make a good buffer of pH=7, but it fails to make a buffer of pH=6. The pH value where NPr_3 activity is higher (fig. 26) has been empirically found to be 7.0-7.5.[13] The typical dependence of ECL intensity on NPr_3 concentration is linear until a plateau is reached at about 20-30 mM (fig. 27).[12]

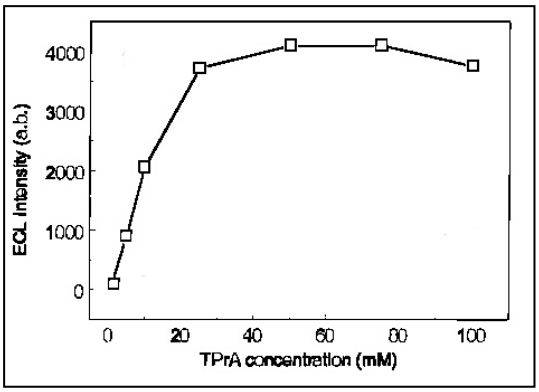

Figure 27. Dependence of ECL intensity on NPr_3 concentration in the flow-through system. Sample solutions contained 1 nM $Ru(bpy)_3^{2+}$ and 0.02 vol % Triton X-100 in the presence of an optimum 1 mM concentration of bromide. Supporting electrolyte: 0.15 M phosphate buffer at pH 7.5. [Adapted from ref. 12]

References

[1] G. Kalyuzhny, M. Buda, J. McNeil, P. Barbara, A. J. Bard, *J.Am. Chem. Soc.*, 125, 6272 (2003).

[2] The washing procedure between a test and the following was the same already described in ECL titration section (3.3.4).

[3] The photon counting unit is however supported by the monochromator.

[4] G. C. Fiaccabrino, M. Koudelka-Hep, Y. –T. Hsueh, S. D. Collins and R. L. Smith, *Anal. Chem.*, 70, 4157 (1998).

[5] X. Zhang and A. J. Bard, *J. Phys. Chem.*, 92, 5566 (1988).

[6] Y. S. Obeng and A. J. Bard; *Langmuir*, 7, 195 (1991).

[7] (a) T. M. Willey, A. L. Vance, C. Bostedt, T. van Buuren, R. W. Meulenberg, L. J. Terminello, C. S. Fadley, *Langmuir*; 20, 4939 (2004); (b) M. Dijksma, B. Kamp, J. C. Hoogvliet, W. P. van Bennekom, *Langmuir*; 16, 3852 (2000); (c) J. Kunze, J. Leitch, A. L. Schwan, R. J. Faragher, R. Naumann, S. Schiller, W. Knoll, J. R. Dutcher, J. Lipkowski, *Langmuir*; 22, 5509 (2006).

[8] J. K. Howie, J. J. Houts and D. T. Sawyer, *J. Am. Chem. Soc.*, 99, 19 (1977).

[9] (a) J. C. Love, L. A. Estroff, J. K. Kriebel, R. G. Nuzzo, G. M. Whitesides, *Chem. Rev.*, 105(4), 1103 (2005); (b) A. Ulman, *Chem. Rev.*, 96, 1533 (1996); (c) R. C. Major, X. –Y. Zhu, *J. Am. Chem. Soc.*, 125, 8454 (2003) ; (d) R. Arnold, W. Azzam, A. Terfort, C. Woll, *Langmuir*, 18, 3980 (2002).

[10] In these experimental conditions the SAM is known to be stable up to an approximate potential of +0.7 V vs. Ag. Consequently in order to oxidize NPr_3 and generate ECL is necessary to detach the SAM from electrode surface.

[11] This appendix is a summary of IGEN inc. dossiers about assay buffers.

[12] Y. Zu and A. J. Bard, *Anal. Chem.*,72, 3223 (2000).

[13] J. K. Leland, M. J. Powell, *J. Electrochem. Soc.*, 137, 3127 (1990).

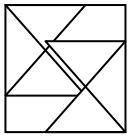

Final remarks

Caminante, no hay camino. Se hace camino al andar.
Antonio Machado

Electrochemiluminescence has proven to be a very versatile method of investigation. During this predoctoral fellowship 14 different Ir and Ru complexes have been studied from the point of view of electrochemical and emission properties. The best behaving new material was found to be Ru(pyr-tet) that evidenced an high ECL emission even in water/air media with a maximum slightly red shifted respect to that of $Ru(bpy)_3^{2+}$. The preliminary tests on his direct interaction with DNA showed a non conventional behaviour that is still under investigation… Some complexes succeeded in preparation of solid devices with light emission in the visible and near IR region. Other compounds, disappointing from the point of view of the wished ECL properties, were unexpectedly impressive in new directions. An interesting example is the Ir(pyr-tet)Br complex that demonstrated the possibility to follow by ECL the kinetics of an electro-induced chemical reaction.

The design of the Bologna ECL instrument was a great occasion to create a flexible and sensitive system introducing many new stimulating possibilities. Last not least the ECL chips electrodes were a surprising source of ideas and know-how exchange. During lab-on-chip preparation, the combination of different disciplines and skills (i. e. engineering, electrochemistry, photochemistry, synthetic chemistry, material sciences, biology, analytical

chemistry, …) resulted in a project of simultaneous academic and applicative interest. Often the multi-discipline approach by combining simple concepts of each subject easily leads to new research directions.
In these three years I learned that an experiment is never a full success or failure but just a knowledge step, whether an objective is reached or not just a new beginning …

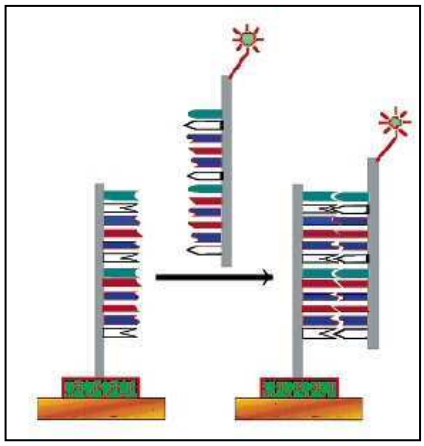

Figure 1. A simple scheme to detect by ECL the DNA hybridization. The target DNA is labelled with an ECL active compound and the complementary strand (probe) is immobilized on electrode surface. [adapted from ref. 1]

Toward nanoparticles and DNA micro-arrays…

The fundamental and mostly realistic objective of ECL investigations seems to be the improving on several aspects of immuno-assay tests. The following research lines are currently in progress in this direction:

- DNA hybridization studies on ECL chips (By using an already reported[1] ibridization scheme shown in fig. 1 a similar experiment will be tried using chips electrodes as substrate).

- MEA (multi electrode array) preparation (by taking as reference the extraordinary micro arrays, containing up to 100,000 electrodes, recently

produced by Combimatrix Corp., a series of 16 electrodes ECL arrays will be prepared and tested to introduce the new detection method in multi-target analysis).

- Synthesis of new ECL labels based on Ru(pyr-tet) (being the ammine modified bpy ligand already available and considering the promising properties of the complex the preparation and testing of the label should easily follow. The hypothetic structure is reported in fig. 2).

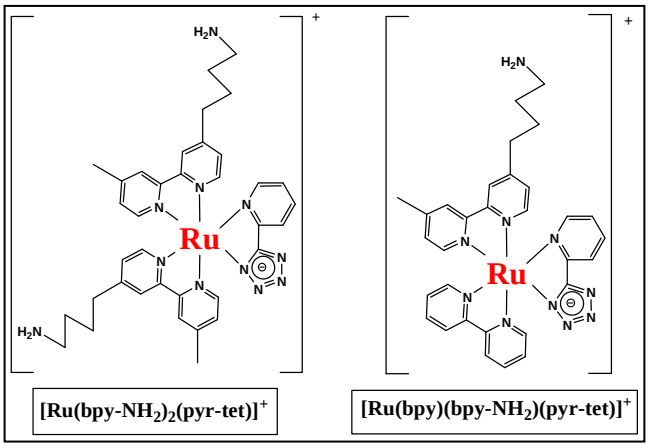

Figure 2. Two possible mixed ligand ECL labels based on Ru(pyr-tet).

- Synthesis and characterization of new complexes containing Ru, Ir, Re and Os as central atom with improved efficiency or shifted emission energy. (unlike fluorescence an ECL multicolour detection system is still unavailable. Four well distinguishable different colours should be necessary to differentiate the nucleotides).

- Synthesis and test of covalently doped silica nanoparticles as ECL labels (The benefits of the use of nanoparticles containing the emitting complex as a label are: the absence of self-quenching due to the fixed position inside the particle; the low concentration of oxygen and water into silica pores that results in higher efficiency; the fact that a great amount of the complex can be

bound to a single molecule of target DNA[2] by greatly increasing the sensitivity).

- Preparation of ECL chip sensors based on the light-switch effect of Ru(dppz) (This type of sensor, depicted in fig. 3, should detect the presence of double helix DNA in solution thank to a great increase of fluorescence efficiency when hybridized DNA is present. The decrease of diffusion coefficient that follows the intercalation of the complex into DNA double strand, discussed in sect. 3.3.2, could be avoided by directly binding the Ru-dppz to the electrode).

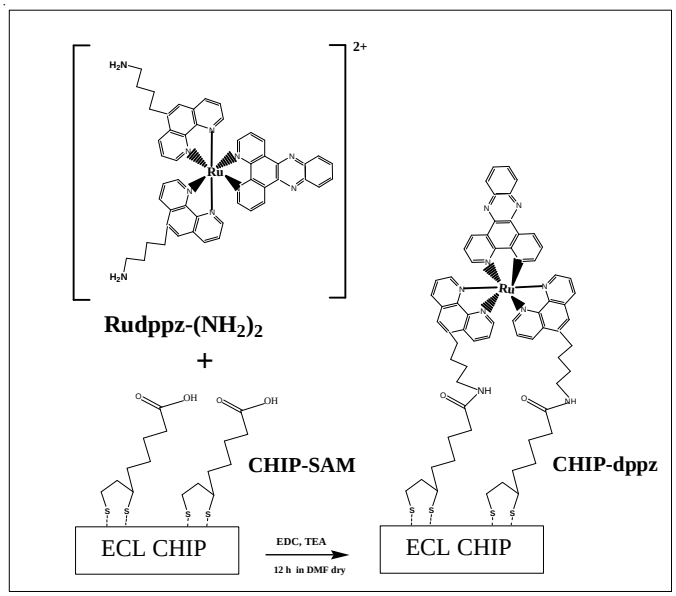

Figure 3. A possible chip functionalization scheme by using the ammine derivative of the Rudppz. This device should detect the presence of DNA double strand thank to the big increase of ECL efficiency in his presence.

References

[1] W. Miao, A. J. Bard, *Anal. Chem.*, 75, 5825 (2003).

[2] W. Miao, A. J. Bard, *Anal. Chem.*, 76,5379 (2004).

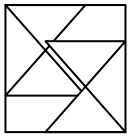

Final Credits

Non c'è nulla di più pericoloso di una grande idea in un piccolo cervello…

E' incredibile come questi tre anni siano trascorsi rapidamente. Sin da quando sono arrivato mi sono accorto di quanto si stesse bene in questo gruppo; qui si lavora e ci si diverte! Qui si pensa alla grande scienza senza dimenticare di prendere un po' in giro chi ti sta attorno. E se c'è festa ci siamo sempre ! La lista di persone da ringraziare è davvero molto lunga… Se dimentico qualcuno non si offenda, sono una persona un po' sbadata ma di sicuro era certo mia intenzione di ringraziarlo. Allora su partiamo:

Massimo e Francesco: come avete potuto accogliere una persona che non conoscevate, insegnargli i vostri segreti e poi mandarlo a fare l'americano ? Beh, comunque grazie davvero ce l'avete fatta !

Demis, Carlo, Giulia, Matteo, Giovanni, Stefania vi ringrazio in ordine sparso perché non ho voglia di mettervi in un qualsiasi ordine; grazie dell'aiuto materiale, psicologico e soprattutto delle sciocchezze che abbiamo detto e fatto insieme.

Ringrazio papa e mamma, grandi lavoratori, grazie alla vostre fatiche e rinunce ho potuto giocare con le luci e l'elettricità fino a più di trent'anni…

Grazie alle due Chiare (mia sorella e la mia ragazza) voi che quotidianamente avete sopportato e quotidianamente sopporterete…

Un ringraziamento speciale va a te mia amata Chiarina ! Nei giorni difficili i tuoi occhi e il tuo sorriso erano sempre con me ! Come una cometa mi hai guidato radiosa verso la gioia !

Come potrei non ricordare Austin ed i suoi personaggi, loro che tanto hanno contribuito a farmi sentire uno scienziato. Ringrazio il Prof. Bard, Frank Fu Ren e tutti gli altri numerosissimi componenti del suo gruppo. Ricordo in particolare quelli dell'officina meccanica ed il mitico soffiatore Michael che hanno assecondato con pazienza tante mie leonardesche creazioni…

Ringrazio Leo della Cyanagen ed il Prof. Luca Prodi per aver sopportato e supportato la mia voglia di fare cose utili all'umanità . Ringrazio i bravissimi Enrico ed Ettore senza i quali i chip sarebbero rimasti nudi…

Ringrazio Roberto di Trento per le misure SIMS-TOF…

Ringrazio il Prof. Palazzi ed il grande Stefano Stagni per le numerose polverine fluorescenti.

Ringrazio l'Ing. Gigi Civera ed il suo braccio destro Danilo per il grande aiuto e l'ospitalità.

Ringrazio Livio Cognolato e gli altri ragazzi dell'Olivetti s.p.a. che camminano con noi verso il sogno "ECL on chip".

Grazie a tutti quelli del progettone LATEMAR….

Insomma basta adesso sono stufo se non avete ancora sentito:

GRAZIEEEEE !

THE END